# Investigating increases in terrestrial carbon uptake

## Michael Dominic O'Sullivan

Submitted in accordance with the requirements for the degree of Doctor of Philosophy

The University of Leeds
School of Earth and Environment

August 2018

# Declaration of Authorship

The candidate confirms that the work submitted is his own, except where work which has formed part of jointly-authored publications has been included. The contribution of the candidate and the other authors to this work has been explicitly indicated below. The candidate confirms that appropriate credit has been given within the thesis where reference has been made to the work of others.

The work in Chapter 2 of the thesis has appeared in publication as follows:

O'Sullivan, M., Rap, A., Reddington, C. L., Spracklen, D. V., Gloor, M., Buermann, W., (2016). Small global effect on terrestrial net primary production due to increased fossil fuel aerosol emissions from East Asia since the turn of the century. Geophysical Research Letters, 40, 8060-8068. The manuscript was written by the candidate with advice from supervisors (W. Buermann, and D. V. Spracklen) and comments from co-authors. The analysis of all model output and comparison with observations was performed by the candidate. The experiment design and model setup was a collaborative effort between the candidate, A. Rap, and W. Buermann. The GLOMAP simulations were performed by C. L. Reddington and the Edwards-Slingo simulations were performed by A. Rap. The candidate performed the JULES simulations.

The work in Chapter 3 of the thesis has been accepted for publication pending major revisions under the following title:

O'Sullivan, M., Spracklen, D. V., Batterman, S. A., Arnold, S. R., Gloor, M., Buermann, W., (2019). Have synergies between nitrogen deposition and atmospheric CO2 driven the recent enhancement of the terrestrial carbon sink? Global Biogeochemical Cycles, **33**. The manuscript was written by the candidate with comments from co-authors. The experiment design was a collaborative effort between the candidate and W. Buermann. The setup, running and analysis of model simulations was performed by the candidate.

The work in Chapter 4 of the thesis is a manuscript soon to be submitted under the following title:

O'Sullivan, M., Spracklen, D. V., Smith, W. K., Sitch, S., Friedlingstein, P., Arora, V. A., Haverd, V., Jain, A. K., Kato, E., Kautz, M., Lombardozzi, D., Nabel J.E.M.S., Tian, H., Vuichard, N., Wiltshire, A., Zhu, D., Buermann, W. (submitted, 2019). Climate-driven variability and trends in plant productivity over the last three decades based on three global products. Global Change Biology. The manuscript was written by the candidate with comments from co-authors. The experiment design was performed by the candidate with input from W. Buermann. The analysis of model output and observation data was performed by the candidate. S. Sitch provided the TRENDY model output, W. K. Smith provided the satellite light-use efficiency dataset, and Martin Jung provided the FLUXCOM dataset.

# Acknowledgements

Firstly, I would like to thank my primary supervisor Wolfgang Buermann for all the help and advice over the years, which I wouldn't have been able to do without. Also, thanks to my other supervisors Dom Spracklen and Manuel Gloor who provided valuable comments and reassurance throughout.

I'd also like to thank Alex Rap and Carly Reddington who had a large contribution to the work presented in Chapter 2, and happily helped out with various modelling issues at the start of the PhD. I would like to thank Steve Arnold who helped me to setup the Community Land Model, used in Chapter 3. A big thanks goes to Richard Rigby who solved all kinds of technical IT issues, saving me countless hours staring at a computer screen!

I'd also like to thank all the members of the Biosphere Atmosphere Group and the Physical Climate Change group, who welcomed me right from the start and were a pleasure to work with. A huge mention to members of my PhD cohort, especially Ollie, Ilkky, George, Lauren, and Hana, who have been on the PhD rollercoaster with me. Also, thanks to all the people who I've played football with over the years.

A special thank you to all my friends and family. Maeve and Patrick in particular who always offered plenty of encouragement. Finally, and most importantly, thank you to my parents for all the support over the years, I couldn't have done this without them.

# Abstract

Anthropogenic $CO_2$ is the most important long-lived greenhouse gas, and with atmospheric concentrations over 40% above pre-industrial levels, it is the main cause of climate change. The terrestrial carbon sink has increased in proportion with anthropogenic $CO_2$ emissions over the last century and dampened climate change. Yet, the mechanisms behind the increase remains a puzzle and this limits our predictive abilities to estimate climate-carbon feedbacks in projections of future climate changes. Since the turn of this century, the terrestrial sink has substantially increased during a time of rapid increase in fossil fuel $CO_2$ emissions.

In this thesis, the influence of increased diffuse radiation (due to anthropogenic aerosol) and nitrogen deposition (and carbon-nitrogen deposition synergies) associated with increased fossil fuel emissions on terrestrial carbon uptake, since the turn of this century is quantified. I also assessed interannual variations (IAV) and trends in climate-driven gross primary productivity (GPP) over the period 1982-2016. The distribution of atmospheric aerosols due to anthropogenic fossil fuel emissions was simulated with chemical transport-aerosol model TOMCAT-GLOMAP over the period 1998-2010. The influence of aerosols on incoming solar radiation was calculated with the radiative transfer model Edwards-Slingo. Subsequently, the impact of variations in direct and diffuse radiation on net primary productivity (NPP) are quantified with the land-surface model JULES. Secondly, the Community Land Model (CLM4.5-BGC) was used to estimate the influence of changes in atmospheric $CO_2$, nitrogen deposition, climate, and their interactions to changes in net primary production (NPP), and net biome production (NBP) over the historical (1901-2016) and modern (1990-2016) periods. Finally, the influence of climate on vegetation productivity is evaluated using upscaled flux tower observations (FLUXCOM), a satellite-based light use efficiency model (LUE), and a set of process based terrestrial biosphere models (TRENDYv6).

I estimate that at global scale, changes in light regimes from fossil fuel aerosol emissions had only a small negative effect (-0.08 PgC/yr) on the increase in terrestrial NPP over the period 1998–2010 (overall increase of 1.7 PgC/yr). Hereby, the substantial increases in fossil fuel aerosol emissions and subsequent plant carbon uptake over East Asia (33% of the 0.53 PgC/yr increase) were effectively cancelled by opposing trends across Europe and North America. Over 1901-2016, nitrogen deposition and carbon-nitrogen synergistic effects contributed ~30% to increase in NBP (overall increase of 2.31 PgC/yr). However, since the turn of this century, nitrogen-related mechanisms had no contribution to the increasing sink. Opposing regional NBP trends due to nitrogen deposition (50 TgC/yr increase in East Asia, and 14 TgC/yr and 6 TgC/yr decreases in North America and East Europe, respectively) cancel at the global scale. Nonetheless, I find that increased nitrogen deposition in East Asia since the early 1990s contributed 50% to the overall increase in NBP over this regions, highlighting the importance of carbon-nitrogen interactions. Therefore, potential large-scale changes in nitrogen deposition could have a significant impact on terrestrial carbon cycling and future climate.

Regarding the impact of climate variations on vegetation productivity, I find large differences in global and regional trends between the observational and modelling products. FLUXCOM has a small positive global GPP trend (0.02±0.01 PgC/yr$^2$) and has a smaller IAV than both other products. The TRENDYv6 models simulate a positive global GPP trend of 0.09±0.06 PgC/yr$^2$, whereas the LUE product has a smaller increase of 0.06±0.02 PgC/yr$^2$. For TRENDYv6 and LUE, the global pattern is predominately driven by a large northern latitude increase (driven by a warming trend). The products agreed on the direction of trend across 60% of the vegetated land surface. Large areas of Eurasia and North America exhibit positive summer trends due to warming. In contrast, warming in central South America has decreased GPP. Negative precipitation trends in South US and Mongolia/China have reduced GPP, whereas a wetting trend in South Africa has enhanced productivity. There are clear differences in the sensitivity of each product to climate forcing, highlighting uncertainty in the processes that influence GPP. These differences in variability and trends in GPP, as well as underlying climatic controls in the three most commonly used products in carbon cycle studies, highlight the need for long-term observations of GPP, particularly in underrepresented regions (e.g. tropical

forests), and the need to better constrain and improve GPP estimates from models.

# Contents

# List of Figures

# List of Tables

# Abbreviations

| | |
|---|---|
| AOD | **A**erosol **O**ptical **D**epth |
| CLM | **C**ommunity **L**and **M**odel |
| CRU | **C**limatic **R**esearch **U**nit |
| DGVM | **D**ynamic **G**lobal **V**egetation **M**odel |
| ENSO | **E**l **N**ino **S**outhern **O**scillation |
| ES | **E**dwards-**S**lingo Radiation Model |
| FACE | **F**ree-**A**ir **C**arbon dioxide **E**nrichment |
| FPAR | **F**raction of absorbed **P**hotosynthetic **A**ctive **R**adiation |
| GCB | **G**lobal **C**arbon **B**udget |
| GPP | **G**ross **P**rimary **P**roduction |
| IAV | **I**nter**a**nnual **V**ariability |
| IPCC | **I**ntergovernmental **P**anel on **C**limate **C**hange |
| LAI | **L**eaf **A**rea **I**ndex |
| LSM | **L**and **S**urface **M**odel |
| LUE | **L**ight-**u**se **E**fficiency |
| NDVI | **N**ormalised **D**ifference **V**egetation **I**ndex |
| NEE | **N**et **E**cosystem **E**xchange |
| NEP | **N**et **E**cosystem **P**roduction |
| NPP | **N**et **P**rimary **P**roduction |
| PFT | **P**lant **F**unctional **T**ype |
| ppm | **p**arts **p**er **m**illion |
| Rh | **H**eterotrophic **R**espiration |
| SDR | **S**urface **D**iffuse **R**adiation |

| | |
|---|---|
| TBM | **T**errestrial **B**iosphere **M**odel |
| TEC | **T**otal **E**cosystem **C**arbon |
| VPD | **V**apour **P**ressure **D**eficit |

# Chapter 1

# Introduction

## 1.1 The global carbon cycle

The cycling of elements in the Earth system is integral in the creation and maintenance of life. The major elements (carbon, oxygen, hydrogen, nitrogen, phosphorus, and sulfur) cycle through four components (biosphere, lithosphere, atmosphere, and hydrosphere) of Earth. Carbon is the main component of all life on Earth and (as carbon-dioxide) partially responsible for the greenhouse effect, warming the planet to hospitable conditions for life. Carbon flows between five major reservoirs; atmosphere, biosphere, oceans, sediments (fossil fuels and soil carbon), and the Earth's interior (mantle and crust).

The Earth's interior contains over 99.9% of all planetary carbon. Only a small fraction (40,000 PgC) of carbon is stored in pools near the Earth's surface. The oceans contain 95% of this biologically active carbon, with majority stored as dissolved inorganic carbon (DIC). Terrestrial carbon is stored as organic forms in soils (1500-2400 PgC) and vegetation (450-650 PgC) (Ciais *et al.*, 2013). Permafrost soils are estimated to contain at least 1700 PgC (Ciais *et al.*, 2013). The atmosphere is the smallest pool, containing over 850 PgC as of 2018 (calculated using a conversion factor of 2.12 PgC/ppm, Prather *et al.* (2012)).

However, these pools are not static and evolve over varying timescales. The carbon cycle is the superposition of two cycles, a slow cycle whereby carbon is exchanged between atmosphere, oceans, land by chemical weathering of rocks and tectonic activity over millions of years; and a fast cycle in which biological and physical processes drive carbon exchange between the atmosphere, oceans, and terrestrial ecosystems on timescales of days to decades.

Terrestrial carbon uptake is the balance of large, uncertain processes. Global photosynthesis, known as Gross Primary Production (GPP) is estimated to be roughly 110 PgC/yr during the pre-industrial era (Ciais *et al.*, 2013). Half of this carbon is respired by plants during maintenance and biomass growth. The remainder is Net Primary Production (NPP) which represents the net production of organic matter in plants. Decomposition of dead organic matter by soil biota, known as heterotrophic respiration (Rh) is a main pathway for carbon to transfer from the land to the atmosphere. The difference between NPP and Rh is Net Ecosystem Production (NEP), which represents the net accumulation of carbon in an ecosystem. Fires and other disturbance processes lead to further carbon release to the atmosphere. The net flux of carbon to the land is known as Net Biome Production (NBP=NEP-disturbances) and is relatively small compared to the total fluxes (~1% of GPP), and therefore small changes in these gross fluxes can lead to relatively large changes in the net carbon flux.

The majority (98%) of ocean carbon is stored as dissolved inorganic carbon (DIC). Deep ocean carbon is relatively stable with a turnover time of thousands of years (Ciais *et al.*, 2013). Conversely, surface DIC is exchanged rapidly with the atmosphere.

Prior to industrialisation the carbon cycle is thought to have been in a relative steady state with no net exchange between the atmosphere, oceans, and land. Human activities have disrupted this natural state. The burning of fossil fuels for heat, electricity and other industrial processes has transferred vast quantities of carbon from the slow carbon cycle to the fast.

In the atmosphere, carbon exists predominately as carbon dioxide ($CO_2$), with current concentrations exceeding 400 ppm (850 PgC). This is an increase of more than 45% since the beginning of the Industrial Revolution, which has been the predominant driver of increased concentrations, through the burning of fossil fuels and deforestation. Human emissions ($E_{TOT}$) have totalled 645±80 PgC since 1750 (Le Quéré *et al.*, 2018). However, less than half (270±5 PgC) of these emissions have remained in the atmosphere ($G_{ATM}$), with the remainder sequestered into the land ($S_{LAND}$) and oceans ($S_{OCEAN}$) (see Figure 1.1). The biospheric sinks provide a valuable service due to the warming nature of atmospheric $CO_2$. Increased $CO_2$ concentrations due to anthropogenic activity has already warmed the planet by 1 °C since 1880 (Hartmann *et al.*, 2013) and will continue to do so into the future (even if emissions stopped immediately) due to the thermal inertia of the oceans (Wigley, 2005). Current (2007-2016) fossil fuel and land-use change emissions are 9.4±0.5 and 1.3±0.7 PgC/yr, respectively. Similarly to the cumulative sink, the atmosphere retained 45% (4.7±0.1) of these emissions.

Air-sea gas exchange is primarily driven by the difference in partial pressure of $CO_2$ between the atmosphere and ocean surface. As such, the ocean sink has increased in proportion with atmospheric concentrations. The ocean has absorbed 160±20 PgC of human emissions since 1750, equating to roughly 25% of total emissions (Le Quéré *et al.*, 2018). This carbon is mainly in the surface waters as oceans take thousands of years to mix fully (Ciais *et al.*, 2013). The current (2007-2016) sink is estimated at 2.4±0.5 PgC/yr and exhibits little inter-annual variability (Le Quéré *et al.*, 2018).

To close the historical global carbon budget, the cumulative terrestrial sink is 215±80 PgC (estimated as the residual term in $S_{LAND} = E_{TOT} - G_{ATM} - S_{OCEAN}$). On an annual basis, the terrestrial sink increased from 1.8±0.8 PgC/yr in the 1960s to 3.6±1.0 PgC/yr in 2007-2016. The increased sink is due to a myriad of factors including; $CO_2$ fertilization of photosynthesis (Schimel *et al.*, 2015), climate warming leading to longer and more favourable growing seasons (Barichivich *et al.*, 2013), regrowth on abandoned farm land (Kondo *et al.*, 2018), and nitrogen deposition stimulating plant growth (Zaehle, 2013) (see Section 1.2). All these effects do not act independently, and as such there may be important synergies between the carbon, nitrogen, and warming effects on plant growth.

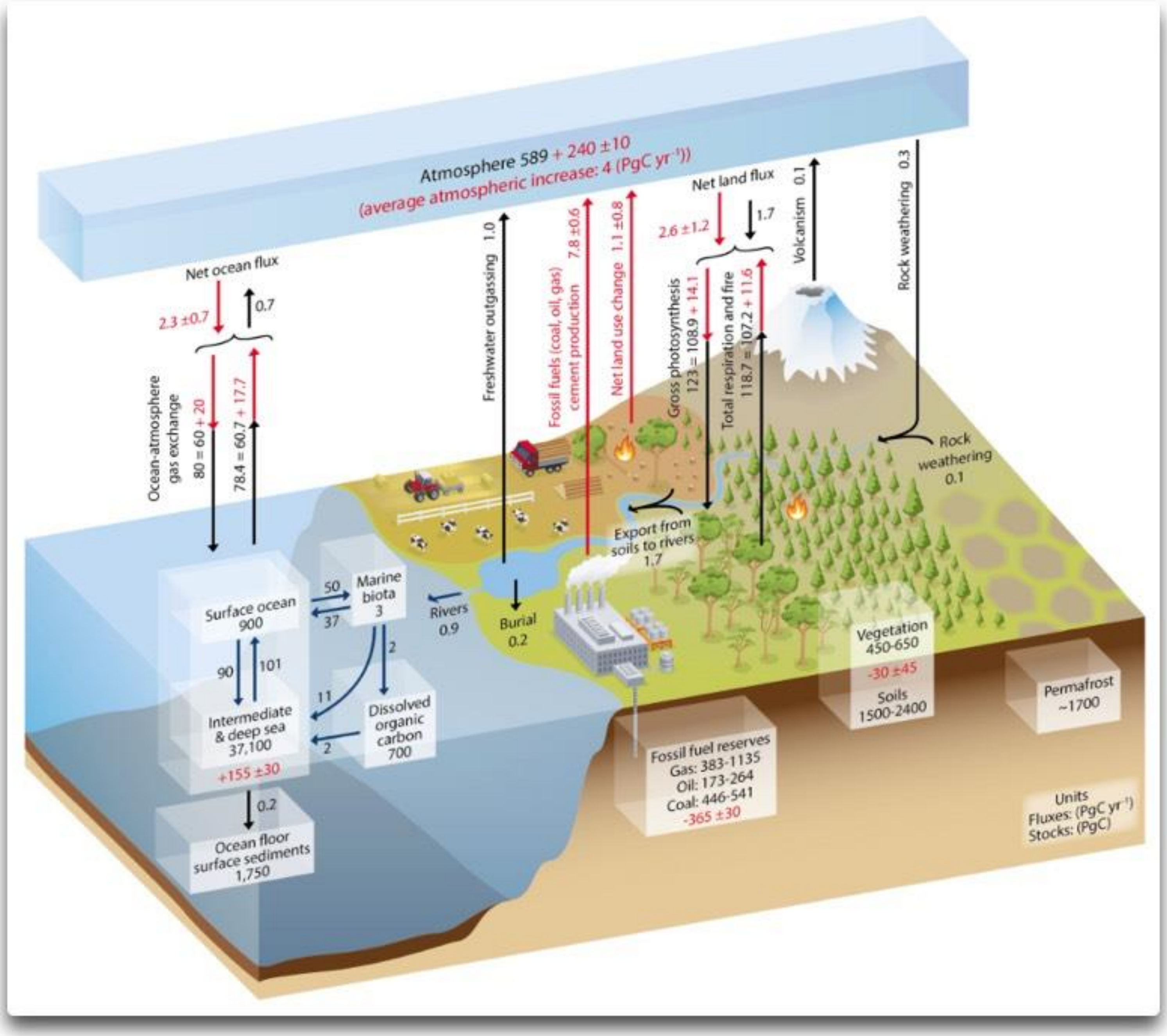

**Figure 1.1 – Schematic of the global carbon cycle. Stores of carbon are shown in boxes (PgC) and fluxes are shown next to arrows (PgC/yr). Numbers and text in black represent preindustrial/natural (year 1750) fluxes and stores. Red numbers in boxes represent the cumulative effect of anthropogenic activity over 1750-2011. Red arrows and number represent annual anthropogenic fluxes averaged over 2000-2009. Figure from Ciais et al. (2013). It should be noted that fluxes and stocks quoted in the text may differ from the figure due to slightly differing averaging periods.**

There is large uncertainty in global terrestrial carbon uptake, and independent methods tend not to agree on the magnitude or spatio-temporal location of the sink. The budget residual estimate mentioned above inherently contains all biases from the other terms in the budget (Le Quéré *et al.*, 2018). Atmospheric $CO_2$ inversions estimate regional land and ocean fluxes using local atmospheric $CO_2$ concentrations and atmospheric transport models (eg. Gurney and Eckels (2011), Piao *et al.* (2013)). The sparse sampling network of $CO_2$ measurements and inaccuracies of the transport models means this approach can only be solved for large scale (continental) fluxes. Further, both these methods offer no understanding of the biospheric processes involved. There are local scale approaches such as using eddy covariance flux towers, which measure local scale NEP using vertical wind velocity and $CO_2$ concentrations. However, the small footprint around the towers makes estimating global fluxes difficult and highly uncertain (Jung *et al.*, 2009, Jung *et al.*, 2011). Carbon stocks and fluxes can be estimated from forest inventories (Pan *et al.*, 2011). However, these inventories suffer from minimal spatial coverage, hence regional flux estimates are uncertain. The gap between spatial scales can be addressed using terrestrial ecosystem models, which simulate GPP, plant growth, litterfall, and respiration and offer an estimate of the residual carbon sink given our current knowledge. The latest version of Global Carbon Budget (Le Quéré *et al.*, 2018) uses a suite of dynamic global vegetation models to estimate the terrestrial sink ($S_{LAND}$) at 3.0±0.8 PgC/yr over 2007-2016, giving a budget imbalance of 0.6 PgC/yr ($B_{IM} = E_{TOT} - G_{ATM} - S_{OCEAN} - S_{LAND}$).

Terrestrial ecosystem functioning can be observed in atmospheric $CO_2$ concentrations. This is clear in the annual Mauna Loa, Hawaii (MLO, 20°N) $CO_2$ record (Figure 1.2) which peaks in boreal winter and troughs in boreal summer – in-line with the growing season. The northern hemisphere dominates the global signal due to the majority of land located there. The amplitude of the seasonal cycle (difference between maximum and minimum concentrations) is larger at higher latitudes, where seasons are more pronounced. The amplitude also reflects terrestrial productivity (Forkel *et al.*, 2016, Graven *et al.*, 2013, Myneni *et al.*, 1997, Randerson *et al.*, 1997). At high latitudes, photosynthesis only occurs during the relatively short growing season, whereas respiration occurs throughout the year. The northern hemisphere (>45°N) seasonal cycle has been increasing since the 1960s indicating a change in ecosystem functioning (Graven *et al.*, 2013). This change is thought to be the response of boreal forests to warmer temperatures, increasing growing season length and carbon uptake (Forkel *et al.*, 2016, Graven *et al.*, 2013). However, warmer temperatures can lead to drier conditions, increasing plant water stress. This has been observed in North American boreal forests where an earlier growing season led to reduced peak summer productivity (Buermann *et al.*, 2013). Further, dry conditions lead to higher chances of fire and insect outbreaks, which can release large quantities of carbon to the atmosphere in a short amount of time (Anderegg *et al.*, 2012).

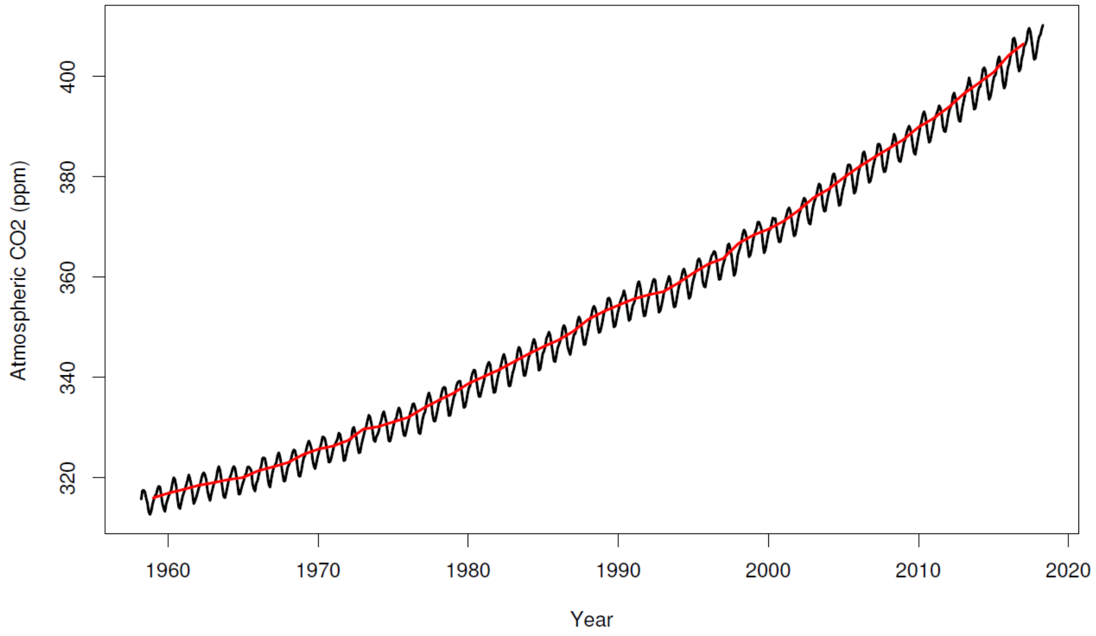

**Figure 1.2 – Monthly mean (black) and annual mean (red) atmospheric CO2 concentration at Mauna Loa, Hawaii 1959-2018. Data from Scripps Institute of Oceanography.**

Climate variability exerts a notable signal on the global carbon cycle, as can be observed with the annual atmospheric $CO_2$ growth rate (Figure 1.3). The predominant climate feature controlling IAV of land carbon fluxes is the El Nino Southern Oscillation (ENSO). During El Nino years, the terrestrial biosphere releases more carbon to the atmosphere, with the converse true for La Nina

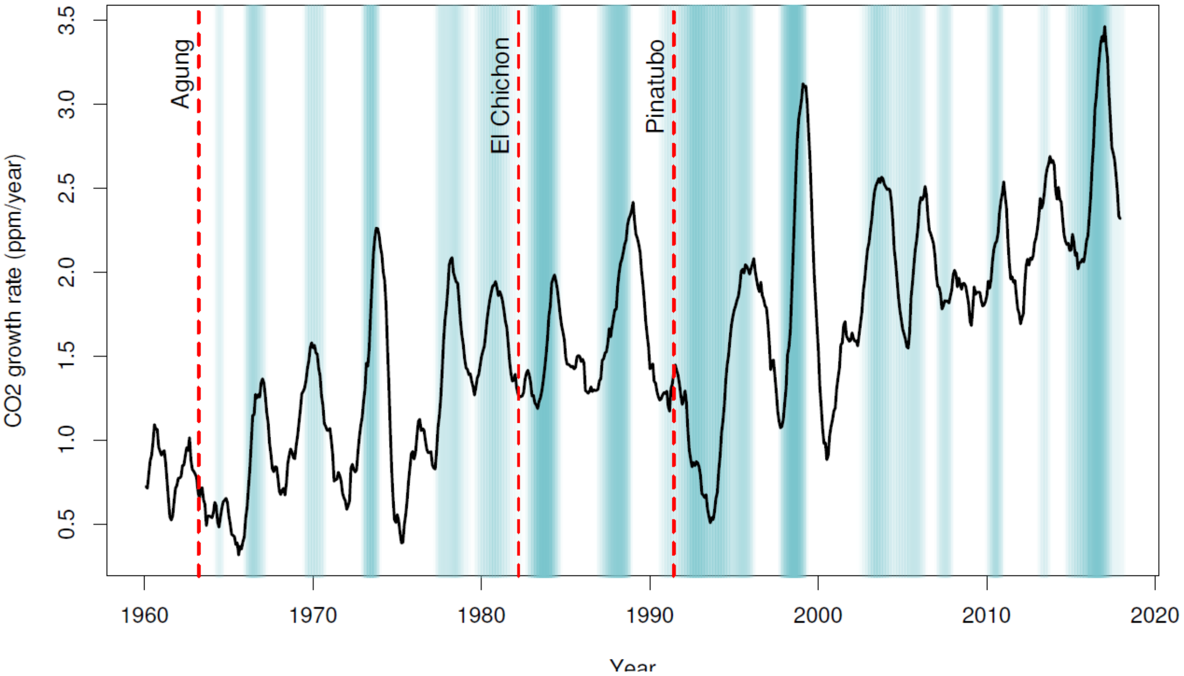

**Figure 1.3 – Annual increase in atmospheric CO2 (ppm/year) 1960-2017. The background shows the intensity and duration of El Nino events based on the MEI. CO2 change is a 12 month running mean of differences for the same month in consecutive years. MEI data is a 12 month running mean. CO2 data is from the Scripps Institute of Oceanography.**

(cool and wet) years. The strong El Nino years of 1997/98 and 2015/16 led to high atmospheric growth rates of 3 ppm/yr (~6 PgC/yr), as a result of reduced plant productivity and increased wildfires (Chatterjee *et al.*, 2017, Liu *et al.*, 2017, Nemani *et al.*, 2003, Van Der Werf *et al.*, 2004).

The low growth rate in the early 1990s can be attributed to the eruption of Mt. Pinatubo which injected substantial sulfate aerosol into the stratosphere. This aerosol cooled the atmosphere, reducing ecosystem respiration and also increased the ratio of diffuse to direct radiation, allowing deeper penetration into forest canopies, increasing NPP (Gu *et al.*, 2003, Lucht *et al.*, 2002). The majority (75%) of the inter-annual variability in the terrestrial carbon flux can be attributed to ENSO and volcanic eruptions (Raupach *et al.*, 2008).

There is no clear consensus on the driving mechanisms or region contributing most to carbon cycle variability. There is evidence for tropical forests responding to temperature variations to be the primary source of variability on inter-annual timescales (Gurney *et al.*, 2008, Peylin *et al.*, 2005). This can be observed in the strong correlation between tropical temperatures and the atmospheric $CO_2$ growth rate (Cox *et al.*, 2013, Wang *et al.*, 2013, Wang *et al.*, 2014). Conversely, recent studies have highlighted the important role of water availability in controlling the carbon variability of semi-arid regions (Ahlstrom *et al.*, 2015, Poulter *et al.*, 2014). A recent study attempted to resolve this issue by considering carbon flux variations to both temperature and water availability at local and global scales (Jung *et al.*, 2017). They conclude that local gross (GPP and Rh) carbon fluxes are controlled by water availability but as this is integrated to the net carbon flux (NEP) and larger spatial scales, temperature variability dominates the signal. This can be explained by two processes. First, the response of GPP and Rh to water availability are highly correlated, so the net flux response is reduced. Secondly, there is a larger spatial consistency in NEP response to temperature (higher temperatures lead to larger loss of carbon), whereas the NEP response to water availability is more heterogeneous. Together, this leads to temperature variability dominating the global carbon signal. Over the latter half of the 20th century (1960-2000) the atmospheric growth rate grew from less than 1 ppm/yr to ~2 ppm/yr (Figure 1.3). However, since the turn of the 21st century the growth rate has been relatively constant (Keenan *et al.*, 2016). Alternatively, fossil fuel emissions of $CO_2$ increased sharply since 2000 at a rate of 3 %/yr almost twice the rate of the prior three decades (Hansen *et al.*, 2013).

An informative metric is the airborne fraction (the ratio of $CO_2$ growth rate and fossil fuel emissions) (Figure 1.4). From this it is clear the biospheric sink has increased in-line with emissions. Interestingly, the airborne fraction seems to decrease from 2000 onwards. The airborne fraction is affected by both changes in the efficiency of sinks and the rate of fossil fuel emissions (Gloor *et al.*, 2010). One would expect a sudden increase in emissions to cause an increase in the airborne fraction, since ocean mixing would not keep pace with additional carbon. Therefore, it is suggested that carbon sinks have increased significantly in the 21st century. Further, Hansen *et al.* (2013) hypothesised that the increased sink is causally linked to the rising emissions themselves. One potential mechanism is increased coal burning (predominately in East Asia) has fertilized the terrestrial biosphere by providing additional nitrogen, which is a crucial determinant of plant productivity (Gruber & Galloway, 2008, LeBauer &

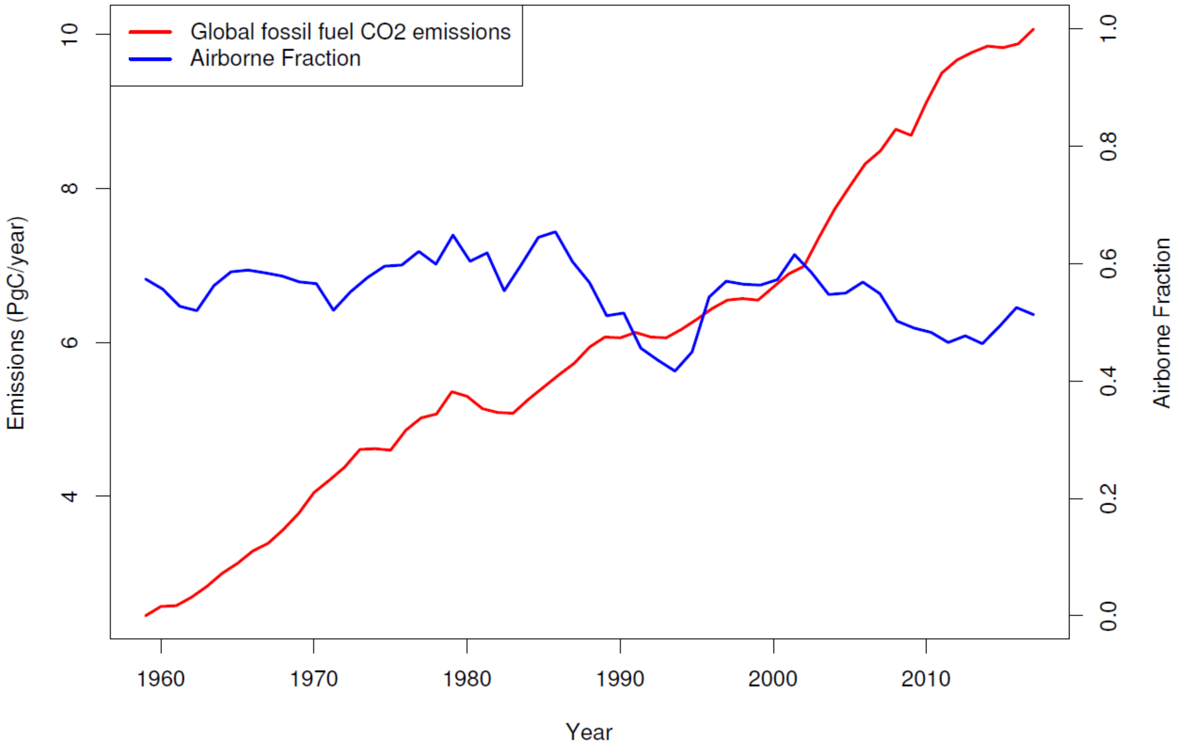

**Figure 1.4 – Fossil fuel $CO_2$ emissions and the airborne fraction (7 year running mean). Data from Le Quere et al 2018.**

Treseder, 2008). Previous modelling (Churkina *et al.*, 2009, Thornton *et al.*, 2007, Zaehle *et al.*, 2010) and observation studies (Oren *et al.*, 2001) have shown the impact of nitrogen deposition working synergistically with $CO_2$ fertilization in increasing global plant productivity, especially in mid-latitude and boreal forests. A second mechanism is increased atmospheric aerosol loading (mainly sulfate aerosol) from coal burning has increased the ratio of diffuse to direct radiation, which allows deeper penetration into forest canopies. Observation (Gu *et al.*, 2003) and modelling (Mercado *et al.*, 2009, Rap *et al.*, 2015) studies have shown forest canopy productivity can drastically increase in a more diffuse radiation regime.

## 1.2 Drivers of the terrestrial carbon cycle

The size and location of the terrestrial carbon sink is uncertain. Certain studies emphasize the role of northern temperate and boreal forests. A recent synthesis of atmospheric $CO_2$ inversion results indicates a northern (>25°N) land sink of 2.2±0.5 PgC/yr (2001-2004 mean) (Piao *et al.*, 2013). There is considerable uncertainty in partitioning this to continental scale fluxes with large spread among inversions. Pan *et al.* (2011) estimate a boreal and temperate forest sink of 1.3±0.1 PgC/yr and a -0.1±0.8 PgC/yr tropical sink (2000-2007 mean) using forest inventories. This implies a tropical sink of ~3 PgC/yr to balance the gross deforestation flux. Further evidence for a tropical sink comes from a subset of atmospheric inversion models which matched the observed vertical gradient of $CO_2$ in the northern hemisphere (Stephens *et al.*, 2007). The “constrained” inversion models found weaker northern uptake of 1.5 PgC/yr and weaker tropical emission of 0.1 PgC/yr compared to the Piao *et al.* (2013) tropical emission estimate of 0.9 PgC/yr.

The consistency of land-surface models (Sitch *et al.*, 2015), forest inventories (Pan *et al.*, 2011), and constrained atmospheric inversions (Stephens *et al.*, 2007) give some confidence into broad location and magnitude of the terrestrial sink (Table 1.1 and Figure 1.5). There are many potential mechanisms behind the increase. For example, increased $CO_2$ concentrations can stimulate photosynthesis. Also, additional nitrogen deposition from agriculture and industrial fossil fuel burning can fertilize ecosystems. Further, changes in climate can influence ecosystem productivity and respiration, leading to changes in the net sink.

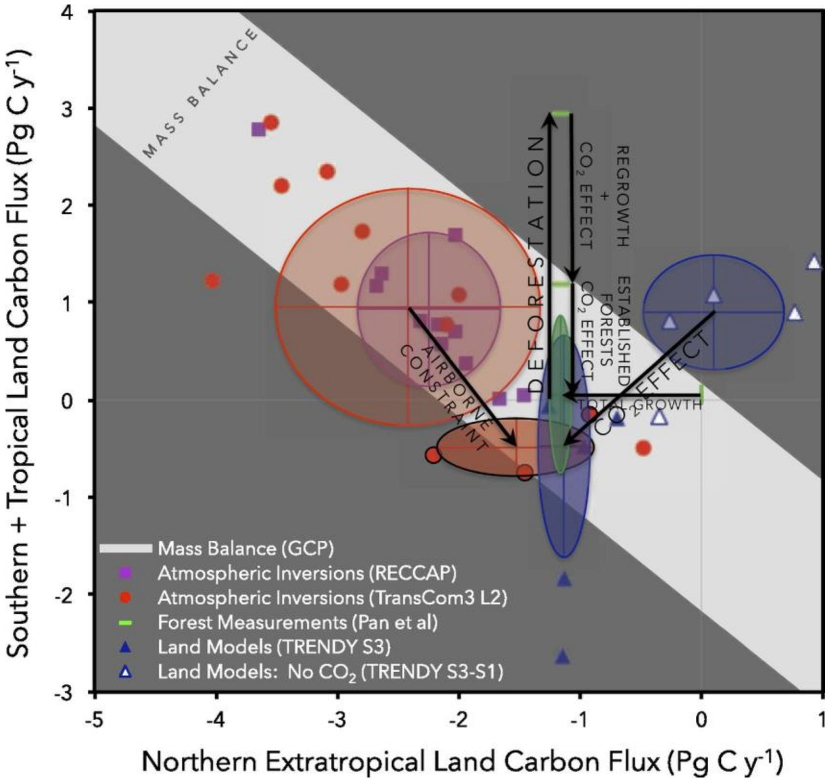

**Figure 1.5 - Comparison of independent carbon flux estimates partitioned into two broad latitude bands (Northern extratropics and southern/tropical lands). Atmospheric inversion estimates in red. The larger red circle shows the mean and standard deviation from Gurney & Eckels (2011) and the smaller red circle shows the three models selected by the additional vertical gradient constraint from Stephens et al. (2007). Light grey band shows the mass balance constraint by the global carbon budget (Le Quéré et al., 2018). Forest inventory estimate for the period 1990-2007 is shown in green (Pan et al., 2011). The upward black arrow shows the gross deforestation flux, reduced by forest regrowth and established forest increased uptake. Finally, blue triangles represent flux estimates from DGVMs for the period 1990-2007 (TRENDY, Sitch et al., 2015). Top right blue circle shows model estimates without the effect of $CO_2$ fertilization, and bottom left blue circle includes $CO_2$ fertilization. Figure and full description can be found in Schimel et al. (2015).**

**Table 1.1 - Summary of land carbon fluxes for the decade 2007-2016 (PgC/yr) from bookkeeping methods, DGVMs, inversions, and budget residuals. DGVM uncertainties represent ±1σ of the decadal estimates from the individual DGVMs. *Inversion estimates are adjusted to account for a preindustrial river flux. Data and full list of references can be found in Le Quere et al., 2018.**

| | 2007-2016 C Flux (PgC/yr) |
|---|---|
| Land-use emissions | |
| Bookkeeping | 1.3±0.7 |
| DGVMs | 1.3±0.4 |
| Terrestrial sink | |
| Residual (Fossil fuel + Land use – atmosphere growth – ocean uptake) | 3.6±1.0 |
| DGVMs | 3.0±0.8 |
| Total land flux | |
| Budget constraint (Fossil fuel – atmosphere growth – ocean uptake) | 2.3±0.7 |
| DGVMs | 1.7±0.7 |
| CTE Inversion* | 1.8 |
| Jena CarboScope Inversion* | 1.4 |
| CAMS Inversion* | 2.3 |

### 1.2.1 $CO_2$ fertilization

Elevated $CO_2$ concentrations increase plant photosynthesis and reduce transpiration, increasing water-use efficiency (carbon gain per unit of water loss). This "$CO_2$ fertilization" effect is the dominant mechanism in terrestrial biosphere models in explaining the global land sink (Sitch *et al.*, 2015), and is estimated to account for 60% of the current (1990-2007) sink (Schimel *et al.*, 2015). However, $CO_2$ fertilization is one of the most unconstrained processes in these models. Free air $CO_2$ enrichment (FACE) experiments enable direct measurement of the $CO_2$ fertilization effect at ecosystem scale, and offer an opportunity to constrain this process. These FACE studies show enhanced photosynthesis, reduced stomatal conductance, and increased productivity in response to elevated $CO_2$ concentrations, with an increase in NPP of 20-25% at double pre-industrial $CO_2$ concentrations (Norby *et al.*, 2005). Norby *et al.* (2005) compared the responses of various species and found the largest response for stands with lowest productivity. However, it is unclear as to whether the $CO_2$ fertilization effect can be sustained long term. The Duke FACE experiment (Duke Forest, North Carolina) showed a sustained NPP and carbon accumulation due to enhanced $CO_2$ over a ten-year period (McCarthy *et al.*, 2010). Conversely, the NPP response declined towards the end of the study at Oak Ridge National Laboratory (ORNL) FACE (Oak Ridge, Tennessee) (Norby *et al.*, 2010). This reduction is attributed to increasing nitrogen limitation. Enhanced $CO_2$ concentration cause an initial increase in plant growth and biomass which sequesters nitrogen, reducing available soil mineral nitrogen (Luo *et al.*, 2004). Moreover, scaling ecosystem responses to global patterns is difficult due to the heterogeneity of the land-surface and varying results from FACE (Hickler *et al.*, 2008).

Terrestrial biosphere models which include a coupled carbon-nitrogen cycle have a reduced $CO_2$ fertilization effect due to increasing nitrogen limitation (Bonan & Levis, 2010, Gerber *et al.*, 2010, Thornton *et al.*, 2007, Zaehle *et al.*, 2010). However, a set of terrestrial ecosystem models which included coupled carbon-nitrogen cycles failed to reproduce the "long-term" behaviour of either the Duke FACE or ORNL FACE experiments (Zaehle *et al.*, 2014). A better representation of above-ground-below-ground interactions and flexible plant stoichiometry have been highlighted as areas for model improvement (Zaehle *et al.*, 2014).

Therefore, our current understanding of $CO_2$ fertilization is still limited. How ecosystems will respond to future $CO_2$ enhancement depends on a myriad of factors such as; stand age, species composition, local climate, nutrient availability. The nitrogen cycle also has an important role in regulating the $CO_2$ fertilization effect through impacts on productivity, allocation, decomposition, mineralisation. For example, if more carbon is allocated to leaves over woody biomass, then the $CO_2$ fertilization effect will be limited. Nonetheless, there is evidence for the $CO_2$ fertilization effect on larger scales. Satellite observations of foliar coverage indicate greening trends due to increased water-use efficiency in arid regions (Donohue *et al.*, 2013). Keenan *et al.* (2013) used eddy covariance towers to show there has been an increase in water-use efficiency (driven by enhanced $CO_2$ concentrations) in temperate and boreal forests of the northern hemisphere in the last two decades.

### 1.2.2 Climate

Variations in climate exert a strong control on terrestrial ecosystem processes and carbon fluxes. Changes in temperature, precipitation, and radiation influence the global carbon cycle on seasonal to decadal scales. One emergent trend since the early 1980s is the lengthening of the growing season, which has increased by 2.6 days per decade (1982-2014) in northern (>45°N) lands (Park *et al.*, 2016). Over a similar period, multiple studies have found widespread northern summer greening, indicating an increase in summer productivity (Barichivich *et al.*, 2013, Park *et al.*, 2016, Xu *et al.*, 2016). These shifts in vegetation activity are thought to be driven by increasing temperature over this period. However, there are conflicting reports as to whether warming leads to a net carbon gain because autumn respiration increases may cancel out increased summer uptake (Keenan *et al.*, 2014, Piao *et al.*, 2008). Further, increased summer uptake with warmer temperatures is not always guaranteed. Studies have shown a reduction in boreal forest peak summer activity, due to earlier springs increasing growing season water stress (Barichivich *et al.*, 2013, Buermann *et al.*, 2013).

Nemani *et al.* (2003) showed global NPP increased by 6% over 1982-1999 due to a relaxation of climatic constraints. The global increase was dominated (42%) by Amazon rainforests where reduced cloud cover increased incoming solar radiation. However, southern hemisphere droughts in the following decade (2000-2009) caused a decline in global NPP (Zhao & Running, 2010). Overall, the net effect of climate on the carbon sink is a delicate balance between uptake and loss processes and their sensitivity to climate changes. Warming leads to a longer growing season in high latitudes, however this increases evaporative demand, which could potentially reduce carbon uptake. Further, warming increases soil decomposition and respiration, counteracting the potential positive effects of warming. A recent modelling study attributed 70% of the greening over 1982-2009 to $CO_2$ fertilization and only 8% to climate change (Zhu *et al.*, 2016). However, on local (grid-cell) scale, climate dominated the greening trend in 28.4% of vegetated regions, compared to $CO_2$ dominating 23.2%. Greening trends due to warming were mostly in high latitudes and the Tibetan Plateau, whereas positive precipitation effects were in the Sahel and South Africa. Further contributing to the small global climate effect is drought conditions in South America leading to a browning over this period, counteracting increases in other regions. Yet, there is evidence of greening in Amazonian tropical forests during higher sunlight dry seasons, suggesting insolation is the dominant climate variable, and not water limitation as modelling studies suggest (Huete *et al.*, 2006, Saleska *et al.*, 2016). In terms of carbon, the same family of models (Trends in net land carbon exchange; TRENDY, see Section 1.3.2) reported a trend in NPP of 0.22±0.08 $PgC/yr^2$ over 1990-2009 with $CO_2$ fertilization explaining 86% (0.19±0.08 $PgC/yr^2$) of the increase and the remainder due to climate (0.03±0.05 $PgC/yr^2$) (Sitch *et al.*, 2015). Focusing on the net carbon flux (NPP – Rh), the land sink trend is 0.06±0.03 $PgC/yr^2$ which is entirely accounted for by $CO_2$ fertilization, indicating respiration trend due to climate balanced the uptake trend. The TRENDY intercomparison project is designed to quantify spatial trends and variability in terrestrial carbon fluxes over the historical period (1901-present), driven with observed atmospheric CO2 concentrations, climate, and land-use change (Sitch *et al*., 2015).

Extreme events such as droughts, heatwaves, and storms can have profound negative impacts on ecosystems, offsetting carbon sinks or causing carbon losses (Ciais *et al.*, 2005, Page *et al.*, 2002, Reichstein *et al.*, 2013). Zscheischler *et al.* (2014) have shown that a few extreme events explain most of the inter-annual variability in GPP. For example, the European heatwave in 2003 caused a net source of 0.5 PgC/yr to the atmosphere, offsetting the previous four years of carbon uptake (Ciais *et al.*, 2005). This was predominantly driven by water shortages reducing plant productivity. Extreme events can cause immediate and lagged responses (fires, insect outbreaks) (Anderegg *et al.*, 2012), therefore their impact on the carbon cycle is non-linear. Further, a small shift in the mean state can have large influences on extremes, which can override the potential benefits of change in the mean state. For example, long term warming in the northern high latitudes is believed to have increased net carbon uptake (Keenan *et al.*, 2014), but the potential increase in water shortages could increase the risk of fires and insect outbreaks, offsetting or outweighing carbon gains from changes in the mean state. Reichstein *et al.* (2013) highlighted key feedbacks triggered by extreme events. For example, heatwaves and dry spells can lead to higher temperatures through reductions in plant transpiration and evaporative cooling (De Boeck & Verbeeck, 2011). Further, low soil moisture increases stress on the hydraulic system of plants which is intensified by higher temperatures.

### 1.2.3 Atmospheric composition

Changes in the composition of the atmosphere impact the carbon cycle. Tropospheric ozone burden varies with the emissions of precursor gases related to fossil fuel emissions (eg. NOx, CO), and concentrations have approximately doubled over the industrial period (Gauss *et al.*, 2006). High levels of ozone can reduce stomatal conductance, leaf photosynthesis, and plant productivity (Ainsworth *et al.*, 2012, Lombardozzi *et al.*, 2015). Lombardozzi *et al.* (2015) estimate current ozone concentrations reduce GPP by 8-12%, and transpiration by 2-2.4%, which works to reduce the land carbon sink.

Further, increased atmospheric aerosols related to fossil fuel emissions influence incoming solar radiation, and the partitioning between direct and diffuse radiation. Leaf photosynthesis increases non-linearly with radiation, saturating at high light levels. Therefore, plants are more efficient in low light conditions. Leaves are often light saturated at the top of the canopy, whereas leaves deeper into the canopy suffer from low light levels. Increased aerosol enhances the diffuse fraction of radiation, and causes deeper penetration into the canopy. This works to increase canopy light-use efficiency and photosynthesis (Roderick *et al.*, 2001). Between 1960 and 1999, variations in the diffuse fraction (associated with changes in cloud cover and aerosol loading) increased the land sink by 25% (Mercado *et al.*, 2009).

### 1.2.4 Land-use and Land Cover Change

Human land use such as deforestation, afforestation and reforestation alter the global carbon balance. The net land use flux is the balance between gross emission terms. Gross emissions include “fast” emissions from deforestation fires and “legacy” emissions from the decomposition of woody debris. Gross uptake includes the regrowth in logged forests or abandoned land (reforestation) and the establishment of forest on new land (afforestation) (Houghton *et al.*, 2012). Overall, the net land use flux is currently (2007-2016) a net source of 1.3±0.7 PgC/yr to the atmosphere (Le Quéré *et al.*, 2018). Whilst this flux is only 12% of total human emissions currently, over the period 1750-2016 changes in land use emitted 225±75 PgC, equating to 35% of total emissions. Tropical deforestation accounted for all the land use emission of carbon during 1990-2007 (Pan *et al.*, 2011). Over the same period, regrowth in previously logged tropical forests and regrowth in abandoned lands on Europe and North America contributed to the land use sink flux (Ciais *et al.*, 2008, Kondo *et al.*, 2018, Pan *et al.*, 2011, Williams *et al.*, 2012).

### 1.2.5 Fire

Although fires are either driven by climate (Section 1.2.2) or human activities (Section 1.2.4), they are a major source of carbon to the atmosphere, and therefore warrant a more detailed outline. Van Der Werf *et al.* (2017) estimate fires emit 2.2 PgC/yr (1997-2016) albeit with substantial inter-annual variability ranging from 1.8 PgC/yr (2013) to 3.0 PgC/yr (1997). Over 50% of global emissions originate in Africa, with savanna fires contributing 90% of the continents total emissions (Van Der Werf *et al.*, 2017). Other fire hotspot regions include savanna and tropical forests of South America (15% of global emissions) and South-East Asia (5%), tropical forest and peat fires in Equatorial Asia (8%), Australian savanna (5%), and temperate and boreal forests in Asia (6%). The burned area in these regions does not scale linearly with emissions. Regions of higher carbon density (eg. forests) contribute relatively more to total emissions, whereas savanna fires largely control burned area (Van Der Werf *et al.*, 2017).

The inter-annual variability in fire emissions contributes a significant proportion (~1/3) of the variability in the land-atmosphere $CO_2$ flux (Keppel-Aleks *et al.*, 2014, Prentice *et al.*, 2011). Fire emission variability is driven by changes in temperature, precipitation, fuel load, and human activities (Van Der Werf *et al.*, 2017).

### 1.2.6 Nitrogen availability

Nitrogen is a key component of living organisms and regulates the land carbon cycle. Even though nitrogen is the most abundant element in the atmosphere, plants cannot use it in its common form, $N_2$. Only reactive forms (NOy and NHx) can be absorbed and used by plants. Therefore, most land regions are nitrogen limited, and plant productivity is often controlled by nitrogen availability (Vitousek & Howarth, 1991). Further, microbial decomposition, and hence soil respiration depends upon nitrogen content of the organic matter (Janssens *et al.*, 2010). This leads to a tight coupling of the carbon and nitrogen cycles. As such, ecosystem net carbon exchange is strongly influenced by nitrogen availability.

However, the inclusion of a coupled carbon-nitrogen scheme in terrestrial biosphere models is relatively new due to the complex interactions in all parts of the ecosystem. Previous modelling studies which fail to include nutrient constraints tend to overestimate the $CO_2$ fertilization effect (Smith *et al.*, 2016, Thornton *et al.*, 2007, Wieder *et al.*, 2015, Zaehle *et al.*, 2015). In future coupled carbon cycle climate projections, this has led to an overprediction of NPP by 19% (Wieder *et al.*, 2015) and net land uptake by 13% by 2100 (Goll *et al.*, 2012, Wieder *et al.*, 2015). This reduction in net land carbon uptake ("carbon-nitrogen" models compared to "carbon-only") is a balance between mostly two processes. Firstly, the $CO_2$ fertilization effect is reduced as nitrogen limitation increases, a process known as progressive nitrogen limitation (Luo *et al.*, 2004). This is countered by an increase in nitrogen mineralisation with warmer temperatures which enhances photosynthesis and carbon uptake (Bonan & Levis, 2010, Thornton *et al.*, 2007, Zaehle *et al.*, 2010). The net carbon effect of including the nitrogen cycle is uncertain however, with most modelling studies projecting smaller land carbon sinks compared to "carbon-only" models (Sokolov *et al.*, 2008, Zaehle *et al.*, 2010). However, other studies project a larger carbon sink by 2100 with the inclusion of a nitrogen cycle (Wårlind *et al.*, 2014).

Over the industrial period humans have doubled nitrogen inputs to the biosphere through fossil fuel burning and agricultural intensification (Gruber & Galloway, 2008). Greatest additions are in the industrialised regions of the northern hemisphere. Additional nitrogen works to fertilize the biosphere, but the impact on carbon uptake depends upon the nature of the underlying vegetation. Forests have a higher potential for carbon storage than shrubs or grasslands due to the high C:N ratio of woody biomass compared to leaves and roots. Studies estimate anthropogenic nitrogen deposition accounts for 0.2-0.5 PgC/yr (10-20% of total sink) of the current carbon sink (Churkina *et al.*, 2009, Liu & Greaver, 2009, Wang *et al.*, 2017, Zaehle, 2013). Further to enhancing photosynthesis, additional nitrogen deposition influences rates of soil microbial decomposition. Rates generally decreases with additional nitrogen (Janssens *et al.*, 2010), but the opposite has also been observed (Janssens *et al.*, 2010, Zhang *et al.*, 2014).

An important indirect effect of additional nitrogen deposition is permitting a further plant response to $CO_2$ fertilization. Synergistic effects can arise when high $CO_2$ concentrations bring about nitrogen limitation, which is alleviated by concurrent rises in nitrogen deposition. This effect has been estimated to be a substantial contributor to increased plant productivity and carbon uptake over the 20th century, accounting for 15-25% of the 1990s sink (Churkina *et al.*, 2009, Zaehle *et al.*, 2010).

### 1.2.7 Current state of play

Many studies have simulated the historical carbon cycle over the industrial period and attempted to attribute processes and mechanisms to the observed changes. Models are forced with varying $CO_2$ concentrations, nitrogen deposition, climate, land use in factorial style combination. This enables the quantification of single driver responses as well as the interactions between them. Most "carbon-only" models explain the increased carbon sink almost entirely through $CO_2$ fertilization (Keenan *et al.*, 2016, Sitch *et al.*, 2015, Smith *et al.*, 2016). However, when nitrogen is included the $CO_2$ fertilization effect is reduced, but still dominant, and losses due to warming are reduced due to increased mineralisation (Thornton *et al.*, 2007, Zaehle *et al.*, 2010).

Since the turn of this century, the land (Keenan *et al.*, 2016, Le Quéré *et al.*, 2018) and ocean (DeVries *et al.*, 2017) sinks have increased. Some studies have attributed this increase to the warming hiatus reducing the increase of respiration (Ballantyne *et al.*, 2017, Keenan *et al.*, 2016). However, this theory has been challenged, arguing that seasonal trends in temperature and respiration do not match on global or regional scales (Ballantyne *et al.*, 2017, Keenan *et al.*, 2016, Zhu *et al.*, 2018). Importantly, Zhu *et al.* (2018) challenge the "warming hiatus" hypothesis, but do not offer an alternative explanation of the sink. As of yet, there has been no certain conclusion on the mechanisms behind the 21st century land sink.

## 1.3 Estimating carbon fluxes

### 1.3.1 Observing terrestrial carbon fluxes

Carbon exchange between the biosphere and atmosphere is widely measured using the eddy covariance technique (Baldocchi *et al.*, 1988). This technique is based on the turbulent transport theory in the atmosphere and calculates carbon, water, and energy fluxes from the covariance of vertical wind speed and gas concentration. There are hundreds of sites around the globe with towers measuring fluxes with this method. Together these towers make up a network named FLUXNET (Baldocchi *et al.*, 2001). The measured $CO_2$ flux represents the Net Ecosystem Exchange between the biosphere and atmosphere and is measured multiple times per second (5 Hz – 40 Hz), which is then aggregated to half hourly intervals (Baldocchi, 2003). For a deeper understanding of ecosystem functioning, the net carbon exchange is partitioned into component land fluxes, GPP and Rh. Two methods are used to partition fluxes. The first uses the fact that only respiratory fluxes are active during the night (Reichstein *et al.*, 2005). Night time observations are used to derive respiration sensitivity to temperature variations, and then GPP is derived as the difference between daytime NEE and respiration. The second method uses a light response curve fit to daytime NEE, whilst accounting for the temperature sensitivity of respiration and the moisture control on photosynthesis (Lasslop *et al.*, 2010). Here, photosynthesis is estimated from canopy light use efficiency, maximum rates of $CO_2$ uptake at light saturation (scaled with moisture availability), and incoming solar radiation. Radiation is estimated using an Arrhenius-type model, used to describe the temperature dependence of ecosystem respiration (Lloyd & Taylor, 1994).

However, the spatial coverage of towers is not uniform, and many areas across the globe are underrepresented (eg. tropical forests). The majority of sites are in temperate forests, and as such are well represented by FLUXNET.

### 1.3.2 Modelling terrestrial carbon fluxes

Terrestrial biosphere models (TBMs) are used to simulate the interactions between the land surface and the atmosphere. TBMs have developed considerably over the last few decades and the current generation include some or all of four groups of sub-models – biogeography, vegetation dynamics, biogeochemistry, and biophysics (Fisher *et al.*, 2014). Initially, biophysical processes involving radiative and water fluxes between soil, vegetation, and the atmosphere were simulated using land-surface models (LSMs). These models (eg. the Simple Biosphere Model, Sellers *et al.* (1986)) had a representation of canopy radiative transfer that treats visible and near-infared, and direct and diffuse radiation separately. They also simulated the influence of vegetation on evapotranspiration and provided the boundary conditions for atmospheric general circulation models.

Biogeochemical sub-models simulate the cycling of carbon, water, and nutrients through ecosystems. One of the most important processes simulated is photosynthesis. Most current TBMs include the same coupling of stomatal conductance (Ball-Berry model, Ball *et al.* (1987)) and photosynthesis (Farquhar model, Farquhar *et al.* (1980)). This coupling was a pivotal step that enabled models to simulate the effect of increased atmospheric $CO_2$ on stomatal conductance and photosynthesis, and allowed climate models to predict changes in atmospheric $CO_2$ concentrations. The additional complexity of the photosynthesis-stomatal conductance model requires an understanding of leaf level processes. Important photosynthetic parameters are $V_{c\ max}$, the maximum rate of carboxylation, and $J_{max}$, the maximum potential rate of electron transport. Further coefficients that relate photosynthesis to stomatal conductance are also required. These parameters are estimated for various plant species (Kattge *et al.*, 2011), but values of $V_{c\ max}$ are highly uncertain (Walker *et al.*, 2014). One important advance is the scaling of leaf photosynthesis to the canopy with the use of a multi-layer canopy scheme. Multi-layer schemes calculate radiation intercepted and photosynthesis at discrete layers in the canopy. Photosynthetic capacity varies with canopy depth depending on vertical profiles of light (potentially treating direct and diffuse separately) and leaf nitrogen content (eg. Mercado *et al.* (2007)).

The land-surface is split into grid cells (spatial resolution eg. 0.5° x 0.5°) and the current generation of TBMs generally represent different land cover (eg. vegetation type, soil, urban, lake, wetland) using sub-grid mosaics (Essery *et al.*, 2003). This splits the grid cell into a number of smaller cells, each with its own surface energy balance in relation to land cover type and the parent grid cell. A feature of current models is the ability to simulate dynamic vegetation in response to changes in climate and competition between species. These models are generally called dynamic global vegetation models (DGVMs) or TBMs when coupled with land-surface and biogeochemical models. The interactions between climate and the distribution of vegetation occur on much slower timescales than the processes mentioned above (eg. decades to millennia). Simple parameterisations exist whereby the plant functional type (PFT) fractional coverage is adjusted once a year depending on annual NPP (eg. TRIFFID, Cox (2001)), as well as more mechanistic approaches where individual plant behaviour and competition for space, light, water, and nutrients is simulated (eg. Hybrid, Friend *et al.* (1997)).

A more recent addition to TBMs is the inclusion of land-use and land-use change. Urban land parameterisations represent the effect of cities on surface energy fluxes and the hydrological cycle (Best *et al.*, 2006). When land-use change is simulated, cropland and pasture plant functional types (PFTs) are included, and the fractional coverage in each grid-cell is updated depending on local land-use. Changes in the carbon balance are tracked by the allocation of removed biomass to product pools with varying decay times (McGuire *et al.*, 2001). Further, biomass regrowth on abandoned land is also considered for each grid-cell (Shevliakova *et al.*, 2009).

Another recent improvement is the inclusion of coupled carbon-nitrogen cycles. The importance of nitrogen on constraining carbon uptake is highlighted in section 1.2.6. Models of terrestrial carbon and nitrogen cycles simulate carbon and nitrogen flows through vegetation and soil pools, the addition of nitrogen through atmospheric deposition and biological nitrogen fixation, and losses through leaching, outgassing, and denitrification (Gerber *et al.*, 2010, Thornton *et al.*, 2007, Zaehle & Friend, 2010).

Modelling communities have developed their own TBMs that often share a representation of processes (eg. many models use the Farquhar model of photosynthesis), but also differ on many other parameterisations (eg. number of PFTs, phenology, allocation, vegetation dynamics). Also, some models may not include all relevant processes (eg. nitrogen cycle, fire). Therefore, there are structural differences between TBMs that lead to varying estimates of fluxes and pools. Work has been done to quantify this uncertainty and constrain the land carbon cycle to changing environmental conditions (climate, $CO_2$, nitrogen deposition, land-use) using a group of TBMs forced with similar protocols. The "TRENDY" model inter-comparison investigated how land carbon fluxes and sinks have changed over the 20th century in response to historical forcing (Sitch *et al.*, 2015). Results from TRENDY are used in Chapter 4 of this thesis.

### 1.3.3 Global estimates of carbon fluxes

Observations of carbon fluxes from FLUXNET occur at point locations (representative of 1-2 $km^2$). Therefore, to obtain global flux estimates requires local observations to be "upscaled". Generally, carbon fluxes are combined with local meteorology to create statistical relationships between global datasets (eg. climate, vegetation type) and local carbon measurements. The FLUXCOM project upscales FLUXNET carbon fluxes to global (gridded 0.5°) coverage with various machine learning methods. FLUXCOM uses 11 different algorithms from four broad families; tree based methods, regression splines, neural networks, and kernel methods (Tramontana *et al.*, 2016). The model tree method was used to estimate a global GPP of 119±6 PgC/yr (Jung *et al.*, 2011), and has been used as a benchmark for TBMs (Piao *et al.*, 2013). One key feature of machine learning methods is that functional relationships are not prescribed, but are found from the patterns in observations. Machine learning algorithms therefore generate multivariate functional relationships between predictor (observed FLUXNET) and target variables. For FLUXCOM GPP, predictor variables include PFT type, mean seasonal cycle of NDVI, air temperature, water availability. Satellite information and climate reanalysis data are used along with the modelled relationships to estimate global scale fluxes.

TBMs are currently the only tool able to predict future impacts of environmental change on the carbon cycle and ecosystem functioning. They have been used to estimate global GPP (Beer *et al.*, 2010), to evaluate the response of ecosystems to climate and $CO_2$ changes (Piao *et al.*, 2013), and how the net carbon balance has changed (Sitch *et al.*, 2015).

Another method of estimating global vegetation productivity is based on satellite observations of optical properties related to vegetation productivity (Myneni *et al.*, 2002). One method uses the fraction of absorbed photosynthetic active radiation (FPAR) in a light-use efficiency model, which assumes a direct proportionality of FPAR with productivity (Monteith, 1972, Monteith & Moss, 1977). Another method uses leaf area index (LAI) to scale up leaf level photosynthesis to canopy, regional, and global scales (Ryu *et al.*, 2011). The benefit of these remote sensing models is the global coverage at relatively high spatial (kilometres) and temporal (days) resolution. Overall, all these methods are used to estimate global and local carbon fluxes, and where estimates converge, more confidence can be placed in their results.

All approaches to estimate global scale carbon fluxes have shortcomings and uncertainties. For example, partitioning FLUXNET NEE observations into gross fluxes (photosynthesis and respiration) is highly uncertain (Lasslop *et al*., 2010, Reichstein *et al*., 2005) and scaling the small spatial footprint of eddy-flux towers to global scale introduces additional uncertainties (Beer *et al*., 2010, Jung *et al*., 2009). The machine learning methods used in FLUXCOM to upscale site level fluxes to global scale contain various sources of uncertainty. Machine learning methods can have different responses when applied beyond the conditions represented in their training data (Jung *et al*., 2009). Furthermore, the information contained in the driving data may not be adequate to capture the variability of carbon fluxes in a variety of conditions (Tramontana *et al*., 2015). For example, soil moisture is a dominant driver of carbon uptake and would improve the machine learning estimates if included (Tramontana *et al*., 2016). However, spatially explicit, long-term soil moisture data is not available, and so machine learning approaches are generally constrained by global gridded data available. Furthermore, another significant uncertainty with FLUXCOM GPP estimates is the poor global representativeness of FLUXNET sites, meaning not all PFTs and climates are represented. For example, few sites exist in tropical forests and extreme (eg. cold and dry) climates.

DGVMs also contain many sources of uncertainty. Model structures can be very different from one another, and as such can diverge in their response to the same forcing (Huntzinger *et al.*, 2017). Fisher *et al.* (2014) highlighted 25 key processes these models simulate, and how differences in their implementation can cause large differences in ecosystem functioning.

## 1.4 Research Aim

The aim of this thesis is:

**To develop a better understanding of the regional distribution of carbon fluxes and sinks as well as associated drivers, processes, and mechanisms by combining model and observational analysis since the turn of this century.**

To address this aim, I had clear hypotheses which I tested by analysing land-surface models and observational data of climate, carbon fluxes from upscaled eddy covariance sites, and satellite-based vegetation indices. Land surface models were used to quantify potential drivers behind the recent changes in land fluxes and sink. Analysing key observational records enabled me to identify regions of significant change in ecosystem functioning using several independent data sources. I place a heavy emphasis on analysing spatiotemporal trends and variability in carbon uptake processes (GPP and NPP) throughout chapters two, three, and four of this thesis. This is because photosynthesis is the primary driver of the global carbon cycle, and so impacts all other fluxes and sinks. Moreover, trends and variability in the net sink have been shown to be predominantly driven by changes in productivity (Ahlstrom *et al.*, 2015, Sitch *et al.*, 2015). Further, I also analyse spatiotemporal changes in the net land sink in Chapter 3, as this work focuses on vegetation and soil processes, in which both photosynthesis and respiration are key aspects of the study. Further, understanding (and quantifying) the driving mechanisms behind variations in past and present carbon fluxes is of vital importance in making realistic projections of future carbon cycling and climate.

All chapters of this thesis make use of DGVMs to estimate changes in local and global scale carbon cycling. Currently, the drivers behind the increased terrestrial sink remain unquantified. To that end, each chapter has a particular novel focus regarding potential drivers of increased carbon uptake; changes in direct/diffuse radiation (Chapter 2), carbon-nitrogen interactions (Chapter 3), and climate change (Chapter 4). The model simulations I perform allow me to attribute changes in carbon uptake to these mechanisms, and address several hypothesis outlined below.

## 1.5 Research hypotheses

In this section the scientific background to each hypothesis is outlined and the research approach taken is discussed.

### 1.5.1 Increases in the fraction of diffuse/direct radiation associated predominantly with East Asian sulfate aerosol emissions have spurred plant photosynthetic rates (Chapter 2)

**Objective**

To understand the relative roles of climate, light-regime, and $CO_2$ concentrations in explaining recent increases in terrestrial plant productivity by performing offline simulations with a land-surface model which simulates canopy photosynthesis by treating direct and diffuse radiation separately.

## Scientific Background

The influence of atmospheric aerosol on the carbon cycle was prominently seen during the eruption of Mt. Pinatubo in 1991, where additional stratospheric aerosol reduced incoming solar radiation by at least 1 W/m$^2$ for over a year after the eruption (Soden *et al.*, 2002). This led to a northern hemisphere cooling of 0.5K in the 1992-1993 growing season (Yang & Schlesinger, 2001). Using a dynamic global vegetation model and atmospheric inversions, Lucht *et al.* (2002) concluded that both NPP and Rh reduced due to this cooling, with the net effect as a net carbon sink due to the eruption. However, increases in atmospheric aerosol increase the diffuse fraction of solar radiation, which has been shown to increase canopy photosynthesis (Roderick *et al.*, 2001). Sunlit leaves are often light saturated and therefore have low light use efficiency. Shaded leaves are more light use efficient but are generally light limited. Under diffuse conditions, top of canopy saturation reduces and total radiation increases deeper into the canopy (Figure 1.6). The net effect on canopy photosynthesis is a balance between a reduction in total radiation and an increase in diffuse radiation (Mercado *et al.*, 2009, Rossow & Schiffer, 1999).

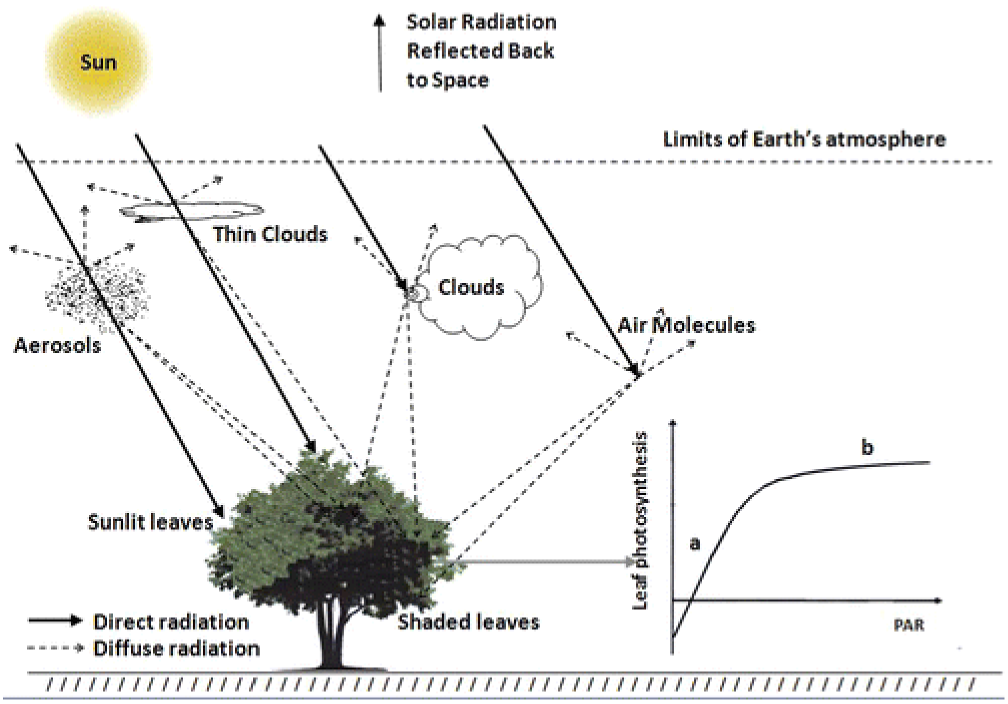

**Figure 1.6 - Schematic diagram of the impact atmospheric particles have on solar radiation. Direct radiation radiates top of vegetation canopy or scatters off aerosols, clouds, air molecules and penetrates deeper into canopies illuminating shaded leaves. The photosynthetic response to increased diffuse (a) and decreased direct (b) radiation is also shown. Figure from Kanniah et al. (2012).**

The year following the Mt. Pinatubo eruption, it was estimated that the increase in diffuse radiation enhanced photosynthesis of a deciduous forest by over 20%, and this finding can likely be extrapolated to a global phenomenon (Gu *et al.*, 2003). In terms of the historical land carbon sink, variations in the diffuse fraction (due to increased anthropogenic aerosol and volcanic emissions) enhanced the land carbon sink by 25% between 1960 and 1999 (Mercado *et al.*, 2009). Since the turn of this century, there has been a sharp increase in fossil fuel emissions (Le Quéré *et al.*, 2018), which has led to higher concentrations of atmospheric aerosols, predominately sulfate aerosol from East Asia (Van Donkelaar *et al.*, 2008). It could be expected that this increase in the diffuse fraction of radiation enhanced photosynthetic activity, increasing carbon uptake (Hansen *et al.*, 2013).

### Research approach

As described in section 1.2, there are many drivers of the terrestrial carbon cycle. As I am interested in process attribution to changes in carbon cycling, I need to perform a series of “offline” simulations in which I prescribe model forcings. This allows me to estimate the combined effect of all forcing factors on carbon uptake as well as the single contributions. In a first step, to accurately simulate the influence fossil fuel aerosol emissions have on carbon uptake via changes in light regime I first needed to reproduce the spatio-temporal distribution of aerosol in the atmosphere. Using these aerosol fields, I can then calculate short-wave direct and diffuse radiative fluxes for use as inputs to a land surface model (Figure 1.7). Although this model cascade approach may miss important feedbacks between the atmosphere and land surface (Berg *et al.*, 2016, Cox *et al.*, 2000), it does allow for process attribution, a focus of this thesis.

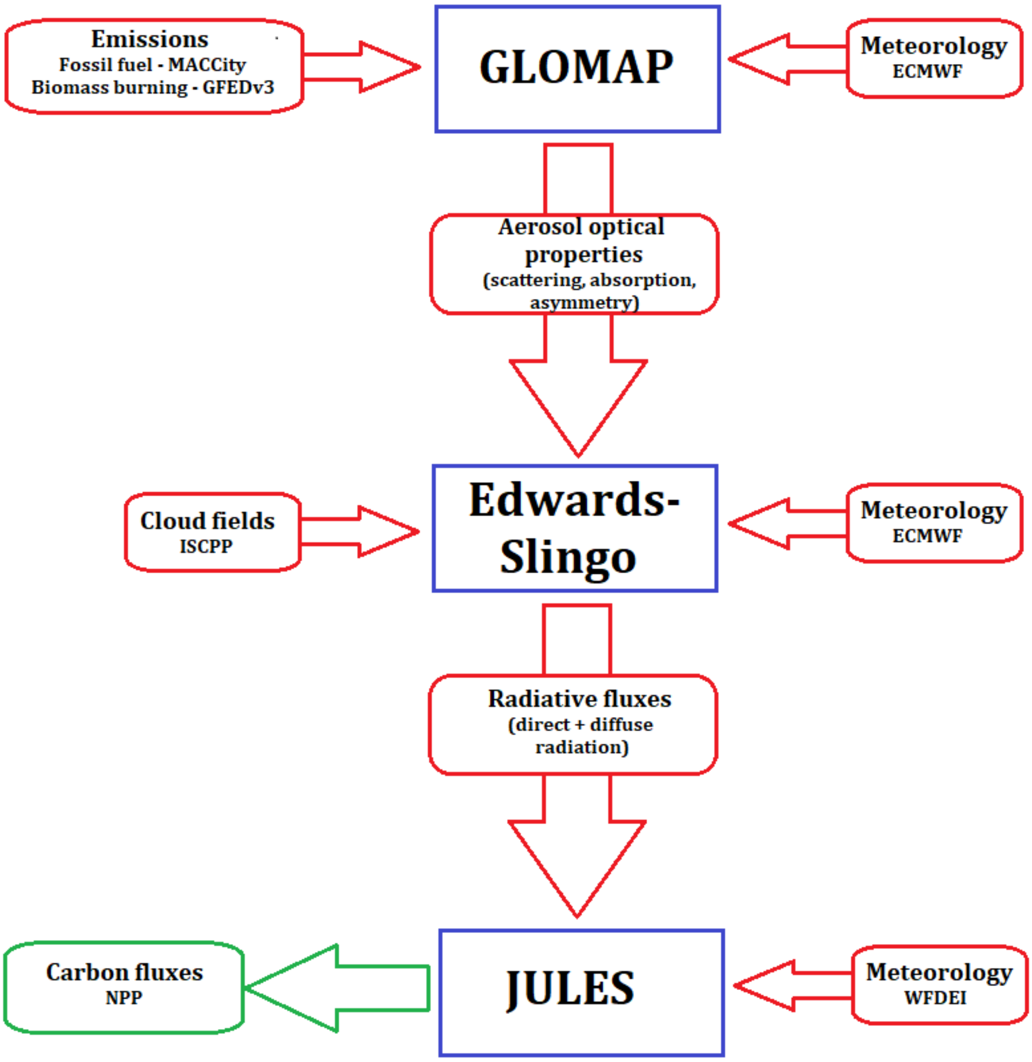

**Figure 1.7 - Model cascade approach used. Fossil fuel and biomass burning emissions are used along with prescribed meteorology to simulate the spatiotemporal distribution of aerosol using GLOMAP. Aerosol optical properties are then subsequently used with cloud fields and meteorology in Edwards-Slingo to simulate direct and diffuse radiation through the atmosphere. Surface radiative fluxes are used with surface climate to force JULES. Net primary production is the main output variable analysed in Chapter 2.**

### Model choice

### Aerosol model

The GLObal Model of Aerosol Processes (GLOMAP) (Spracklen *et al.*, 2005a, Spracklen *et al.*, 2005b) is an extension to the TOMCAT three-dimensional, Eulerian chemical transport model (Chipperfield, 2006). GLOMAP is a global aerosol model, calculating particle size, concentration, and chemical composition. GLOMAP includes various aerosol processes, including nucleation, condensation, growth, coagulation, dry and wet deposition, and cloud processing. In the GLOMAP version used here, the aerosol species included are black carbon (BC), particulate organic matter, sulfate, sea salt, and dust. The horizontal resolution is 2.8° × 2.8°, with 31 vertical levels ranging from the surface to 10 hPa, with the layer thickness varying from 60 m (surface) to 1 km (tropopause). The model is driven with historical meteorology (wind, temperature, humidity) from the European Centre for Medium-Range Weather Forecasts (ECMWF) at 6-hourly intervals and interpolated onto the model time step (30 min). Annually varying anthropogenic emissions (BC, organic carbon (OC), and SO2) including fossil fuel and biofuel emissions are taken from the MACCity inventory (Granier *et al.*, 2011). This data set is based on historical Atmospheric Chemistry and Climate Model Intercomparison Project (ACCMIP) (for years 1990 and 2000) and RCP 8.5 (2005 and 2010) emissions. The emissions were linearly interpolated for the years between those given. Biomass burning emissions (BC, OC, and SO2) are taken from the Global Fire Emissions Database version 3 (van der Werf *et al.*, 2010) and are supplied as annually varying monthly means.

This work uses the modal version of GLOMAP (Mann *et al.*, 2010), which simulates the concentration, size, and mass of aerosol particles using a two moment (mass per particle and number concentration) modal scheme. The version used here has seven log-normal size modes, each containing particles with a range of geometric mean diameters ($D_g$) (Nucleation, $D_g < 10$nm; Aitken, $10 < D_g < 100$ nm; Accumulation, $100 < D_g < 1\mu$m; Coarse, $D_g > 1\mu$m). Four are treated hydrophilic with a three non-hydrophilic Aitken, Accumulation, and Coarse modes. The original version of GLOMAP used a sectional scheme (Spracklen *et al.*, 2005a). However, a sectional model can be computationally expensive for multidecadal coupled aerosol-climate simulations (Spracklen *et al.*, 2005a). Realistic aerosol schemes are still required in climate models but at increased computational efficiency. I planned a series of factorial runs to simulate the changes in aerosol due to changes in various emission sources with a total length of 26 years. Therefore, GLOMAP-mode was the appropriate model to use in our study.

Further, GLOMAP-mode has been evaluated extensively in previous studies and has been shown to capture observed aerosol concentrations (Mann *et al.*, 2012, Mann *et al.*, 2010, Reddington *et al.*, 2016, Schmidt *et al.*, 2012, Spracklen *et al.*, 2011a, Spracklen *et al.*, 2011b) and aerosol optical depth (AOD) (Bellouin *et al.*, 2013, Rap *et al.*, 2015, Reddington *et al.*, 2015, Reddington *et al.*, 2016) in various regions and conditions. I also compare modelled AOD with satellite derived AOD (Chapter 2).

A two-moment aerosol model that calculates aerosol number and mass has an advantage over “mass-only” models when interested in accurately simulating processes that affect the aerosol size distribution. The addition of aerosol in mass only models results in increased concentrations (Bellouin *et al.*, 2013). However, additional aerosol in two-moment schemes (eg. via condensation) may grow particles and not alter number concentrations. Accurately representing particle mass and number is important for quantification of aerosol radiative forcing as this requires knowledge on the spatial and temporal distributions of mass, number, chemical composition, size, and shape of aerosols (Bellouin *et al.*, 2013).

### Radiative transfer model

To most accurately describe radiative transfer through the atmosphere, the use of “line-by-line” calculations is required. This method loops through each frequency and calculates the radiance. This requires the calculation of each spectral line for all molecules in the atmosphere. A more efficient method is to define a small number of spectral bands to represent the whole spectra and calculate radiance for each band. These “parameterisations” have been shown to agree well with corresponding line-by-line calculations (Pincus *et al.*, 2015). Therefore, in many coupled-climate modelling studies (eg. CMIP5, Taylor *et al.*

(2012)) and offline studies (Rap *et al.*, 2013, Rap *et al.*, 2015, Scott *et al.*, 2018) radiative parameterisations are used for computational speed.

The offline Edwards-Slingo (ES) radiative transfer model (Edwards & Slingo, 1996) was an appropriate choice due to its computational efficiency, extensive inclusion of physical processes, and heavy use throughout the scientific community (Edwards & Slingo, 1996, Haywood *et al.*, 1997, Sun, 2011). ES calculates radiative fluxes for a given atmospheric state (eg. water vapour, cloud cover, temperature, aerosol loading). The radiative spectrum is split into six bands in the shortwave region and nine bands in the longwave region. Modelled surface short wave direct and diffuse radiative fluxes have been shown to match well to observations (Rap *et al.*, 2015). The model was configured with a horizontal resolution of 2.8° x 2.8° on 32 vertical levels. The model is forced with monthly mean ECMWF climate (water vapour and temperature) and ozone reanalysis data. Cloud fields (liquid water path and cloud fraction) and surface albedo are taken from the International Satellite Cloud Climatology Project (ISCCP-D2) (Rossow and Shiffer, 1999).

Further, aerosol radiative effects are calculated for four of the seven possible size modes (Aitken soluble, accumulation soluble and insoluble, and coarse soluble). Insoluble accumulation and coarse modes only contain dust aerosol, which is not a focus of this thesis.

### Land surface model

The Joint UK Land Environment Simulator (JULES) land surface model is used to quantify the changes in direct and diffuse radiation have on carbon fluxes. JULES simulates the exchange of carbon, water, energy, and momentum between the land surface and atmosphere (Best *et al.*, 2011, Clark *et al.*, 2011). The model includes a multilayer canopy parameterisation to scale leaf photosynthesis to canopy (Mercado *et al.*, 2009, Mercado *et al.*, 2007). Photosynthesis is calculated on each level and the scheme considers variations in direct and diffuse radiation on sunlit and shaded leaves. The multilayer scheme contrasts with the original “big leaf” approach where the canopy is treated as a single leaf. “Big leaf” parameterisations do not distinguish between direct and diffuse radiation, a distinction which has been shown to have a large impact on carbon uptake (Gu *et al.*, 2003, Mercado *et al.*, 2009, Roderick *et al.*, 2001). The multilayer scheme has been evaluated against eddy covariance data in a temperate coniferous site in the Netherlands (Jogireddy *et al.*, 2006), temperate broad leaved and needle leaved sites (Mercado *et al.*, 2009), and tropical broadleaf sites (Mercado *et al.*, 2007, Rap *et al.*, 2015) and matches the diurnal cycle and light response at high radiance well, an improvement on previous model versions. A more detailed description of JULES is given in Text A1.

In this thesis, JULES is forced with ERA-Interim climate fields (Weedon *et al.*, 2014) and runs at 0.5° spatial resolution with 3-hourly time steps. The climate drivers consist of 2 m air temperature, specific humidity, precipitation, 10 m wind speed, and surface pressure. Further, JULES is forced with time varying atmospheric $CO_2$ concentrations derived from National Oceanic and Atmospheric Administration (NOAA) monitoring stations. Model drivers also include downward surface radiation (short-wave direct and diffuse and long wave) from the ES model.

## Experiments

The driving mechanisms behind the post-2000 land sink are unknown. Studies highlight the role of $CO_2$ fertilization (Keenan *et al.*, 2016, Schimel *et al.*, 2015), climate (Ballantyne *et al.*, 2017, Keenan *et al.*, 2016), nitrogen deposition (Quinn Thomas *et al.*, 2010), and diffuse radiation (Mercado *et al.*, 2009) in driving the carbon sink. I therefore performed a set of factorial simulations with JULES to estimate the carbon uptake response to combined and singular forcings. The version of JULES used (v3.2) does not include a coupled carbon-nitrogen scheme and so I could not evaluate the carbon response to changes in nitrogen deposition. I did however, quantify the response to changes in $CO_2$ concentrations, climate, and light regime (direct/diffuse radiation). I further separated changes in light regime due to either fossil fuel aerosol, fire aerosol, and cloud cover (Table 1.2).

First, GLOMAP was used to simulate the changes in aerosol distribution over the period 1998-2010. Three simulations were performed, by either varying emissions of fossil fuel or biomass burning or keeping them fixed at year 2000 levels (Table 1, blue box). Aerosol optical properties were then used in the ES model along with cloud fields to perform four more factorial simulations (Table 1.2, red box). These four ES simulations provided varying spatiotemporal fields of surface direct and diffuse radiation to force JULES. Five JULES simulations were performed. The impact of changing surface radiation to 1) Fire aerosol, 2) fossil fuel aerosol, and 3) Cloud cover, as well as changes in 4) Climate, and 5) $CO_2$ was quantified (Table 1.2).

I had a sole focus on analysing changes in NPP as changes in light regime predominately affect carbon uptake processes. This shortened the modelling time required as I only needed to equilibrate the vegetation with our initial conditions rather than the whole carbon cycle (eg soil pools). The model was spun-up for 60 years using a repeated 1995 meteorology. I performed 5 factorial simulations in which drivers were varied or held constant in turn (see Chapter 2). Further, within the vegetation dynamics module TRIFFID (see Text A1), competition between species is disabled as simulations are over a small number of years.

**Table 1.2 - Summary of simulations performed by GLOMAP (blue box), Edwards-Slingo (red box), and JULES (whole table). The impact of changing emissions on aerosol distributions from fire and fossil fuel was quantified with GLOMAP, the subsequent impact of fire and fossil fuel aerosol and changing cloud cover on surface radiation was quantified with ES. Finally, the impact of changing climate, $CO_2$, and changes in surface radiation due to fire aerosol, fossil fuel aerosol, and clouds was quantified with JULES. F stands for fixed and V stands for varying.**

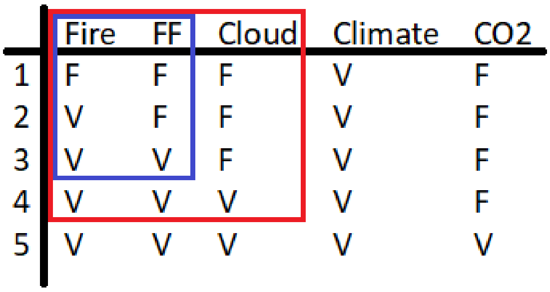

| | Fire | FF | Cloud | Climate | CO2 |
|---|---|---|---|---|---|
| 1 | F | F | F | V | F |
| 2 | V | F | F | V | F |
| 3 | V | V | F | V | F |
| 4 | V | V | V | V | F |
| 5 | V | V | V | V | V |

### 1.5.2 Increases in nitrogen deposition from East Asian fossil fuel burning have increased plant carbon uptake (Chapter 3)

**Objective**

Perform offline simulations with a land-surface model with a coupled carbon-nitrogen scheme to understand the relative roles of climate, nutrient, and $CO_2$ concentrations in explaining recent increases in terrestrial plant productivity and carbon sinks.

**Scientific Background**

The importance of nitrogen availability for plant growth is outlined in sections 1.2.5 and 3.1. Process based (Thornton *et al.*, 2009, Thornton *et al.*, 2007, Zaehle *et al.*, 2010) and empirical (Wang *et al.*, 2017, Zhu *et al.*, 2017) modelling, as well as field studies (de Vries *et al.*, 2014, Maaroufi *et al.*, 2015, Magnani *et al.*, 2007, Schulte-Uebbing & de Vries, 2018) show the impact of nitrogen deposition on carbon uptake. One field study estimates boreal and temperate forest sensitivities (uptake of carbon per unit nitrogen deposition) as high as 300 gC/gN (Magnani *et al.*, 2007). However, many more field studies give estimates between 5-30 gC/gN (de Vries *et al.*, 2014, Maaroufi *et al.*, 2015, Schulte-Uebbing & de Vries, 2018). Schulte-Uebbing and de Vries (2018) derived a nitrogen induced global carbon sink of 0.2 PgC/yr, a result not dissimilar from process model estimates of ~0.3 PgC/yr (Zaehle *et al.*, 2010).

How ecosystems respond to additional nitrogen depends on other factors (vegetation age, climate, $CO_2$ concentrations, land-use) and the interactions between them (synergistically or antagonistically). Synergistic effects can arise when an ecosystem is co-limited by several factors and these limitations are relieved simultaneously (Oren *et al.*, 2001). For example, carbon-nitrogen synergies can arise when additional nitrogen alleviates nitrogen limitation brought about by rising $CO_2$ concentrations (Churkina *et al.*, 2009, Oren *et al.*, 2001, Zaehle *et al.*, 2010). Carbon-nitrogen synergy has been estimated to be a substantial contributor of the 1990s land sink, from 0.3 PgC/yr (13% of total sink) (Zaehle *et al.*, 2010) to 1.2 PgC/yr (47% of total sink) (Churkina *et al.*, 2009). Therefore, I hypothesize that the rapid increase in fossil fuel emissions since 2000 has contributed to the land carbon sink through a combination of $CO_2$ fertilization, nitrogen deposition, and the synergy between the two. Similarly to our "diffuse radiation" hypothesis, the location of nitrogen emissions/deposition is an important factor when considering the global carbon response. For example, increased deposition in agricultural regions will likely not elicit a response as these ecosystems are nitrogen saturated, whereas increased deposition over temperate and boreal forests will potentially see large carbon gains (Fisher *et al.*, 2012).

Many terrestrial ecosystem models now include a coupled carbon-nitrogen cycle (Zaehle & Dalmonech, 2011). All models reduce the strength of $CO_2$ fertilization as nitrogen availability increases and reduce climate induced losses as mineralisation increases. Despite similar features these models differ in how they link carbon and nitrogen, and the degree of detail to which different processes are included. There is difficulty in knowing the "best" way to model the coupled carbon-nitrogen cycle due to the complexities in evaluating non-linear processes that cannot be directly measured. When compared to FACE experiments, models do not capture important ecosystem processes due to model simplifications or missing mechanisms entirely (Zaehle *et al.*, 2014).

To address the second hypothesis, I decided to use the Community Land Model version 4.5 (CLM4.5). One benefit of CLM is its long standing in the scientific community, having been developed and evaluated for many years (Bonan *et al.*, 2011, Bonan *et al.*, 2012, Duarte *et al.*, 2017, Koven *et al.*, 2013, Lawrence *et al.*, 2011, Oleson *et al.*, 2008). A new feature in CLM4.5 is the inclusion of vertically resolved soil carbon-nitrogen dynamics (Koven *et al.*, 2013), which is vital in accurately simulating nitrogen uptake and mineralisation (Zaehle *et al.*, 2014). However, CLM4.5 has fixed CN stoichiometry. Field experiments have shown both ecosystem stoichiometry to change with changing

$CO_2$ concentrations and nitrogen deposition (Norby *et al.*, 2005, Zaehle *et al.*, 2014). By not allowing these to vary, CLM is missing key processes, for example; plants adapting to nitrogen stress with rising $CO_2$ concentrations. Nevertheless, CLM4.5 is an established model for studying carbon-nitrogen interactions (Thornton *et al.*, 2009, Thornton *et al.*, 2007) and so appropriate in addressing our hypothesis.

## Research Approach

### Model

CLM4.5 simulates biophysical, hydrological, and biogeochemical exchange between the land and the atmosphere (Oleson *et al.*, 2013). CLM4.5 is fully prognostic with regards to carbon and nitrogen state variables in the vegetation, litter, and soil organic matter pools. Nitrogen availability limits carbon uptake by downregulating GPP if plant demand (determined from fixed carbon-nitrogen stoichiometry) is higher than available nitrogen. This approach offers a direct link between plant nitrogen and carbon uptake but is not entirely realistic. Plant photosynthesis is controlled by leaf nitrogen content, not by available soil nitrogen that downregulates the photosynthetic rate (Evans, 1989). Nonetheless, modelled GPP has been shown to have good agreement with observations (Bonan *et al.*, 2011, Koven *et al.*, 2013). Alternative approaches exist where CN stoichiometry is flexible meaning nutrient limitation is not represented by an instantaneous downregulation of potential GPP, but instead by leaf nitrogen content (Ghimire *et al.*, 2016, Zaehle & Friend, 2010). The latest version of CLM (version 5) uses this "foliar nitrogen content" method, but was not available for use at the time of this study. Nevertheless, CLM4.5 has been shown to capture the 20th century change in terrestrial carbon cycling (Koven *et al.*, 2013). A more detailed description of CLM is given in Text A2.

Climate driver data (precipitation, temperature, solar radiation, atmospheric pressure, specific humidity, and winds) used stem from the CRU-NCEP dataset (Harris *et al.*, 2014, Viovy, 2016) (0.5° spatial and 6h temporal resolution), which is aggregated/interpolated to the CLM4.5 spatial resolutions of 1.25° x 0.9° and 30 min time step. Further, I also used prescribed annual, globally averaged $CO_2$ concentrations from the Earth Systems Research Laboratory (Dlugokencky & Tans, 2017). I used fixed present-day land cover as described in Oleson *et al.* (2013), meaning I did not consider land-use and land-cover change in this study since my focus was broadly on carbon-nitrogen interactions.

### Experiments

I decided to run two sets of experiments, an “extended period” (1901-2016) and a “recent period” (1990-2016). Both sets were factorial simulations, whereby the land carbon response to atmospheric $CO_2$, climate, and nitrogen deposition (and their interactions/synergies) was tested (Table 1.3). I first perform a model spin-up by cycling early 20th century climate and preindustrial $CO_2$ concentrations and nitrogen deposition. When the model reaches a steady state (soil carbon pools are in equilibrium), the extended simulations would provide me with a historical evolution of the terrestrial carbon cycle and attribution to its underlying drivers, enabling a comparison to previous long-term studies (eg. Zaehle *et al.* (2010), Thornton *et al.* (2007)). Further, the extended simulations provide initial conditions for the recent simulations starting in 1990. The recent period is chosen as such to enable me to quantify changes in carbon cycling relative to a modern baseline (in line with our hypothesis) and provide a long enough time-series for trends and changes to be analysed.

**Table 1.3 - Summary of factorial model simulations performed with CLM. C (constant) indicated 1900 (or 1990 for “recent” simulations) values are used for atmospheric CO2 and nitrogen deposition and 1901-1920 (or 1990 for “recent” simulations) is recycled. T (transient) indicates historically varying CO2, nitrogen deposition, and climate is used.**

| Experiment | $CO_2$ | Nitrogen deposition | Climate |
|---|---|---|---|
| **S1** | C | C | C |
| **S2** | T | C | C |
| **S3** | C | T | C |
| **S4** | C | C | T |
| **S5** | T | T | C |
| **S6** | T | C | T |

| | | | |
|---|---|---|---|
| **S7** | C | T | T |
| **S8** | T | T | T |

### 1.5.3 A progressive relaxation of climatic constraints has led to increased plant productivity (Chapter 4)

**Objective**

Analyse variability and trends over the last three decades in key model and observational records including climate, and gross primary productivity from terrestrial biosphere models, upscaled eddy covariance data, and satellite derived vegetation observations. Objective is to identify regions of significant change in ecosystem functioning due to variations in climate alone.

**Scientific Background**

Gross primary productivity (GPP) is the largest global carbon flux, and as such, small variations can have a large influence on the net carbon balance. Further, it drives other major components of the carbon cycle, such as respiration and growth. Climate controls GPP inter-annual variability (IAV) and influences long-term trends. Global IAV is dominated by certain “hotspot” regions such as tropical forests (Cox *et al.*, 2013) and semi-arid (Ahlstrom *et al.*, 2015, Poulter *et al.*, 2014) regions. Zscheischler *et al.* (2014) found that just 7% of the spatio-temporal domain explains 78% of the global GPP IAV. GPP variability is often linked to extreme climate events such as; drought, heatwaves, and heavy precipitation, which can lead to large increases (Bastos *et al.*, 2013) or decreases (Zhao & Running, 2010) in vegetation productivity. The carbon cycle response to climate variations depends upon the underlying vegetation type, mean climate state, and previous conditions/disturbances, and as such is a result of many complex, interacting processes (Reichstein *et al.*, 2013). Long-term warming in the northern high latitudes has been hypothesised to lead to increase annual carbon uptake via an increase in length of the growing season (Keenan *et al.*, 2014, Myneni *et al.*, 1997, Piao *et al.*, 2007). However, spring warming can also reduce peak summer productivity due to increased moisture stress (Buermann *et al.*, 2013). There have been noticeable drying trends in large regions reducing carbon uptake as well such as; Southern USA (Anderegg *et al.*, 2012), and South America (Zhao & Running, 2010).

There are three popular methodologies to calculating global GPP. These are: upscaling eddy covariance measurements using statistical (Jung *et al.*, 2009) or empirical (Beer *et al.*, 2009) techniques, the use of optical satellite data related to vegetation productivity, generally absorbed photosynthetic active radiation (APAR) or leaf-area index (LAI), and finally terrestrial biosphere models which simulate bio-physical/chemical processes on leaf to biome scales (eg. Sitch *et al.* (2008); Piao *et al.* (2009)). These methods rely on various assumptions and as such are inherently uncertain (Anav *et al.*, 2015).

Therefore, analysing the consistency between independent products in terms of IAV, trends, and sensitivity to climate variability on different spatial scales will provide valuable insight into the confidence that can be placed in local and regional estimates and the underlying climatic controls.

## Research Approach

I assess the consistency in seasonal and inter-annual variability and long-term trends of three independent GPP datasets over the period 1982-2016 in relation to climate variability alone. I use the FLUXCOM RS+METEO product (Jung *et al.*, 2017, Tramontana *et al.*, 2016), TRENDYv6 model inter-comparison (a suite of process based terrestrial biosphere models, Sitch *et al.* (2015)), and a satellite based light-use efficiency model (Running *et al.*, 2004, Smith *et al.*, 2016). I focus on the influence of climate alone, and ignore greening due to $CO_2$ fertilization because this is a highly uncertain process in which models and observations disagree on (Smith *et al.*, 2016). Secondly, the climate effect in the TRENDY models was calculated by subtracting the “S1” simulations (varying $CO_2$) from the “S2” simulations (varying $CO_2$ and climate). Further, FLUXCOM GPP does not include any greening effects due to $CO_2$ fertilization, and so just evaluating the climate response leads to a more consistent comparison.

I use multiple linear regression to calculate the sensitivity of GPP to individual climate (temperature and precipitation) forcings on local (grid-cell, 0.5°) and regional scales. I use the raw GPP output (as opposed to detrended) to calculate "trend correlations", as I am interested in how climate has influenced GPP in the long-term as well. I further compare the datasets in terms of the dominant climate driver of GPP by evaluating which climate forcing contributes most to the explained variance (see Section 4.2). I omit incoming solar radiation from the regression analysis as it has been shown that anomalies in temperature and precipitation dominate local, regional, and global scale carbon flux variability (Jung *et al.*, 2017).

# References

Ahlstrom A, Raupach MR, Schurgers G *et al.* (2015) The dominant role of semi-arid ecosystems in the trend and variability of the land $CO_2$ sink. Science, **348**, 895-899.

Ainsworth EA, Yendrek CR, Sitch S, Collins WJ, Emberson LD (2012) The Effects of Tropospheric Ozone on Net Primary Productivity and Implications for Climate Change. Annual Review of Plant Biology, **63**, 637-661.

Anav A, Friedlingstein P, Beer C *et al.* (2015) Spatiotemporal patterns of terrestrial gross primary production: A review. Reviews of Geophysics, **53**, 785-818.

Anderegg WRL, Berry JA, Smith DD, Sperry JS, Anderegg LDL, Field CB (2012) The roles of hydraulic and carbon stress in a widespread climate-induced forest die-off. Proceedings of the National Academy of Sciences of the United States of America, **109**, 233-237.

Baldocchi D (2003) Assessing the eddy covariance technique for evaluating carbon dioxide exchange rates of ecosystems: past, present and future. Global Change Biology*,* **9**, 479-492.

Baldocchi D, Falge E, Gu L *et al.* (2001) FLUXNET: A New Tool to Study the Temporal and Spatial Variability of Ecosystem–Scale Carbon Dioxide, Water Vapor, and Energy Flux Densities. Bulletin of the American Meteorological Society*,* **82**, 2415-2434.

Baldocchi DD, Hincks BB, Meyers TP (1988) Measuring Biosphere-Atmosphere Exchanges of Biologically Related Gases with Micrometeorological Methods. Ecology*,* **69**, 1331-1340.

Ball JT, Woodrow IE, Berry JA (1987) A Model Predicting Stomatal Conductance and its Contribution to the Control of Photosynthesis under Different Environmental Conditions. pp Page. Dordrecht, Springer Netherlands.

Ballantyne A, Smith W, Anderegg W *et al.* (2017) Accelerating net terrestrial carbon uptake during the warming hiatus due to reduced respiration. Nature Climate Change*,* **7**.

Barichivich J, Briffa KR, Myneni RB *et al.* (2013) Large-scale variations in the vegetation growing season and annual cycle of atmospheric CO <sub>2</sub> at high northern latitudes from 1950 to 2011. Global Change Biology*,* **19**, 3167-3183.

Bastos A, Running SW, Gouveia C, Trigo RM (2013) The global NPP dependence on ENSO: La Niña and the extraordinary year of 2011. Journal of Geophysical Research: Biogeosciences*,* **118**, 1247-1255.

Beer C, Ciais P, Reichstein M *et al.* (2009) Temporal and among-site variability of inherent water use efficiency at the ecosystem level. Global Biogeochemical Cycles*,* **23**, n/a-n/a.

Beer C, Reichstein M, Tomelleri E *et al.* (2010) Terrestrial Gross Carbon Dioxide Uptake: Global Distribution and Covariation with Climate. Science*,* **329**, 834-838.

Bellouin N, Mann GW, Woodhouse MT, Johnson C, Carslaw KS, Dalvi M (2013) Impact of the modal aerosol scheme GLOMAP-mode on aerosol forcing in the Hadley Centre Global Environmental Model. Atmos. Chem. Phys*,* **13**, 3027-3044.

Berg A, Findell K, Lintner B *et al.* (2016) Land–atmosphere feedbacks amplify aridity increase over land under global warming. Nature Climate Change*,* **6**, 869-874.

Best MJ, Grimmond CSB, Villani MG (2006) Evaluation of the Urban Tile in MOSES using Surface Energy Balance Observations. Boundary-Layer Meteorology*,* **118**, 503-525.

Best MJ, Pryor M, Clark DB *et al.* (2011) The Joint UK Land Environment Simulator (JULES), model description. Part 1: Energy and water fluxes. Geoscientific Model Development*,* **4**, 677-699.

Bonan GB, Lawrence PJ, Oleson KW *et al.* (2011) Improving canopy processes in the Community Land Model version 4 (CLM4) using global flux fields empirically inferred from FLUXNET data. JOURNAL OF GEOPHYSICAL RESEARCH*,* **116**, 1-22.

Bonan GB, Levis S (2010) Quantifying carbon-nitrogen feedbacks in the Community Land Model (CLM4). Geophysical Research Letters*,* **37**, L07401-L07401.

Bonan GB, Oleson KW, Fisher RA, Lasslop G, Reichstein M (2012) Reconciling leaf physiological traits and canopy flux data: Use of the TRY and FLUXNET databases in the Community Land Model version 4. Journal of Geophysical Research: Biogeosciences, **117**, n/a-n/a.

Buermann W, Bikash PR, Jung M, Burn DH, Reichstein M (2013) Earlier springs decrease peak summer productivity in North American boreal forests. Environmental Research Letters, **8**, 024027-024027.

Chatterjee A, Gierach MM, Sutton AJ *et al.* (2017) Influence of El Niño on atmospheric CO <sub>2</sub> over the tropical Pacific Ocean: Findings from NASA's OCO-2 mission. Science, **358**, eaam5776-eaam5776.

Chipperfield MP (2006) New version of the TOMCAT/SLIMCAT off-line chemical transport model: Intercomparison of stratospheric tracer experiments. Quarterly Journal of the Royal Meteorological Society, **132**, 1179-1203.

Churkina G, Brovkin V, Von Bloh W, Trusilova K, Jung M, Dentener F (2009) Synergy of rising nitrogen depositions and atmospheric CO <sub>2</sub> on land carbon uptake moderately offsets global warming. Global Biogeochemical Cycles, **23**, n/a-n/a.

Ciais P, Reichstein M, Viovy N *et al.* (2005) Europe-wide reduction in primary productivity caused by the heat and drought in 2003. Nature, **437**, 529-533.

Ciais P, Sabine C, Bala G *et al.* (2013) Carbon and Other Biogeochemical Cycles. In. Climate Change 2013: The Physical Science Basis. Contribution of Working Group I to the Fifth Assessment Report of the Intergovernmental Panel on Climate Change.

Ciais P, Schelhaas MJ, Zaehle S *et al.* (2008) Carbon accumulation in European forests. Nature Geoscience, **1**, 425-429.

Clark DB, Mercado LM, Sitch S *et al.* (2011) The Joint UK Land Environment Simulator (JULES), model description. Part 2: Carbon fluxes and vegetation dynamics. pp Page.

Cox PM (2001) Description of the TRIFFID dynamic global vegetation model, Hadley Centre Technical Note 24, Hadley Centre, Met Office, Bracknell, UK.

Cox PM, Betts RA, Jones CD, Spall SA, Totterdell IJ (2000) Erratum: Acceleration of global warming due to carbon-cycle feedbacks in a coupled climate model. Nature, **408**, 184-187.

Cox PM, Pearson D, Booth BB, Friedlingstein P, Huntingford C, Jones CD, Luke CM (2013) Sensitivity of tropical carbon to climate change constrained by carbon dioxide variability. Nature, **494**, 341-344.

De Boeck HJ, Verbeeck H (2011) Drought-associated changes in climate and their relevance for ecosystem experiments and models. Biogeosciences, **8**, 1121-1130.

De Vries W, Du E, Butterbach-Bahl K (2014) Short and long-term impacts of nitrogen deposition on carbon sequestration by forest ecosystems. Current Opinion in Environmental Sustainability, **9-10**, 90-104.

Devries T, Holzer M, Primeau F (2017) Recent increase in oceanic carbon uptake driven by weaker upper-ocean overturning. Nature, **542**, 215-218.

Dlugokencky E, Tans PP (2017) NOAA/ESRL. pp Page.

Donohue RJ, Roderick ML, Mcvicar TR, Farquhar GD (2013) Impact of CO <sub>2</sub> fertilization on maximum foliage cover across the globe's warm, arid environments. Geophysical Research Letters, **40**, 3031-3035.

Duarte HF, Raczka BM, Ricciuto DM *et al.* (2017) Evaluating the Community Land Model (CLM4.5) at a coniferous forest site in northwestern United States using flux and carbon-isotope measurements. Biogeosciences, **145194**, 4315-4340.

Edwards JM, Slingo A (1996) Studies with a flexible new radiation code. I: Choosing a comnfiguration for a large-scale model. Quarterly Journal of the Royal Meteorological Society, **122**, 689-719.

Essery RLH, Best MJ, Betts RA, Cox PM, Taylor CM (2003) Explicit Representation of Subgrid Heterogeneity in a GCM Land Surface Scheme. Journal of Hydrometeorology, **4**, 530-543.

Evans JR (1989) Photosynthesis and nitrogen relationships in leaves of C3 plants. Oecologia, **78**, 9-19.

Farquhar GD, Von Caemmerer S, Berry JA (1980) A biochemical model of photosynthetic $CO_2$ assimilation in leaves of C3 species. Planta, **149**, 78-90.

Fisher JB, Badgley G, Blyth E (2012) Global nutrient limitation in terrestrial vegetation. Global Biogeochemical Cycles, **26**.

Fisher JB, Huntzinger DN, Schwalm CR, Sitch S (2014) Modeling the Terrestrial Biosphere. Annual Review of Environment and Resources, **39**, 91-123.

Forkel M, Carvalhais N, Rödenbeck C *et al.* (2016) Enhanced seasonal CO 2 exchange caused by amplified plant productivity in northern ecosystems. Science, **351**, 696-699.

Friend AD, Stevens AK, Knox RG, Cannell MGR (1997) A process-based, terrestrial biosphere model of ecosystem dynamics (Hybrid v3.0). Ecological Modelling, **95**, 249-287.

Gauss M, Myhre G, Isaksen ISA *et al.* (2006) Radiative forcing since preindustrial times due to ozone change in the troposphere and the lower stratosphere. Atmospheric Chemistry and Physics, **6**, 575-599.

Gerber S, Hedin LO, Oppenheimer M, Pacala SW, Shevliakova E (2010) Nitrogen cycling and feedbacks in a global dynamic land model. Global Biogeochemical Cycles, **24**, 1-15.

Ghimire B, Riley WJ, Koven CD, Mu M, Randerson JT (2016) Representing leaf and root physiological traits in CLM improves global carbon and nitrogen cycling predictions. Journal of Advances in Modeling Earth Systems, **8**, 598-613.

Gloor M, Sarmiento JL, Gruber N (2010) What can be learned about carbon cycle climate feedbacks from the CO 2 airborne fraction? Atmos. Chem. Phys. Atmospheric Chemistry and Physics, **10**, 7739-7751.

Goll DS, Brovkin V, Parida BR *et al.* (2012) Nutrient limitation reduces land carbon uptake in simulations with a model of combined carbon, nitrogen and phosphorus cycling. Biogeosciences, **9**, 3547-3569.

Granier C, Bessagnet B, Bond T *et al.* (2011) Evolution of anthropogenic and biomass burning emissions of air pollutants at global and regional scales during the 1980–2010 period. Climatic Change, **109**, 163-190.

Graven HD, Keeling RF, Piper SC *et al.* (2013) Enhanced seasonal exchange of $CO_2$ by northern ecosystems since 1960. Science (New York, N.Y.), **341**, 1085-1089.

Gruber N, Galloway JN (2008) An Earth-system perspective of the global nitrogen cycle. Nature, **451**, 293-296.

Gu L, Baldocchi DD, Wofsy SC, Munger JW, Michalsky JJ, Urbanski SP, Boden T (2003) Response of a Deciduous Forest to the Mount Pinatubo Eruption: Enhanced Photosynthesis. Science, **299**, 2035-2038.

Gurney KR, Baker D, Rayner P, Denning S (2008) Interannual variations in continental-scale net carbon exchange and sensitivity to observing networks estimated from atmospheric CO <sub>2</sub> inversions for the period 1980 to 2005. Global Biogeochemical Cycles, **22**, n/a-n/a.

Gurney KR, Eckels WJ (2011) Regional trends in terrestrial carbon exchange and their seasonal signatures. Tellus B: Chemical and Physical Meteorology, **63**, 328-339.

Hansen J, Kharecha P, Sato M (2013) Climate forcing growth rates: doubling down on our Faustian bargain. Environmental Research Letters, **8**, 011006-011006.

Harris I, Jones PD, Osborn TJ, Lister DH (2014) Updated high-resolution grids of monthly climatic observations - the CRU TS3.10 Dataset. International Journal of Climatology, **34**, 623-642.

Hartmann DL, Klein Tank AMG, Rusticucci M *et al.* (2013) Observations: Atmosphere and Surface. In. Climate Change 2013: The Physical Science Basis. Contribution of Working Group I to the Fifth Assessment Report of the Intergovernmental Panel on Climate Change.

Haywood JM, Roberts DL, Slingo A *et al.* (1997) General Circulation Model Calculations of the Direct Radiative Forcing by Anthropogenic Sulfate and Fossil-Fuel Soot Aerosol. Journal of Climate, **10**, 1562-1577.

Hickler T, Smith B, Prentice IC, Mjöfors K, Miller P, Arneth A, Sykes MT (2008) $CO_2$ fertilization in temperate FACE experiments not representative of boreal and tropical forests. Global Change Biology, **14**, 1531-1542.

Houghton RA, House JI, Pongratz J *et al.* (2012) Carbon emissions from land use and land-cover change. Biogeosciences, **9**, 5125-5142.

Huete AR, Didan K, Shimabukuro YE *et al.* (2006) Amazon rainforests green-up with sunlight in dry season. Geophysical Research Letters, **33**, L06405-L06405.

Huntzinger DN, Michalak AM, Schwalm C *et al.* (2017) Uncertainty in the response of terrestrial carbon sink to environmental drivers undermines carbon-climate feedback predictions. Scientific Reports, **7**, 4765-4765.

Janssens IA, Dieleman W, Luyssaert S *et al.* (2010) Reduction of forest soil respiration in response to nitrogen deposition. Nature Geoscience, **3**, 315-322.

Jogireddy V, Cox PM, Huntingford C, Harding RJ, Mercado LM (2006) An improved description of canopy light intercep- tion for use in a GCM land-surface scheme: calibration and testing against carbon fluxes at a coniferous forest. In. Haddley Centre Technical Note 63.

Jung M, Reichstein M, Bondeau A (2009) Towards global empirical upscaling of FLUXNET eddy covariance observations: validation of a model tree ensemble approach using a biosphere model. Biogeosciences, **6**, 2001-2013.

Jung M, Reichstein M, Margolis HA *et al.* (2011) Global patterns of land-atmosphere fluxes of carbon dioxide, latent heat, and sensible heat derived from eddy covariance, satellite, and meteorological observations. JOURNAL OF GEOPHYSICAL RESEARCH, **116**, G00J07-G00J07.

Jung M, Reichstein M, Schwalm CR *et al.* (2017) Compensatory water effects link yearly global land $CO_2$ sink changes to temperature. Nature, **541**, 516-520.

Kanniah KD, Beringer J, North P, Hutley L (2012) Control of atmospheric particles on diffuse radiation and terrestrial plant productivity: A review. Progress in Physical Geography, **36**, 209-237.

Kattge J, Díaz S, Lavorel S *et al.* (2011) TRY - a global database of plant traits. Global Change Biology, **17**, 2905-2935.

Keenan TF, Gray J, Friedl MA *et al.* (2014) Net carbon uptake has increased through warming-induced changes in temperate forest phenology. Nature Climate Change, **4**, 598-604.

Keenan TF, Hollinger DY, Bohrer G, Dragoni D, Munger JW, Schmid HP, Richardson AD (2013) Increase in forest water-use efficiency as atmospheric carbon dioxide concentrations rise. Nature, **499**, 324-327.

Keenan TF, Prentice IC, Canadell JG, Williams CA, Wang H, Raupach M, Collatz GJ (2016) Recent pause in the growth rate of atmospheric $CO_2$ due to enhanced terrestrial carbon uptake. Nature Communications, **7**, 13428-13428.

Keppel-Aleks G, Wolf AS, Mu M *et al.* (2014) Separating the influence of temperature, drought, and fire on interannual variability in atmospheric CO <sub>2</sub>. Global Biogeochemical Cycles, **28**, 1295-1310.

Kondo M, Ichii K, Patra PK *et al.* (2018) Plant Regrowth as a Driver of Recent Enhancement of Terrestrial $CO_2$ Uptake. Geophysical Research Letters, **45**, 4820-4830.

Koven CD, Riley WJ, Subin ZM *et al.* (2013) The effect of vertically resolved soil biogeochemistry and alternate soil C and N models on C dynamics of CLM4. Biogeosciences, **10**, 7109-7131.

Lasslop G, Reichstein M, Papale D *et al.* (2010) Separation of net ecosystem exchange into assimilation and respiration using a light response curve approach: critical issues and global evaluation. Global Change Biology, **16**, 187-208.

Lawrence DM, Oleson KW, Flanner MG *et al.* (2011) Parameterization improvements and functional and structural advances in Version 4 of the Community Land Model. Journal of Advances in Modeling Earth Systems, **3**, n/a-n/a.

Le Quéré C, Andrew RM, Friedlingstein P *et al.* (2018) Global Carbon Budget 2017. Earth Syst. Sci. Data, **1010333739**, 405-448.

Lebauer DS, Treseder KK (2008) NITROGEN LIMITATION OF NET PRIMARY PRODUCTIVITY IN TERRESTRIAL ECOSYSTEMS IS GLOBALLY DISTRIBUTED. Ecology, **89**, 371-379.

Liu J, Bowman KW, Schimel DS *et al.* (2017) Contrasting carbon cycle responses of the tropical continents to the 2015–2016 El Niño. Science, **358**, eaam5690-eaam5690.

Liu L, Greaver TL (2009) A review of nitrogen enrichment effects on three biogenic GHGs: the $CO_2$ sink may be largely offset by stimulated N2O and CH4 emission. Ecology Letters, **12**, 1103-1117.

Lloyd J, Taylor JA (1994) On the temperature dependence of soil respiration. Functional Ecology, **8**, 315-323.

Lombardozzi D, Levis S, Bonan G *et al.* (2015) The Influence of Chronic Ozone Exposure on Global Carbon and Water Cycles. Journal of Climate, **28**, 292-305.

Lucht W, Prentice IC, Myneni RB *et al.* (2002) Climatic control of the high-latitude vegetation greening trend and Pinatubo effect. Science (New York, N.Y.), **296**, 1687-1689.

Luo Y, Su B, Currie WS *et al.* (2004) Progressive Nitrogen Limitation of Ecosystem Responses to Rising Atmospheric Carbon Dioxide. BioScience, **54**, 731-739.

Maaroufi NI, Nordin A, Hasselquist NJ, Bach LH, Palmqvist K, Gundale MJ (2015) Anthropogenic nitrogen deposition enhances carbon sequestration in boreal soils. Global Change Biology, **21**, 3169-3180.

Magnani F, Mencuccini M, Borghetti M *et al.* (2007) The human footprint in the carbon cycle of temperate and boreal forests. Nature, **447**, 849-851.

Mann GW, Carslaw KS, Ridley DA *et al.* (2012) Intercomparison of modal and sectional aerosol microphysics representations within the same 3-D global chemical transport model. Atmos. Chem. Phys. Atmospheric Chemistry and Physics, **12**, 4449-4476.

Mann GW, Carslaw KS, Spracklen DV *et al.* (2010) Description and evaluation of GLOMAP-mode: a modal global aerosol microphysics model for the UKCA composition-climate model. Geoscientific Model Development Discussions, **3**, 651-734.

Mccarthy HR, Oren R, Johnsen KH *et al.* (2010) Re-assessment of plant carbon dynamics at the Duke free-air CO 2 enrichment site: interactions of atmospheric [CO 2 ] with nitrogen and water availability over stand development. New Phytologist, **185**, 514-528.

Mcguire AD, Sitch S, Clein JS *et al.* (2001) Carbon balance of the terrestrial biosphere in the Twentieth Century: Analyses of CO <sub>2</sub> , climate and land use effects with four process-based ecosystem models. Global Biogeochemical Cycles, **15**, 183-206.

Mercado LM, Bellouin N, Sitch S, Boucher O, Huntingford C, Wild M, Cox PM (2009) Impact of changes in diffuse radiation on the global land carbon sink. Nature, **458**, 1014-1017.

Mercado LM, Huntingford C, Gash JHC, Cox PM, Jogireddy V (2007) Improving the representation of radiation interception and photosynthesis for climate model applications. Tellus, Series B: Chemical and Physical Meteorology, **59**, 553-565.

Monteith JL (1972) Solar Radiation and Productivity in Tropical Ecosystems. The Journal of Applied Ecology, **9**, 747-747.

Monteith JL, Moss CJ (1977) Climate and the Efficiency of Crop Production in Britain [and Discussion]. Philosophical Transactions of the Royal Society B: Biological Sciences, **281**, 277-294.

Myneni RB, Hoffman S, Knyazikhin Y *et al.* (2002) Global products of vegetation leaf area and fraction absorbed PAR from year one of MODIS data. Remote Sensing of Environment, **83**, 214-231.

Myneni RB, Keeling CD, Tucker CJ, Asrar G, Nemani RR (1997) Increased plant growth in the northern high latitudes from 1981 to 1991. Nature, **386**, 698-702.

Nemani RR, Keeling CD, Hashimoto H *et al.* (2003) Climate-driven increases in global terrestrial net primary production from 1982 to 1999. Science (New York, N.Y.), **300**, 1560-1563.

Norby RJ, Delucia EH, Gielen B *et al.* (2005) Forest response to elevated $CO_2$ is conserved across a broad range of productivity. Proceedings of the National Academy of Sciences of the United States of America, **102**, 18052-18056.

Norby RJ, Warren JM, Iversen CM, Medlyn BE, Mcmurtrie RE (2010) $CO_2$ enhancement of forest productivity constrained by limited nitrogen availability. Proceedings of the National Academy of Sciences of the United States of America, **107**, 19368-19373.

Oleson KW, Lawrence DM, Authors L *et al.* (2013) Technical Description of version 4.5 of the Community Land Model (CLM).

Oleson KW, Niu GY, Yang ZL *et al.* (2008) Improvements to the Community Land Model and their impact on the hydrological cycle. J. Geophys. Res, **113**.

Oren R, Ellsworth DS, Johnsen KH *et al.* (2001) Soil fertility limits carbon sequestration by forest ecosystems in a $CO_2$-enriched atmosphere. Nature, **411**, 469-472.

Page SE, Siegert F, Rieley JO, Boehm H-DV, Jaya A, Limin S (2002) The amount of carbon released from peat and forest fires in Indonesia during 1997. Nature, **420**, 61-65.

Pan Y, Birdsey RA, Fang J *et al.* (2011) A large and persistent carbon sink in the world's forests. Science (New York, N.Y.), **333**, 988-993.

Park T, Ganguly S, Tømmervik H *et al.* (2016) Changes in growing season duration and productivity of northern vegetation inferred from long-term remote sensing data. Environmental Research Letters, **11**, 084001-084001.

Peylin P, Bousquet P, Le Quéré C *et al.* (2005) Multiple constraints on regional CO <sub>2</sub> flux variations over land and oceans. Global Biogeochemical Cycles, **19**.

Piao S, Ciais P, Friedlingstein P, De Noblet-Ducoudré N, Cadule P, Viovy N, Wang T (2009) Spatiotemporal patterns of terrestrial carbon cycle during the 20th century. Global Biogeochemical Cycles, **23**, n/a-n/a.

Piao S, Ciais P, Friedlingstein P *et al.* (2008) Net carbon dioxide losses of northern ecosystems in response to autumn warming. Nature, **451**, 49-52.

Piao S, Friedlingstein P, Ciais P, Viovy N, Demarty J (2007) Growing season extension and its impact on terrestrial carbon cycle in the Northern Hemisphere over the past 2 decades. Global Biogeochemical Cycles, **21**, n/a-n/a.

Piao S, Sitch S, Ciais P *et al.* (2013) Evaluation of terrestrial carbon cycle models for their response to climate variability and to $CO_2$ trends. Global Change Biology, **19**.

Pincus R, Mlawer EJ, Oreopoulos L *et al.* (2015) Geophysical Research Letters Radiative flux and forcing parameterization error in aerosol-free clear skies. Geophysical Research Letters, **42**, 5485-5492.

Poulter B, Frank D, Ciais P *et al.* (2014) Contribution of semi-arid ecosystems to interannual variability of the global carbon cycle. Nature, **509**, 600-603.

Prather MJ, Holmes CD, Hsu J (2012) Reactive greenhouse gas scenarios: Systematic exploration of uncertainties and the role of atmospheric chemistry. Geophysical Research Letters, **39**, n/a-n/a.

Prentice IC, Kelley DI, Foster PN, Friedlingstein P, Harrison SP, Bartlein PJ (2011) Modeling fire and the terrestrial carbon balance. Global Biogeochemical Cycles, **25**, n/a-n/a.

Quinn Thomas R, Canham CD, Weathers KC, Goodale CL (2010) Increased tree carbon storage in response to nitrogen deposition in the US. Nature Geoscience, **3**, 13-17.

Randerson JT, Thompson MV, Conway TJ, Fung IY, Field CB (1997) The contribution of terrestrial sources and sinks to trends in the seasonal cycle of atmospheric carbon dioxide. Global Biogeochemical Cycles, **11**, 535-560.

Rap A, Scott CE, Spracklen DV *et al.* (2013) Natural aerosol direct and indirect radiative effects. Geophysical Research Letters, **40**, 3297-3301.

Rap A, Spracklen DV, Mercado L *et al.* (2015) Fires increase Amazon forest productivity through increases in diffuse radiation. 1-9.

Raupach MR, Canadell JG, Le Quéré C (2008) Anthropogenic and biophysical contributions to increasing atmospheric CO 2 growth rate and airborne fraction. Biogeosciences, **5**, 1601-1613.

Reddington CL, Butt EW, Ridley DA, Artaxo P, Morgan WT, Coe H, Spracklen DV (2015) Air quality and human health improvements from reductions in deforestation-related fire in Brazil. **8**, 1-6.

Reddington CL, Spracklen DV, Artaxo P, Ridley D, Rizzo LV, Arana A (2016) Analysis of particulate emissions from tropical biomass burning using a global aerosol model and long-term surface observations. Atmospheric Chemistry and Physics Discussions, 1-49.

Reichstein M, Bahn M, Ciais P *et al.* (2013) Climate extremes and the carbon cycle. Nature, **500**, 287-295.

Reichstein M, Falge E, Baldocchi D *et al.* (2005) On the separation of net ecosystem exchange into assimilation and ecosystem respiration: review and improved algorithm. Global Change Biology, **11**, 1424-1439.

Roderick ML, Farquhar GD, Berry SL, Noble IR (2001) On the direct effect of clouds and atmospheric particles on the productivity and structure of vegetation. Oecologia, **129**, 21-30.

Rossow WB, Schiffer RA (1999) Advances in Understanding Clouds from ISCCP. Bulletin of the American Meteorological Society, **80**, 2261-2287.

Running SW, Running SNW, Nemani RR, Heinsch FA, Zhao M, Reeves M, Hashimoto H (2004) A Continuous Satellite-Derived Measure of Global Terrestrial Primary Production. BioScience, **54**.

Ryu Y, Baldocchi DD, Kobayashi H *et al.* (2011) Integration of MODIS land and atmosphere products with a coupled-process model to estimate gross primary productivity and evapotranspiration from 1 km to global scales.

Saleska SR, Wu J, Guan K, Araujo AC, Huete A, Nobre AD, Restrepo-Coupe N (2016) Dry-season greening of Amazon forests. Nature, **531**, E4-E5.

Schimel D, Stephens BB, Fisher JB (2015) Effect of increasing $CO_2$ on the terrestrial carbon cycle. Proceedings of the National Academy of Sciences of the United States of America, **112**, 436-441.

Schmidt A, Carslaw KS, Mann GW *et al.* (2012) Importance of tropospheric volcanic aerosol for indirect radiative forcing of climate. Atmos. Chem. Phys. Atmospheric Chemistry and Physics, **12**, 7321-7339.

Schulte-Uebbing L, De Vries W (2018) Global-scale impacts of nitrogen deposition on tree carbon sequestration in tropical, temperate, and boreal forests: A meta-analysis. Global Change Biology, **24**, e416-e431.

Scott CE, Monks SA, Spracklen DV *et al.* (2018) Impact on short-lived climate forcers increases projected warming due to deforestation. Nature Communications, **9**, 157-157.

Sellers PJ, Mintz Y, Sud YC *et al.* (1986) A Simple Biosphere Model (SIB) for Use within General Circulation Models. Journal of the Atmospheric Sciences, **43**, 505-531.

Shevliakova E, Pacala SW, Malyshev S *et al.* (2009) Carbon cycling under 300 years of land use change: Importance of the secondary vegetation sink. Global Biogeochemical Cycles, **23**, n/a-n/a.

Sitch S, Friedlingstein P, Gruber N *et al.* (2015) Recent trends and drivers of regional sources and sinks of carbon dioxide. Biogeosciences, **12**, 653-679.

Sitch S, Huntingford C, Gedney N *et al.* (2008) Evaluation of the terrestrial carbon cycle, future plant geography and climate-carbon cycle feedbacks using five Dynamic Global Vegetation Models (DGVMs). Global Change Biology, **14**, 2015-2039.

Smith KW, Reed SC, Cleveland CC *et al.* (2016) Large divergence of satellite and Earth system model estimates of global terrestrial $CO_2$ fertilization. Nature Climate Change, **6**, 306-310.

Soden BJ, Wetherald RT, Stenchikov GL, Robock A (2002) Global cooling after the eruption of Mount Pinatubo: a test of climate feedback by water vapor. Science (New York, N.Y.), **296**, 727-730.

Sokolov AP, Kicklighter DW, Melillo JM *et al.* (2008) Consequences of Considering Carbon–Nitrogen Interactions on the Feedbacks between Climate and the Terrestrial Carbon Cycle. Journal of Climate, **21**, 3776-3796.

Spracklen DV, Carslaw KS, Pöschl U, Rap A, Forster PM (2011a) Global cloud condensation nuclei influenced by carbonaceous combustion aerosol. Atmos. Chem. Phys. Atmospheric Chemistry and Physics, **11**, 9067-9087.

Spracklen DV, Jimenez JL, Carslaw KS *et al.* (2011b) Aerosol mass spectrometer constraint on the global secondary organic aerosol budget. Atmos. Chem. Phys. Atmospheric Chemistry and Physics, **11**, 12109-12136.

Spracklen DV, Pringle KJ, Carslaw KS, Chipperfield MP, Mann GW (2005a) A global off-line model of size-resolved aerosol microphysics: I. Model development and prediction of aerosol properties. Atmos. Chem. Phys, **5**, 2227-2252.

Spracklen DV, Pringle KJ, Carslaw KS, Chipperfield MP, Mann GW (2005b) A global off-line model of size-resolved aerosol microphysics: II. Identification of key uncertainties. Atmospheric Chemistry and Physics, **5**, 3233-3250.

Stephens BB, Gurney KR, Tans PP *et al.* (2007) Weak Northern and Strong Tropical Land Carbon Uptake from Vertical Profiles of Atmospheric $CO_2$. Science, **316**, 1732-1735.

Sun Z (2011) Improving transmission calculations for the Edwards–Slingo radiation scheme using a correlated-k distribution method. Quarterly Journal of the Royal Meteorological Society Q. J. R. Meteorol. Soc*,* **137**, 2138-2148.

Taylor KE, Stouffer RJ, Meehl GA, Taylor KE, Stouffer RJ, Meehl GA (2012) An Overview of CMIP5 and the Experiment Design. Bulletin of the American Meteorological Society*,* **93**, 485-498.

Thornton PE, Doney SC, Lindsay K *et al.* (2009) Carbon-nitrogen interactions regulate climate-carbon cycle feedbacks: results from an atmosphere-ocean general circulation model. Biogeosciences*,* **6**.

Thornton PE, Lamarque J-F, Rosenbloom NA, Mahowald NM (2007) Influence of carbon-nitrogen cycle coupling on land model response to CO 2 fertilization and climate variability. Global Biogeochemical Cycles*,* **21**, GB4018-GB4018.

Tramontana G, Ichii K, Camps-Valls G *et al*. (2015) Uncertainty analysis of gross primary production upscaling using Random Forests, remote sensing and eddy covariance data. Remote Sensing of Environment, **168**, 360-373.

Tramontana G, Jung M, Schwalm CR *et al.* (2016) Predicting carbon dioxide and energy fluxes across global FLUXNET sites with regression algorithms. Biogeosciences*,* **13**, 4291-4313.

Van Der Werf GR, Randerson JT, Collatz GJ *et al.* (2004) Continental-Scale Partitioning of Fire Emissions During the 1997 to 2001 El Niño/La Niña Period. Science*,* **303**, 73-76.

Van Der Werf GR, Randerson JT, Giglio L *et al.* (2010) Global fire emissions and the contribution of deforestation, savanna, forest, agricultural, and peat fires (1997–2009). Atmospheric Chemistry and Physics*,* **10**, 11707-11735.

Van Der Werf GR, Randerson JT, Giglio L *et al.* (2017) Global fire emissions estimates during 1997–2016. Earth Syst. Sci. Data*,* **95194**, 697-720.

Van Donkelaar A, Martin RV, Leaitch WR *et al.* (2008) Analysis of aircraft and satellite measurements from the Intercontinental Chemical Transport Experiment (INTEX-B) to quantify long-range transport of East Asian sulfur to Canada. Atmos. Chem. Phys. Atmospheric Chemistry and Physics*,* **8**, 2999-3014.

Viovy N (2016) CRUNCEP data set. pp Page.

Vitousek PM, Howarth RW (1991) Nitrogen Limitation on Land and in the Sea: How Can It Occur? pp Page, Springer.

Walker AP, Beckerman AP, Gu L *et al.* (2014) The relationship of leaf photosynthetic traits - <i>V</i> <sub>cmax</sub> and <i>J</i> <sub>max</sub> - to leaf nitrogen, leaf phosphorus, and specific leaf area: a meta-analysis and modeling study. Ecology and Evolution*,* **4**, 3218-3235.

Wang R, Goll D, Balkanski Y *et al.* (2017) Global forest carbon uptake due to nitrogen and phosphorus deposition from 1850 to 2100. Global Change Biology*,* **23**, 4854-4872.

Wang W, Ciais P, Nemani RR *et al.* (2013) Variations in atmospheric $CO_2$ growth rates coupled with tropical temperature. Proceedings of the National Academy of Sciences of the United States of America*,* **110**, 13061-13066.

Wang X, Piao S, Ciais P *et al.* (2014) A two-fold increase of carbon cycle sensitivity to tropical temperature variations. Nature*,* **506**, 212-215.

Wårlind D, Smith B, Hickler T, Arneth A (2014) Nitrogen feedbacks increase future terrestrial ecosystem carbon uptake in an individual-based dynamic vegetation model. Biogeosciences, **11**, 6131-6146.

Weedon GP, Balsamo G, Bellouin N, Gomes S, Best MJ, Viterbo P (2014) Data methodology applied to ERA-Interim reanalysis data. Water Resources Research, **50**, 7505-7514.

Wieder WR, Cleveland CC, Smith WK, Todd-Brown K (2015) Future productivity and carbon storage limited by terrestrial nutrient availability. Nature Geoscience, **8**, 441-444.

Wigley TML (2005) The Climate Change Commitment. Science, **307**, 1766-1769.

Williams CA, Collatz GJ, Masek J, Goward SN (2012) Carbon consequences of forest disturbance and recovery across the conterminous United States. Global Biogeochemical Cycles, **26**, 1-13.

Xu Z, Hou Y, Zhang L, Liu T, Zhou G (2016) Ecosystem responses to warming and watering in typical and desert steppes. Scientific Reports, **6**, 34801-34801.

Yang F, Schlesinger ME (2001) Identification and separation of Mount Pinatubo and El Niño-Southern Oscillation land surface temperature anomalies. JOURNAL OF GEOPHYSICAL RESEARCH, **106770**, 757-714.

Zaehle S (2013) Terrestrial nitrogen-carbon cycle interactions at the global scale. Philosophical transactions of the Royal Society of London. Series B, Biological sciences, **368**, 20130125-20130125.

Zaehle S, Dalmonech D (2011) Carbon–nitrogen interactions on land at global scales: current understanding in modelling climate biosphere feedbacks. Current Opinion in Environmental Sustainability, **3**, 311-320.

Zaehle S, Friend AD (2010) Carbon and nitrogen cycle dynamics in the O-CN land surface model: 1. Model description, site-scale evaluation, and sensitivity to parameter estimates. Global Biogeochemical Cycles, **24**.

Zaehle S, Friend AD, Friedlingstein P, Dentener F, Peylin P, Schulz M (2010) Carbon and nitrogen cycle dynamics in the O-CN land surface model: 2. Role of the nitrogen cycle in the historical terrestrial carbon balance. Global Biogeochemical Cycles, **24**, GB1005-GB1005.

Zaehle S, Jones CD, Houlton B *et al.* (2015) Nitrogen Availability Reduces CMIP5 Projections of Twenty-First-Century Land Carbon Uptake*. Journal of Climate, **28**, 2494-2511.

Zaehle S, Medlyn BE, De Kauwe MG *et al.* (2014) Evaluation of 11 terrestrial carbon-nitrogen cycle models against observations from two temperate Free-Air $CO_2$ Enrichment studies. New Phytologist, **202**, 803-822.

Zhang C, Niu D, Hall SJ *et al.* (2014) Effects of simulated nitrogen deposition on soil respiration components and their temperature sensitivities in a semiarid grassland. Soil Biology and Biochemistry, **75**, 113-123.

Zhao M, Running SW (2010) Drought-Induced Reduction in Global Terrestrial Net Primary Production from 2000 Through 2009. Science, **329**, 940-943.

Zhu J, He N, Zhang J *et al.* (2017) Estimation of carbon sequestration in China's forests induced by atmospheric wet nitrogen deposition using the principles of ecological stoichiometry. Environmental Research Letters, **12**, 114038-114038.

Zhu Z, Piao S, Myneni RB *et al.* (2016) Greening of the Earth and its drivers. Nature Climate Change, **6**, 791-795.

Zhu Z, Piao S, Yan T, Ciais P, Bastos A, Zhang X, Wang Z (2018) The Accelerating Land Carbon Sink of the 2000s May Not Be Driven Predominantly by the Warming Hiatus. Geophysical Research Letters, **45**, 1402-1409.

Zscheischler J, Mahecha MD, Von Buttlar J *et al.* (2014) A few extreme events dominate global interannual variability in gross primary production. Environmental Research Letters, **9**, 35001-35013.

# Chapter 2

# Small global effect on terrestrial net primary production due to increased fossil fuel aerosol emissions from East Asia since the turn of the century

**M. O'Sullivan[1],** A. Rap[1], C. L. Reddington[1], D. V. Spracklen[1], E. Gloor[2], and W. Buermann[1]

[1]Institute for Climate and Atmospheric Science, School of Earth and Environment, University of Leeds, Leeds LS2 9JT, UK.

[2]School of Geography, University of Leeds, Leeds LS2 9JT, UK.

## Abstract

The global terrestrial carbon sink has increased since the start of this century at a time of growing carbon emissions from fossil fuel burning. Here we test the hypothesis that increases in atmospheric aerosols from fossil fuel burning enhanced the diffuse light fraction and the efficiency of plant carbon uptake. Using a combination of models, we estimate that at global scale changes in light regimes from fossil fuel aerosol emissions had only a small negative effect on the increase in terrestrial net primary production over the period

1998-2010. Hereby, the substantial increases in fossil fuel aerosol emissions and plant carbon uptake (14 TgC $yr^{-2}$) over East Asia were effectively cancelled by opposing trends across Europe (-8 TgC $yr^{-2}$) and North America (-10 TgC $yr^{-2}$). This suggests that changes in the direct/diffuse light ratio has a large impact on photosynthesis. However, if the recent increase in the land carbon sink would be causally linked to fossil fuel emissions it is unlikely via the effect of aerosols but due to other factors such as nitrogen deposition or nitrogen-carbon interactions.

## 2.1 Introduction

Fossil fuel (FF) emissions of $CO_2$ have sharply increased since the turn of the century at a rate of 3% $yr^{-1}$, almost twice the rate of the prior three decades (Hansen *et al.*, 2013). In contrast, global atmospheric $CO_2$ growth rates were relatively constant during this period (Ballantyne *et al.*, 2012). A coincident decline in land use carbon emissions (Harris *et al.*, 2012) as well as a moderate strengthening of ocean carbon uptake (Le Quéré *et al.*, 2015, Rödenbeck *et al.*, 2014) may have played a role but these contributions appear insufficient to explain the slow atmospheric growth rate of $CO_2$, implying that terrestrial carbon sinks must have substantially increased in this period (Sarmiento *et al.*, 2010).

The recent divergence of trends in carbon emissions and atmospheric $CO_2$ growth rates led to speculations that key carbon sink processes may be strongly controlled by the increasing emissions themselves, namely increased nitrogen deposition and a larger fraction of diffuse versus direct solar radiation from predominantly increased sulfate aerosol emissions originating from East Asia (Hansen *et al.*, 2013). In regards to the latter, multiple studies have shown that the efficiency of plant photosynthesis increases under more diffuse light conditions (e.g. resulting from increased scattering of light by aerosols or clouds) since under such conditions radiation can penetrate deeper into the canopy, illuminating previously shaded leaves (Gu *et al.*, 2003, Mercado *et al.*, 2009, Roderick *et al.*, 2001). However, these studies also show that a corresponding reduction in total radiation may have a negative impact upon photosynthesis, whereby GPP tends to decline if the diffuse fraction surpasses 0.4 (Mercado *et al.*, 2009). The overall effect on photosynthesis and net primary production (NPP) thus depends upon the balance between these two mechanisms. Recent model results showed that increases in the fraction of diffuse radiation due to anthropogenic aerosols in the period 1960-1999 (the global dimming period) enhanced the global carbon sink by 24% (Mercado *et al.*, 2009). The extent at which the rapid increase in East Asian FF aerosol emissions since the turn of the century may have impacted plant growth and the global carbon sink is however not clear since anthropogenic aerosol emissions in Europe and United States have decreased persistently since the late 1980s (Wild *et al.*, 2009).

Here we therefore test the hypothesis that an increase in the fraction of diffuse light associated with increased FF aerosol emissions predominantly from East Asia have contributed to increased global plant carbon uptake which would provide a mechanism for a potential link between global carbon emissions and the land carbon sink. Using atmospheric models, including an aerosol model with size-resolved aerosol microphysics, we first simulate aerosol distributions (originating from fossil fuel and fires) and corresponding effects on light regimes over 1998 to 2010. We then use these to drive a land surface model to estimate their relative contributions to changes in regional and global NPP.

## 2.2 Methodology

The distribution of anthropogenic aerosols was simulated using a global aerosol model (Mann *et al.*, 2010). The impact of aerosols and clouds on surface radiation was simulated using a radiative transfer model (Edwards & Slingo, 1996). Plant carbon uptake was simulated using a land surface model (Best *et al.*, 2011, Clark *et al.*, 2011). A similar combination of models has also been used in a recent study by Rap *et al.* (2015).

### 2.2.1 Aerosol Model

The aerosol distribution was simulated using the GLObal Model of Aerosol Processes (GLOMAP) (Mann *et al.*, 2010), which is an extension to the TOMCAT 3-D chemical transport model (Chipperfield, 2006). GLOMAP is a global aerosol microphysical model that simulates the concentration, size, and mass of aerosol particles using a two-moment (mass per particle and number concentration) modal scheme. This model includes various aerosol processes, including nucleation, condensation, growth, coagulation, dry and wet deposition, and cloud processing. In the GLOMAP version used here, the aerosol species included are black carbon (BC), particulate organic matter (POM), sulfate, sea salt, and mineral dust. The horizontal resolution is 2.8º x 2.8º, with 31 vertical levels ranging from the surface to 10hPa, with the layer thickness varying from 60 m (surface) to 1 km (tropopause). The model is driven with historical meteorology from the European Centre for Medium-Range Weather Forecasts (ECMWF) at 6-hourly intervals and interpolated onto the model time-step (30 minutes). Annually varying anthropogenic emissions (BC, organic carbon (OC), $SO_2$) including fossil fuel and biofuel emissions are taken from the MACCity inventory (Granier *et al.*, 2011). This dataset is based on historical ACCMIP (for years 1990 and 2000) and RCP 8.5 (2005 and 2010) emissions. The emissions were linearly interpolated for the years between those given. Biomass burning emissions (BC, OC, $SO_2$) are taken from the Global Fire Emissions Database version 3 (GFED3) (van der Werf *et al.*, 2010) and are supplied as annually varying monthly means.

GLOMAP has been evaluated extensively in previous work and generally found to match ground-based station observations (e.g. AERONET) well (Mann *et al.*, 2010, Rap *et al.*, 2015, Reddington *et al.*, 2016, Reddington *et al.*, 2014). In this study, we compared trends in simulated aerosol optical depth (AOD) with satellite-based (MODIS, SeaWiFS) estimates for the period of overlapping data records 2001-2010. Results showed generally good agreement between the modelled and observed AOD trends specifically in areas where fossil fuel emissions dominate the AOD trends (Figure 2.1 and Figures B1-B3 in the supporting information). In this study we are interested in trends in AOD driven by changing anthropogenic aerosol emissions. To exclude a contamination from dust, we calculate AOD only for the 4 aerosol size modes (aitken-soluble, aitken-insoluble, accumulation-soluble, and coarse-soluble) that do not include dust. We demonstrated that satellite aerosol trends are similar both during periods with and without a large contribution from dust in East Asia (Figure B1), demonstrating that observed trends are not due to trends in dust.

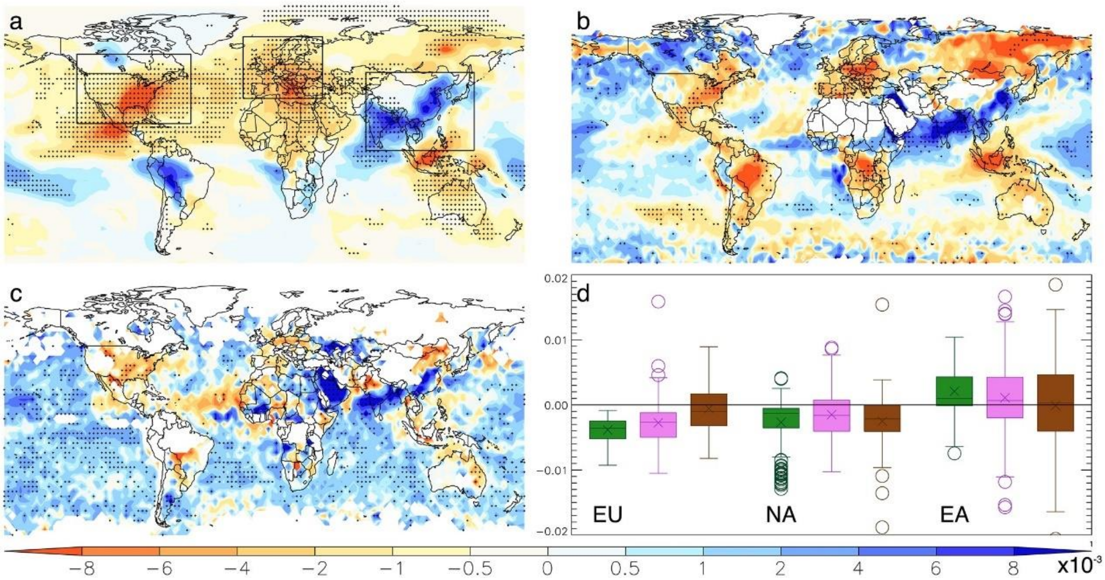

**Figure 2.1 - Comparison between modeled and satellite annual mean AOD trends (year-1) for the period of overlapping data records 2001–2010. Panels depict linear trends for (a) GLOMAP, (b) MODIS, and (c) SeaWiFS. (d) Linear trends in AOD (year-1) between 2001 and 2010 are shown for the three focus regions (outlined in Figure 2.1a; land points only): Europe (EU), North America (NA), and East Asia (EA) based on GLOMAP (green), MODIS (violet), and SeaWiFS (brown). The crosses represent the mean trend, the middle bars the median, the boxes the 25th and 75th percentile values, and the error bars the minimum and maximum values with circles representing outliers (greater than 1.5 times interquartile range). White areas in Figures 2.1b and 2.1c indicate regions where satellite retrievals were not available, and in all maps statistically significant ($P<0.05$; Student's t-test) trends are highlighted with stippling. Spatial resolutions in the original data sets differ between modeled (2.8°) and satellite (MODIS (1.0°) and SeaWiFS (0.5°)), and for this comparison the satellite AOD fields were aggregated to the coarser model resolution.**

### 2.2.2 Radiative transfer model

The Edwards and Slingo (1996) radiative transfer model is used to quantify the aerosol effect on direct and diffuse radiation (Rap *et al.*, 2013). We used the aerosol optical properties (scattering, absorption, and asymmetry coefficients) for each aerosol mode and spectral band based on Bellouin *et al.* (2013). The model is forced with monthly mean ECMWF climate (water vapour, temperature) and ozone reanalysis data together with cloud fields and surface albedo from the International Satellite Cloud Climatology Project (ISCCP-D2) (Rossow & Schiffer, 1999). The simulated total and direct radiation fluxes are used to calculate diffuse radiation (diffuse = total – direct). Due to the uncertainty in aerosol-cloud interactions we do not allow changes in aerosol to alter cloud properties (aerosol indirect effect). The Edwards-Slingo (ES) model has been validated in recent studies to some extent (e.g. Rap *et al.* (2015)). We performed additional validations at four FluxNet sites in Europe and North America and found reasonable model performance (Figures B4 and B5).

### 2.2.3 Land surface model

The Joint UK Land Environment Simulator (JULES) land surface model used here simulates the exchange of carbon, water, energy and momentum between the land surface and atmosphere (Best *et al.*, 2011, Clark *et al.*, 2011). The model includes a multilayer (10 levels) canopy parameterization to scale photosynthesis from leaf to the canopy (Mercado *et al.*, 2009, Mercado *et al.*, 2007). Photosynthesis is calculated at each level, and treats sunlit and shaded leaves separately. In our simulations, we used the dynamic phenology (TRIFFID) version of JULES. To ensure the plant pools and NPP are at steady state, the model was spun up for 60 years (10 in equilibrium mode and 50 in dynamical mode (see *Cox (2001)*) using a repeated driver climatology for 1995. The control simulation was then run with transient driving input for 1996-1998, providing a steady-state to start our simulations from. The model is forced with ERA-Interim climate fields (Weedon *et al.*, 2014), and runs at 0.5° spatial resolution with three hourly time steps. The climate drivers consist of 2m air temperature, specific humidity, precipitation, 10m wind speed and surface pressure. Model drivers also include downwards surface radiation (short-wave direct and diffuse, long-wave) from the ES model. The JULES plant carbon uptake response to changes in solar radiation has also been validated to some extent at temperate needleleaf and broadleaf forest sites (Mercado *et al.*, 2009) and in tropical rainforests (Rap *et al.*, 2015). We conducted further validations at the same four FluxNet sites that were used in the ES validations (see above). Also in this case, the modelled GPP responses to increases in PAR under both total and diffuse light regimes agree generally well with observed responses (Figure B6).

We performed a set of factorial simulations with JULES over the period 1998-2010 to isolate the impact of single drivers on NPP. The five drivers considered include (1) climate, (2) atmospheric $CO_2$, and incoming solar radiation due to aerosols associated with (3) anthropogenic emissions, (4) fire emissions as well as (5) cloud cover. We started with a 'control' simulation in which only climate variables were varied and anthropogenic and fire aerosol emissions remained at year 2000 values to avoid the anomalous 1998 ENSO year and atmospheric $CO_2$ was held fixed at 1998 levels whereas cloud cover was based on a climatology for whole study period 1998-2010. Four additional simulations were carried out whereby in each simulation one additional driver was varied, so that our final simulation had monthly varying fire emissions and cloud cover for the whole period and anthropogenic emissions and the atmospheric $CO_2$ level varied annually. We first calculated the trend (based on linear regression) in annual AOD, surface diffuse radiation (SDR), and NPP for each simulation. The climate effect and combined effect can be inferred directly from the first (only climate varied) and last (all drivers varied) model runs. To isolate the impact of the remaining single drivers, the difference between the trends of two simulations that only differ by that driver was used.

## 2.3 Results

The simulated impact of anthropogenic aerosol emissions on AOD and SDR from 1998 to 2010 is shown in Figure 2.2. As anticipated, AOD changes were largest in regions of significant FF aerosol emission change over this period. For example, East Asia show substantial increases in AOD and SDR coinciding with increasing anthropogenic aerosol and aerosol precursor emissions (Granier *et al.*, 2011). In contrast, Europe and North America experienced declining AOD and SDR trends driven by a reduction in FF aerosol emissions (Figure 2.2, Table 2.1 and Figure B3). The spatial distribution of these trends in AOD and SDR are greatest close to the vicinity of the respective source regions, although changes extend for thousands of km due to atmospheric transport of the aerosols. Our results also show that changes in fossil fuel aerosol emissions play an important role in the AOD trends compared to natural (e.g. sea spray) and fire induced changes in all three regions of interest (Figure B1). A subsequent analysis that isolates the contribution of each factor (FF, fire, and clouds) to trends in SDR further confirms this result, with fossil fuel burning also dominating the trend in the three focus regions of East Asia, Europe and North America (Figure B7).

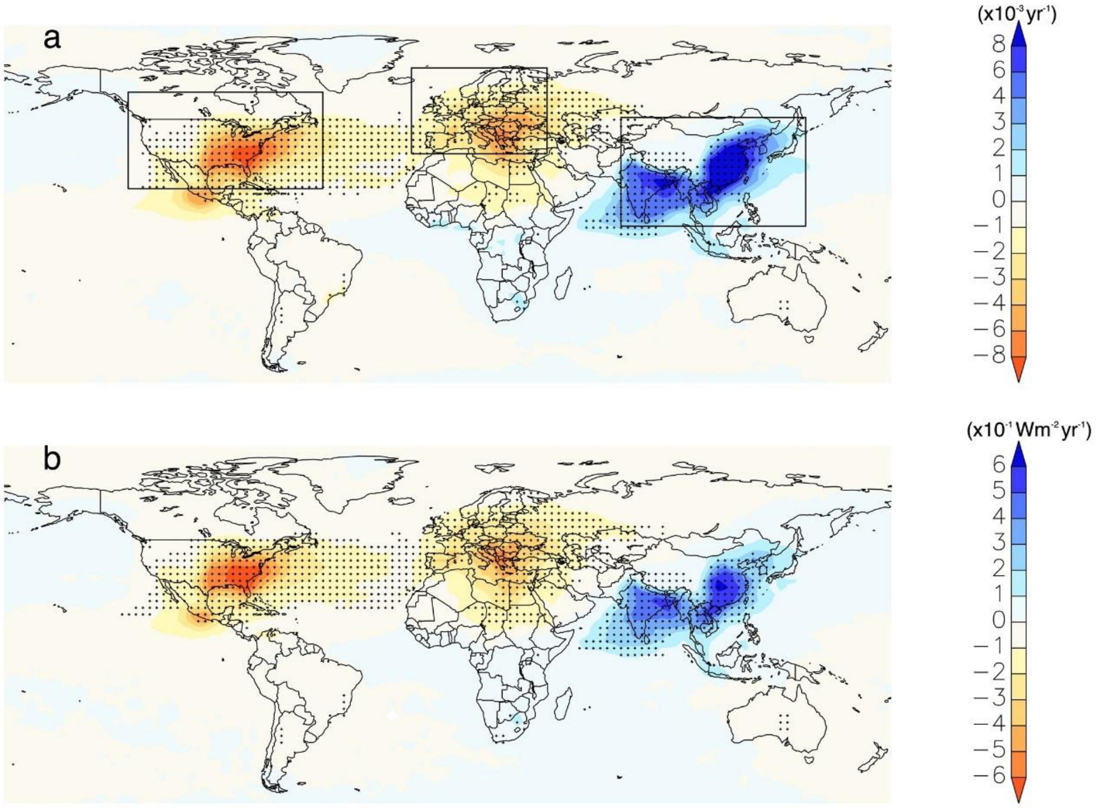

**Figure 2.2 - Spatial pattern of linear trends in simulated annual (a) AOD and (b) SDR due to changes in fossil fuel aerosol emissions over the period 1998–2010. In Figures 2.2a and 2.2b, trends are calculated as the difference in the trends based on two single simulations, with varying anthropogenic aerosol emissions as the only difference between the two (see section 2.2). Statistically significant (P<0.05) trends are highlighted with stippling.**

**Table 2.1 - Trends in AOD, SDR, and NPP over the period 1998-2010 for global land and three focus regions. The linear trends shown are based on simulations in which all drivers are varied and where the effect of FF aerosol emissions is isolated (in parentheses). The three focus regions (only land areas) are outlined in Figure 2.2a and number of asterisks indicate statistical significance of trends at P<0.05 (*), P<0.01(**) and P<0.001 (***) levels, respectively.**

| Region | AOD ($yr^{-1}$) | SDR ($W\ m^{-2}\ yr^{-1}$) | NPP ($TgC\ yr^{-2}$) |
|---|---|---|---|
| East Asia | 0.0037*** (0.0035***) | 0.31** (0.21***) | 44.13* (14.44) |
| Europe | -0.0052*** (-0.0050***) | -0.56*** (-0.47***) | 19.10 (-8.09) |
| North America | -0.0021*** (-0.0021***) | -0.16 (-0.18***) | 17.32 (-9.78) |
| Global | -0.0002 (-0.0001) | -0.002 (-0.03) | 140.13 (-6.82) |

A factorial analysis based on multiple runs with the JULES land surface model (see Methods) was used to quantify the contribution of single drivers (changes in light regimes due to FF and fire emissions as well as changes in cloud cover, in addition to changes in near-surface climate and increased atmospheric $CO_2$ concentrations) to the trend in NPP in the study period 1998-2010. Results show that the spatial patterns in the overall NPP trends (Figure 2.3a) were generally dominated by trends in near-surface climate (Figure 2.3b and Figure B8). In this regard, warming across northern Eurasia and cooling across Canada appeared to be responsible for the pronounced positive and negative NPP trends in these regions, respectfully (Figure 2.3b and Figure B9). Over many land regions outside the northern high latitudes, trends in precipitation appeared to be the dominant driver for trends in NPP (Figure 2.3b and Figure B9).

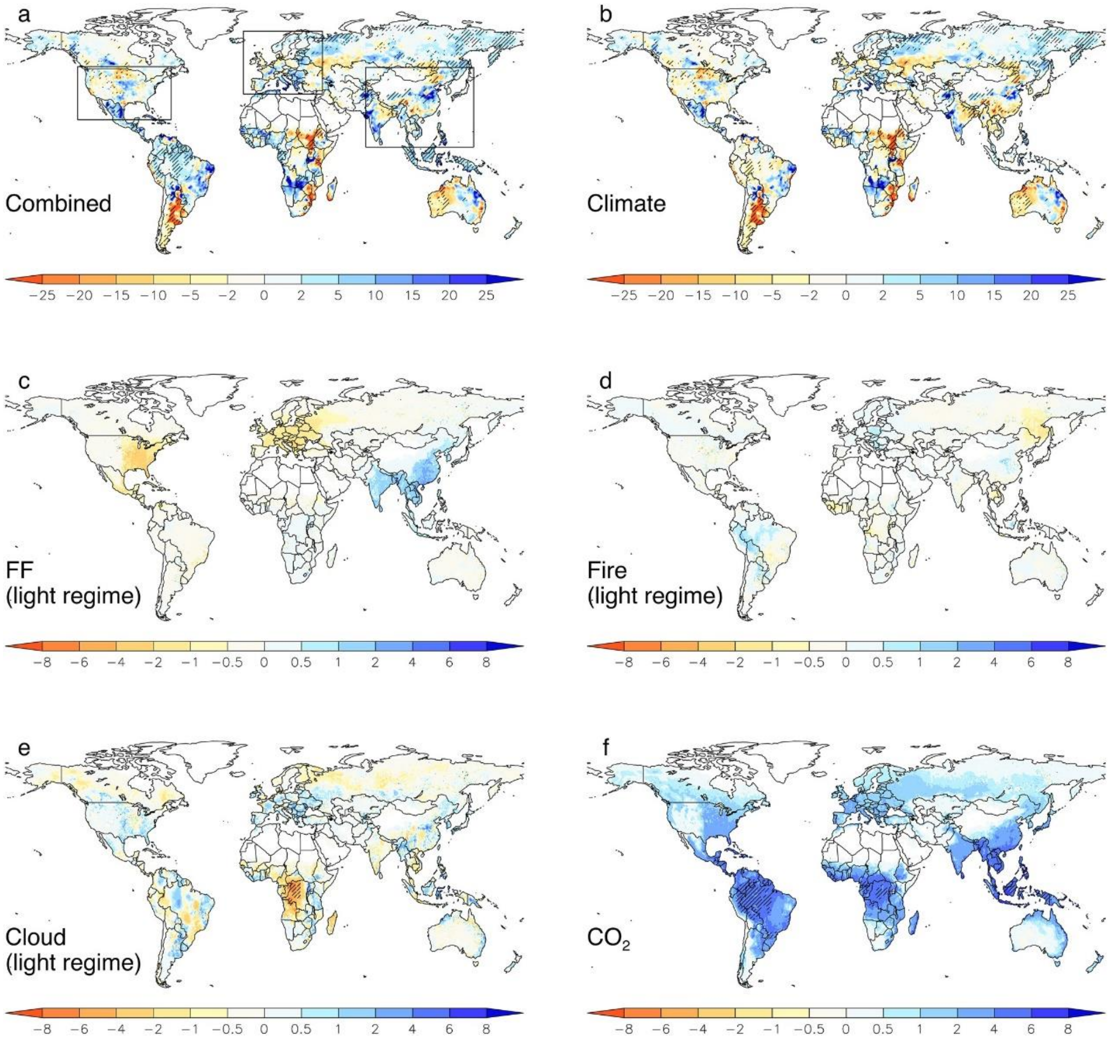

**Figure 2.3 - Spatial pattern of linear trends (gCm$^{-2}$yr$^{-2}$) in annual NPP for the period 1998–2010. The maps depict trends in NPP based on factorial JULES simulations with (a) all drivers varied and corresponding to single drivers including (b) climate, as well as light regimes associated with (c) fossil fuel aerosol emissions, (d) fire aerosol emissions, and (e) cloud cover. (f) Trends in NPP associated with atmospheric CO$_2$. Statistically significant ($P<0.05$) trends are highlighted with stippling.**

At more regional levels, changes in SDR associated with FF aerosols had a sizeable impact on trends in NPP in East Asia, Europe, and Eastern USA (Figure 2.3c) broadly in line with the spatial pattern of the corresponding AOD and SDR trends (Figure 2.2). Changes in NPP due to trends in SDR resulting from changes in fire emissions and cloud cover were of similar magnitude but displayed a more heterogeneous pattern across the continents (Figures 2.3d and 2.3e). Over central African rainforests, a relatively strong cloud cover – SDR effect was observed, where a reduction in SDR associated with a strong trend towards lower cloud cover (Figure B7) led to markedly lower NPP. Conversely, and as expected, the $CO_2$ fertilization effect (Figure 2.3f) led to consistent increases in NPP across most of the vegetated land surface, with the largest impact in the highly productive tropics.

In Figure 2.4, regionally aggregated and global contributions from each single driver to the overall NPP trends over the 1998-2010 study period are shown. Corresponding results show that over East Asia, changes in climate (negative contribution) as well as atmospheric $CO_2$ (positive) were the most dominant drivers of trends in NPP (Figure 2.4a). However, increases in SDR due to increasing FF aerosol emissions caused a sizeable positive NPP trend (14 TgC $yr^{-2}$; see also Table 2.1), which amounted to a substantial proportion (33%) of the total positive NPP trend over this region. In Europe and North America, changes in climate and atmospheric $CO_2$ were generally also the dominant drivers of NPP changes, whereas declining SDR (from decreasing FF aerosol emissions) led to significant negative contributions to the overall NPP trends (Figure 2.4b and 2.4c; Table 2.1). At global scale, we estimated an overall increasing NPP trend of 0.14 PgC $yr^{-2}$ over the study period 1998-2010 with changes in atmospheric $CO_2$ (0.25 PgC $yr^{-2}$) and near-surface climate (-0.09 PgC $yr^{-2}$) playing a dominant role (Figure 2.4d). At this global level, the aerosol radiative effects from changes in FF emissions are relatively small (-6.8 TgC $yr^{-2}$, -4.9% of total NPP trend) since the increasing contributions over East Asia are effectively cancelled out by the declining contributions from Europe and North America.

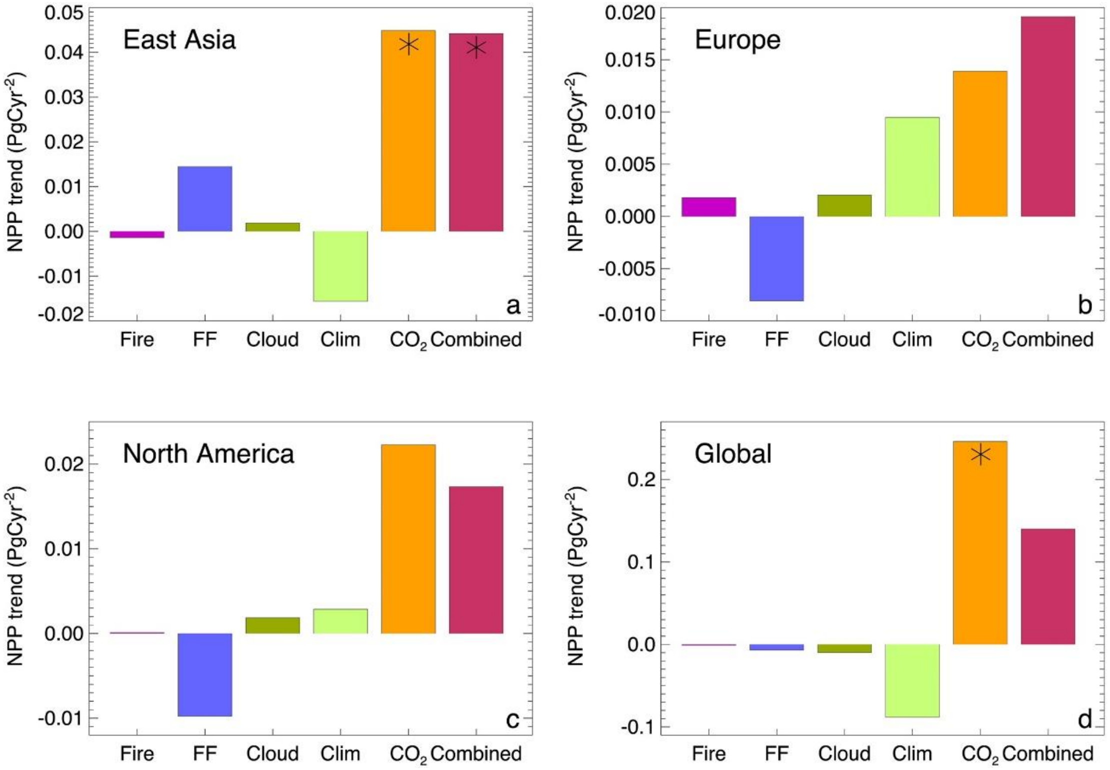

**Figure 2.4 - Global, regional, and mechanistic attribution of trends in annual NPP for the period 1998–2010. Trends are based on annual means of spatially aggregated NPP for the three focus regions (a) East Asia, (b) Europe, and (c) North America as well as for (d) all land regions. The three focus regions are depicted in Figure 2.3a. Statistically significant ($P < 0.05$) trends are highlighted (asterisk).**

## 2.4 Discussion

Our results suggest that the simulated increase in global NPP (0.14 PgC yr$^{-2}$) over the period 1998 to 2010 is largely driven by increasing atmospheric $CO_2$, through a combination of direct $CO_2$ fertilization and the indirect effects of improved water use efficiency in line with previous model studies (Schimel *et al.*, 2015, Sitch *et al.*, 2015). The dominant contribution of the $CO_2$ fertilization effect on trends in NPP should however be viewed with caution as more recent studies showed that land surface models may overestimate corresponding impacts considerably (Brienen *et al.*, 2015, Smith *et al.*, 2016). At the global scale, climatic trends over this period contributed negatively to changes in global NPP consistent with results based on a more data-constrained approach (Zhao & Running, 2010).

Radiative effects associated with aerosol emissions from FF and fire activity and those related to clouds on trends in NPP played only a minor role at global scale. Our results however do show that at more regional levels, FF aerosol emissions and corresponding effects on diffuse radiation are potent drivers of NPP changes, particularly over East Asia where they contribute 33% to the total NPP trend. In this region, the recent trend in fossil fuel aerosol emissions are mainly driven by increases in coal burning and associated sulfate aerosols (Granier *et al.*, 2011, Lu *et al.*, 2010). Our results must be viewed with some caution since for example we did not consider potential adverse effects of acidic sulfate deposition on NPP (Büntgen *et al.*, 2014). But one important inference is that due to the importance of this 'FF aerosol driver' and the relatively short atmospheric lifetime of aerosols (days to weeks), a decline in regional-scale FF aerosols (e.g. through implementing more strict air pollution standards) may reduce NPP and net carbon uptake substantially at relatively short time scales.

Our findings presented here thus indicate that the marked post-2000 increase in the global land carbon sink may not be explained by changes in light regimes resulting from coincident changes in fossil fuel aerosol emissions and corresponding effects on NPP. This is to a large part a result of the opposing contributions from Asia and from Europe and North America leading to a relatively small global impact. This opens the door for investigations of alternative carbon sink mechanisms that are causally linked to increasing FF emissions. In this regard, nitrogen deposition may act as a potent driver through both its direct effect on photosynthesis, plant respiration and soil respiration (Zaehle, 2013) as well as indirectly through easing nutrient constraints for NPP enhancements via the $CO_2$ fertilization effect (Norby *et al.*, 2010). In addition, decadal climatic trends that are largely independent of FF emission trajectories may induce strong impacts on NPP (as shown here) and also on plant and soil respiration. In this regard, the recent 'hiatus' in global temperatures (IPCC, 2013) may have reduced respiratory carbon fluxes thereby contributing to the enhanced land carbon sink in this time frame.

## Acknowledgements

We gratefully acknowledge funding for this study through a EU Marie Curie Integration grant (CIG PCIG14-GA-2013- 631812) to W.B. This work used eddy covariance data acquired by the FLUXNET community and in particular by the AmeriFlux and CarboEuropeIP networks. AmeriFlux was supported by the U.S. Department of Energy, Biological and Environmental Research, Terrestrial Carbon Program (grants DE-FG02-04ER63917, DE-FG02-04ER63911, and DE-SC0006708). We acknowledge financial support of the eddy covariance data harmonization provided by CarboEuropeIP, FAO-GTOS-TCO, iLEAPS, the Max-Planck Institute for Biogeochemistry, National Science Foundation, University of Tuscia, Université Laval and Environment Canada, and U.S. Department of Energy and of the database development and technical support from Berkeley Water Center, Lawrence Berkeley National Laboratory, Microsoft Research eScience, Oak Ridge National Laboratory, University of California-Berkeley, and University of Virginia. This work was supported by the Natural Environment Research Council (grant numbers NE/J004723/1 and NE/J009822/1).

## References

Ballantyne AP, Alden CB, Miller JB, Tans PP, White JWC (2012) Increase in observed net carbon dioxide uptake by land and oceans during the past 50 years. Nature*,* **488**, 70-72.

Bellouin N, Mann GW, Woodhouse MT, Johnson C, Carslaw KS, Dalvi M (2013) Impact of the modal aerosol scheme GLOMAP-mode on aerosol forcing in the Hadley Centre Global Environmental Model. Atmos. Chem. Phys*,* **13**, 3027-3044.

Best MJ, Pryor M, Clark DB *et al.* (2011) The Joint UK Land Environment Simulator (JULES), model description. Part 1: Energy and water fluxes. Geoscientific Model Development*,* **4**, 677-699.

Brienen RJW, Phillips OL, Feldpausch TR *et al.* (2015) Long-term decline of the Amazon carbon sink. Nature*,* **519**, 344-348.

Büntgen U, Tegel W, Kaplan JO *et al.* (2014) Placing unprecedented recent fir growth in a European-wide and Holocene-long context. Frontiers in Ecology and the Environment*,* **12**, 100-106.

Chipperfield MP (2006) New version of the TOMCAT/SLIMCAT off-line chemical transport model: Intercomparison of stratospheric tracer experiments. Quarterly Journal of the Royal Meteorological Society*,* **132**, 1179-1203.

Clark DB, Mercado LM, Sitch S *et al.* (2011) The Joint UK Land Environment Simulator (JULES), model description. Part 2: Carbon fluxes and vegetation dynamics. pp Page.

Cox PM (2001) Description of the TRIFFID dynamic global vegetation model, Hadley Centre Technical Note 24, Hadley Centre, Met Office, Bracknell, UK.

Edwards JM, Slingo A (1996) Studies with a flexible new radiation code. I: Choosing a comnfiguration for a large-scale model. Quarterly Journal of the Royal Meteorological Society*,* **122**, 689-719.

Granier C, Bessagnet B, Bond T *et al.* (2011) Evolution of anthropogenic and biomass burning emissions of air pollutants at global and regional scales during the 1980–2010 period. Climatic Change*,* **109**, 163-190.

Gu L, Baldocchi DD, Wofsy SC, Munger JW, Michalsky JJ, Urbanski SP, Boden T (2003) Response of a Deciduous Forest to the Mount Pinatubo Eruption: Enhanced Photosynthesis. Science*,* **299**, 2035-2038.

Hansen J, Kharecha P, Sato M (2013) Climate forcing growth rates: doubling down on our Faustian bargain. Environmental Research Letters*,* **8**, 011006-011006.

Harris NL, Brown S, Hagen SC *et al.* (2012) Baseline map of carbon emissions from deforestation in tropical regions. Science (New York, N.Y.)*,* **336**, 1573-1576.

IPCC (2013) Climate Change 2013: The Physical Science Basis. Contribution of Working Group I to the Fifth Assessment Report of the Intergovernmental Panel on Climate Change [Stocker, T.F., D. Qin, G.-K. Plattner, M. Tignor, S.K. Allen, J. Boschung, A. Nauels, Y. Xia, V. Bex and P.M. Midgley (eds.)]. Cambridge University Press, Cambridge, United Kingdom and New York, NY, USA, 1535 pp.

Le Quéré C, Moriarty R, Andrew RM *et al.* (2015) Global carbon budget 2014. Earth System Science Data*,* **7**, 47-85.

Lu Z, Streets DG, Zhang Q *et al.* (2010) Sulfur dioxide emissions in China and sulfur trends in East Asia since 2000. Atmospheric Chemistry and Physics*,* **10**, 6311-6331.

Mann GW, Carslaw KS, Spracklen DV *et al.* (2010) Description and evaluation of GLOMAP-mode: a modal global aerosol microphysics model for the UKCA composition-climate model. Geoscientific Model Development Discussions*,* **3**, 651-734.

Mercado LM, Bellouin N, Sitch S, Boucher O, Huntingford C, Wild M, Cox PM (2009) Impact of changes in diffuse radiation on the global land carbon sink. Nature*,* **458**, 1014-1017.

Mercado LM, Huntingford C, Gash JHC, Cox PM, Jogireddy V (2007) Improving the representation of radiation interception and photosynthesis for climate model applications. Tellus, Series B: Chemical and Physical Meteorology*,* **59**, 553-565.

Norby RJ, Warren JM, Iversen CM, Medlyn BE, Mcmurtrie RE (2010) $CO_2$ enhancement of forest productivity constrained by limited nitrogen availability. Proceedings of the National Academy of Sciences of the United States of America*,* **107**, 19368-19373.

Rap A, Scott CE, Spracklen DV *et al.* (2013) Natural aerosol direct and indirect radiative effects. Geophysical Research Letters*,* **40**, 3297-3301.

Rap A, Spracklen DV, Mercado L *et al.* (2015) Fires increase Amazon forest productivity through increases in diffuse radiation. 1-9.

Reddington CL, Spracklen DV, Artaxo P, Ridley D, Rizzo LV, Arana A (2016) Analysis of particulate emissions from tropical biomass burning using a global aerosol model and long-term surface observations. Atmospheric Chemistry and Physics Discussions, 1-49.

Reddington CL, Yoshioka M, Balasubramanian R, Ridley D, Toh YY, Arnold SR, Spracklen DV (2014) Contribution of vegetation and peat fires to particulate air pollution in Southeast Asia. Environmental Research Letters, **9**, 094006-094006.

Rödenbeck C, Bakker DCE, Metzl N *et al.* (2014) Interannual sea–air CO&lt;sub&gt;2&lt;/sub&gt; flux variability from an observation-driven ocean mixed-layer scheme. Biogeosciences, **11**, 4599-4613.

Roderick ML, Farquhar GD, Berry SL, Noble IR (2001) On the direct effect of clouds and atmospheric particles on the productivity and structure of vegetation. Oecologia, **129**, 21-30.

Rossow WB, Schiffer RA (1999) Advances in Understanding Clouds from ISCCP. Bulletin of the American Meteorological Society, **80**, 2261-2287.

Sarmiento JL, Gloor M, Gruber N *et al.* (2010) Trends and regional distributions of land and ocean carbon sinks. Biogeosciences, **7**, 2351-2367.

Schimel D, Stephens BB, Fisher JB (2015) Effect of increasing $CO_2$ on the terrestrial carbon cycle. Proceedings of the National Academy of Sciences of the United States of America, **112**, 436-441.

Sitch S, Friedlingstein P, Gruber N *et al.* (2015) Recent trends and drivers of regional sources and sinks of carbon dioxide. Biogeosciences, **12**, 653-679.

Smith KW, Reed SC, Cleveland CC *et al.* (2016) Large divergence of satellite and Earth system model estimates of global terrestrial $CO_2$ fertilization. Nature Climate Change, **6**, 306-310.

Van Der Werf GR, Randerson JT, Giglio L *et al.* (2010) Global fire emissions and the contribution of deforestation, savanna, forest, agricultural, and peat fires (1997–2009). Atmospheric Chemistry and Physics, **10**, 11707-11735.

Weedon GP, Balsamo G, Bellouin N, Gomes S, Best MJ, Viterbo P (2014) Data methodology applied to ERA-Interim reanalysis data. Water Resources Research, **50**, 7505-7514.

Wild M, Trussel B, Ohmura A, Long CN, Konig-Langlo G, Dutton EG, Tsvetkov A (2009) Global dimming and brightening: An update beyond 2000. Journal of Geophysical Research Atmospheres, **114**, 1-14.

Zaehle S (2013) Terrestrial nitrogen-carbon cycle interactions at the global scale. Philosophical transactions of the Royal Society of London. Series B, Biological sciences, **368**, 20130125-20130125.

Zhao M, Running SW (2010) Drought-Induced Reduction in Global Terrestrial Net Primary Production from 2000 Through 2009. Science, **329**, 940-943.

# Chapter 3

# Have synergies between nitrogen deposition and atmospheric $CO_2$ driven the recent enhancement of the terrestrial carbon sink?

**Michael O'Sullivan[1],** Dominick V. Spracklen[1], Sarah A. Batterman[2], Steve R. Arnold[1], Manuel Gloor[2] and Wolfgang Buermann[1]

[1]Institute for Climate and Atmospheric Science, School of Earth and Environment, University of Leeds, Leeds, UK

[2]School of Geography, University of Leeds, Leeds, UK

## Abstract

The terrestrial carbon sink has increased since the turn of this century at a time of increased fossil fuel burning, yet the mechanisms enhancing this sink are not fully understood. Here, we assess the hypothesis that regional increases in nitrogen deposition since the early 2000s has alleviated nitrogen limitation and worked in tandem with enhanced $CO_2$ fertilization to increase ecosystem productivity and carbon sequestration providing a causal link between the parallel increases in emissions and the global land carbon sink. We use the Community Land Model (CLM4.5-BGC) to estimate the influence of changes in atmospheric $CO_2$, nitrogen deposition, climate, and their interactions to changes in net primary production (NPP), and net biome production (NBP). We focus on two periods, 1901-2016 and 1990-2016 to estimate changes in land carbon

fluxes relative to historical and contemporary baselines, respectively. We find that over the historical period nitrogen deposition (14%) and carbon-nitrogen synergy (14%) were significant contributors to the current terrestrial carbon sink, suggesting that long-term increases in nitrogen deposition led to a substantial increase in $CO_2$ fertilization. However, relative to the contemporary baseline, changes in nitrogen deposition and carbon-nitrogen synergy had no substantial contribution to the 21st century increase in global carbon uptake. Nonetheless, we find that increased nitrogen deposition in East Asia since the early 1990s contributed 50% to the overall increase in NBP over this region, highlighting the importance of carbon-nitrogen interactions. Therefore, potential large-scale changes in nitrogen deposition could have a significant impact on terrestrial carbon cycling and future climate.

## 3.1 Introduction

Fossil fuel $CO_2$ emissions have rapidly increased since the turn of this century, at rates almost doubling those of the previous three decades (Hansen *et al.*, 2013). Annual growth rates of atmospheric $CO_2$ have been, somewhat surprisingly, relatively low during this period which may imply that the global carbon sink has considerably strengthened (Ballantyne *et al.*, 2012, Keenan *et al.*, 2016). During the same epoch there is also evidence of a decrease in land use and land cover change (LULCC) emissions (Houghton *et al.,* 2012, Le Quéré *et al.*, 2018) and a parallel increase in the strength of the ocean carbon sink (DeVries *et al.*, 2017, Le Quéré *et al.*, 2018, Rödenbeck *et al.*, 2014), but both of these trends appear insufficient to account for the low growth of atmospheric $CO_2$ (Le Quéré *et al.*, 2018). As a result, the terrestrial carbon sink (estimated as the 'residual' in the global carbon budget (Le Quéré *et al.*, 2016)) does exhibit a sharp increase since the early 2000s. An increasing terrestrial carbon sink since the early 2000s is also consistent with independent lines of evidence based on forest inventories (Pan *et al.*, 2011), and process-based modelling studies (eg. Le Quéré *et al.* (2018)).

Various observation-based (Clark *et al.*, 2013, Los, 2013, Norby *et al.*, 2005, Terrer *et al.*, 2016) and modelling (Cheng *et al.*, 2017, Keenan *et al.*, 2016, Schimel *et al.*, 2015, Sitch *et al.*, 2015, Zhu *et al.*, 2016) studies have highlighted the role elevated $CO_2$ levels have on photosynthesis and water-use efficiency in explaining the increase in the terrestrial carbon sink over recent decades. Schimel *et al.* (2015) estimated that 60% of the contemporary (1990-2007) terrestrial sink is due to increased atmospheric $CO_2$ concentrations. However, if increased plant carbon uptake via the $CO_2$ fertilization effect alone was the main driver behind the increase in global net carbon uptake since the turn of this century, we would expect a more transient increase over time (in line with gradual changes in atmospheric $CO_2$ concentrations) than what is observed. Further, the strength of the $CO_2$ fertilization effect based on carbon cycle simulations has been disputed by others, arguing that models tend to overestimate this effect (Gerber *et al.*, 2013, Gerber *et al.*, 2010, Hungate *et al.*, 2003, Huntzinger *et al.*, 2017, Smith *et al.*, 2016, Wieder *et al.*, 2015) because they neglect important processes (e.g. role of colimitation by nutrients) that potentially limit the $CO_2$ fertilization effect.

Nitrogen availability may constrain the response of ecosystem productivity to rising levels of atmospheric $CO_2$ (Bonan & Levis, 2010, Churkina *et al.*, 2009, Norby *et al.*, 2010, Thornton *et al.*, 2007, Zaehle, 2013, Zaehle & Dalmonech, 2011) via its role as an essential plant nutrient that constrains productivity globally (LeBauer & Treseder, 2008, Vitousek & Howarth, 1991). Nitrogen has been found to be particularly important for plant productivity in mid- and high-latitudes, but may also be important in tropical regions (Elser *et al.*, 2007, Fisher *et al.*, 2012, LeBauer & Treseder, 2008). Any additional nitrogen added to the terrestrial biosphere, could therefore enhance carbon storage directly by alleviating nitrogen limitation on plant productivity and indirectly by permitting a further plant response to $CO_2$ fertilization (referred to as carbon-nitrogen synergy). Synergistic effects can arise when high $CO_2$ concentrations bring about nitrogen limitation, which is alleviated by concurrent rises in nitrogen deposition. Recent studies indicate enhanced terrestrial carbon uptake in the range of 0.2-0.5 PgC/yr (Churkina *et al.*, 2009, Liu & Greaver, 2009, Wang *et al.*, 2017, Zaehle, 2013) due to the direct effect of increased terrestrial nitrogen deposition from anthropogenic activities (~30 TgN/yr in 1850 to ~80 TgN/yr presently (Kanakidou *et al.*, 2016)). This enhancement of terrestrial carbon uptake would be equivalent to 10-20% of the total modern carbon sink. Since 1860, humans have doubled nitrogen inputs to the biosphere predominately through fossil fuel burning and agricultural intensification (Galloway *et al.*, 2004, Gruber & Galloway, 2008). Over the last two decades the trends of nitrogen emissions and subsequent deposition have differed regionally. East Asian deposition has increased substantially (Jia *et al.*, 2016, Jia *et al.*, 2014, Liu *et al.*, 2013), whereas European (Banzhaf *et al.*, 2015, de Vries & Posch, 2011, Waldner *et al.*, 2014) and North American (Du *et al.*, 2014) nitrogen deposition is thought to have decreased during this time.

The influence of climate variability (via alterations in temperature, precipitation, cloudiness, seasonal pattern) on changes in terrestrial carbon fluxes and storage may also be substantial (Ahlstrom *et al.*, 2015, Baldocchi *et al.*, 2016, Cox *et al.*, 2013, Frank *et al.*, 2015, Reichstein *et al.*, 2013). The recent "warming hiatus" (1998-2013) was identified as a potential key mechanism behind the increased land sink during this period via reduced ecosystem respiration (Ballantyne *et al.*, 2017). Hansen *et al.* (2013) speculated that the parallel increase in global fossil fuel emission and the land carbon sink since the turn of this century maybe a result of carbon uptake mechanisms that are controlled by the emissions themselves, namely a larger fraction of diffuse solar radiation from increased sulfate aerosol emissions, and increased nitrogen deposition. However, the "diffuse radiation" mechanism has been shown to play only a minor role at global scale (O'Sullivan *et al.*, 2016). Alternatively, the concurrent rise in both anthropogenic carbon and nitrogen emissions (predominantly from East Asia) could have worked in tandem to fertilize the terrestrial biosphere via a combination of direct fertilization by increased nitrogen deposition along with an increased $CO_2$ fertilization effect due to alleviation of nitrogen limitation. The latter synergistic effect can be observed in ecosystems co-limited by various factors, which when relieved together lead to a strong synergistic response (de Vries *et al.*, 2014, de Vries *et al.*, 2009, Finzi *et al.*, 2007).

In this study, we investigated the hypothesis that the parallel increases in fossil fuel emissions and the land carbon sink since the turn of this century are causally linked through the individual and synergistic effects of increased atmospheric $CO_2$ concentrations and nitrogen deposition on ecosystem productivity. We used a process-based model of the terrestrial biosphere with fully interactive carbon-nitrogen cycling. We analysed sets of factorial simulations for two different periods (1900-2016 and 1990-2016) in order to quantify the effects of various model drivers ($CO_2$, nitrogen, and climate) relative to historical and contemporary baselines.

## 3.2 Methodology

### 3.2.1 Model description

For this study, we used the Community Land Model version 4.5 (CLM4.5-BGC), which simulates biophysical, hydrological, and biogeochemical exchange processes between the land and the atmosphere (Oleson *et al.*, 2013). CLM4.5-BGC is fully prognostic with regards to carbon and nitrogen state variables in the vegetation, litter, and soil organic matter pools. The model also prognostically simulates the seasonal cycle of vegetation growth/decay, leaf area index (LAI), and vegetation height and includes explicit parameterizations of fire and harvest disturbance processes. We use a version of the model which includes an improved biogeochemistry scheme (CLM4.5-BGC) (Thornton *et al.*, 2007). Compared to previous versions of the model, these improvements include vertically-resolved carbon and nitrogen soil dynamics, a new decomposition scheme, and a more detailed representation of nitrification and denitrification (Koven *et al.*, 2013). As a result of these updates, simulated fluxes and pools (of carbon and nitrogen) more closely reflect observational data (Koven *et al.,* 2013). Also 20th century carbon dynamics are more realistic due to higher terrestrial carbon uptake because of reduced nitrogen constraints and longer turnover times for decomposing carbon (Koven *et al.*, 2015).

While CLM4.5-BGC has been described in detail (Oleson *et al.*, 2013), we briefly summarize some key processes that are of relevance for this study. In

CLM4.5-BGC, leaf stomatal conductance ($g_s$) is coupled to photosynthesis based on the Ball -Berry model (Collatz *et al.,* 1991, Sellers *et al.,* 1996):

$$g_s = m\frac{A_n}{c_s/P_{atm}}h_s + b\beta_t, \tag{1}$$

where $A_n$ is the leaf photosynthesis rate, $c_s$ is the CO2 partial pressure at the leaf surface, $P_{atm}$ is the atmospheric pressure, $h_s$ is the relative humidity at the leaf surface, $m$ is a plant functional type (PFT) specific slope coefficient, and $b$ is a PFT specific minimum stomatal conductance, regulated by the soil moisture stress factor $\beta_{t.}$ $\beta_t$ ranges between 0 (maximum water stress) and 1 (minimum water stress), and works to reduce the minimum stomatal conductance $b$. Further, $\beta_t$ impacts $g_s$ through its influence on $A_n$, by scaling the maximum rate of carboxylation ($\beta_t\,V_{cmax}$).

Additionally, $A_n$ depends (in part) upon the internal leaf CO2 partial pressure ($c_i$) via Fick's law as follows:

$$c_i = c_a - (1.4r_b + 1.6r_s)P_{atm}A_n, \tag{2}$$

where $c_a$ is the atmospheric CO2 partial pressure, $r_b$ is the leaf boundary layer resistance, and $r_s$ is the stomatal resistance. The equations for $c_i$, $g_s$, and $A_n$ (not shown) are solved iteratively until $c_i$ converges. This formulation couples the carbon and water cycles and both photosynthesis and stomatal conductance are reduced in dry conditions. Both $g_s$, and $A_n$ are solved separately for sunlit and shaded conditions and scaled through the canopy (as a function of LAI) to determine canopy level conductance and potential GPP ($\mathrm{GPP_{pot}}$).

Nitrogen limitation is modelled through downscaling $\mathrm{GPP_{pot}}$ depending on available nitrogen and required nitrogen by new carbon growth (Oleson *et al.,* 2013; Thornton *et al.,* 2007). Actual GPP is defined as

$$\mathrm{GPP}{=}\mathrm{GPP_{pot}}(1 - f), \tag{3}$$

with the nitrogen scaling factor (*f*) defined as

$$f = \frac{\mathrm{CF_{avail\_alloc}}\text{-}\mathrm{CF_{alloc}}}{\mathrm{GPP_{pot}}}, \tag{4}$$

where $\mathrm{CF_{avail\_alloc}}$ is the carbon flux from photosynthesis available for new growth, after accounting for maintenance respiration, and $\mathrm{CF_{alloc}}$ is the carbon allocation to new growth. In a first step, plant nitrogen demand is calculated depending on the amount of carbon available for growth ($CF_{avail\_alloc}$) and fixed C:N stoichiometry for each part of the vegetation (leaves, roots, wood) for each PFT on the soil column. The plant demand for nitrogen is (partially) compensated for by translocating nitrogen from senescing leaves. Total plant nitrogen demand is reduced by this translocating flux to give the plant demand for mineral nitrogen from the soil. The combined nitrogen demand for all PFTs and heterotrophic demand from the soil (immobilization) compete for available soil nitrogen. Plant nitrogen uptake is then calculated (depending on the ratio of demand to supply), which is then used along with allometric relationships and C:N stoichiometry to calculate $CF_{alloc}$.

Soil decomposition rates are also influenced by nitrogen availability. For decomposition from each upstream to downstream pool, a nitrogen source/sink term is calculated depending on the carbon and nitrogen content of each pool. Therefore, depending on plant demand for soil nitrogen, decomposition fluxes can be downregulated if nitrogen supply is limited. In addition to the rapid cycling of nitrogen in the plant-litter-soil system, CLM4.5 simulates dynamics of the ‘external’ nitrogen cycle, with inputs of bioavailable nitrogen entering the terrestrial ecosystem through biological fixation and atmospheric deposition. Nitrogen leaves the system through losses due to fire, denitrification, and leaching. Additions from deposition and biological fixation (BNF) are added straight to the mineral $NH_4^+$ pool, where plants and microbes compete for the nitrogen. This representation of carbon-nitrogen interactions in CLM4.5-BGC leads to a strong coupling between heterotrophic respiration and plant productivity, as respiration depends on organic matter produced, and productivity depends on the nutrients made available through the decomposition of this organic matter (Thornton *et al.*, 2007). Hence, further to the positive impact nitrogen deposition has upon plant productivity another important pathway for nitrogen to fertilize plant growth is through warming induced increases in nitrogen mineralisation a process which is also simulated in CLM4.5-BGC (Thornton *et al.*, 2007).

The model driver data used include nitrogen deposition for the period 1850-2000 from simulations based on the Community Atmosphere Model version 3.5 (CAM3.5) using historical nitrogen emissions (Lamarque *et al.*, 2010). For the more recent period 2000-2016, we use nitrogen deposition fields generated following the emissions from Representative Concentration Pathway 8.5 (also using CAM3.5) (Lamarque *et al.*, 2011), as this most closely matches current emission levels (Peters *et al.*, 2013). Due to the temporal averaging of emissions data (linear interpolation between decadal means), there is a smooth transition (no step changes between years) between emission inventories at the year 2000, and hence the deposition fields used.

Climate driver data used stem from the CRU-NCEP (version 7) dataset (Viovy, 2018) (0.5° spatial and 6h temporal resolution), which is designed to drive CLM over long timer periods and aggregated/interpolated to the CLM4.5 spatial resolutions of 1.25° x 0.9375° and 30 min time step. CRUNCEP is a combination of two datasets; CRU TS3.2 0.5° x 0.5° monthly data over the period 1901-2002 (Harris *et al.*, 2014), and the NCEP reanalysis 2.5° x 2.5° 6-hourly data covering 1948-2016 (Kalnay *et al.*, 1996). Further, we also used prescribed annual, globally averaged $CO_2$ concentrations from the Earth Systems Research Laboratory (Dlugokencky & Tans, 2017). We used fixed present-day land cover as described in section 21.3.3 of Oleson *et al.* (2013) , meaning we did not consider land-use and land-cover change in this study since our focus was broadly on carbon-nitrogen interactions.

## 3.2.2 Model experiments

### 3.2.2.1 The extended period 1901-2016

We performed a set of factorial simulations to assess the land carbon cycle response to increasing atmospheric $CO_2$, nitrogen deposition, and climate changes, as well as the interactions between these drivers. This design allowed estimation of the effects of individual drivers on carbon pools and fluxes, and hence on the overall terrestrial carbon budget during the period 1901-2016. Global annual means of model drivers (climate, nitrogen deposition, atmospheric $CO_2$) are shown in Figure C1 (in the supporting information), and the spatial distribution of changes over this period are shown in Figure C2. Our model spin-up procedure followed that of the multi-model TRENDY study (Sitch *et al.*, 2015) to be able to compare the results of this study to the TRENDY ensembles. It entails cycling early 20th century climate (1901-1920) with atmospheric $CO_2$ concentrations and nitrogen deposition of the year 1860 until carbon pools and fluxes were in a steady state. The model then ran from 1861-1900 with varying $CO_2$ and nitrogen deposition and the same climate cycles as in the first step. We then ran a set of factorial off-line experiments over 1901-2016 with varying $CO_2$, climate, nitrogen deposition, and fixed present-day land use (see Table 3.1).

From this set of eight simulations, we estimated the contribution from each driver to changes in net primary production (NPP), heterotrophic respiration (RH), and net biome production (NBP) (estimated through NBP=NPP-RH-fire), and total ecosystem carbon as following: $CO_2$ fertilization = (S2 – S1), nitrogen deposition = (S3 – S1), climate (S4 – S1*), carbon-nitrogen synergy = (S5 – S2) – (S3 – S1), carbon-climate synergy = (S6 – S4) – (S2 – S1), and the combined effect = (S8 – S1*). Here, simulation S1* represents the linear trend (from 1901-2016) in annual means of NPP, NBP, and total ecosystem carbon based on experiment S1. We use the trend in S1 rather than annual means to preserve the inter-annual variability of climate in the "Climate" and "Combined" contributions. Taking the difference between the simulations removes the background carbon trends from the non-equilibrium initial conditions (see Bonan and Levis (2010)).

We calculate the change in NPP and NBP due to each driver over the study period by differencing the 2007-2016 and 1901-1910 means. To statistically test for a difference between the two decades we use a Mann-Whitney U test. As a result of our experiment design, contributions from $CO_2$ fertilization, nitrogen deposition, carbon-nitrogen synergy, and carbon-climate synergy use early 20th century climate as a source of variance in both decades (1901-1910 and 2007-2016). For the contributions from climate, and "combined", the "actual" climate variability in each decade is the source of variance.

**Table 3.1 - Summary of Factorial Model Simulations With CLM4.5-BGC.**

| Experiment | $CO_2$ | Nitrogen deposition | Climate |
|---|---|---|---|
| **S1** | C | C | C |
| **S2** | T | C | C |
| **S3** | C | T | C |
| **S4** | C | C | T |
| **S5** | T | T | C |
| **S6** | T | C | T |
| **S7** | C | T | T |
| **S8** | T | T | T |

*Note.* C (constant) indicates 1900 values are used for atmospheric $CO_2$ and nitrogen deposition and 1901-1920 climate is recycled. T (transient) indicates historically varying $CO_2$, nitrogen deposition and climate is used.

#### 3.2.2.2 The recent period 1990-2016

We performed a second set of experiments for the more recent period (1990-2016) using initial conditions obtained from experiment S8 (at 1990) by branching out of experiment S8 (Table 3.1). Simulations are performed in a similar manner to the extended period; however, our constant values were from 1990 for atmospheric $CO_2$, nitrogen deposition, and climate. We performed these simulations of the recent period to quantify recent changes in carbon/nitrogen cycling relative to a more contemporary baseline. Such an analysis would be more closely aligned with the time frame of our main aim of evaluating explanations for the terrestrial sink increase since the turn of this century. Contributions from each factor are calculated through factorial simulations, similar to the extended period.

### 3.2.3 Diagnosing model results

Nitrogen limitation (N-lim) is a key metric in assessments of carbon-nitrogen coupling and is directly estimated in CLM4.5-BGC through the ratio of actual GPP to potential GPP (GPP that would occur without nitrogen limitation) at each time step, and thus is a scalar between 0-1, with high/low N-lim values indicate low/high nitrogen limitation.

In diagnosing our model results we evaluate N-lim along with the Γ factor which expresses the sensitivity of terrestrial carbon storage to atmospheric $CO_2$. For the Γ factor, we adopt the definition: $\Gamma_X = \frac{\Delta TEC_X}{\Delta C_a} = \frac{\Delta(TEC_Y - TEC_Z)}{\Delta C_a}$, where $\Delta TEC_X$ is the change in total ecosystem carbon (PgC) due to factor $X$ over a certain period, calculated as the difference between simulations $Y$ and $Z$ (see Table 3.2). $\Delta C_a$ is the change in atmospheric $CO_2$ (ppm) over the same period. For the extended period we focus on the change in $TEC$ and $C_a$ from 1901-1910 to 2007-2016 and for the recent period on the change from 1990-1996 to 2010-2016.

**Table 3.2 - Summary of Simulations Used in the Calculations for Γ.**

| $\Gamma_{CO2}$ | $\Gamma_{CO2+CNsyn}$ | $\Gamma_{CO2+CNsyn+NDEP}$ |
|---|---|---|
| $\Delta(TEC_{S2} - TEC_{S1})/\Delta C_a$ | $\Delta(TEC_{S5} - TEC_{S3})/\Delta C_a$ | $\Delta(TEC_{S5} - TEC_{S1})/\Delta C_a$ |

*Note.* Γ is calculated for the direct $CO_2$ effect $\Gamma_{CO2}$, the direct $CO_2$ and carbon-nitrogen synergy effects $\Gamma_{CO2+CNsyn}$, and finally the direct $CO_2$, direct nitrogen deposition effects, and the synergy between them $\Gamma_{CO2+CNsyn+NDEP}$.

## 3.3 Results

### 3.3.1 Long-term changes in net terrestrial carbon uptake and attribution of underlying drivers

To evaluate our hypothesis that nitrogen deposition, $CO_2$ fertilization, and their interactions have enhanced the terrestrial carbon sink, we first analyse our CLM4.5-BGC model simulations of the carbon component fluxes NPP and RH, as well as NBP covering the extended period over the last century.

At the global scale, simulated NPP increased substantially over the 20th century to present day from 56.2 (mean of 1901-1910) to 66.0 PgC/yr (mean of 2007-2016) with positive contributions from all drivers considered, including rising $CO_2$ concentrations (referred to as $CO_2$ fertilization), nitrogen deposition, climate, and carbon-nitrogen as well as carbon-climate synergies (Figure 3.1, Table 3.3). The relative contribution of these drivers to this overall NPP increase amounts to 60% for increased $CO_2$, 15% for nitrogen deposition, 8% for carbon-nitrogen synergy, 9% for carbon-climate synergy and 8% for climate. Both $CO_2$ fertilization and nitrogen deposition individually caused a smooth, transient increase in NPP, in line with the trajectory of the corresponding drivers (see Figure 3.1 and Figure C1). The positive carbon-nitrogen synergistic contribution to NPP implies that (as expected) the efficiency of the $CO_2$ fertilization effect is enhanced as nitrogen limitation is diminished (through nitrogen deposition). In addition, a similar positive contribution of comparable magnitude is observed for the carbon-climate synergistic effect.

**Table 3.3 - Change in Global NPP and NBP (PgC/yr) for the extended ((2007-2016) - (1901-1910)) and recent ((2010-2016) - (1990-1996)) periods.**

| **Period** | **Variable** | **Change due to each driver (PgC/yr)** | | | | | | |
|---|---|---|---|---|---|---|---|---|
| | | $CO_2$ | **NDEP** | **CLIMATE** | **CN-SYN** | **CC-SYN** | **SUM of three effects (% of COMBINED)** | **COMBINED** |
| **Extended** | **NPP** | 5.93 | 1.50 | 0.84 | 0.77 | 0.86 | 8.27 (85%) | 9.75 |
| | **NBP** | 2.39 | 0.34 | -1.07 | 0.35 | 0.44 | 1.66 (72%) | 2.31 |
| **Recent** | **NPP** | 1.91 | 0.03 | 1.22 | 0.01 | 0.24 | 3.16 (93%) | 3.41 |
| | **NBP** | 1.22 | 0.03 | -1.17 | 0.00 | 0.18 | 0.08 (30%) | 0.27 |

*Note.* Positive values for NBP indicate a sink of carbon to the land surface. SUM of three effects indicates the sum of $CO_2$, NDEP, and CLIMATE.

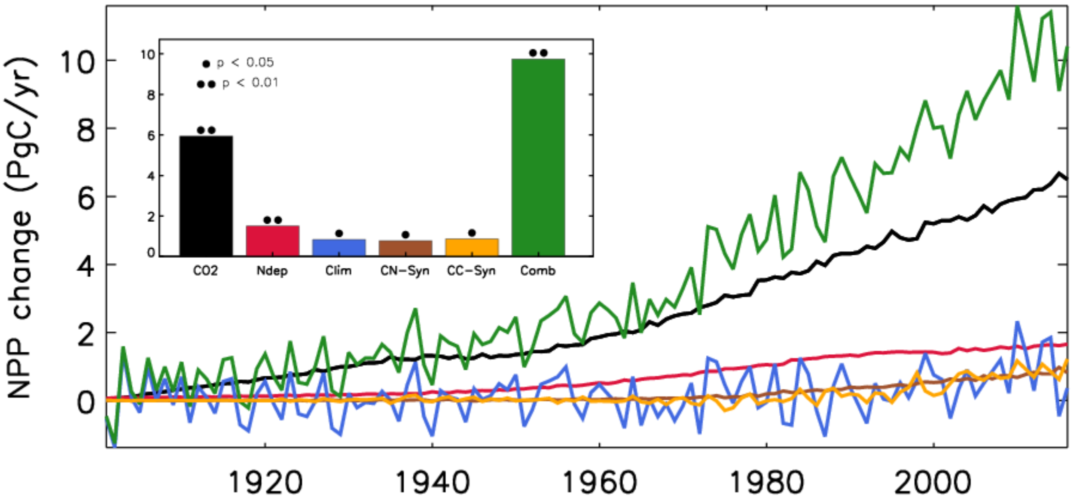

**Figure 3.1 - Global, annual mean change in NPP (PgC/yr) relative to the control simulation (S1) during 1901-2016 due to $CO_2$ fertilization ($CO_2$), nitrogen deposition (Ndep), climate change (Clim), carbon-nitrogen synergy (CN-Syn), carbon-climate synergy (CC-Syn) and the combined effects (Comb). Inset shows the change in NPP from 1901-1910 to 2007-2016. Statistically significant (• $p<0.05$, •• $p<0.01$; Mann-Whitney U test) changes are highlighted.**

A spatially explicit analysis of the factorial simulations shows that the $CO_2$ fertilization effect is most profound in tropical regions (Figure 3.2a). Substantial contributions from nitrogen deposition are also evident over the industrialised regions of Europe, East Asia, and North America, and the agricultural regions of India and South-East Asia (Figure 3.2b). Whilst NPP increases due to nitrogen deposition have the largest footprint in industrialised regions, the associated NPP response also depends on the nitrogen limitation of a given ecosystem. This is apparent in the grasslands of Africa and South America, where nitrogen deposition (Figure C2) induced a substantial NPP response (Figure 3.2b). The increase in NPP due to climate can be attributed to mid and high northern latitudes, where warming has led to a longer growing season and increased soil moisture (Figure C3), enhancing annual net plant carbon uptake (Figure 3.2c). Further, warming enhanced nitrogen mineralisation in these soils (Figure C4) increasing plant productivity, which is also captured in the climate response. The positive carbon-nitrogen synergistic contribution is prevalent in tropical forests and East Asia (Figure 3.2d), regions that are also exhibiting high sensitivity to $CO_2$ fertilization (Figure 3.2a). Similarly, positive carbon-climate synergistic effects are substantial in the tropics, as well as regions in the mid/high latitudes (Figure 3.2e).

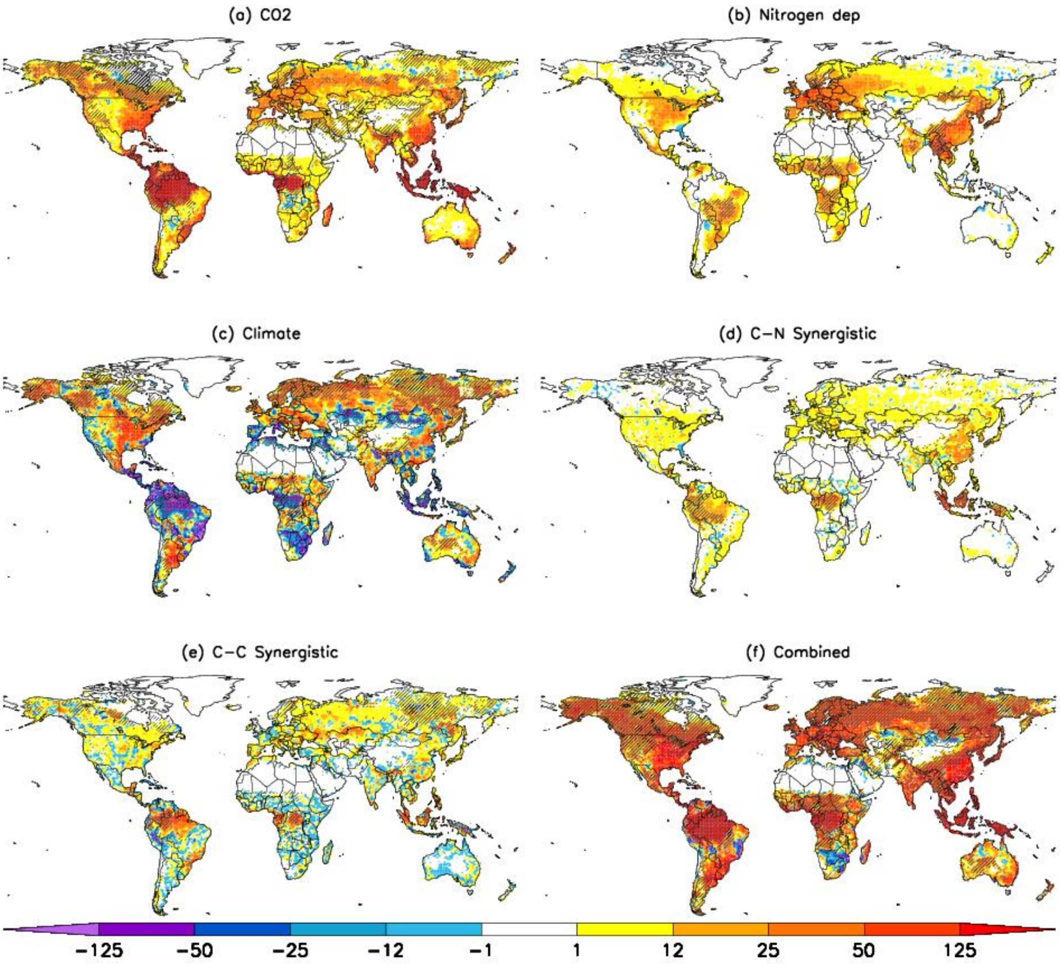

**Figure 3.2 - Spatial patterns of NPP change (gC/m²/yr) as a result of all drivers considered. Maps show single driver contribution from a) $CO_2$ fertilization, b) nitrogen deposition, c) Climate, d) CN-synergy, e) CC-synergy, and f) the combined effect, respectively. The patterns are based on a set of factorial simulations (see Methods). NPP changes shown here are calculated as the difference between 2007-2016 (final decade) and 1901-1910 (first decade) mean values. Significant ($p<0.05$; Mann-Whitney U test) changes highlighted with hatching.**

Globally, NBP has increased from 0.8 to 3.2 PgC/yr (1901-1910 to 2007-2016 means) with positive contributions from $CO_2$ fertilization, nitrogen deposition, carbon-nitrogen synergy, and carbon-climate synergy whilst an overall negative contribution from climate (Figure 3.3, Table 3.3). The relative contribution of these drivers to this overall NBP increase amounts to 99% for increased $CO_2$, 14% for nitrogen deposition, 14% for carbon-nitrogen synergy, 18% for carbon-climate synergy and -45% for climate. Whilst the $CO_2$ fertilization effect steadily contributed to NBP changes throughout the whole period, nitrogen deposition induced NBP increases became significant from the 1970s onwards (Figure 3.3), a period of increased anthropogenic nitrogen deposition (fossil fuel NOx and agricultural NHx) (Lamarque *et al.*, 2010). Results also show that the carbon-nitrogen synergistic effect is as large as the effect from nitrogen deposition alone, implying additional nitrogen had a large positive impact on $CO_2$ fertilization. NBP is highly sensitive to climatic changes especially at inter-annual time scales (Figure 3.3 and Figure C1). Overall, changes in climate have led to a net carbon source, with accelerated losses since the 1990s, due to warming induced soil respiration rates increasing faster than NPP.

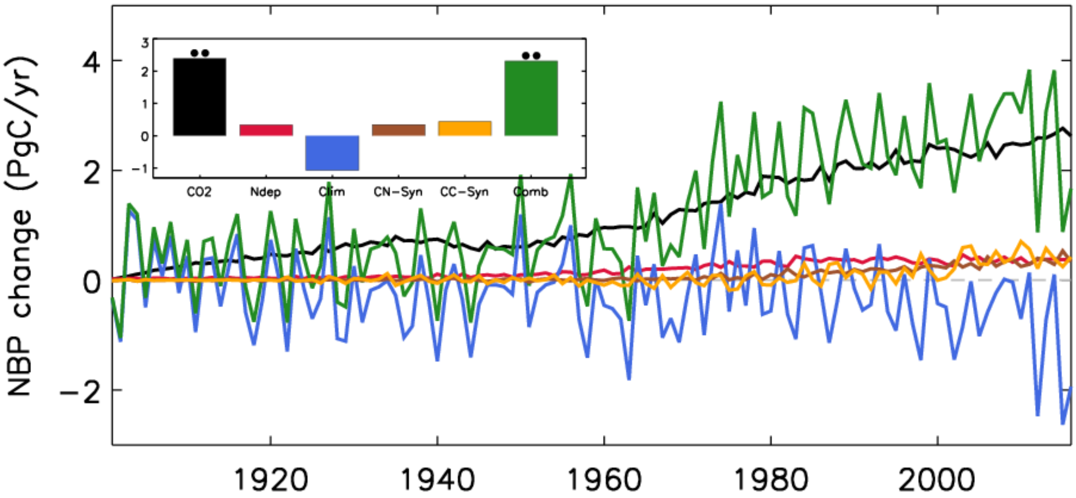

**Figure 3.3 - Global, annual mean change in NBP (PgC/yr) relative to the control simulation (S1) during 1901-2016 due to $CO_2$ fertilization ($CO_2$), nitrogen deposition (Ndep), climate change (Clim), the combined effect (Comb), carbon-nitrogen synergy (CN-Syn), and carbon-climate synergy (CC_Syn). Zero line is shown in grey. Inset is the change in NPP from (1901-1910) to (2007-2016). Statistically significant (• p<0.05, •• p<0.01; Mann-Whitney U test) changes are highlighted.**

The spatial distribution of changes in NBP over roughly the last century from $CO_2$ fertilization and nitrogen deposition mirrors those seen in NPP (Figure 3.4a,b and Figure 3.2a,b) and is consistent with the notion of a strong influence of NPP on net carbon uptake. Interestingly, increased nitrogen deposition seems to have had no direct effect on tropical forest net carbon uptake (but instead increased the efficiency of $CO_2$ fertilization: the CN synergistic effect as discussed below). NBP decreases due to climate can be attributed predominately to tropical regions as well as large areas across Eurasia and North America (Figure 3.4c). Both the carbon-nitrogen and carbon-climate synergistic effects follow the NPP patterns of large tropical increases, as well as vast areas of the mid-high latitudes (Figure 3.4d,e). These synergistic effects occur when there is both a high sensitivity to CO2 fertilization and a concurrent release of nitrogen limitation. This is seen in the case of tropical forests where increased atmospheric $CO_2$ concentrations increases nitrogen limitation that is then alleviated with simultaneous increases in nitrogen deposition (Figure 3.4d). Overall, the majority of the vegetated land surface has increased net carbon uptake over the historical period, with the tropics, East Asia, North America, and northern Eurasia dominating (Figure 3.4f). However, areas in South America, Southern Africa, and the Eurasian Steppe are now carbon sources to the atmosphere.

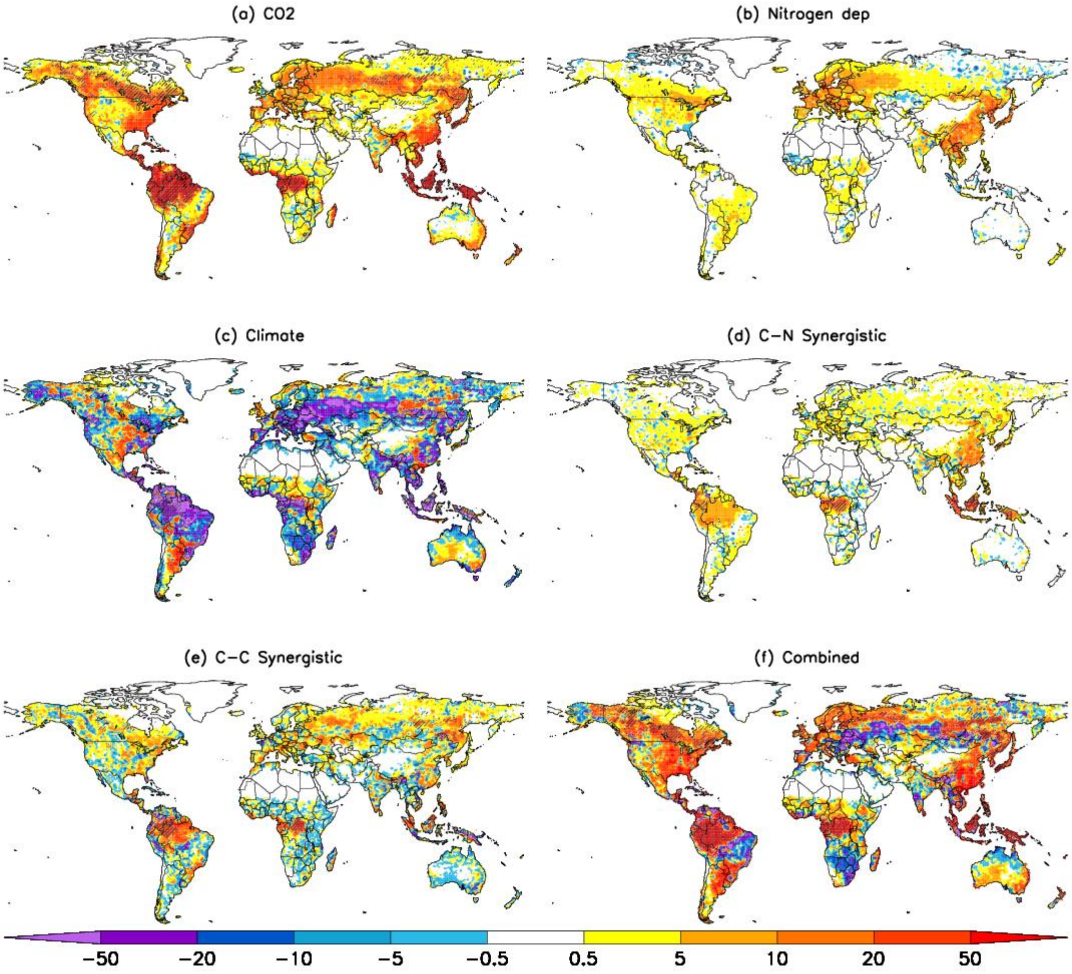

**Figure 3.4 - Spatial patterns of NBP change (gC/m$^2$/yr) due to a) CO$_2$ fertilization, b) nitrogen deposition, c) Climate, d) CN-synergy, e) CC-synergy, and f) combined effect. The synergistic effect is calculated as the difference between 2007-2016 and 1901-1910 mean values. Significant ($p<0.05$; Mann-Whitney U test) changes highlighted with hatching.**

Recent published findings based on the Global Carbon Budget (GCB) show that the land carbon sink has increased over the last five decades (Le Quéré *et al.*, 2018). In the GCB, the land sink is estimated as the 'residual' in the global carbon mass balance between fossil fuel and land-use emissions, atmospheric CO$_2$ growth rates, and ocean uptake. This 'residual' sink has increased from ~1.5 PgC/yr to ~3 PgC/yr from the 1960s to the 2000s (Figure 3.5). The estimated decadal carbon sinks in our study are in general agreement and within the uncertainties of the GCB estimates, giving some confidence in our modelled magnitude (Figure 3.5).

We also compared our results to those based on the recent TRENDY multi-model inter-comparison, which consider the influence of varying atmospheric $CO_2$ concentrations and climate on carbon fluxes (S2 simulations) (Sitch *et al.*, 2015). As carbon-nitrogen interactions are a focal point of this study, we compared our results with the TRENDY models that include a coupled carbon-nitrogen scheme (CLM4-CN and OCN) separately to the ‘carbon-only’ models. Whilst CLM4-CN and OCN tend to simulate lower net carbon uptake compared to the “carbon-only” mean, they are both still within the range spanned by the TRENDY ‘carbon-only’ ensemble (Figure 3.5). Therefore, while introducing a coupled carbon-nitrogen scheme tends to have a strong influence on land carbon uptake in DGVMs (Friedlingstein & Prentice, 2010, Thornton *et al.*, 2007, Zaehle *et al.*, 2010), the structural difference between models is a larger source of uncertainty. Our results match the mean TRENDY carbon sink estimate well on decadal scales, albeit with noticeable differences in the 1960s and 1980s.

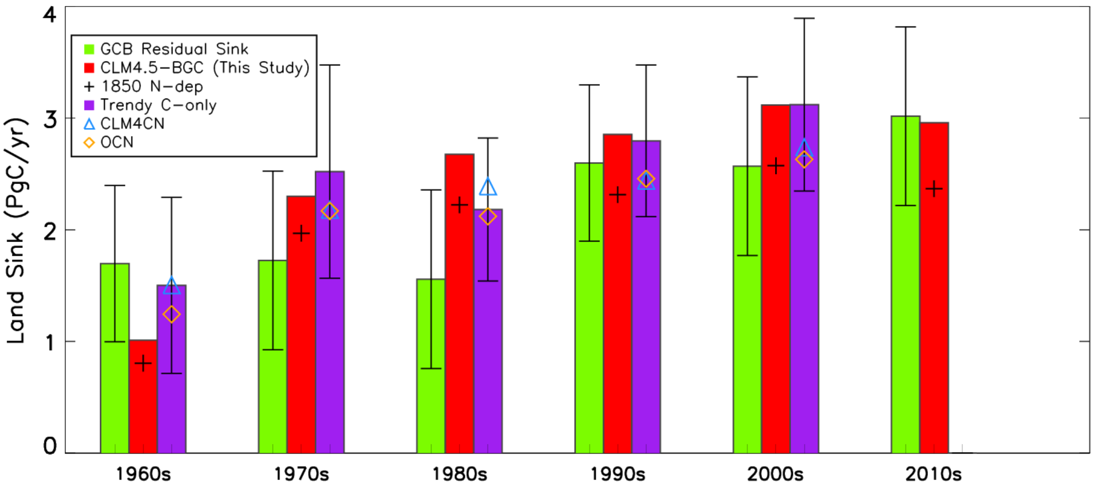

**Figure 3.5 - Multiple estimates of the decadal mean land carbon sink for the 1960s – 2010s based on the GCB, TRENDY (S2) and this study. Note that the TRENDY simulations and our results do not consider LULCC, and the GCB residual sink inherently accounts for LULCC fluxes. Carbon sink (PgC/yr) estimates correspond to the GCB 'residual' (green bars), this study (red bars), this study with 1900 nitrogen deposition (black crosses), and the ensemble-mean from Trendy based on "carbon-only" models (purple bars). Estimates for the two Trendy models with interactive nitrogen are also shown: CLM4CN (blue triangles) and OCN (orange diamonds). The GCB error bars represent the uncertainty in the corresponding sink estimate as provided by Le Quere et al [2018]. The error bars for the Trendy estimate represent one standard deviation based on the multi-model ensemble mean. The final decade (2010s) captures the mean land sink for the period 2010-2016. For our study, the influence of anthropogenic nitrogen deposition (direct and synergistic effects) can be inferred by the difference between the black cross and red bar. This effect has grown from 0.2 PgC/yr in 1960s to 0.7 PgC/yr in 2010s.**

### 3.3.2 Recent changes in net terrestrial carbon uptake and attribution of underlying drivers

We next evaluated whether the marked strengthening of the terrestrial carbon sink since the turn of this century was due to the hypothesised causal link between concurrent changes in the sink and anthropogenic fossil fuel emissions (Hansen *et al.*, 2013, Keenan *et al.*, 2016). In a first step, we tested to what extent the model (with all drivers varied) captures the uptick in the ‘residual’ land carbon sink since the turn of the century. The trend in the residual sink increased by 0.33 PgC/yr$^2$ between 1990-2002 and 2002-2014 (Figure C5). Our model simulated a smaller increase of 0.08 PgC/yr$^2$, in line with the change simulated by the TRENDY multi-model mean, 0.09 PgC/yr$^2$ (Figure C5)

Next, we performed factorial simulations starting from contemporary 1990 baseline conditions (see Methods) to attribute drivers and processes in the context of the more recent uptick in the terrestrial carbon sink. Corresponding results show a global NPP increase of 3.4 PgC/yr between the early 1990s (mean of 1990-1996) and the end of our study period (2010-2016), with $CO_2$ fertilization and climate being the dominant drivers, accounting for 56% and 35% of the overall change, respectively (Table 3.3). On a global scale, terrestrial nitrogen deposition increased by 3% over this period (70 TgN/yr to 72 TgN/yr), hence had little impact on NPP changes (Table 3.3). However, the effect of deposition differed across regions, reflecting the spatial pattern of nitrogen deposition. East Asia and Western Europe experienced enhanced NPP consistent with the positive change in nitrogen deposition over this period, whilst Eastern Europe, North America, and the African savannah had a decline in NPP consistent with a decrease in nitrogen deposition (Figure 3.6b and Figure C6, Table C1). Northern hemisphere warming between the two focal epochs (1990-1996 and 2010-2016) led to widespread NPP increases in boreal regions of Eurasia and North America (Figure 3.6c and Figure C7). In regions outside of the northern high latitudes, changes in water availability (e.g. soil moisture) also drove positive NPP changes (Figure C8). In contrast to the extended study period (1900-2016, see above), the carbon-nitrogen synergistic effect is near zero over the recent period, with only a small increase in East Asia (Figure 3.6d). Conversely, carbon-climate synergy has a small but noticeable positive contribution to NPP (Figure 3.6e). In this case, tropical forests in South America and Central Africa have a positive response, whilst most other regions exhibit small and spatially heterogenous responses. Potential factors underlying the difference in simulated synergistic effects between the extended and the more recent periods are discussed below.

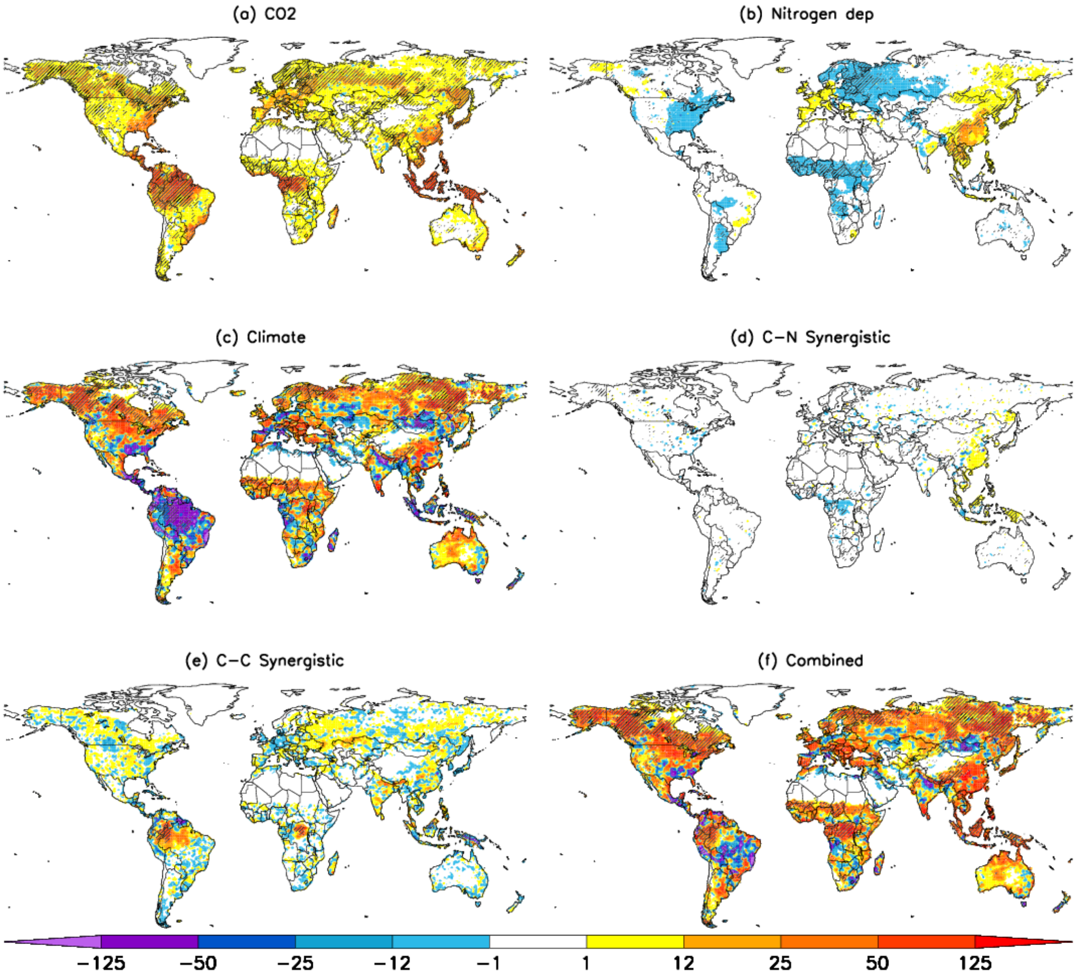

**Figure 3.6 - Spatial patterns of NPP change (gC/m$^2$/yr) due to a) CO$_2$ fertilization, b) nitrogen deposition, c) climate, d) CN-synergy, e) CC-synergy, and f) combined effect. The synergistic effect is calculated as the difference between the combined effect and sum of effects. NPP changes shown here are calculated as the difference between 2010-2016 and 1990-1996 mean values. Significant ($p<0.05$; Mann-Whitney U test) changes highlighted with hatching.**

At global scale, changes in climate led to a loss of NBP by 1.17 PgC/yr between the two focal periods 1990-1996 and 2010-2016, whereas CO$_2$ fertilization increased NBP by 1.22 PgC/yr (Table 3.3). Changes in nitrogen deposition played only a minor role, sequestering an additional 0.03 PgC/yr, whilst carbon-nitrogen synergy had an insignificant contribution. Carbon-climate synergy effects induced a relatively small (but important) positive increase in NBP of 0.18 PgC/yr, which in combination with all other drivers considered led to an overall increase of 0.27 PgC/yr between 1990-1996 and 2010-2016, with $CO_2$ fertilization dominating the response (Table 3.3).

The spatial pattern of changes in NBP between 1990-1996 and 2010-2016 due to $CO_2$ fertilization, nitrogen deposition, and CN-synergy effects (Figure 3.7a,b,d) were similar to the associated NPP pattern (see Figure 3.6) as expected since these drivers predominantly influence NBP through their effect on plant carbon uptake. Conversely, climate variations caused widespread declines in NBP due to either a combination of reduced NPP and increased soil respiration (such as in the Amazon) or respiration increases being larger than NPP increases, as observed over the mid/high latitudes (Figures 3.7c and Figure C9). Carbon-climate interactions led to significant increases in tropical forests and the forests of North America, Eurasia, and China (Figure 3.7e). The overall pattern of NBP change is dominated (on grid-box scale) by climate variability, although $CO_2$ fertilization effects are visible across the tropics (Figure 3.7c,f).

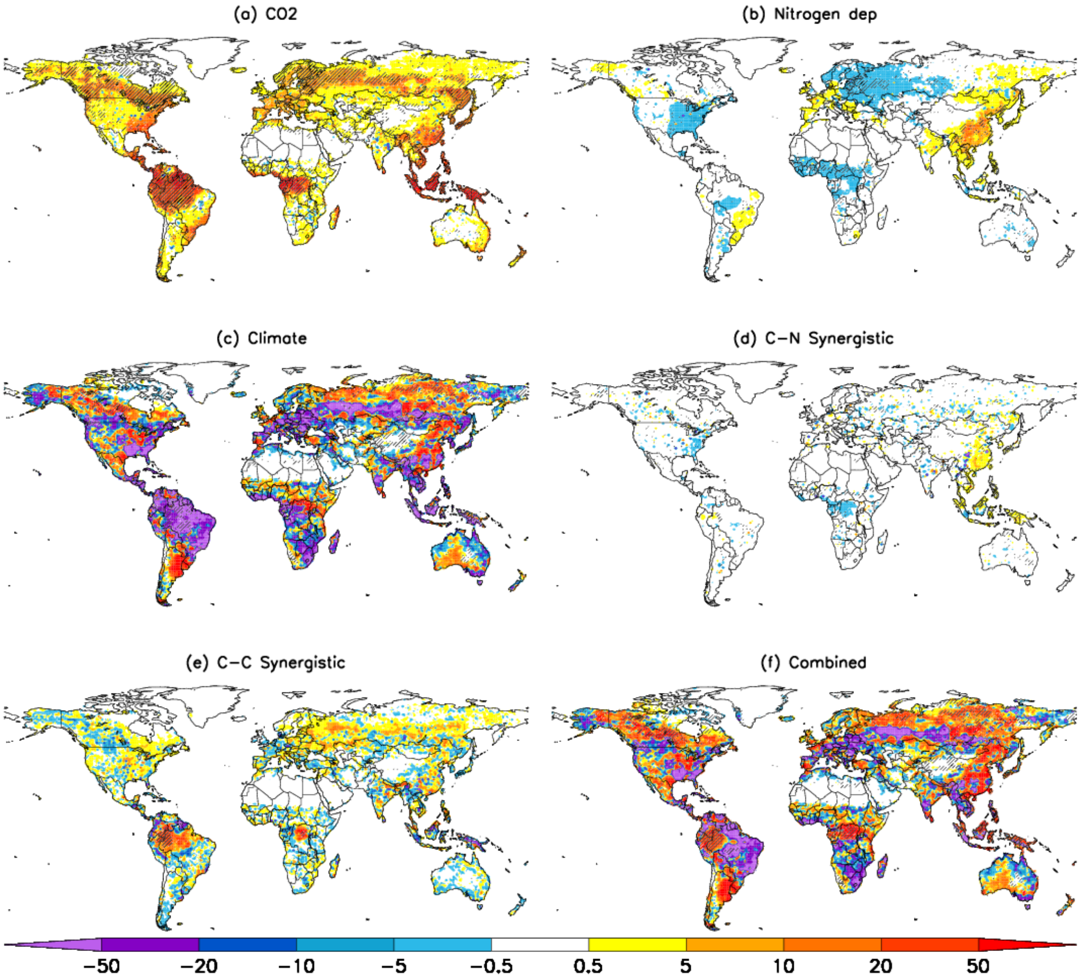

**Figure 3.7 - Spatial patterns of NBP change (gC/m$^2$/yr) due to a) $CO_2$ fertilization, b) nitrogen deposition, c) climate, d) CN-synergy, e) CC-synergy, and f) the combined effect. The synergistic effect is calculated as the difference between the combined effect and sum of effects. NBP changes shown here are calculated as the difference between 2010-2016 and 1990-1996 mean values. Significant ($p<0.05$; Mann-Whitney U test) changes highlighted with hatching.**

### 3.3.3 Sensitivity of carbon-nitrogen interactions for the more recent and extended study periods

We next examined the extent to which additional nitrogen deposition has changed the efficiency of the $CO_2$ fertilization effect, in order to evaluate our hypothesis that nitrogen deposition has interacted with $CO_2$ to increase the terrestrial carbon sink. Hence in a next step, we considered the sensitivity of carbon storage to atmospheric $CO_2$ concentrations ($\Gamma = \frac{\Delta TEC}{\Delta Ca}$) and how this is modulated by carbon-nitrogen interactions (see Methods). For the extended period covering roughly the last century, we find $\Gamma_{CO2} = 1.32$ PgC/ppm $CO_2$ (Table 3.4). Including the carbon-nitrogen synergistic contribution increased Γ by 0.08 PgC/ppm $CO_2$, and direct nitrogen deposition increased Γ by a further 0.21 PgC/ppm. These estimates indicate that additional nitrogen enabled higher plant carbon uptake via more effective $CO_2$ fertilization, and that the direct effects from additional nitrogen were approximately twice that of the synergistic contribution (increase of 0.21 PgC/ppm compared to 0.08 PgC/ppm) (Table 3.4).

**Table 3.4 - Γ values (PgC/ppm) for the extended (1901-1910 to 2007-2016) and recent (1990-1996 to 2010-2016) periods**

| **Period** | $\Gamma_{CO2}$ | $\Gamma_{CO2+CNsyn}$ | $\Gamma_{CO2+CNsyn+NDEP}$ |
|---|---|---|---|
| **Extended** | 1.32 | 1.40 | 1.61 |
| **Recent** | 0.45 | 0.45 | 0.45 |

*Note.* Estimates are provided for Γ factors associated with the direct $CO_2$ effect ($CO_2$), $CO_2$ and CN-synergistic effects ($CO_2$+CNsyn), and the combined $CO_2$ and nitrogen deposition effects, including CN-synergy ($CO_2$+CNsyn+NDEP).

The magnitude of Γ and the impact of nitrogen are sensitive to the baseline of simulations because of the influence of background carbon trends and the current state of carbon and nitrogen pools. Therefore, we also focus on the recent period (1990-2016), enabling us to quantify the contribution from changes in nitrogen deposition to $CO_2$ fertilization relative to a more contemporary baseline. Our method of calculating Γ removes background trends in total ecosystem carbon from non-equilibrium conditions (see Methods) and so purely captures the response to rising $CO_2$ and nitrogen deposition relative to the chosen baseline. For the recent period (1990-2016) the removal of a background trend in total ecosystem carbon and the relatively large $\Delta C_a$ since 1990 led to much lower Γ values of 0.45 PgC/ppm (Table 3.4). The impact of direct nitrogen deposition on Γ is limited due to opposing regional impacts (increases in Western Europe and China, decreases in North America, Eastern Eurasia, and Africa) leading to an insignificant global effect (Table 3.4, Figure C6 and Figure C10f). Furthermore, the rate of nitrogen deposition globally changed little between the two periods (1990-1996 to 2010-2016), and the small spatial extent of increased deposition (restricted to Western Europe and East Asia, Figure C6a) also limited the global synergistic response. Although Γ increases in China due to carbon-nitrogen synergy, there is no response in Western Europe (Figure C10e). This lack of a synergistic effect is possibly due to the relatively low increase (7%) in deposition in Western Europe over this period, compared to the larger increase observed in East Asia (27%) (Table C1).

Overall, nitrogen deposition and associated synergistic effects have increased the sensitivity of the biosphere to atmospheric $CO_2$ over the 20th century. However, relative to a modern baseline, (which approximates the real-world situation in regard to attributing mechanisms of the accelerated 21st century sink more closely), there are no synergistic effects.

### 3.3.4 Tracking nitrogen limitation for the extended and more recent study period

We also evaluated how nitrogen availability regulates carbon uptake using a “Nitrogen limitation scalar” (N-lim) the ratio of actual GPP to “potential-GPP” (simulated GPP before nitrogen limitation is imposed, see Methods). Globally, at the baseline of our extended study period (1901) nitrogen limitation reduced GPP by 20% (161.3 PgC/yr to 129.3 PgC/yr). At global scale, our trajectories of N-lim showed decreases (increasing limitation) under increasing atmospheric CO2 (Figure 3.8a). Increased nitrogen deposition reduced the limitation, in line with expectations (Figure 3.8a). But N-lim is also sensitive to changes in climate, exhibiting large inter-annual variability with a positive trend (reduced limitation) from 1980s onwards. Climate has a complex relationship with N-lim due to the influence on both the amount of required nitrogen for climate-driven changes in photosynthesis and available nitrogen (through impact on nitrogen soil remineralisation rates), meaning the exact cause of the simulated behaviour is difficult to diagnose. Carbon-nitrogen synergy (the interaction of rising $CO_2$ concentrations and rising nitrogen deposition) reduced nitrogen limitation from 1980 onwards (Figure 3.8a), matching the period in which we see a synergistic response in NPP and NBP (Figures 3.1 and 3.3). For the carbon-nitrogen synergistic contribution to be significant, additional nitrogen deposition needs to alleviate the progressive nitrogen limitation (PNL) brought about by rising $CO_2$ concentrations. This synergistic contribution only occurs when additional nitrogen is required by vegetation due to rising $CO_2$ concentrations (as additional carbon inputs increase immobilization of nitrogen by plants and microbes), which in some ecosystems takes years to develop. This can be seen in the Amazon where N-lim is constant until the 1970s, and then decreases (higher nitrogen limitation) due to rising $CO_2$, inducing an increase (reduced nitrogen limitation) in N-lim from carbon-nitrogen synergy (Figure C11).

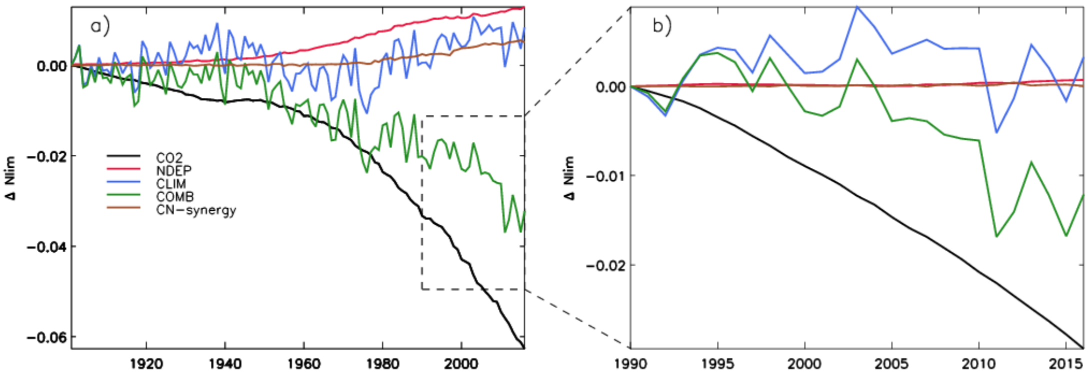

**Figure 3.8 - Changes in the global N limitation scalar for (a) extended simulations (1901-2016) and (b) short simulations (1990-2016). Changes are relative to a control simulation with no variables changing. Also note that the short simulations are relative to 1990 baseline. Contributions from $CO_2$ (black), nitrogen deposition (red), climate (blue), combined (green), and CN-synergy (yellow) are shown. Note that negative values indicate a higher nitrogen limitation.**

With a focus on the more recent study period (1990 baseline), increased $CO_2$ concentrations increase nitrogen limitation at global scale similar to the extended period (Figure 3.8b). In addition, climate warming has increased nitrogen mineralisation rates, reducing the limitation , albeit this is masked to some extent by substantial inter-annual variability (Figure 3.8b). Importantly, over this timescale nitrogen deposition and carbon-nitrogen synergy had a near zero contribution to changes in N-lim. This is partly because the change in global nitrogen deposition between 1990-2016 was relatively small (Figure C12). However, nitrogen deposition increases in East Asia and West Europe, and decreases in North America over this period had noticeable but opposing influences on global N-lim (Figure C13). Furthermore, the direct influence of nitrogen deposition on N-lim was noticeable (in Western Europe and East Asia), there was however, virtually no change due to carbon-nitrogen synergy (Figure C13b,c). Therefore, additional nitrogen deposition in these regions was insufficient to alleviate substantially the nitrogen limitation brought about by high $CO_2$ concentrations. It is difficult to pinpoint the exact cause of our simulated responses, but as previously stated, this is potentially due to the short time period considered, limiting the time for synergistic effects to arise.

## 3.4 Discussion

Understanding the mechanisms behind the ongoing changes in the terrestrial carbon cycle is critical for reliably predicting how the Earth system may change into the future. Here, we assessed the hypothesis that increases in $CO_2$ concentrations and nitrogen deposition (both linked to increasing rates in fossil fuel burning) worked synergistically to increase the terrestrial carbon sink since the turn of this century using a modelling approach. Significant effects are found over the historical period (1901-2016, Figure 3.1), however, relative to a modern baseline (1990) we find that both nitrogen deposition and carbon-nitrogen synergy had no substantial contribution to the increased land sink since the turn of this century (Figures 3.6 and 3.7) (Le Quéré *et al.*, 2018), likely because global nitrogen deposition changed little during this period. Importantly however, there have been significant shifts in the spatial patterns of nitrogen deposition and subsequent impacts on the carbon sink since the 1990s (Figures 3.7 and C6). This highlights the pivotal role nitrogen availability has upon the local carbon cycle. Several studies suggest vegetation productivity is limited by nitrogen (Fisher *et al.*, 2012, Janssens *et al.*, 2010), and enhanced nitrogen deposition, predominantly from anthropogenic fossil fuel burning is thought to have contributed positively to the historical terrestrial carbon sink (Fleischer *et al.*, 2015, Thornton *et al.*, 2007, Wang *et al.*, 2017, Zaehle *et al.*, 2010). Our current (2010-2016) sink estimate of 0.36 PgC/yr (Table 3.3) is in agreement with these previous studies (0.2-0.5 PgC/yr). We found that nitrogen deposition induced effects start to occur towards the latter decades of the 20th century when the additional nitrogen worked to offset the increased nitrogen limitation brought about by increasing $CO_2$ concentrations (Figures 3.1 and 3.3) (Finzi *et al.*, 2006).

Tropical ecosystems are considered not limited by nitrogen (Hedin *et al.*, 2009), but can become nitrogen limited as atmospheric $CO_2$ concentrations rise. In our simulations, this process begins in the 1980s, at which point the direct $CO_2$ fertilization effect is reduced (Figure C11). This increased nitrogen limitation is also an indication of when synergistic effects can develop, because from this time any additional nitrogen deposition can alleviate this limitation. Further, tropical forests can often be limited by phosphorus availability due to the typical old, weathered soils found in these regions (Vitousek & Sanford, 1986). However, carbon-nitrogen-phosphorus dynamics are not currently included in CLM4.5-BGC, and so we do not capture the limitation on tropical carbon uptake by phosphorus availability.

Our estimate (1990s mean) of the synergistic contribution to the terrestrial sink (0.32 PgC/yr) is similar to that of Zaehle *et al.* (2010) (0.4 PgC/yr) but smaller than the Churkina *et al.* (2009) estimate of 0.7 PgC/yr (Table 3.3). Differences between estimates are not surprising given the complex interactions between the carbon and nitrogen cycles, different model parameterisations and the use of off-line (Zaehle *et al.*, 2010) or coupled (Churkina *et al.*, 2009) model simulations.

However, most studies that look to quantify the influence of nitrogen deposition on the land carbon sink perform long-term multi-decadal/century-scale simulations (Bala *et al.*, 2013, Churkina *et al.*, 2009, Devaraju *et al.*, 2016, Thornton *et al.*, 2007, Wang *et al.*, 2017, Zaehle *et al.*, 2010), and so quantify changes in carbon cycling over given historical periods. In these modelling studies (and including this one), interaction effects are shown to develop over the course of many decades, and so highlight how the magnitude of simulated non-linear effects depend on the timescale and baseline considered. In this regard, the scientific community has given less attention to process attribution behind the post-2000 carbon sink. Our analysis indicates that for the most recent decade, changes in nitrogen deposition and corresponding effects on $CO_2$ fertilization had no influence on global carbon uptake (Figure 3.3). Thus, from our long-term historical simulations we conclude additional nitrogen deposition has increased the sink by ~0.7 PgC/yr, but recent regional changes in deposition have not altered the nitrogen induced global sink. This is primarily due to opposing responses from nitrogen deposition increases in East Asia and Western Europe and decreases in North America and Eastern Europe, respectively, resulting in a small overall impact globally (Figures 3.6 and 3.7). Furthermore, increased uptake from carbon-nitrogen synergy only occurs in regions of increased deposition (Churkina *et al.*, 2009, Zaehle *et al.*, 2010), however we find that in both East Asia and Western Europe high nitrogen limitation brought about by high atmospheric $CO_2$ concentrations in this period inhibits carbon uptake, a constraint which is not fully alleviated by the extra nitrogen deposited. Despite the fact that evidence points towards nitrogen deposition induced East Asian greening and carbon sink increases in the last three decades (Gu *et al.*, 2015, Piao *et al.*, 2015, Piao *et al.*, 2012, Zhu *et al.*, 2017), our results suggest that a significant contribution from additional nitrogen deposition to the enhanced global land sink since the turn of this century is unlikely.

Thus, what processes and mechanisms are behind the post-2000 increase in the land carbon sink? Firstly, it should be noted that our modelled land carbon sink does not fully capture the magnitude of the uptick seen in the residual land sink since ~2000 (Figure 3.5 and Figure C5), exhibiting a more transient increase. While the limited ability of reproducing this uptick appears to be model specific (Le Quéré *et al.*, 2016), this may indicate that the model used is inadequately capturing and/or missing key processes. Yet, our analysis indicates that even in a scenario with high nitrogen limitation, $CO_2$ fertilization is the main driver behind the increased sink, a result consistent with previous modelling studies (Keenan *et al.*, 2016, Schimel *et al.*, 2015, Sitch *et al.*, 2015), with nitrogen deposition and its interactions with $CO_2$ fertilization providing secondary drivers. However, this "transient" $CO_2$ fertilization hypothesis contradicts the observed behaviour of the residual land sink, which seems to experience a step increase from ~2000 onwards (Le Quéré *et al.*, 2016).

Furthermore, variations in climate have a strong influence on carbon cycling (Friedlingstein *et al.*, 2006), and we simulated a net loss of carbon due to surface warming since the turn of this century. However, the impact of climate on the recent behaviour of the land sink is relatively uncertain (Friedlingstein, 2015, Mystakidis *et al.*, 2016). The findings of this study are contrary to the conclusions of Ballantyne *et al.* (2017), who argue that relatively cool surface temperatures (over 1998-2012 – 'warming hiatus') reduced soil respiration, inducing a carbon sink. However, this 'warming hiatus' hypothesis itself has been called into question because the changes in seasonal land sink trends between warming (1982-1998) and hiatus (1998-2014) periods do not match the changes in seasonal temperature trends (Zhu *et al.*, 2018), and so changes in seasonal temperature are unlikely to be drivers of reduced annual ecosystem respiration. Thus, following contradictory studies, the mechanism(s) behind the increased terrestrial carbon sink since 2000 remain elusive.

Although our results provide a useful indication of competing factors controlling the land carbon sink over the historical period, there are a number of process simplifications and limitations in our modelling methods that need to be considered. For example, we do not consider the effects of LULCC in this study. However, LULCC emissions are used directly in calculating the residual land sink, and so any errors in LULCC emissions propagate through to the residual sink estimate. So, if the 21st century decline in LULCC emissions is underestimated (Andela *et al.*, 2017, Kondo *et al.*, 2018, Liu *et al.*, 2015), the uptick in the residual sink will be overestimated, meaning our modelled results would be more in agreement with the "observed" sink.

Further, the low temporal resolution (decadal mean) of our nitrogen deposition driver data will mask to some extent any abrupt related changes in the coupled carbon-nitrogen cycles. However, as our analysis is based on decadal scales we are reasonably confident in capturing the main response to changing nitrogen deposition. Regarding changes in spatial patterns of nitrogen deposition in the recent period, Chinese and North American trends are well validated (Liu *et al.*, 2013, Xing *et al.*, 2015). The simulated trends in nitrogen deposition over Western Europe seem, however, less robust as suggested by a recent satellite study indicating opposing trends (Jia *et al.*, 2016). This discrepancy can be reconciled as Jia *et al.* (2016) did not include the contribution from ammonia to the total deposition flux due to lack of observations, yet ammonia could be an important component of changes in total nitrogen fluxes in agricultural and biomass burning regions (Warner *et al.*, 2017). Nonetheless, as the large-scale changes seems to be realistic, we are satisfied we accurately capture recent changes in deposition.

Additionally, even though CLM4.5-BGC simulates detailed carbon and nitrogen cycles, there are still a number of shortcomings associated with carbon-nitrogen biogeochemistry schemes (Thomas *et al.*, 2013). One example is the fixed C:N ratios for plant tissues, which prevents ecosystems adapting to new conditions. In-situ studies have shown that ecosystems exhibit increasing C:N ratios under increasing $CO_2$, enabling high carbon storage per unit nitrogen (Dybzinski *et al.*, 2015, Finzi *et al.*, 2006). Further, CLM4.5-BGC does not account for the varying dynamics of above/below ground carbon allocation, whereby there is increased root allocation under elevated atmospheric $CO_2$ and nitrogen stress. This process has been shown to mediate plant response to elevated $CO_2$ levels (Drake *et al*. 2011).

Newer versions of CLM improve upon the formulation used in this study, by introducing dynamic allocation and a more sophisticated representation of plant nitrogen uptake (Ghimire *et al.,* 2016). Finally, our model does not consider the considerable uncertainty caused by biological fixation (Cleveland *et al.*, 1999), which provides a major input of new nitrogen to terrestrial ecosystems, and which has been found to up-regulate during periods when net carbon uptake rates are high (Batterman *et al.*, 2013a). Our model formulation scales biological nitrogen fixation to NPP, which does not accurately reflect the up- and down-regulation that plants use in response to differences in nitrogen demand versus supply (Batterman *et al.*, 2013a, Batterman *et al.*, 2013b). Such an alternative modelling structure is recommended (Wieder *et al.*, 2015). Furthermore, the carbon cost for acquiring nutrients, including from soil vs. nitrogen fixation, is not currently simulated and modelling studies have shown the importance of this in accurately simulating how plants respond to altered nitrogen availability (Brzostek *et al.*, 2014, Shi *et al.*, 2016).

## 3.5 Conclusion

Our results highlight the importance of synergistic effects between rising atmospheric $CO_2$, nitrogen deposition, and a changing climate in regard to the evolution of the terrestrial carbon sink over the 20th century. However, with respect to the recent (post 2000) strengthening of the terrestrial carbon sink, our findings suggest that such synergistic effects between carbon, nitrogen and climate are not key factors because of the relatively small change in global nitrogen deposition over the last two decades. We find that CO2 fertilization to be a main driver behind the increased carbon sink since 2000, in line with previous studies (eg. Keenan *et al.* (2016)), although the recently-observed decline in the carbon sink across the Amazonian tropical forests suggest another factor, such as nitrogen, may be limiting the size of the sink (Brienen *et al.*, 2015, Hedin, 2015). Alternatively, variations in climate have the potential to drive changes in carbon storage. Our analysis suggests climate variations weakened the carbon sink over the recent period. The response of the biosphere to recent variations in climate is, however, uncertain with conflicting conclusions about the magnitude of change in the post-2000 carbon sink (Ballantyne *et al.*, 2017, Zhu *et al.*, 2018).

With signs of the “warming hiatus” ending (Fyfe *et al.*, 2016) and the potential for increased nutrient limitation in the future with higher demand under enhanced $CO_2$, along with the potential for reductions in nitrogen deposition in some regions (Kanakidou *et al.*, 2016), it remains unclear how long the terrestrial carbon sink can continue to grow in line with fossil fuel emissions. Resolving this question is critical for resolving nutrient cycling and global change in the future.

## Acknowledgments

We gratefully acknowledge funding for this study though a EU Marie Curie Integration grant (CIG PCIG14-GA-2013-631812) to W.B. This work was supported by the Natural Environment Research Council (grant number NE/N006895/1). All model simulation data is available at https://doi.org/10.5518/470

## References

Ahlstrom A, Raupach MR, Schurgers G *et al.* (2015) The dominant role of semi-arid ecosystems in the trend and variability of the land CO2 sink. Science, **348**, 895-899.

Andela N, Morton D, Giglio L *et al.* (2017) A human-driven decline in global burned area. Science, **356**, 1356-1362.

Bala G, Devaraju N, Chaturvedi RK, Caldeira K, Nemani R (2013) Nitrogen deposition: how important is it for global terrestrial carbon uptake? Biogeosciences, **10**, 7147-7160.

Baldocchi D, Ryu Y, Keenan T (2016) Terrestrial Carbon Cycle Variability. F1000Research, **5**, 2371-2371.

Ballantyne A, Smith W, Anderegg W *et al.* (2017) Accelerating net terrestrial carbon uptake during the warming hiatus due to reduced respiration. Nature Climate Change, **7**.

Ballantyne AP, Alden CB, Miller JB, Tans PP, White JWC (2012) Increase in observed net carbon dioxide uptake by land and oceans during the past 50 years. Nature, **488**, 70-72.

Banzhaf S, Schaap M, Kranenburg R *et al.* (2015) Dynamic model evaluation for secondary inorganic aerosol and its precursors over Europe between 1990 and 2009. Geoscientific Model Development, **8**, 1047-1070.

Batterman SA, Hedin LO, Van Breugel M, Ransijn J, Craven DJ, Hall JS (2013a) Key role of symbiotic dinitrogen fixation in tropical forest secondary succession. Nature, **502**, 224-227.

Batterman SA, Wurzburger N, Hedin LO (2013b) Nitrogen and phosphorus interact to control tropical symbiotic $N_2$ fixation: a test in *Inga punctata*. Journal of Ecology, **101**, 1400-1408.

Bonan GB, Levis S (2010) Quantifying carbon-nitrogen feedbacks in the Community Land Model (CLM4). Geophysical Research Letters*,* **37**, L07401-L07401.

Brienen RJW, Phillips OL, Feldpausch TR *et al.* (2015) Long-term decline of the Amazon carbon sink. Nature*,* **519**, 344-348.

Brzostek ER, Fisher JB, Phillips RP (2014) Modeling the carbon cost of plant nitrogen acquisition: Mycorrhizal trade-offs and multipath resistance uptake improve predictions of retranslocation. Journal of Geophysical Research: Biogeosciences*,* **119**, 1684-1697.

Cheng L, Zhang L, Wang YP *et al.* (2017) Recent increases in terrestrial carbon uptake at little cost to the water cycle. Nature Communications*,* **8**.

Churkina G, Brovkin V, Von Bloh W, Trusilova K, Jung M, Dentener F (2009) Synergy of rising nitrogen depositions and atmospheric $CO_2$ on land carbon uptake moderately offsets global warming. Global Biogeochemical Cycles*,* **23**.

Clark DA, Clark DB, Oberbauer SF (2013) Field-quantified responses of tropical rainforest aboveground productivity to increasing $CO_2$ and climatic stress, 1997-2009. Journal of Geophysical Research: Biogeosciences*,* **118**, 783-794.

Cleveland CC, Townsend AR, Schimel DS *et al.* (1999) Global patterns of terrestrial biological nitrogen ($N_2$) fixation in natural ecosystems. Global Biogeochemical Cycles*,* **13**, 623-645.

Collatz GJ, Ball JT, Grivet C, Berry JA (1991) Physiological and environmental regulation of stomatal conductance, photosynthesis and transpiration: a model that includes a laminar boundary layer. Agricultural and Forest Meteorology, **54**, 107-136.

Cox PM, Pearson D, Booth BB, Friedlingstein P, Huntingford C, Jones CD, Luke CM (2013) Sensitivity of tropical carbon to climate change constrained by carbon dioxide variability. Nature*,* **494**, 341-344.

De Vries W, Du E, Butterbach-Bahl K (2014) Short and long-term impacts of nitrogen deposition on carbon sequestration by forest ecosystems. Current Opinion in Environmental Sustainability*,* **9-10**, 90-104.

De Vries W, Posch M (2011) Modelling the impact of nitrogen deposition, climate change and nutrient limitations on tree carbon sequestration in Europe for the period 1900–2050. Environmental Pollution*,* **159**, 2289-2299.

De Vries W, Solberg S, Dobbertin M, Sterba H (2009) The impact of nitrogen deposition on carbon sequestration by European forests and heathlands. Forest Ecology and Management*,* **258**, 1814-1823.

Devaraju N, Bala G, Caldeira K, Nemani R (2016) A model based investigation of the relative importance of CO2-fertilization, climate warming, nitrogen deposition and land use change on the global terrestrial carbon uptake in the historical period. Climate Dynamics*,* **47**, 173-190.

Devries T, Holzer M, Primeau F (2017) Recent increase in oceanic carbon uptake driven by weaker upper-ocean overturning. Nature*,* **542**, 215-218.

Dlugokencky E, Tans PP (2017) NOAA/ESRL. pp Page.

Drake JE, Gallet-Budynek A, Hofmockel KS *et al*. (2011) Increases in the flux of carbon belowground stimulate nitrogen uptake and sustain the long-term enhancement of forest productivity under elevated $CO_2$. Ecology Letters, **14**, 349-357.

Du E, Wim De V, James NG, Xueyang H, Jingyun F (2014) Changes in wet nitrogen deposition in the United States between 1985 and 2012. Environmental Research Letters, **9**, 095004.

Dybzinski R, Farrior CE, Pacala SW (2015) Increased forest carbon storage with increased atmospheric CO2 despite nitrogen limitation: a game-theoretic allocation model for trees in competition for nitrogen and light. Global Change Biology, **21**, 1182-1196.

Elser JJ, Bracken MES, Cleland EE *et al.* (2007) Global analysis of nitrogen and phosphorus limitation of primary producers in freshwater, marine and terrestrial ecosystems. Ecology Letters, **10**, 1135-1142.

Finzi AC, Moore DJP, Delucia EH *et al.* (2006) PROGRESSIVE NITROGEN LIMITATION OF ECOSYSTEM PROCESSES UNDER ELEVATED $CO_2$ IN A WARM-TEMPERATE FOREST. Ecology, **87**, 15-25.

Finzi AC, Norby RJ, Calfapietra C *et al.* (2007) Increases in nitrogen uptake rather than nitrogen-use efficiency support higher rates of temperate forest productivity under elevated CO2. Proceedings of the National Academy of Sciences of the United States of America, **104**, 14014-14019.

Fisher JB, Badgley G, Blyth E (2012) Global nutrient limitation in terrestrial vegetation. Global Biogeochemical Cycles, **26**.

Fleischer K, Wårlind D, Van Der Molen MK *et al.* (2015) Low historical nitrogen deposition effect on carbon sequestration in the boreal zone. Journal of Geophysical Research: Biogeosciences, **120**, 2542-2561.

Frank D, Reichstein M, Bahn M *et al.* (2015) Effects of climate extremes on the terrestrial carbon cycle: concepts, processes and potential future impacts. Global Change Biology, **21**, 2861-2880.

Friedlingstein P (2015) Carbon cycle feedbacks and future climate change. Philosophical Transactions of the Royal Society A: Mathematical, Physical and Engineering Sciences, 1-22.

Friedlingstein P, Cox P, Betts R *et al.* (2006) Climate–Carbon Cycle Feedback Analysis: Results from the C 4 MIP Model Intercomparison. Journal of Climate, **19**, 3337-3353.

Friedlingstein P, Prentice IC (2010) Carbon–climate feedbacks: a review of model and observation based estimates. Current Opinion in Environmental Sustainability, **2**, 251-257.

Fyfe JC, Meehl GA, England MH *et al.* (2016) Making sense of the early-2000s warming slowdown. Nature Climate Change, **6**, 224-228.

Galloway JN, Dentener FJ, Capone DG *et al.* (2004) Nitrogen Cycles: Past, Present, and Future. Biogeochemistry, **70**, 153-226.

Gerber S, Hedin LO, Keel SG (2013) Land use change and nitrogen feedbacks constrain the trajectory of the land carbon sink. Geophysical Research Letters, **40**, 5218-5222.

Gerber S, Hedin LO, Oppenheimer M, Pacala SW, Shevliakova E (2010) Nitrogen cycling and feedbacks in a global dynamic land model. Global Biogeochemical Cycles, **24**, 1-15.

Ghimire B, Riley WJ, Koven CD *et al*. (2016) Representing leaf and root physiological traits in CLM improves global carbon and nitrogen cycling predictions. Journal of Advances in Modelling Earth Systems, **8**, 598-613.

Gruber N, Galloway JN (2008) An Earth-system perspective of the global nitrogen cycle. Nature, **451**, 293-296.

Gu F, Zhang Y, Huang M, Tao B (2015) Nitrogen deposition and its effect on carbon storage in Chinese forests during 1981–2010. Atmospheric Environment, **123**, 171-179.

Hansen J, Kharecha P, Sato M (2013) Climate forcing growth rates: doubling down on our Faustian bargain. Environmental Research Letters, **8**, 011006-011006.

Harris I, Jones PD, Osborn TJ, Lister DH (2014) Updated high-resolution grids of monthly climatic observations - the CRU TS3.10 Dataset. International Journal of Climatology, **34**, 623-642.

Hedin LO (2015) BIOGEOCHEMISTRY Signs of saturation in the tropical carbon sink. Nature, **519**, 295-296.

Hedin LO, Brookshire ENJ, Menge DNL, Barron AR (2009) The Nitrogen Paradox in Tropical Forest Ecosystems. Annual Review of Ecology, Evolution, and Systematics, **40**, 613-635.

Houghton RA, House JI, Pongratz J *et al.* (2012) Carbon emissions from land use and land-cover change. Biogeosciences, **9**, 5125-5142.

Hungate BA, Dukes JS, Shaw MR, Luo YQ, Field CB (2003) Nitrogen and climate change. Science, **302**, 1512-1513.

Huntzinger DN, Michalak AM, Schwalm C *et al.* (2017) Uncertainty in the response of terrestrial carbon sink to environmental drivers undermines carbon-climate feedback predictions. Scientific Reports, **7**, 4765-4765.

Janssens IA, Dieleman W, Luyssaert S *et al.* (2010) Reduction of forest soil respiration in response to nitrogen deposition. Nature Geoscience, **3**, 315-322.

Jia Y, Yu G, Gao Y, He N, Wang Q, Jiao C, Zuo Y (2016) Global inorganic nitrogen dry deposition inferred from ground- and space-based measurements. Scientific Reports, **6**, 19810-19810.

Jia Y, Yu G, He N *et al.* (2014) Spatial and decadal variations in inorganic nitrogen wet deposition in China induced by human activity. Scientific Reports, **4**, 3763.

Kalnay E, Kanamitsu M, Kistler R *et al.* (1996) The NCEP/NCAR 40-Year Reanalysis Project. Bulletin of the American Meteorological Society, **77**, 437-471.

Kanakidou M, Myriokefalitakis S, Daskalakis N *et al.* (2016) Past, Present, and Future Atmospheric Nitrogen Deposition. Journal of the Atmospheric Sciences, **73**, 2039-2047.

Keenan TF, Prentice IC, Canadell JG, Williams CA, Wang H, Raupach M, Collatz GJ (2016) Recent pause in the growth rate of atmospheric CO2 due to enhanced terrestrial carbon uptake. Nature Communications, **7**, 13428-13428.

Kondo M, Ichii K, Patra PK *et al.* (2018) Plant Regrowth as a Driver of Recent Enhancement of Terrestrial CO2 Uptake. Geophysical Research Letters, **45**, 4820-4830.

Koven CD, Lawrence DM, Riley WJ (2015) Permafrost carbon-climate feedback is sensitive to deep soil carbon decomposability but not deep soil nitrogen dynamics. Proceedings of the National Academy of Sciences of the United States of America, **112**, 3752-3757.

Koven CD, Riley WJ, Subin ZM *et al.* (2013) The effect of vertically resolved soil biogeochemistry and alternate soil C and N models on C dynamics of CLM4. Biogeosciences, **10**, 7109-7131.

Lamarque J-F, Kyle GP, Meinshausen M *et al.* (2011) Global and regional evolution of short-lived radiatively-active gases and aerosols in the Representative Concentration Pathways. Climatic Change*,* **109**, 191-212.

Lamarque JF, Bond TC, Eyring V *et al.* (2010) Historical (1850–2000) gridded anthropogenic and biomass burning emissions of reactive gases and aerosols: methodology and application. Atmospheric Chemistry and Physics*,* **10**, 7017-7039.

Le Quéré C, Andrew RM, Canadell J *et al.* (2016) Global Carbon Budget 2016. Earth Syst. Sci. Data*,* **8**, 605-649.

Le Quéré C, Andrew RM, Friedlingstein P *et al.* (2018) Global Carbon Budget 2017. Earth Syst. Sci. Data*,* **10**, 405-448.

Lebauer DS, Treseder KK (2008) NITROGEN LIMITATION OF NET PRIMARY PRODUCTIVITY IN TERRESTRIAL ECOSYSTEMS IS GLOBALLY DISTRIBUTED. Ecology*,* **89**, 371-379.

Liu L, Greaver TL (2009) A review of nitrogen enrichment effects on three biogenic GHGs: the CO2 sink may be largely offset by stimulated N2O and CH4 emission. Ecology Letters*,* **12**, 1103-1117.

Liu X, Zhang Y, Han W *et al.* (2013) Enhanced nitrogen deposition over China. Nature*,* **494**, 459-462.

Liu Y, van Dijk A, de Jeu R *et al.* (2015) Recent reversal in loss of global terrestrial biomass. Nature Climate Change, **5**, 470-474.

Los SO (2013) Analysis of trends in fused AVHRR and MODIS NDVI data for 1982-2006: Indication for a $CO_2$ fertilization effect in global vegetation. Global Biogeochemical Cycles*,* **27**, 318-330.

Mystakidis S, Davin EL, Gruber N, Seneviratne SI (2016) Constraining future terrestrial carbon cycle projections using observation-based water and carbon flux estimates. Global Change Biology*,* **22**, 2198-2215.

Norby RJ, Delucia EH, Gielen B *et al.* (2005) Forest response to elevated CO2 is conserved across a broad range of productivity. Proceedings of the National Academy of Sciences of the United States of America*,* **102**, 18052-18056.

Norby RJ, Warren JM, Iversen CM, Medlyn BE, Mcmurtrie RE (2010) CO2 enhancement of forest productivity constrained by limited nitrogen availability. Proceedings of the National Academy of Sciences of the United States of America*,* **107**, 19368-19373.

O'Sullivan M, Rap A, Reddington CL, Spracklen DV, Gloor M, Buermann W (2016) Small global effect on terrestrial net primary production due to increased fossil fuel aerosol emissions from East Asia since the turn of the century. 8060-8068.

Oleson KW, Lawrence DM, Authors L *et al.* (2013) Technical Description of version 4.5 of the Community Land Model (CLM).

Pan Y, Birdsey RA, Fang J *et al.* (2011) A large and persistent carbon sink in the world's forests. Science (New York, N.Y.)*,* **333**, 988-993.

Peters GP, Andrew RM, Boden T *et al.* (2013) The challenge to keep global warming below 2 °C. Nature Climate Change*,* **3**, 4-6.

Piao S, Yin G, Tan J *et al.* (2015) Detection and attribution of vegetation greening trend in China over the last 30 years. Global Change Biology*,* **21**, 1601-1609.

Piao SL, Ito A, Li SG *et al.* (2012) The carbon budget of terrestrial ecosystems in East Asia over the last two decades. Biogeosciences*,* **9**, 3571-3586.

Reichstein M, Bahn M, Ciais P *et al.* (2013) Climate extremes and the carbon cycle. Nature, **500**, 287-295.

Rödenbeck C, Bakker DCE, Metzl N *et al.* (2014) Interannual sea–air CO&lt;sub&gt;2&lt;/sub&gt; flux variability from an observation-driven ocean mixed-layer scheme. Biogeosciences, **11**, 4599-4613.

Schimel D, Stephens BB, Fisher JB (2015) Effect of increasing CO2 on the terrestrial carbon cycle. Proceedings of the National Academy of Sciences of the United States of America, **112**, 436-441.

Sellers PJ, Randall DA, Collatz GJ *et al.* (1996) A Revised Land Surface Parameterization (SiB2) for Atmospheric GCMS. Part I: Model Formulation. Journal of Climate, **9**, 676-705.

Shi M, Fisher JB, Brzostek ER, Phillips RP (2016) Carbon cost of plant nitrogen acquisition: global carbon cycle impact from an improved plant nitrogen cycle in the Community Land Model. Global Change Biology, **22**, 1299-1314.

Sitch S, Friedlingstein P, Gruber N *et al.* (2015) Recent trends and drivers of regional sources and sinks of carbon dioxide. Biogeosciences, **12**, 653-679.

Smith KW, Reed SC, Cleveland CC *et al.* (2016) Large divergence of satellite and Earth system model estimates of global terrestrial CO2 fertilization. Nature Climate Change, **6**, 306-310.

Terrer C, Vicca S, Hungate BA, Phillips RP, Prentice IC (2016) Mycorrhizal association as a primary control of the $CO_2$ fertilization effect. Science (New York, N.Y.), **353**, 72-74.

Thomas RQ, Bonan GB, Goodale CL (2013) Insights into mechanisms governing forest carbon response to nitrogen deposition: a model–data comparison using observed responses to nitrogen addition. Biogeosciences, **10**, 3869-3887.

Thornton PE, Lamarque J-F, Rosenbloom NA, Mahowald NM (2007) Influence of carbon-nitrogen cycle coupling on land model response to $CO_2$ fertilization and climate variability. Global Biogeochemical Cycles, **21**, GB4018-GB4018.

Viovy N (2018) CRUNCEP Version 7 - Atmospheric Forcing Data for the Community Land Model. pp Page, Boulder, CO, Research Data Archive at the National Center for Atmospheric Research, Computational and Information Systems Laboratory.

Vitousek PM, Howarth RW (1991) Nitrogen Limitation on Land and in the Sea: How Can It Occur? pp Page, Springer.

Vitousek PM, Sanford RL (1986) Nutrient Cycling in Moist Tropical Forest. Ann. Rev. Ecol. Syst, **17**, 137-167.

Waldner P, Marchetto A, Thimonier A *et al.* (2014) Detection of temporal trends in atmospheric deposition of inorganic nitrogen and sulphate to forests in Europe. Atmospheric Environment, **95**, 363-374.

Wang R, Goll D, Balkanski Y *et al.* (2017) Global forest carbon uptake due to nitrogen and phosphorus deposition from 1850 to 2100. Global Change Biology, **23**, 4854-4872.

Warner JX, Dickerson RR, Wei Z, Strow LL, Wang Y, Liang Q (2017) Increased atmospheric ammonia over the world's major agricultural areas detected from space. Geophysical Research Letters, **44**, 2875-2884.

Wieder WR, Cleveland CC, Lawrence DM, Bonan GB (2015) Effects of model structural uncertainty on carbon cycle projections: biological nitrogen fixation as a case study. Environmental Research Letters*,* **10**, 044016-044016.

Xing J, Mathur R, Pleim J *et al.* (2015) Observations and modeling of air quality trends over 1990–2010 across the Northern Hemisphere: China, the United States and Europe. Atmos. Chem. Phys*,* **15**, 2723-2747.

Zaehle S (2013) Terrestrial nitrogen-carbon cycle interactions at the global scale. Philosophical transactions of the Royal Society of London. Series B, Biological sciences*,* **368**, 20130125-20130125.

Zaehle S, Dalmonech D (2011) Carbon–nitrogen interactions on land at global scales: current understanding in modelling climate biosphere feedbacks. Current Opinion in Environmental Sustainability*,* **3**, 311-320.

Zaehle S, Friend AD, Friedlingstein P, Dentener F, Peylin P, Schulz M (2010) Carbon and nitrogen cycle dynamics in the O-CN land surface model: 2. Role of the nitrogen cycle in the historical terrestrial carbon balance. Global Biogeochemical Cycles*,* **24**, GB1005-GB1005.

Zhu J, He N, Zhang J *et al.* (2017) Estimation of carbon sequestration in China's forests induced by atmospheric wet nitrogen deposition using the principles of ecological stoichiometry. Environmental Research Letters*,* **12**, 114038-114038.

Zhu Z, Piao S, Myneni RB *et al.* (2016) Greening of the Earth and its drivers. Nature Climate Change*,* **6**, 791-795.

Zhu Z, Piao S, Yan T, Ciais P, Bastos A, Zhang X, Wang Z (2018) The Accelerating Land Carbon Sink of the 2000s May Not Be Driven Predominantly by the Warming Hiatus. Geophysical Research Letters*,* **45**, 1402-1409.

# Chapter 4

# Climate-driven trends and variability in terrestrial vegetation productivity over 1982-2016

**Michael O'Sullivan**[1,2], Dominick. V. Spracklen[2], W. Kolby Smith[3], Stephen Sitch[4], Pierre Friedlingstein[1], Vivek K. Arora[5], Vanessa Haverd[6], Atul Jain[7], Etsushi Kato[8], Markus Kautz[9,10], Danica Lombardozzi[11], Julia E.M.S. Nabel[12], Hanqin Tian[13], Nicolas Vuichard[14], Andy Wiltshire[15], Dan Zhu[14], and Wolfgang Buermann[2,16]

[1]College of Engineering, Mathematics and Physical Sciences, University of Exeter, Exeter EX4 4QF, UK

[2]Institute for Climate and Atmospheric Science, School of Earth and Environment, University of Leeds, Leeds, UK

[3]School of Natural Resources and the Environment, University of Arizona, Tucson, AZ 85721, USA

[4]College of Life and Environmental Sciences, University of Exeter, Exeter EX4 4RJ, UK

[5]Canadian Centre for Climate Modelling and Analysis, Environment and Climate Change Canada, University of Victoria, Victoria, British Columbia, Canada V8W2Y2

[6]CSIRO Oceans and Atmosphere, Canberra, ACT 2601, Australia

[7]Department of Atmospheric Sciences, University of Illinois, Urbana, IL 61801, USA

[8]Institute of Applied Energy (IAE), Minato, Tokyo 105-0003, Japan

[9]Institute of Meteorology and Climate Research – Atmospheric Environmental Research (IMK-IFU), Karlsruhe Institute of Technology (KIT), Garmisch-Partenkirchen, Germany

[10]Forest Research Institute Baden- Württemberg, 79100 Freiburg, Germany

[11]Climate and Global Dynamics Division, National Center for Atmospheric Research, Boulder, CO 80302, USA

[12]Max Planck Institute for Meteorology, Hamburg 20146, Germany

[13]International Center for Climate and Global Change Research, School of Forestry and Wildlife Sciences, Auburn University, 602 Duncan Drive, Auburn, AL 36849, USA

[14]Laboratoire des Sciences du Climat et de l'Environnement, UMR8212 CEA-CNRS-UVSQ, Université Paris-Saclay, IPSL, Gif-sur-Yvette 91191, France

[15]Met Office Hadley Centre, Exeter EX1 3PB, UK

[16]Institute of Geography, University of Augsburg, 86159 Augsburg, Germany

## Abstract

Geographical variations in climate control the productivity of vegetation (gross primary productivity; GPP), and therefore have a large impact on the amount of carbon stored in the terrestrial biosphere. However, direct observations of global GPP are not possible, and current estimates rely on different modelling and quasi-observed approaches. Here, we assess the consistency in GPP estimates based on three widely used approaches; two observation-based approaches, the upscaling of FLUXNET site observations (FLUXCOM) and a satellite derived light-use efficiency model (LUE), and GPP estimates from a suite of terrestrial biosphere models (TRENDYv6). We compare climate-driven interannual variability (IAV) and trends in GPP from local to global scales over the period 1982-2016. We find large GPP differences across the multiple temporal and spatial scales considered between the products. FLUXCOM IAV and trends are systematically smaller than those based on the other two products at local and global scales. Large northern GPP increases for TRENDYv6 and LUE dominate positive global trends in these two approaches. Locally, we find robust year-to-year correlation in the various estimates, with

exception of tropical and high northern latitude regions. Further, there are large regions (58% of the vegetated land surface) where all products agree on the direction of trends. However, there are clear differences in variability and trends in GPP as well as underlying climatic controls, highlighting uncertainty in the processes that influence GPP. These results emphasise the need for long-term observations of GPP, particularly in underrepresented regions (e.g. tropical forests), and the need to better constrain and improve relevant processes in models, to more accurately quantify the climate sensitivity of terrestrial carbon uptake.

## 4.1 Introduction

Gross primary production (GPP), the amount of carbon fixed by photosynthesis per unit area in time, is the pathway for transferring atmospheric $CO_2$ to the terrestrial biosphere. It is the largest carbon flux in the Earth system, and as such any small change can significantly alter the net carbon balance at the surface, atmospheric $CO_2$ concentrations, and subsequently feedbacks to climate (Friedlingstein *et al.*, 2014). Therefore, quantifying variations in GPP and attributing underlying drivers and mechanisms is an important area of research. GPP responds to changes in atmospheric $CO_2$ concentrations, nutrient availability, and climate (Ciais *et al.*, 2005, Nemani *et al.,* 2003, Schimel *et al.,* 2015, Zaehle & Dalmonech, 2011). Moreover, land use and land-cover change (e.g. deforestation) alter the spatial distribution of vegetation and therefore also impact GPP and carbon uptake.

Variations in climate can influence both IAV and long-term trends in GPP. IAV in global GPP has been found to be controlled by certain hotspot regions, specifically tropical forests (Jung *et al.*, 2011, Wang *et al.*, 2013, Wang *et al.*, 2014) and semi-arid regions (Ahlstrom *et al.*, 2015, Poulter *et al.*, 2014). IAV in GPP in these hotspot regions is dominated by climate variability associated with the El Nino Southern Oscillation (ENSO) (Ahlstrom *et al.*, 2015, Bastos *et al.*, 2013, Zhao & Running, 2010), and other climate extreme climatic events (Zscheischler *et al.*, 2014). With more frequent climate extremes under projected climate change (Seneviratne *et al.*, 2012), the impact of GPP IAV on the global carbon cycle is also likely to increase (Reichstein *et al.*, 2013).

In regard to longer-term variations, there is evidence that recent large-scale climatic shifts have profoundly influenced global plant carbon uptake and the land carbon sink (Buermann *et al*., 2016). Specifically, the accelerated warming over northern latitudes appears to have substantially increased carbon uptake by plants (Keeling *et al*., 1996, Keenan *et al.*, 2014, Myneni *et al.*, 1997, Piao *et al.*, 2007). However, northern warming during colder seasons can lead to moisture stress later in the year, offsetting the initial positive effects (Buermann *et al.*, 2018, Buermann *et al.*, 2013)**.** Warming-induced drying trends with adverse impacts on GPP have also been identified in large regions of the southern hemisphere (Huang *et al.*, 2016, Zhao & Running, 2010, Zscheischler *et al.*, 2014).

GPP studies over large spatial scales (including those mentioned above) rely on modelling approaches. This is because observation-based estimates of GPP are only available at leaf levels through chambers (Welp *et al.*, 2011) or local levels through eddy-covariance flux towers (Baldocchi *et al.*, 2001). Scaling leaf-level observations to global scale is challenging due to the artificial nature of lab experiments and challenges associated with scaling leaf-level values to the entire canopy (Baldocchi, 2003). Furthermore, partitioning eddy-covariance data into component fluxes is an uncertain procedure (Lasslop *et al.*, 2010, Reichstein *et al.*, 2005, Wehr & Saleska, 2015, Wehr *et al*., 2016) and scaling the small spatial footprint of eddy-flux towers to global scale introduces additional uncertainties (Beer *et al.*, 2010, Jung *et al*., 2009). Machine learning methods are often utilised to perform this upscaling from local flux tower levels to regional and global scales (e.g. Beer *et al.,* 2010, Jung *et al.,* 2011). The FLUXCOM initiative uses a variety of methods (including different partitioning methods and machine learning algorithms) to integrate site level observations, satellite remote sensing, and meteorological data to produce wall-to-wall estimates of carbon fluxes (Tramontana *et al.,* 2016, Jung *et al.,* 2017).

An alternative data-driven approach to estimate GPP is using satellite observations of vegetation activity, such as the fraction of absorbed photosynthetic active radiation absorbed by plants (FPAR), combined with a light-use efficiency formulation (Running *et al.*, 2004, Zhu *et al.*, 2013). Such satellite-driven production efficiency models can provide benefits of high spatiotemporal information owing to the satellites unique sampling capabilities. However, satellite observations often suffer from data contamination due to cloud cover and signal saturation in dense canopied regions and these influences together with uncertainties in LUE theory propagate into uncertainties in GPP (Smith, WK *et al.*, 2016).

Dynamic global vegetation models (DGVMs) offer another method of estimating global GPP. These prognostic process-based models represent our current understanding of the major processes of the terrestrial carbon cycle and other biogeochemical cycles (Fisher *et al.*, 2014), and offer the only way to project future changes in carbon cycling. However, given the high complexity of terrestrial ecosystems, simplifications must be made, and often such simplifying assumptions are different and sometimes divergent across models. More specifically, differences arise between modelled estimates of GPP due to different sets of equations and parameterisations of processes, such as photosynthesis, physiology, phenology, and element cycling (Fisher *et al.*, 2014).

These observation-based and process-based modelling approaches all have their own merits and limitations and they do not necessarily agree with each other on various spatial and temporal scales (Smith, WK *et al.*, 2016). Yet, corresponding model outputs have been used independently or in conjunction with one another in multiple studies focussing on the variability of the terrestrial carbon cycle (Ballantyne *et al.*, 2017, Beer *et al.*, 2010, Jung *et al.*, 2017, Zhu *et al.*, 2016). It is thus important to assess the consistency of these 'state of the art' GPP products across multiple temporal and spatial scales including their sensitivity to climate variability. Highlighting similarities and discrepancies will provide information on the level of confidence we can place in the products and hence previously made inferences.

The aim of this study is to compare climate-driven GPP estimates (see Methods) from an empirical approach based on eddy-covariance data (FLUXCOM, Jung *et al.* (2017)), a light-use efficiency model (Smith WK *et al.*, 2016), and a set of DGVMs from TRENDYv6 (Le Quéré *et al*., 2018). Specifically, over the 35-year study period 1982-2016, we investigate (i) to what extent are these climate-driven GPP estimates consistent on seasonal, interannual, and longer-term timescales across multiple spatial scales and (ii) how do they differ in regards to their sensitivity to key climate drivers.

## 4.2 Methods

### 4.2.1 GPP Datasets

FLUXCOM

We used GPP obtained from FLUXCOM (version RS+METEO) (Jung *et al.*, 2017, Tramontana *et al.*, 2016) at 0.5° spatial resolution and monthly time scale over the period 1982-2016. FLUXCOM GPP is based on machine learning methods that upscale FLUXNET (Baldocchi *et al.*, 2001) site level information (carbon fluxes and local meteorology derived from flux towers) using gridded climate and satellite data. Three machine learning methods are used for the upscaling process; Artificial Neural Networks, Random Forests, and Multivariate Adaptive Regression (Jung *et al.*, 2017, Tramontana *et al.*, 2016). Flux towers measure net carbon exchange between land and the atmosphere. The component GPP flux is derived by estimating the temperature sensitivity of ecosystem respiration (TER) from night time flux data and then extrapolated to daytime to determine TER and GPP (Reichstein *et al.*, 2005). Gridded (0.5°) predictor variables (e.g. local climate, vegetation type, normalized difference vegetation index (NDVI)) are used to produce spatio-temporal grids of GPP. Climate variables are from the CRUNCEPv8 product, which is based on a combination of Climate Research Unit monthly 0.5° dataset and the 6-hourly time resolution National Centres for Environmental Prediction (NCEP) reanalysis. Overall, there are three different GPP estimates (three upscaling products with different machine learning algorithms to form the FLUXCOM ensemble) and the spread in these ensemble members as a measure of uncertainty (see also below). By design, the FLUXCOM RS+METEO GPP product does not capture the effects associated with $CO_2$ fertilization, vegetation greening or disturbances since in its generation only climatic input variables are time-varying. The FLUXCOM product therefore largely captures the response of GPP to instantaneous climate variability alone and does not capture vegetation and soil moisture memory effects.

In a complementary analysis, we also use another GPP product (0.5° over the period 1982-2008) based on upscaled FLUXNET observations (FluxNetG; Jung *et al.*, 2011). FluxNetG is driven with a single satellite vegetation dataset (NDVIg), and unlike FLUXCOM, includes information on interannual variations in vegetation activity. Therefore, we assess to what degree including additional (interannual) satellite information influences upscaled GPP variability and trends.

TRENDY

We also used GPP data over the period 1982-2016 from twelve DGVMs that participated in the TRENDYv6 multi-model inter-comparison, which were all forced with a common protocol (Sitch *et al.*, 2015). Models included are CABLE (Haverd *et al.*, 2018), CLASS-CTEM (Melton & Arora, 2016), CLM4.5-BGC (Oleson *et al.,* 2013), DLEM (Tian *et al.*, 2015), ISAM (Jain *et al.*, 2013), LPJ-GUESS (Smith *et al.*, 2014), JSBACH (Reick *et al.*, 2013), JULES (Clark *et al.*, 2011), ORCHIDEE (Krinner *et al.*, 2005), ORCHIDEE-MICT (Guimberteau *et al.*, 2018), VEGAS (Zeng *et al.*, 2005), and VISIT (Kato *et al.*, 2013). In order to isolate the climate-driven GPP portion in the TRENDYv6 model runs (consistent with our study aim) the following procedure was applied. We used the "CO2 varied only (S1)" and "(Climate and CO2 varied (S2)" simulations from the full set of simulations performed for TRENDYv6. Although the simulations were run from 1700 onwards, we use data from the period 1901-2016. The "S1" simulation is forced with time varying atmospheric $CO_2$ concentrations derived from ice cores and National Oceanic and Atmospheric Administration (NOAA) monitoring stations but meteorological data from the early 20th century (1901-1920) (CRUNCEPv8) is used repeatedly. Consequently, the S1 simulation does not capture changes in climate. To derive the desired "climate only" response for each model we first calculated the trend over 35 years using non-linear least squares (from the 'stats' package in R (Bates & Watts, 1988)) (1982-2016) for each month and grid cell in the S1 simulations. Then this trend was subtracted from that in the S2 simulations (the S2 simulations are run with both time varying $CO_2$ concentrations and meteorological data). This preserves interannual variability but removes the influence of rising $CO_2$ concentrations over this period. We then created an ensemble mean and represent uncertainty by the standard deviation based on the 12 ensemble members (see below).

Light use efficiency (LUE)

LUE models offer an additional tool to estimate GPP patterns (Running *et al.*, 2004). Thus, we have also included a 35-year estimate (1982-2016) based on Global Inventory Modelling and Mapping Studies (GIMMS3g) FPAR from NOAA-AVHRR satellites (Zhu *et al.*, 2013) and meteorological data using the MODIS GPP algorithm (Running *et al.*, 2004, Smith WK *et al.*, 2016) such that:

$$GPP = FPAR \times PAR \times LUE_{\max} \times f(T_{\min}) \times f(VPD) \qquad (1)$$

FPAR over this extended study period is derived from the Normalised Difference Vegetation Index version 3g (NDVI3g) using a neural network algorithm (Zhu *et al.*, 2013). PAR represents incoming photosynthetically active radiation. The maximum light-use efficiency ($LUE_{max}$), minimum temperature function ($f(T_{min})$), and vapour pressure deficit function (f(VPD)) vary depending on biome type. Gridded, monthly mean $T_{min}$ and VPD from CRUNCEPv8 are used. This formulation assumes a temporally invariant *LUE*, and therefore doesn't capture the primary photosynthetic response to increased $CO_2$ concentrations (Norby *et al*., 2005, De Kauwe *et al.,* 2016). Consequently, changes in GPP based on equation (1) are largely driven by climate variability. We use two sets of parameters for $LUE_{max}$, $f(T_{min})$, and f(VPD) to provide an estimate of uncertainty in model structure (Robinson *et al.,* 2018, Zhao & Running, 2010). We then formed an ensemble mean of the two estimates and use the spread as a measure of uncertainty (see also below).

### 4.2.2 Climate datasets

We calculate the sensitivity of each GPP dataset to mean annual surface air temperature (MAT) and precipitation (MAP) from the CRUNCEPv8 reanalysis at 0.5° resolution. All three products are driven by surface air temperature, however only TRENDYv6 is driven with precipitation directly. In the FLUXCOM approach, moisture limitations are represented through a water stress function based on a soil water balance model (Tramontana *et al.*, 2016), whereas in the

LUE formulation a VPD scalar is used (Running *et al.*, 2004). Precipitation is a crucial parameter influencing VPD and soil moisture, and thus we use it consistently across datasets to estimate corresponding GPP sensitivities to water availability.

### 4.2.3 Data processing

To produce spatially consistent products, DGVM output is regridded to 0.5°x0.5° to match both FLUXCOM and LUE. All products are available on monthly time steps from 1982-2016. For each ensemble member (3 for FLUXCOM, 12 for TRENDY, 2 for LUE) we calculated grid-cell and regional (see Figure D1 for regional definitions) anomalies by subtracting the 35-year mean at monthly, seasonal, and annual timescales. We then created ensemble means of these anomalies for each product and use the spread (1 stdev) as a measure of uncertainty in the various approaches. We focus on anomalies rather than absolute GPP as there are large differences between GPP estimates across all 17 datasets (Figure D2). Also, we are interested in how climate-driven GPP has changed over the study period so focusing on anomalies is more appropriate.

### 4.2.4 Statistical analysis

In order to assess the climate sensitivity of the various products, we decomposed the annual GPP anomalies for each region (r) and year (y) into the components forced by temperature and precipitation as:

$$GPP_{r,y} = \gamma_r \times \mathrm{TEMP}_{r,y} + \lambda_r \times \mathrm{PREC}_{r,y} + \varepsilon_{r,y} \qquad (2)$$

where $\gamma_r$ represents the sensitivity of GPP to temperature anomalies ($\mathrm{TEMP}_{r,y}$), $\lambda_r$ the sensitivity of GPP to precipitation anomalies ($\mathrm{PREC}_{r,y}$), and $\varepsilon_{r,y}$ is the residual error. We did not detrend the GPP data before performing the multiple regression since we are interested in how both IAV and long-term variations have influenced GPP. Importantly, the fitted regression coefficients ($\gamma_r$ and $\lambda_r$) represent apparent GPP sensitivities to variations in temperature and precipitation. These are not actual sensitivities because temperature and precipitation are not fully independent and there are also missing explanatory variables in the multiple regression (e.g. radiation, humidity). We omit incoming solar radiation from the regression analysis as it has been previously shown to have a minor contribution to IAV in local and global GPP (Jung *et al*., 2017). Note that this multiple linear regression approach accounts for the covariation between temperature and precipitation. The regression coefficients are calculated using linear least squares and uncertainty in the coefficients is obtained from the standard error. Further, GPP sensitivity to temperature and precipitation may change over time and so here they represent mean sensitivities over the 35-year period. To derive the relative importance of the two climate regressors in determining GPP variability, we use the Lindeman-Merenda-Gold (LMG) method (from the 'relaimpo' package in R (Grömping, 2006)) which calculates the contribution of each regressor to the overall $R^2$ of the linear model.

For trend analysis, we first calculate trends for each ensemble member and report the ensemble mean trend. Uncertainty associated with the trend is calculated from the spread in trends among ensemble members.

## 4.3 Results

### 4.3.1 Large-scale GPP IAV and trends

In a first step, we compared IAV and trends in large-scale climate-driven GPP based on the three approaches, FLUXCOM, LUE and TRENDYv6. At global scale, all three GPP products show a positive trend over the study period 1982-2016 (Figure 4.1a, Table 4.1). However, the FLUXCOM GPP data show a substantially smaller non-significant increase (0.002±0.017 PgC/yr$^2$; $P$>0.05) compared to TRENDYv6 (0.092±0.057 PgC/yr$^2$; $P$<0.01) and LUE (0.062±0.022 PgC/yr$^2$; $P$<0.01) (Figure 4.1a, Table 4.1). We also find that individual FLUXCOM ensemble members do not agree on the direction of the trend, hence the large range compared to the mean (Figure D3). This highlights the influences of the choice of upscaling method on GPP estimates (Tramontana *et al*., 2016).

A focus on regional scales shows that the northern latitudes dominate the global trend for all three products, with significant ($P$<0.01) increases for TRENDYv6 and LUE, but non-significant ($P$>0.05) increases for FLUXCOM (Figure 4.1b, Table 4.1). In the tropics, TRENDYv6 shows a significant positive trend of 0.023±0.031 PgC/yr$^2$ ($P<0.05$), whereas LUE and FLUXCOM show no significant change. Importantly, individual ensemble members of all three products disagree on the direction of trend, highlighting the uncertainty in tropical GPP estimates (Figure D3). All products agree on no GPP trends in the southern latitudes (Figure 4.1d).

Differences in the IAV between the three GPP products (estimated through the standard deviation (σ) of annual (detrended) GPP over the period 1982-2016) are also noteworthy. FLUXCOM GPP displays much lower IAV (0.34 PgC/yr) than the other two products, (TRENDYv6: 1.21 PgC/yr and LUE: 1.01 PgC/yr; Figure 4.1a). Similar differences in IAV between the three products are obtained for northern and tropical regions (Fig. 4.1b,c), but for the southern extratropics TRENDYv6-based GPP is twice as high as in the other products (Fig. 4.1d). FLUXCOM captures only a portion (the instantaneous) of the climate-driven GPP signal whereas the other products contain vegetation and soil memory effects (see also Methods). Namely, FLUXCOM has a climatological fixed seasonal cycle of satellite leaf area index (LAI), so LAI does not vary inter-annually. Therefore, lower FLUXCOM IAV is expected. This is further corroborated by analysing trends and variability in FluxNetG (see Methods). We find the magnitude of trends and variability (over the period 1982-2008) of FluxNetG are more comparable to TRENDYv6 and LUE in all regions (Figure D4). Therefore, the inclusion of solely seasonal satellite data in FLUXCOM significantly reduces GPP IAV and trends.

How well do the three GPP products agree at interannual time scales? To answers this, we computed correlations between the respective detrended annual GPP timeseries. The three GPP products are significantly ($P<0.05$) correlated in all large spatial domains, with the exception of FLUXCOM and LUE over northern latitudes and TRENDYv6 and LUE at global scales (Table 4.1). Generally, the correlations between FLUXCOM and TRENDYv6 at both regional and global scales are much higher compared to the other products and the agreement in IAV between all three products tends to be also greater in tropical and southern latitudes (Table 4.1). LUE simulates large negative tropical anomalies in 2005 (Figure 4.1c), in response to large-scale drought (Phillips *et al.*, 2009, Zhao & Running, 2010), a feature not shared with the other two products, however. Therefore, it seems the satellite based LUE model captures unique information compared to FLUXCOM and TRENDYv6, and generally satellite-driven models agree better with in-situ data than approaches without satellite data (Raczka *et al.*, 2013). This implies that both FLUXCOM and TRENDYv6 are potentially missing important information about GPP variability.

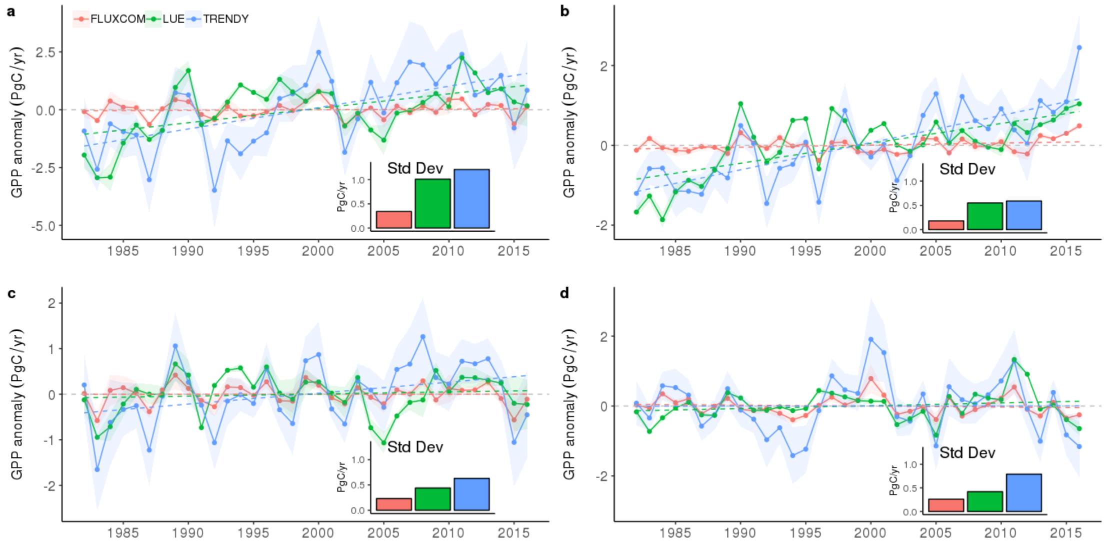

**Figure 4.1 - Global and regional variations in annual GPP based on three GPP products. Annual gross primary production (GPP) anomalies (PgC/yr) over the period 1982-2016 estimated by upscaled flux tower observations, FLUXCOM (red), a subset of terrestrial biosphere models from TRENDYv6 inter-comparison (blue), and a satellite based light use efficiency model (green). GPP anomalies are shown for a) Global, b) Northern, c) Tropical, and d) Southern regions, as defined in Figure D1. Shading represents 1σ spread among each products ensemble members (see Methods). Linear trends are depicted with a dashed line. Bar charts show the inter-annual variability of each product as the 1σ (PgC/yr) of the detrended timeseries.**

**Table 4.1 - Global and regional trends in climate-driven GPP for each product and correlation coefficients between each product. Trends show ensemble mean and the uncertainty is the standard deviation of the trends of each group of ensemble members. Correlations are performed on detrended data in each product combination; FLUXCOM-TRENDYv6 (FT), FLUXCOM-LUE (FL), and TRENDY-LUE (TL). Trends significantly different from zero and significant correlations are marked with an asterisk (*P<0.05, **P<0.01). Regions are shown in Figure D1.**

| Region | Trend (PgC/yr$^2$) | | | Correlation (r) | | |
|---|---|---|---|---|---|---|
| | FLUXCOM | TRENDY | LUE | FT | FL | TL |
| Global | 0.002±0.017 | 0.092±0.057** | 0.062±0.022** | 0.84** | 0.36* | 0.27 |
| North | 0.005±0.004 | 0.068±0.024** | 0.050±0.010** | 0.80** | 0.33 | 0.37* |
| Tropics | 0.000±0.012 | 0.023±0.031* | 0.005±0.010 | 0.90** | 0.52** | 0.46** |
| South | -0.003±0.003 | 0.000±0.022 | 0.008±0.003 | 0.91** | 0.57** | 0.55** |

### 4.3.2 Local-scale IAV and trends

We further examined the temporal agreement between datasets at more local scales by performing grid-cell correlations between the detrended GPP timeseries. There are large areas of significant ($P<0.05$) positive agreement between the products (Figure 4.2), namely in temperate US, grasslands of Eurasia, and savannas and shrublands of the southern hemisphere (as classified by MODIS landcover product MCD12C1 (Friedl *et al.*, 2010) Figures D5 and D6). Furthermore, for FLUXCOM and TRENDYv6, positive correlations are found across the globe (Figure 4.2a). Both FLUXCOM and TRENDYv6 GPP in the tropics have low agreement at these interannual time scales with GPP derived from LUE. Disagreement between FLUXCOM/TRENDYv6 and LUE in central Amazon and South East Asia is due to FLUXCOM and TRENDYv6 having relatively low variance, whereas the lack of correlation in Africa is primarily driven by low covariance (Figure D7). Differences also exist in boreal regions, where FLUXCOM and LUE GPP have low agreement, but TRENDYv6 and LUE are ubiquitously significantly positively correlated. FLUXCOM GPP has very low variance in the northern high latitudes, which is likely adding to the low correlation with LUE (Figure D7). With a focus on seasonal timescales, the good agreement between FLUXCOM and TRENDYv6 is evident for all seasons (Figure D8). For TRENDYv6 and LUE, strong positive correlations in the extratropics are apparent in all seasons, matching the annual correlation pattern (Figures 4.2 and D8). However, the seasonal patterns for FLUXCOM and LUE differ from the annual correlations. For high northern latitudes, for example, the GPP of each product in March-April-May (MAM) is positively correlated, whereas there are no significant correlations in June-July-August (JJA) FLUXCOM and LUE (Figure D8). Other seasonal disparities exist, for example in the US and South Africa, where summer correlations tend to be higher than other seasons (Figure D8). The cause of the seasonal discrepancies is difficult to diagnose. Potential reasons could include; structural differences in the products (e.g. photosynthetic and/or phenological parameterisation, land cover parameterisation, method of including climatic constraints), or, e.g. for high northern latitudes biases in satellite data and lack of eddy covariance flux towers.

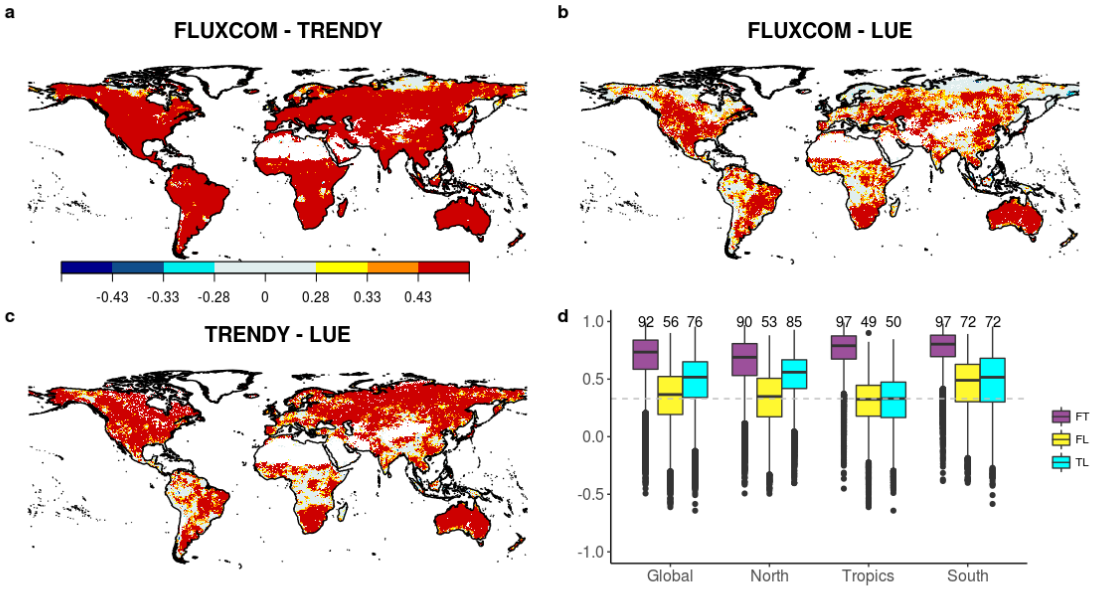

**Figure 4.2 - Grid-cell correlation coefficient (Pearson's r) patterns between detrended annual mean GPP anomalies (1982-2016) for a) FLUXCOM and TRENDYv6, b) FLUXCOM and LUE, c) TRENDY and LUE. (r=0.28, 0.33, 0.43 corresponds to p<0.1, p<0.05, p<0.01). Panel d) shows boxplots of grid-scale correlations for each product combination (FLUXCOM-TRENDY; FT, FLUXCOM-LUE; FL, and TRENDY-LUE; TL) and region. Regions are defined in Figure D1. Grey dashed line at r=0.33 (p<0.05). Numbers above each box represent the percentage of grid cells in the region with a correlation of at least 0.33.**

An ensuing trend analysis on annual GPP shows that all three products exhibit consistently positive trends for large areas across Boreal Eurasia, Europe, North America, West and South Africa, and Australia (Figure 4.3). However, for the northern high latitudes in general only TRENDYv6 and LUE predict large-scale significant increases ($P<0.05$), whereas in the case of FLUXCOM such widespread positive trends are less frequent (Figure 4.3). Northern hemisphere GPP increases are most likely due to a combination of enhanced photosynthesis within the growing season and a lengthening of the growing season (Forkel *et al.*, 2016, Keenan *et al.*, 2014; Figure D9a). The largest positive GPP trends in all three products are over Southern and West Africa, owing to increased precipitation trends (Figure D9b). Southern USA, South America, and East Africa exhibit a declining trend in GPP in all datasets (Figure 4.3d). Warming temperatures in these regions could have led to increases in evaporative demand, leading to a reduction in photosynthesis (Zhao & Running, 2010). There is no clear consensus in Central Africa, with LUE showing large areas of declining GPP but corresponding patterns for FLUXCOM and TRENDYv6 are much more heterogeneous due to no significant trends (Figure 4.3). Overall, the three products agree in regard to the direction of trends over 58% of the vegetated land surface (45% and 13% for positive and negative trends, respectively (Figure 4.3d).

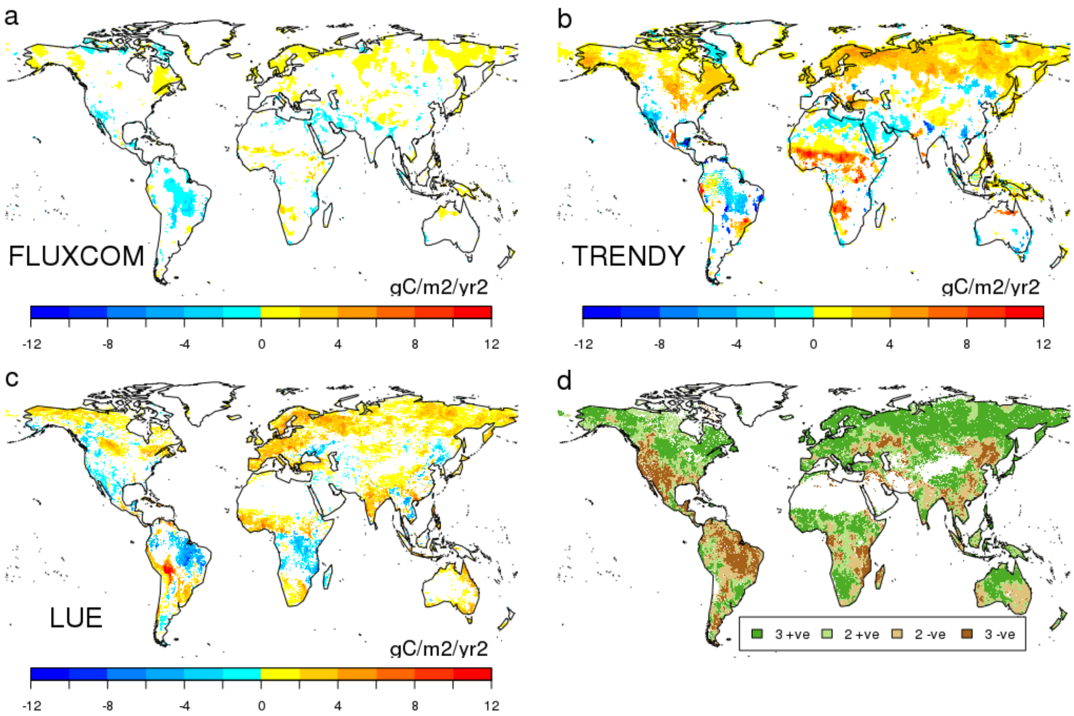

**Figure 4.3 - Spatial pattern of climate-driven trends in annual mean GPP for each product. a, b, c, The maps depict significant (*P*<0.05) trends in annual GPP (gC/m$^2$/yr$^2$) over 1982-2016 for a) FLUXCOM, b) TRENDYv6, c) LUE. d, Agreement in the direction of trend between the three products. Dark areas are where all agree on the direction of trend and light areas indicate disagreement (two products agree, and one differs).**

The large annual GPP increases observed in northern latitudes in TRENDYv6 and LUE (and FLUXCOM to a smaller extent) stem from contributions throughout the growing season (March through November in Eurasia and June through November in North America; Figures 4.4 and D10). The three products also agree on the spring/summer decline in productivity over southern portions of North America. There is further agreement on the positive Western and Southern Africa trends in September through February and December through August, respectively. Further, the central South American decrease in annual GPP captured by all products is also consistently concentrated in the dry season

(Aug-Oct) (Figure 4.4). Apart from this, there is generally poor agreement over tropical forests in all seasons, with no clear patterns emerging (Figure D10). This highlights the potential lack of significant trends in tropical regions and/or deficiencies in all three products. Errors could be due to underrepresentation of tropical FLUXNET sites that form the basis of the FLUXCOM product (Tramontana *et al.*, 2016), inadequacies in how process-based models simulate tropical GPP (e.g. due to phenology (Restrepo-Coupe *et al.*, 2017) or physiology (Wu *et al.*, 2016) parameterisations), low quality optical data driving the LUE model or how the MODIS GPP algorithm parameterises tropical forests. Since GPP and its IAV in tropical regions responds primarily to water stress and not temperature (as in the high-latitude regions) this also likely points to differing response of GPP to water stress in different models and approaches.

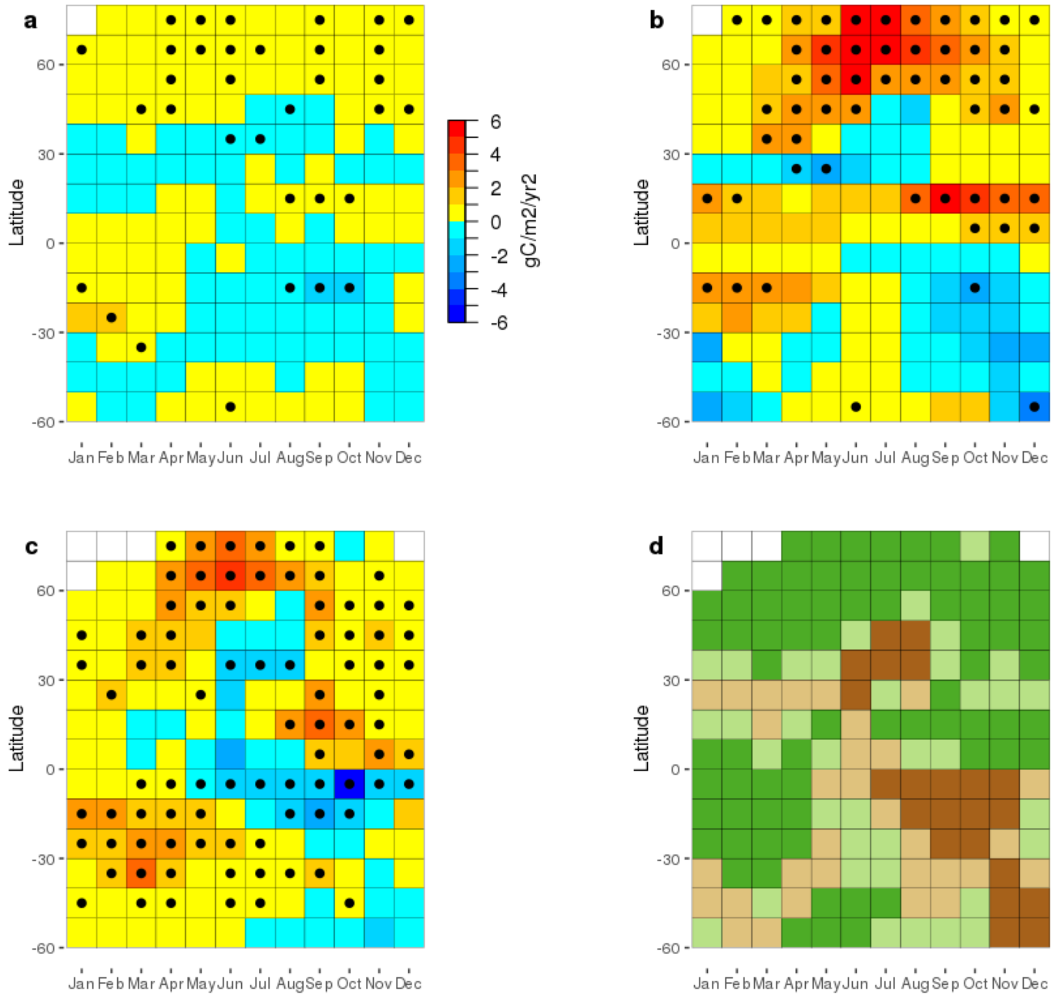

**Figure 4.4 - Trends in regionally averaged monthly GPP based on each product and the level of agreement between them. Panels show latitude (y-axis) - month (x-axis) plots of the linear trend in monthly GPP over 1982-2016 (gC/m$^2$/yr$^2$) in 10° latitude bins between 60°S and 80°N for a) FLUXCOM, b) TRENDYv6, and c) LUE. Significant trends (*P*<0.05) are highlighted with a black circle. Panel d) summarizes agreement in monthly GPP trends amongst the products (Dark green – 3 products agree on positive trend, light green – 2 products agree on positive trend, light brown – 2 products agree on negative trend, dark brown – 3 products agree on negative trend).**

### 4.3.3 Attribution to climate drivers

#### 4.3.3.1 Large-scale sensitivity

We next analysed the sensitivity of GPP based on the three products to changes in temperature and precipitation over the 35-year study period. For FLUXCOM, globally-averaged annual GPP anomalies are inversely associated with MAT anomalies (-0.26 PgC/yr/°C; *P*<0.1), whereas for TRENDYv6 and LUE these relationships are significantly (*P*<0.05) positive with similar sensitivities of 1.48 PgC/yr/°C and 1.30 PgC/yr/°C, respectively (Figure 4.5). Global annual GPP anomalies based on FLUXCOM and TRENDYv6 have a significant (*P*<0.05) positive sensitivity to mean annual precipitation, although in TRENDYv6 (4.24±0.65 PgC gained per 100mm) this sensitivity is over four times higher than in FLUXCOM (0.94±0.18 PgC/100mm; Figure 4.5). Further, LUE-based annual GPP is only weakly (*P*=0.25) positively related to annual precipitation on a global scale.

In northern regions, temperature provides a key constraint on boreal vegetation growth. A warming trend of 0.04 °C/yr (Figure D11c) between 1982-2016 has enhanced growing season photosynthesis and lengthened the growing season, and in turn increased annual GPP (Sitch *et al.*, 2015). In these northern regions all three products agree on the (positive) sign of the sensitivity between annual GPP and MAT, but differ in regards to magnitude (Figure 4.5). While GPP from TRENDYv6 and LUE exhibit significant (*P*<0.05) positive temperature sensitivities of 1.46±0.17 PgC/yr/°C and 1.32±0.20 PgC/yr/°C, respectively, GPP based on FLUXCOM lacks a strong relationship with temperature ($\gamma_r$ = 0.09±0.06 PgC/yr/°C, $P$=0.52). Further, annual GPP from FLUXCOM and TRENDYv6 show significant positive sensitivities to MAP anomalies of 0.78±0.17 PgC/yr/100mm and 2.15±0.53 PgC/yr/100mm, respectively, whereas LUE (0.93±0.78 PgC/yr/100mm) shows a positive but non-significant sensitivity to precipitation across these northern regions.

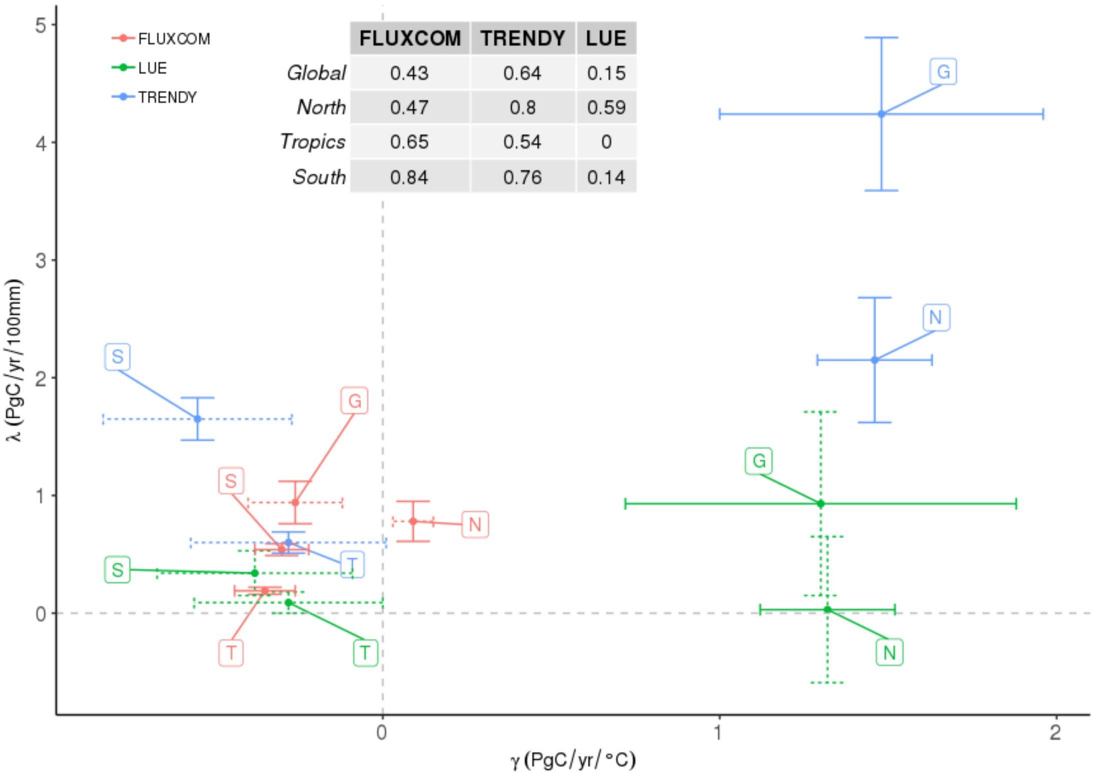

|  | FLUXCOM | TRENDY | LUE |
|---|---|---|---|
| *Global* | 0.43 | 0.64 | 0.15 |
| *North* | 0.47 | 0.8 | 0.59 |
| *Tropics* | 0.65 | 0.54 | 0 |
| *South* | 0.84 | 0.76 | 0.14 |

**Figure 4.5 - Sensitivity of global (G), northern (N), tropical (T), and southern (S) annual GPP to temperature (γ) and precipitation (λ) anomalies. Regions are defined in Figure D1. γ and λ are estimated from equation (2) over the period 1982-2016 (see Methods). Error bars show the standard error of the sensitivity estimates (see Methods). Dashed error bars indicate the multiple regression coefficient is statistically insignificant (P>0.05). Inset table shows the proportion of variance in GPP that is explained by the multiple regression (using $R^2$).**

In the tropics and southern latitudes, all products consistently show a positive relationship between annual GPP and MAP and a negative link between annual GPP and MAT. FLUXCOM has a significant ($P$<0.05) negative sensitivity of GPP to temperature ($\gamma_{Tropics\_FLUXCOM}$ = -0.35±0.09 PgC/yr/°C; $\gamma_{South\_FLUXCOM}$ = -

0.30±0.08 PgC/yr/°C), whereas both TRENDYv6 and LUE do not have a significant temperature response in either the tropics or southern latitudes. FLUXCOM and TRENDYv6 have significant ($P$<0.05) sensitivities to precipitation ($\lambda_{Tropics\_FLUXCOM}$ = 0.54±0.05 PgC/yr/100mm, $\lambda_{Tropics\_TRENDYv6}$ 1.65±0.18 PgC/yr/100mm; $\lambda_{South\_FLUXCOM}$ = 0.19±0.03 PgC/yr/100mm, $\lambda_{South\_TRENDYv6}$ 0.60±0.09 PgC/yr/100mm), but LUE has no significant ($P$>0.05) precipitation sensitivity. This lack of response of LUE-based GPP to precipitation is likely due to the use of VPD (and not precipitation) in the LUE approach, since VPD is more sensitive to temperature than precipitation (Smith, WK *et al.*, 2016). Thus, neither temperature nor precipitation explain substantial portions of the variance in LUE-based tropical and southern GPP (Figure 4.5). Moreover, the negative response of tropical GPP to increasing temperatures implies that tropical ecosystems are already functioning near their temperature optimum and any further increases in temperature will negatively affect their GPP (Corlett, 2011).

#### 4.3.3.2 Local scale sensitivity

We also calculated GPP sensitivities to temperature and precipitation at local scales based on our regression framework (see equation (2) in Methods). The geographic distribution for annual GPP against MAT is similar across the three products, with a positive relationship in Eurasia and North America and a negative relationship in the tropics and southern latitudes (Figure 4.6a,c,e). For FLUXCOM, annual GPP response to MAT is much lower than for TRENDYv6 and LUE (on average 4 gC/m$^2$/yr/°C (FLUXCOM) compared to 23 gC/m$^2$/yr/°C (TRENDYv6) and 18 gC/m$^2$/yr/°C (LUE)) and corresponding robust ($P$<0.05) sensitivities are not as widespread (35% of vegetated northern land (> 30°N) for FLUXCOM compared to 65% for TRENDYv6 and 61% for LUE). All products exhibit a similar spatial pattern of significant negative annual GPP responses to MAT across large parts of South America, Southern Asia, and Australia (Figure 4.6a,c,e). Some differences are apparent, however, with FLUXCOM and TRENDYv6 showing significant negative GPP sensitivities to MAT in the Amazon, whereas the LUE approach does not. Further, negative GPP responses in respect to MAT for TRENDYv6 and FLUXCOM in Africa are predominately located in the south of the continent, whereas in the case of LUE corresponding sensitivities include also Central Africa.

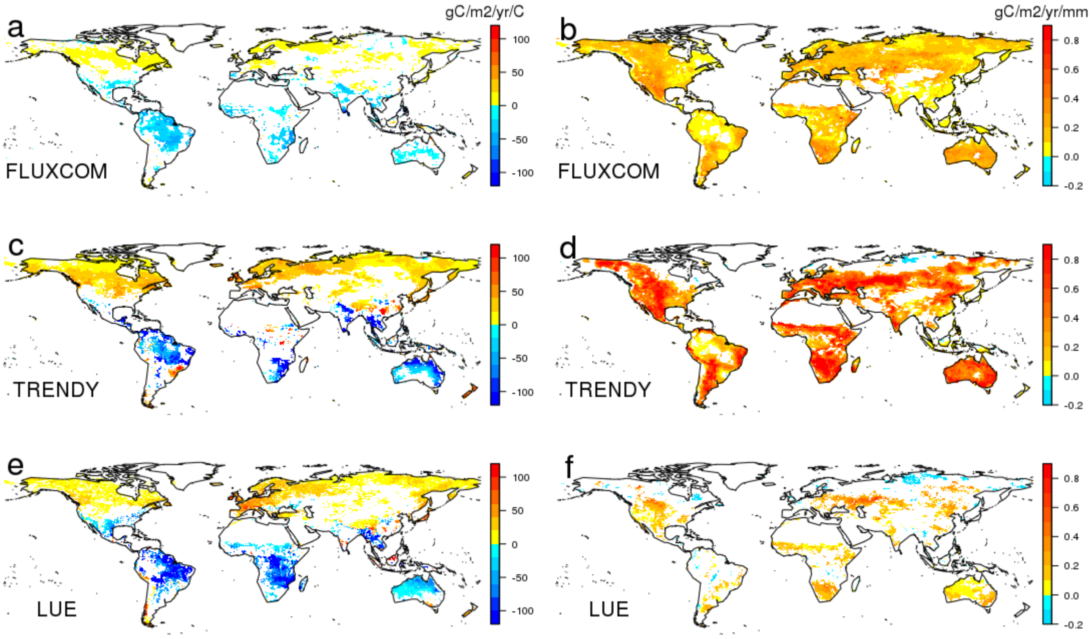

**Figure 4.6 - Spatial pattern of the response of GPP to variability in mean annual temperature (MAT) and mean annual precipitation (MAP). Sensitivity of annual GPP to variations in (a, c, e) MAT (gC/m$^2$/yr/°C) and (b, d, f) MAP (gC/m$^2$/yr/100mm) for (a,b) FLUXCOM, (c,d) TRENDYv6, and (e,f) LUE. Sensitivities are calculated from multiple linear regression of annual GPP against MAT and MAP at each grid cell (see equation (2) in Methods). Only significant (*P*<0.05) sensitivities are shown.**

In regards to annual GPP responses to MAP, the three products agree on significant positive sensitivities in the northern mid-latitudes (30°N-50°N), and the savannas and shrublands of South America, South Africa, and Australia (Figure 4.6b,d,f). However, FLUXCOM GPP is also positively correlated with precipitation at high northern latitudes, whereas for TRENDYv6 and LUE such responses are not apparent (or even of opposite sign; Figure 4.6d,f). Negative precipitation sensitivities are potentially due to increased cloud cover with increased rainfall, leading to a reduction in incoming solar radiation and consequently GPP (Nemani *et al.*, 2003). For FLUXCOM and TRENDYv6, annual GPP across the tropics is robustly positively related to MAP but for LUE such positive sensitivities are less widespread or non-existent.

In a final step, we examined which climatic factor dominates GPP variability in the various products. Using equation (2), we combine the sensitivity parameters and the actual variability in precipitation and temperature. Precipitation is the dominant factor (compared to temperature) on 90% of the vegetated land surface for FLUXCOM, while this reduces to 64% and 34% for TRENDYv6 and LUE, respectively (Figure 4.7). This major difference is due to contrasting sensitivity patterns in the high northern latitudes where MAT only dominates 9% of the land for FLUXCOM GPP variability, whereas this is 47% for TRENDYv6 and 70% for LUE (Figure 4.6 and Figure 4.7d). There are further differences in the dominant factors in the tropics and southern regions, with FLUXCOM GPP being almost entirely dominated by MAP variability but GPP from TRENDYv6 and LUE showing more areas that are controlled by MAT. Tropical South America GPP is dominated by MAT variability in all three products. There is further agreement in Southern Africa, temperate USA, north east China, and parts of east Russia, where precipitation is the primary driver of GPP variability.

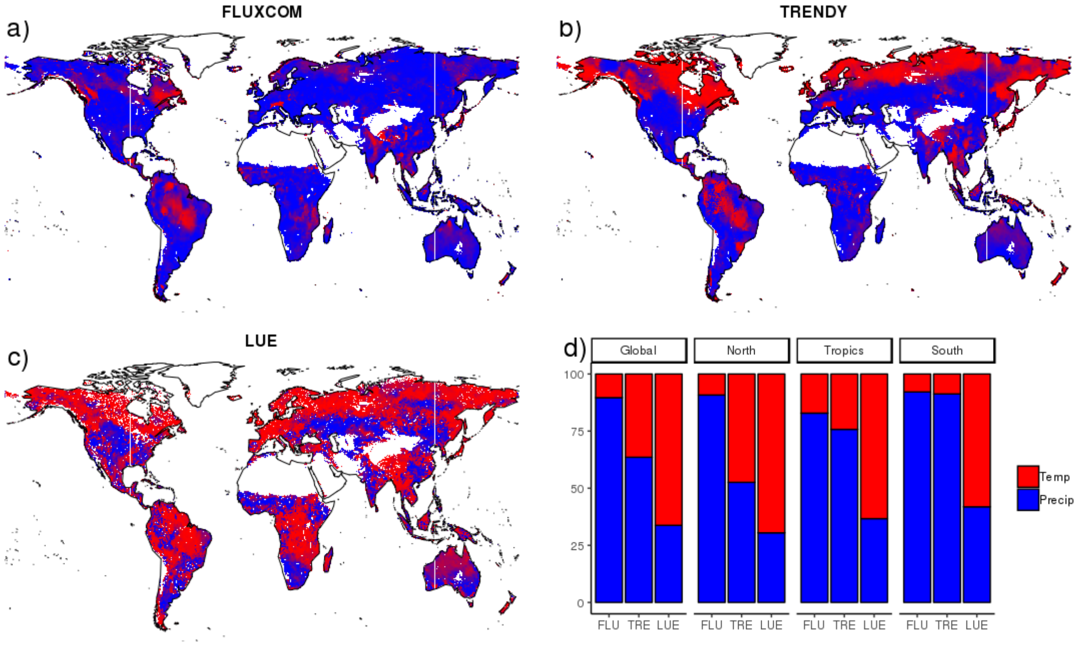

**Figure 4.7 - Spatial pattern of the relative importance of temperature and precipitation in explaining annual GPP variability for a) FLUXCOM, b) TRENDY, and c) LUE (see Methods). Percentage of dominance for temperature and precipitation for four large scale regions is also shown (d). A climate variable is dominant if it contributes more than 50% to the explained variance in the multiple linear regression.**

## 4.4 Discussion

In this study, we examined the consistency amongst climate-driven GPP data (at multiple spatial and temporal scales) from three widely used products (FLUXCOM, LUE, and TRENDYv6). Understanding and quantifying how GPP responds to past climate change is a necessary step in correct model parameterisations and future projections of carbon fluxes and sinks. The three GPP products investigated represent independent ‘state-of-the-art’ datasets and therefore any discrepancies in IAV, trends, and climate sensitivity need to be highlighted.

One key result is that the FLUXCOM IAV in GPP is much lower than for TRENDYv6 and LUE, an issue discussed previously (Jung *et al.*, 2009, Piao *et al.*, 2013). This underestimation could be due to several reasons. First, FLUXCOM does not capture vegetation and soil moisture memory effects and represents more instantaneous GPP responses to climate (see Methods). This contrasts with FluxNetG GPP, which has significantly larger interannual variability and trends, with magnitudes more in line with TRENDYv6 and LUE (Figure D4). Therefore, this highlights the large influence the choice of input data has on the machine learning GPP estimates used in FLUXCOM and FluxNetG. Secondly, there are very few sites in regions that dominate the global IAV, such as tropical forests (Cox *et al.*, 2013) and semi-arid regions (Ahlstrom *et al.*, 2015), which could lead to biases at regional/global scales. Aside from differences in magnitude of variability, the GPP products show generally a good agreement in the their IAV at global and relatively broad regional scales (respective correlations are significant ($P$<0.05) in all regions (Table 4.1)). In general, FLUXCOM and TRENDYv6 year-to-year correlations were substantially higher when either are compared to LUE, also consistent with a previous study (Anav *et al.*, 2015). On a grid-cell scale LUE does not correlate with FLUXCOM in the tropics and high northern latitudes, or with TRENDYv6 in the tropics (Figure 4.2). There are known issues with satellite optical data in these regions due to cloud contamination, which could influence derived FPAR data used in the LUE algorithm (Zhao *et al*., 2005, Smith, WK *et al*., 2016). Alternatively, the LUE algorithm could be a source of error and might not capture climate sensitivity correctly (Anav *et al.*, 2015, Chen *et al.*, 2017, Medlyn, 2011, Piao *et al.*, 2013). For example, the ability of VPD to fully capture the down regulation of GPP, particularly in drought conditions, has been called into question (Stocker *et al*., 2018). However, it is important to note that both FLUXCOM and TRENDYv6 GPP are also highly uncertain in tropical regions. FLUXCOM suffers from poor data coverage in the tropics and as such tropical GPP is poorly constrained (Anav *et al.*, 2015). In addition, both FLUXCOM and TRENDYv6 have low variability in the Amazon and South East Asia compared to LUE, which can mask agreement amongst the products (Figure D7). In summary, all three GPP products have severe limitations in tropical regions, and so a lack of correlation at interannual timescales between them in this region is not surprising.

We further analysed the long-term trends in GPP and explored linkages to underlying climatic controls. We find that the climate-driven GPP trends based on TRENDYv6 and LUE are consistent, with both simulating a large northern increase (Figures 4.1 and 4.3). FLUXCOM GPP trends are systematically lower than other GPP estimates in all regions (Anav *et al.*, 2015, Piao *et al.*, 2013). Large scale northern warming led to increased uptake in the TRENDYv6 and LUE models, a finding in line with studies showing a lengthening of the growing season (Keenan *et al.*, 2014, Richardson *et al.*, 2010), and increases in annual carbon uptake (Keenan *et al.*, 2014). FLUXCOM northern trends could be smaller for several reasons. By design, FLUXCOM has no greening trend, and so neglect a potential climate effect on plant biomass which could be captured by the TRENDYv6 models through increases in LAI or earlier leaf onset as well as in LUE through satellite FPAR. However, a previous TRENDY model inter-comparison study simulated no trend in northern NPP due to climate variations over the period 1990-2009 (Sitch *et al.*, 2015). Further, these contrasting results could be due to differences in GPP and NPP trends, or because this version of TRENDY (version 6) contains a different set of models to previous versions. Moreover, a difference in the time periods (three decades in this study compared to two decades in Sitch *et al.* (2015)) could influence trend analysis. Nonetheless, this difference between TRENDY versions highlights uncertainty in model structure and parameterisations. As mentioned previously, plant physiological response to climate controls GPP variability (Xia *et al.*, 2015, Zhou *et al.*, 2017). Incorrect (or missing) representation of related processes, such as the sensitivity and acclimation of photosynthesis to changes in temperature, can lead to errors in simulated GPP (Booth *et al.*, 2012, Lombardozzi *et al.*, 2015, Mercado *et al.*, 2018). It is not clear how the inclusion of temperature acclimation would affect simulated GPP trends (in all regions) with studies showing both increased and decreased photosynthesis in a warming scenario with temperature acclimation included, depending on the underlying PFT and exact acclimation formulation (Lombardozzi *et al.*, 2015, Mercado *et al.*, 2018, Smith NG *et al.*, 2016).

It is important to note that precipitation variability is also important for temperate GPP (Anderegg *et al.*, 2012), and corresponding influences are captured consistently in the three products. Examples include the large negative GPP trends in West and Southern USA due to precipitation declines (Figure 4.3). Further, GPP declines in China and Mongolia are consistent with previous modelling and satellite studies that also highlighted the China/Mongolia pattern, attributing the decrease in GPP to negative precipitation trends (Poulter *et al.*, 2013). Over the tropics, we find similar and contrasting GPP trends amongst the products, and differences in the underlying climate sensitivities. All three products exhibit comparable negative GPP trends in central South America, driven by rising temperatures increasing evaporative demand (Zhao & Running, 2010). Precipitation increases in the Sahel led to positive GPP trends in all products, a feature highlighted previously (Brandt *et al.*, 2015, Hickler *et al.*, 2005). Further, positive precipitation trends in South East Asia led to a spatially uniform (albeit small) increase in TRENDYv6 GPP. However, FLUXCOM and LUE simulate no change in the majority of South East Asia (and other tropical forest regions). As stated previously, all three products suffer from uncertainties (e.g. from model structure or underlying observations) in the tropics, making tropical trends less robust (Chen *et al.*, 2017, Wu *et al.*, 2018).

In regard to comparative analysis of climate sensitivities, we find GPP from both TRENDYv6 and LUE exhibit widespread positive sensitivities to MAT in northern latitudes, a result in-line with previous observation-based studies (Keenan *et al*., 2014, Xu *et al*., 2013, Zhou *et al*., 2001; Figures 4.5 and 4.6). In contrast, GPP from FLUXCOM shows significant sensitivities to MAT in relatively few regions across the northern latitudes, a result found previously (Jung *et al*., 2017; Figure 4.6). Further, GPP from FLUXCOM and TRENDYv6 have significant positive sensitivities to MAP in northern temperate latitudes (Figure 4.6), a region previously shown where water availability is a dominant driver of GPP (Ahlstrom *et al*., 2015, Anderegg *et al*., 2012). However, contrary to TRENDYv6 and LUE, GPP IAV in boreal latitudes from FLUXCOM is predominantly driven by MAP variability. Potential reasons for this pattern include that FLUXCOM is driven with seasonally varying climatology of satellite FPAR, and so could be missing an important inter-annual climate signal (see Figure D4). Further, FLUXCOM is known to have poor performance in cold regions as GPP magnitudes and variability are generally low which causes issues in explaining variability using empirical models (Tramontana *et al*., 2016). There are large regions across the tropics and southern latitudes where GPP has a negative relationship to MAT (Piao *et al*., 2013, Zhao & Running, 2010), however when integrated from local to regional scales (see Figure D1), variability in GPP is not correlated to regional MAT anomalies. For both FLUXCOM and TRENDYv6, variability in MAP is a dominant driver of GPP IAV at local and regional scales in tropical and southern latitudes. This is consistent with previous work showing water availability to be a principal driver of productivity across much of the tropical/southern latitudes (Ahlstrom *et* al., 2015, Jung *et* al., 2017, Piao *et* al., 2013, Zscheischler *et al.*, 2014). Interestingly, we find tropical LUE GPP does not correlate significantly with MAP in any grid cells (Figure 4.6), although increased precipitation has been shown to enhance tropical GPP (Beer *et al.*, 2010). This disparity between products is most likely due to both FLUXCOM and TRENDYv6 being driven by soil water availability which is strongly related to precipitation, whereas LUE is driven with VPD, which is more strongly related to temperature. Nevertheless, previous work (using FLUXCOM and TRENDYv6) explains tropical GPP variability through moisture availability, giving confidence in our explanatory analysis (Jung *et al.*, 2017).

Strikingly, the spatial pattern of the dominant climatic driver on GPP variability is not consistent amongst the products. TRENDYv6 and LUE agree on the general pattern of temperature controlling GPP in the northern-high latitudes and precipitation controlling GPP in northern temperate, tropical, and southern regions (Nemani *et al.*, 2003, Piao *et al.*, 2009). In stark contrast, FLUXCOM GPP variability is dominated by precipitation almost everywhere globally, including the northern high-latitude boreal regions. The latter is somewhat inconsistent with our general understanding of climatic constraints on plant productivity (Nemani *et al.*, 2003).

## 4.5 Conclusion

We observed notable similarities and differences in the IAV and long-term trends in GPP from three key products in carbon cycle science (FLUXCOM, TRENDY, and LUE). GPP IAV and trends from FLUXCOM are systematically lower than satellite (LUE) and process-based (TRENDYv6) products, indicating significant uncertainties exist. Temperature increases in the northern latitudes appear to have significantly increased GPP on the global scale. However, changes in tropical GPP due to variations in climate are not consistent, with products disagreeing on the spatial pattern and underlying drivers of trends. The northern warming and increased GPP trend is more robust, with temperature limitation of high latitude productivity exerting a primary control (Nemani *et al.*, 2003), and the gradual relaxation of this constraint has been observed via independent methods (Barichivich *et al.*, 2013, Graven *et al.*, 2013, Keenan *et al.*, 2014, Myneni *et al.*, 1997).

All three products agreed on the direction of trend across 60% of the vegetated land surface, however magnitudes of trends were generally less consistent among the three products and thus are more uncertain. Differences in GPP estimates between TRENDY models indicate that models need to be improved since processes are either not included or misrepresented. For example, large uncertainties associated with the parameterisation, acclimation, and scaling (vertically through the canopy and spatially across the landscape) of photosynthesis have been highlighted (Rogers *et al.*, 2017). However, including more processes does not necessarily improve a model as the added complexity can lead to more uncertain parameterisations (Prentice *et al.*, 2015, Zaehle *et al.*, 2014).

Furthermore, there are key similarities and differences in GPP sensitivity to climate forcings between the products. All products agree on a general pattern of positive GPP correlations to MAT in northern regions, and negative correlations in tropical/southern lands. However, spatial patterns and magnitudes of GPP sensitivity to MAP are not consistent. Interannual variability in GPP from FLUXCOM is seemingly driven solely by MAP anomalies in majority of regions whereas LUE shows few regions sensitive to MAP variability. Thus, isolating the regional/local sensitivity of GPP to individual climate forcings is not straightforward. Firstly, by design, different methodologies of calculating GPP will inherently lead to different sensitivities to environmental drivers. In addition, products use different variables and data sources to represent the same environmental stresses (e.g. temperature and moisture). However, as moisture availability and temperature are key climatic constraints on plant productivity, we have confidence in our regression framework and analysis.

Nonetheless, there is a need for more long-term, direct observations of GPP especially in underrepresented regions (e.g. tropical forests) to reduce uncertainties in all products. With novel satellite measurements capturing photosynthesis more directly (e.g. chlorophyll fluorescence and new optical metrics, Badgley *et al.* (2017)), in the future there will be a new means to reliably constrain interannual variability and long-term trends of GPP on local and global scales.

## Acknowledgments

We gratefully acknowledge funding for this study though a EU Marie Curie Integration grant (CIG PCIG14-GA-2013-631812) to W.B. This work was supported by the Natural Environment Research Council (grant number NE/N006895/1). The data used are listed in the references. We would also like to thank Martin Jung for providing FLUXCOM data and valuable comments on the manuscript.

## References

Ahlstrom A, Raupach MR, Schurgers G *et al.* (2015) The dominant role of semi-arid ecosystems in the trend and variability of the land CO2 sink. Science, **348**, 895-899.

Anav A, Friedlingstein P, Beer C *et al.* (2015) Spatiotemporal patterns of terrestrial gross primary production: A review. Reviews of Geophysics, **53**, 785-818.

Anderegg WRL, Berry JA, Smith DD, Sperry JS, Anderegg LDL, Field CB (2012) The roles of hydraulic and carbon stress in a widespread climate-induced forest die-off. Proceedings of the National Academy of Sciences of the United States of America, **109**, 233-237.

Badgley G, Field CB, Berry JA (2017) Canopy near-infrared reflectance and terrestrial photosynthesis. Science Advances, **3**, e1602244-e1602244.

Baldocchi D (2003) Assessing the eddy covariance technique for evaluating carbon dioxide exchange rates of ecosystems: past, present and future. Global Change Biology, **9**, 479-492.

Baldocchi D, Falge E, Gu L *et al.* (2001) FLUXNET: A New Tool to Study the Temporal and Spatial Variability of Ecosystem–Scale Carbon Dioxide, Water Vapor, and Energy Flux Densities. Bulletin of the American Meteorological Society, **82**, 2415-2434.

Ballantyne A, Smith W, Anderegg W *et al.* (2017) Accelerating net terrestrial carbon uptake during the warming hiatus due to reduced respiration. Nature Climate Change, **7**.

Barichivich J, Briffa KR, Myneni RB *et al.* (2013) Large-scale variations in the vegetation growing season and annual cycle of atmospheric $CO_2$ at high northern latitudes from 1950 to 2011. Global Change Biology, **19**, 3167-3183.

Bastos A, Running SW, Gouveia C, Trigo RM (2013) The global NPP dependence on ENSO: La Niña and the extraordinary year of 2011. Journal of Geophysical Research: Biogeosciences, **118**, 1247-1255.

Bates, D. M. and Watts, D. G. (1988) *Nonlinear Regression Analysis and Its Applications,* Wiley

Beer C, Reichstein M, Tomelleri E *et al.* (2010) Terrestrial Gross Carbon Dioxide Uptake: Global Distribution and Covariation with Climate. Science, **329**, 834-838.

Booth BBB, Jones CD, Collins M *et al.* (2012) High sensitivity of future global warming to land carbon cycle processes. Environmental Research Letters, **7**, 024002-024002.

Brandt M, Mbow C, Diouf AA, Verger A, Samimi C, Fensholt R (2015) Ground- and satellite-based evidence of the biophysical mechanisms behind the greening Sahel. Global Change Biology, **21**, 1610-1620.

Buermann W, Bikash PR, Jung M, Burn DH, Reichstein M (2013) Earlier springs decrease peak summer productivity in North American boreal forests. Environmental Research Letters, **8**, 024027-024027.

Buermann W, Beaulieu C, Parida B *et al.*, (2016) Climate-driven shifts in continental net primary production implicated as a driver of a recent abrupt increase in the land carbon sink. Biogeosciences, **13**, 1597-1607.

Buermann W, Forkel M, O'Sullivan M *et al.* (2018) Widespread seasonal compensation effects of sring warming on northern plant productivity. Nature, **562**, 110-114.

Chen M, Rafique R, Asrar GR *et al.* (2017) Regional contribution to variability and trends of global gross primary productivity. Environmental Research Letters, **12**, 105005-105005.

Ciais P, Reichstein M, Viovy N *et al.*, (2005) Europe-wide reduction in primary productivity caused by the heat and drought in 2003. Nature, **437**, 529-533.

Clark DB, Mercado LM, Sitch S *et al.,* (2011) The Joint UK Land Environment Simulator (JULES), model description - Part 2: carbon fluxes and vegetation dynamics. Geoscientific Model Development, **4**, 701-722.

Corlett RT (2011) Impacts of warming on tropical lowland rainforests. Trends in Ecology & Evolution, **26**, 606-613.

Cox PM, Pearson D, Booth BB, Friedlingstein P, Huntingford C, Jones CD, Luke CM (2013) Sensitivity of tropical carbon to climate change constrained by carbon dioxide variability. Nature*,* **494**, 341-344.

De Kauwe MG, Keenan TF, Medlyn BE *et al*., (2016) Satellite based estimates underestimate the effect of CO2 fertilization on net primary productivity. Nature Climate Change, **6**, 892-893.

Dee DP, Uppala SM, Simmons AJ *et al.* (2011) The ERA-Interim reanalysis: configuration and performance of the data assimilation system. Quarterly Journal of the Royal Meteorological Society*,* **137**, 553-597.

Fisher JB, Huntzinger DN, Schwalm CR, Sitch S (2014) Modeling the Terrestrial Biosphere. Annual Review of Environment and Resources*,* **39**, 91-123.

Forkel M, Carvalhais N, Rodenbeck C *et al*., (2016) Enhanced seasonal $CO_2$ exchange caused by amplified plant productivity in northern ecosystems. Science, **351**, 696-699.

Friedl MA, Sulla-Menashe D, Tan B *et al*., (2010) MODIS Collection 5 global land cover: Algorithm refinements and characterization of new datsets. Remote Sensing of Environment, **114**, 168-182.

Friedlingstein P, Meinshausen M, Arora VK *et al*. (2014) Uncertainties in CMIP5 Climate Projections due to Carbon Cycle Feddbacks, Journal of Climate, **27**, 511-526

Graven HD, Keeling RF, Piper SC *et al.* (2013) Enhanced seasonal exchange of CO2 by northern ecosystems since 1960. Science (New York, N.Y.)*,* **341**, 1085-1089.

Grömping U (2006) Relative Importance for Linear Regression in R: The Package relaimpo. Journal of Statistical Software*,* **17**, 1-27.

Guimberteau M, Zhu D, Maignan F *et al.,* (2018) ORCHIDEE-MICT (v8.4.1), a land surface model for the high latitudesL model description and validation. Geosci. Model Dev, **11**, 121-163.

Haverd V, Smith B, Nieradzik L *et al.* (2018) A new version of the CABLE land surface model (Subversion revision r4601) incorporating land use and land cover change, woody vegetation demography, and a novel optimisation-based approach to plant coordination of photosynthesis. Geosci. Model Dev*,* **11**, 2995-3026.

Hickler T, Eklundh L, Seaquist JW *et al.* (2005) Precipitation controls Sahel greening trend. Geophysical Research Letters*,* **32**, L21415-L21415.

Huang J, Yu H, Guan X, Wang G, Guo R (2016) Accelerated dryland expansion under climate change. Nature Climate Change*,* **6**, 166-171.

Jain AK, Meiyappan P, Song Y, House JI (2013) $CO_2$ emissions from land-use change affected more by nitrogen cycle, than by the choice of land-cover data. Global Change Biology*,* **19**, 2893-2906.

Jung M, Reichstein M, Bondeau A (2009) Towards global empirical upscaling of FLUXNET eddy covariance observations: validation of a model tree ensemble approach using a biosphere model. Biogeosciences*,* **6**, 2001-2013.

Jung M, Reichstein M, Margolis H *et al.* (2011) Global patterns of land-atmosphere fluxes of carbon dioxide, latent heat, and sensible heat derived from eddy covariance, satellite, and meteorological observations. Journal of Geophysical Research, **116**, G00J07.

Jung M, Reichstein M, Schwalm CR *et al.* (2017) Compensatory water effects link yearly global land CO2 sink changes to temperature. Nature, **541**, 516-520.

Kalnay E, Kanamitsu M, Kistler R *et al.* (1996) The NCEP/NCAR 40-Year Reanalysis Project. Bulletin of the American Meteorological Society, **77**, 437-471.

Kato E, Kinoshita T, Ito A, Kawamiya M, Yamagata Y (2013) Evaluation of spatially explicit emission scenario of land-use change and biomass burning using a process-based biogeochemical model. Journal of Land Use Science, **8**, 104-122.

Keeling CD, Chin JS, Whorf TP (1996) Increased activity of northern vegetation inferred from atmospheric $CO_2$ measuremets. Nature, **382**, 146-149.

Keenan TF, Gray J, Friedl MA *et al.* (2014) Net carbon uptake has increased through warming-induced changes in temperate forest phenology. Nature Climate Change, **4**, 598-604.

Krinner G, Viovy N, de Noblet-Ducoudre N *et al*., (2005) A dynamic global vegetation model for studies of the coupled atmosphere-biosphere system. Global Biogeochemical Cycles, **19**, 1-33.

Le Quéré C, Andrew RM, Friedlingstein P *et al*., (2018) Global Carbon Budget 2017. Earth System Science Data, **10**, 405-448.

Lombardozzi DL, Bonan GB, Smith NG, Dukes JS, Fisher RA (2015) Temperature acclimation of photosynthesis and respiration: A key uncertainty in the carbon cycle-climate feedback. Geophysical Research Letters, **42**, 8624-8631.

Melton JR, Arora VK (2016) Competition between plant functional types in the Canadian Terrestrial Ecosystem Model (CTEM) v.2.0. Geoscientific Model Development, **9**, 323-361.

Medlyn B (2011) Comment on "Drought-Induced Reduction in Global Terrestrial Net Primary Production from 2000 Through 2009". Science, **333**, 1093.

Mercado LM, Medlyn BE, Huntingford C *et al.* (2018) Large sensitivity in land carbon storage due to geographical and temporal variation in the thermal response of photosynthetic capacity. New Phytologist, **218**, 1462-1477.

Myneni RB, Keeling CD, Tucker CJ, Asrar G, Nemani RR (1997) Increased plant growth in the northern high latitudes from 1981 to 1991. Nature, **386**, 698-702.

Nemani RR, Keeling CD, Hashimoto H *et al.* (2003) Climate-driven increases in global terrestrial net primary production from 1982 to 1999. Science (New York, N.Y.), **300**, 1560-1563.

Norby RJ, Delucia EH, Gielen B *et al.* (2005) Forest response to elevated CO2 is conserved across a broad range of productivity. Proceedings of the National Academy of Sciences of the United States of America, **102**, 18052-18056.

Oleson K, Lawrence DM, Bonan GB, *et al.* (2013) Technical description of version 4.5 of the community land model (CLM). Boulder, CO: NCAR.

Phillips OL, Aragão LEOC, Lewis SL *et al.* (2009) Drought sensitivity of the Amazon rainforest. Science (New York, N.Y.), **323**, 1344-1347.

Piao S, Ciais P, Friedlingstein P, De Noblet-Ducoudré N, Cadule P, Viovy N, Wang T (2009) Spatiotemporal patterns of terrestrial carbon cycle during the 20th century. Global Biogeochemical Cycles, **23**, GB4026.

Piao S, Friedlingstein P, Ciais P, Viovy N, Demarty J (2007) Growing season extension and its impact on terrestrial carbon cycle in the Northern Hemisphere over the past 2 decades. Global Biogeochemical Cycles*,* **21**, GB3018.

Piao S, Sitch S, Ciais P *et al.* (2013) Evaluation of terrestrial carbon cycle models for their response to climate variability and to CO2 trends. Global Change Biology*,* **19**.

Poulter B, Frank D, Ciais P *et al.* (2014) Contribution of semi-arid ecosystems to interannual variability of the global carbon cycle. Nature*,* **509**, 600-603.

Poulter B, Pederson N, Liu H *et al.* (2013) Recent trends in Inner Asian forest dynamics to temperature and precipitation indicate high sensitivity to climate change. Agricultural and Forest Meteorology*,* **178-179**, 31-45.

Prentice IC, Liang X, Medlyn BE, Wang YP (2015) Reliable, robust and realistic: the three R's of next-generation land-surface modelling. Atmospheric Chemistry and Physics*,* **15**, 5987-6005.

Raczka BM, Davis KJ, Huntzinger D *et al*. (2013) Evaluation of continental carbon cycle simulations with North American flux tower observations. Ecological Monographs, **83**, 531-556.

Reichstein M, Bahn M, Ciais P *et al.* (2013) Climate extremes and the carbon cycle. Nature*,* **500**, 287-295.

Reichstein M, Falge E, Baldocchi D *et al.* (2005) On the separation of net ecosystem exchange into assimilation and ecosystem respiration: review and improved algorithm. Global Change Biology*,* **11**, 1424-1439.

Reick CH, Raddatz T, Brovkin V *et al*., (2013) The representation of natural and anthropogenic land cover changes in MPI-ESM. Jounral of Advances in Modeling Earth Systems, **5**, 459-482.

Restrepo-Coupe N, Levine NM, Christoffersen BO *et al.* (2017) Do dynamic global vegetation models capture the seasonality of carbon fluxes in the Amazon basin? A data-model intercomparison. Global Change Biology*,* **23**, 191-208.

Richardson AD, Black TA, Ciais P *et al.* (2010) Influence of spring and autumn phenological transitions on forest ecosystem productivity. Philosophical transactions of the Royal Society of London. Series B, Biological sciences*,* **365**, 3227-3246.

Rienecker MM, Suarez MJ, Gelaro R *et al.* (2011) MERRA: NASA's Modern-Era Retrospective Analysis for Research and Applications. Journal of Climate*,* **24**, 3624-3648.

Robinson NP, Alfred BW, Smith WK *et al*., (2018) Terrestrial primary production for the conterminous United States derived from Landsat 30m and MODIS 250m. Remote Sensing in Ecology and Conservation, **4**, 264-280.

Rogers A, Medlyn BE, Dukes JS *et al.* (2017) A roadmap for improving the representation of photosynthesis in Earth system models. New Phytologist*,* **213**, 22-42.

Running SW, Running SNW, Nemani RR, Heinsch FA, Zhao M, Reeves M, Hashimoto H (2004) A Continuous Satellite-Derived Measure of Global Terrestrial Primary Production. BioScience*,* **54**.

Schimel D, Stephens BB, Fisher JB (2015) Effect of inreasing $CO_2$ on the terrestrial carbon cycle. Procedings of the National Academy of Sciences of the United States of America, **112**, 436-441.

Seneviratne SI, Nicholls N, Easterling D *et al.* (2012) Changes in climate extremes and their impacts on the natural physical environment. Managing the Risks of Extreme Events and Disasters to Advance Climate Change Adaptation. A Special Report of Working Groups I and II of the Intergovernmental Panel on Climate Change (IPCC)*,* **6**, 109-203.

Sitch S, Friedlingstein P, Gruber N *et al.* (2015) Recent trends and drivers of regional sources and sinks of carbon dioxide. Biogeosciences*,* **12**, 653-679.

Smith B, Wårlind D, Arneth A *et al*. (2014) Implications of incorporating N cycling and N limitations on primary production in an individual-based dynamic vegetation model. Biogeosciences, 11, 2027-2054.

Smith WK, Reed SC, Cleveland CC *et al.* (2016) Large divergence of satellite and Earth system model estimates of global terrestrial CO2 fertilization. Nature Climate Change*,* **6**, 306-310.

Smith NG, Malyshev SL, Shevliakova E, Kattge J, Dukes JS (2016) Foliar temperature acclimation reduces simulated carbon sensitivity to climate. Nature Climate Change*,* **6**, 407-411.

Stocker BD, Zscheischler J, Keenan TF *et al*. (2018) Quantifying soil moisture impacts on light use efficiency acros biomes. New Phytologist, **218**, 1430-1449.

Tian H, Chen G, Lu C *et al.* (2015) North American terrestrial CO2 uptake largely offset by CH4 and N2O emissions: toward a full accounting of the greenhouse gas budget. Climatic Change*,* **129**, 413-426.

Tramontana G, Jung M, Schwalm CR *et al.* (2016) Predicting carbon dioxide and energy fluxes across global FLUXNET sites with regression algorithms. Biogeosciences*,* **13**, 4291-4313.

Wang W, Ciais P, Nemani RR *et al.* (2013) Variations in atmospheric CO2 growth rates coupled with tropical temperature. Proceedings of the National Academy of Sciences of the United States of America*,* **110**, 13061-13066.

Wang X, Piao S, Ciais P *et al.* (2014) A two-fold increase of carbon cycle sensitivity to tropical temperature variations. Nature*,* **506**, 212-215.

Wehr R, Saleska SR (2015) An improved isotopic method for partitioning net ecosystem–atmosphere CO2 exchange. Agricultural and Forest Meteorology*,* **214-215**, 515-531.

Wehr R, Munger JW, McManus JB *et al*. (2016) Seasonality of temperate forest photosynthesis and daytime respiration. Nature **534**, 680-683.

Welp LR, Keeling RF, Meijer HaJ *et al.* (2011) Interannual variability in the oxygen isotopes of atmospheric CO2 driven by El Niño. Nature*,* **477**, 579-582.

Wu J, Albert LP, Lopes AP *et al.* (2016) Leaf development and demography explain photosynthetic seasonality in Amazon evergreen forests. Science (New York, N.Y.)*,* **351**, 972-976.

Wu Z, Boke-Olén N, Fensholt R, Ardö J, Eklundh L, Lehsten V (2018) Effect of climate dataset selection on simulations of terrestrial GPP: Highest uncertainty for tropical regions. PLOS ONE*,* **13**, e0199383-e0199383.

Xia J, Niu S, Ciais P *et al.* (2015) Joint control of terrestrial gross primary productivity by plant phenology and physiology. Proceedings of the National Academy of Sciences of the United States of America*,* **112**, 2788-2793.

Xu L, Myneni RB, Chapin III FS *et al*., (2013) Temperature and vegetation seasonality diminshment over northern lands. Nature Climate Change, **3**, 581-586.

Zaehle S, Medlyn BE, De Kauwe MG *et al.* (2014) Evaluation of 11 terrestrial carbon–nitrogen cycle models against observations from two temperate Free-Air $CO_2$ Enrichment studies. New Phytologist*,* **202**, 803-822.

Zaehle S, Dalmonech D (2011) Carbon–nitrogen interactions on land at global scales: current understanding in modelling climate biosphere feedbacks. Current Opinion in Environmental Sustainability*,* **3**, 311-320.

Zeng N, Mariotti A, Wetzel P (2005) Terrestrial mechanisms of interannual $CO_2$ variability. Global Biogeochemical Cycles*,* **19**.

Zhao M, Heinsch FA, Nemani RR *et al*., (2005) Improvements of the MODIS terrestrial gross and net primary production global data set. Remote Sensing of Environment, **95**, 164-176.

Zhao M, Running SW (2010) Drought-Induced Reduction in Global Terrestrial Net Primary Production from 2000 Through 2009. Science*,* **329**, 940-943.

Zhou L, Tucker CJ, Kaufmann RK *et al.* (2001) Variations in northern vegetation activity inferred from satellite data of vegetation index during 1981 to 1999. Journal of Geophysical Research: Atmospheres, **106**, 20069-20083.

Zhou S, Zhang Y, Ciais P *et al.* (2017) Dominant role of plant physiology in trend and variability of gross primary productivity in North America. Scientific Reports*,* **7**, 41366-41366.

Zhu Z, Bi J, Pan Y *et al.* (2013) Global Data Sets of Vegetation Leaf Area Index (LAI)3g and Fraction of Photosynthetically Active Radiation (FPAR)3g Derived from Global Inventory Modeling and Mapping Studies (GIMMS) Normalized Difference Vegetation Index (NDVI3g) for the Period 1981 to 2011. Remote Sensing*,* **5**, 927-948.

Zhu Z, Piao S, Myneni RB *et al.* (2016) Greening of the Earth and its drivers. Nature Climate Change*,* **6**, 791-795.

Zscheischler J, Mahecha MD, Von Buttlar J *et al.* (2014) A few extreme events dominate global interannual variability in gross primary production. Environmental Research Letters*,* **9**, 35001-35013.

# Chapter 5

# Discussion

The terrestrial carbon sink has increased over the past decades, however the exact driving processes and mechanisms remain unquantified. Increased $CO_2$ concentrations, nitrogen deposition, changes in climate, and land-use / land-cover change have all played a role on uptake and release processes on various spatial and temporal scales. Locating the changing carbon fluxes and sinks and the finding driving mechanisms is a primary research goal for the scientific community because to make any predictions about the future of the carbon cycle and climate, we need to correctly understand the past.

The aim of this thesis was to study the recent changes in the terrestrial carbon cycle, and to identify drivers, processes, and mechanisms behind observed changes. A combination of models was used to study the influence of anthropogenic fossil fuel emissions on atmospheric aerosol distribution, surface radiation, and net primary productivity, as well as the impact of nitrogen deposition on the net carbon balance. I also analysed observational and model data of vegetation productivity to quantify the influence of climate on carbon uptake over the period 1982-2016.

I used a variety of modelling and observational tools to address the three hypotheses:

**H1**: Increases in the fraction of diffuse/direct radiation associated predominantly with East Asian sulfate aerosol emissions have spurred plant photosynthetic rates (Chapter 2)

**H2**: Increases in nitrogen deposition from East Asian fossil fuel burning have increased plant carbon uptake (Chapter 3)

**H3**: A progressive relaxation of climatic constraints has led to increased plant productivity (Chapter 4)

The following sections provide a summary of the results from each chapter in relation to the thesis hypotheses.

## 5.1 Small global effect on terrestrial net primary production due to increased fossil fuel aerosol emissions from East Asia since the turn of the century

A three-model cascade was used to quantify the influence of changes in anthropogenic fossil fuel emissions had on atmospheric aerosol (GLOMAP), surface radiation (Edwards-Slingo), and NPP (JULES) over 1998-2010. GLOMAP is compared to satellite observations of aerosol optical depth, and both Edward-Slingo radiation and JULES GPP are compared to tower site observations. A summary of the findings from this study in relation to the first hypothesis is presented below:

a) There have been large regional changes in modelled aerosol optical depth (AOD) over 1998-2010, with an increase of 0.04 in East Asia, and decreases of 0.06 and 0.03 in Europe and North America, respectively. Trends in fossil fuel emissions dominate the AOD trends in these industrialised regions, accounting for 95% of the overall change. The absolute magnitude of modelled AOD is systematically lower than satellite observations. However, in fossil fuel aerosol dominated regions, modelled trends matched satellite observations well. Potential reasons for an underestimation in modelled aerosol loading include; uncertainty in observations, overestimation in deposition processes, coarse spatial and temporal model resolution, and omission of various atmospheric species (eg. dust, nitrate).

b) In the industrialised northern hemisphere changes in surface diffuse radiation (SDR) are dictated by fossil fuel aerosol, with higher/lower aerosol loading leading to higher/lower SDR. Isolating the fossil fuel aerosol effect over 1998-2010, SDR increased in East Asia by +2.5 W/m$^2$, and decreased in Europe and North America by 5.6 W/m$^2$ and 2.2 W/m$^2$, respectively. These opposing regional trends led to a small global reduction in SDR of 0.36 W/m$^2$. Compared to site level observations, the model under predicts SDR and over predicts total surface radiation, with the main differences in summer months, when radiation is highest. This could be due to the underestimation of the modelled aerosol loading.

c) Global changes in NPP over the study period are dominated by $CO_2$ fertilization (+2.9 PgC/yr) and climate variations (-0.96 PgC/yr), with an overall increase of 1.7 PgC/yr over 1998-2010. Changes in SDR due to fossil fuel aerosol contribute less than 5% of the overall NPP change (-0.08 PgC/yr). Regionally, changes in SDR due to fossil fuel emissions have a large influence on NPP trends, contributing 33% of the 0.53 PgC/yr increase in East Asia. In Europe and North America, reductions in SDR led to NPP decreases of similar magnitudes of $CO_2$ fertilization, in the opposing direction. Climate variability dominates NPP trends on 74% of vegetated land, with $CO_2$ fertilization dominating 22%, predominately in tropical forests. Warming in the high northern latitudes spurred on plant growth and increased annual NPP, whereas wetting and drying trends in the mid and southern latitudes controlled annual NPP changes.

d) Modelled GPP sensitivity to direct and diffuse radiation generally matches flux tower observations, with increased GPP at higher radiation levels. GPP is higher under diffuse light conditions than direct light, as expected from the theory of radiative transfer in vegetation canopies. The model does underestimate GPP sensitivity to diffuse light in the two needleleaf forests (Hyytiala and Loobos). The model parameters (eg. Vcmax) were left at global values for the comparison and could be the reason behind this discrepancy. This could potentially lead to an underestimation of the "fossil fuel – diffuse light" effect in these forest biomes. However, as diffuse radiation is underestimated in our study, the diffuse effect on NPP is potentially overestimated due to the nonlinearity of plant carbon uptake to changes radiation.

## 5.2 Have synergies between nitrogen deposition and atmospheric $CO_2$ driven the recent enhancement of the terrestrial carbon sink?

CLM4.5-BGC was used to simulate changes in carbon uptake and storage, with a focus on two time periods (with different baselines). Extended factorial simulations were performed over 1901-2016 to attribute drivers to changes in carbon uptake, with a focus on nitrogen deposition and carbon-nitrogen synergy. Recent simulations over the period 1990-2016 were also performed to quantify changes relative to a more contemporary baseline. A summary of the findings from this study in relation to the second hypothesis is presented below:

a) Fossil fuel emission and atmospheric deposition of nitrogen increased over the 20th century due to industrialisation in many regions across the globe. Global nitrogen deposition increased from 24 TgN/yr in 1900 to 70 TgN/yr in 2016 due to a combination of increased fossil fuel burning and agricultural intensification. Regional deposition patterns are dictated by emission sources, with major source regions of USA, Europe, and East Asia. More recently (1990-2016), global deposition has been relatively constant, however regional changes have occurred. Air quality measures in Europe and the US have decreased nitrogen deposition by 0.13 TgN/yr and 0.89 TgN/yr, respectively. Contrary, large increases in fossil fuel burning increased nitrogen deposition by 3.74 TgN/yr in East Asia.

b) Over the 20th century, NPP increased by 10 PgC/yr (+17%), with the largest contribution from $CO_2$ fertilization (60%). Increased nitrogen deposition accounted for 15% of the increase, with non-linear interactions between carbon, nitrogen, and climate accounting for 17%. Similarly, increases in the net land flux were dominated by $CO_2$

fertilization, with nitrogen deposition and synergistic effects each amounting to 15% of the overall 2.3 PgC/yr increase. Changes in climate decreased net carbon uptake as warming increased soil respiration and drying trends reduced photosynthesis.

c) There are regional differences between the contribution of each driver to changes in net carbon uptake. $CO_2$ fertilization predominates in tropical and northern hemisphere forests, whereas the influence nitrogen deposition is most apparent in North America, Europe, and East Asia. Carbon-nitrogen synergistic effects arise in tropical regions as well as in China, where additional nitrogen deposited worked to offset the limitation brought about by increased $CO_2$ fertilization. Climate trends caused widespread losses of carbon across parts of temperate Eurasia, tropical regions, and southern Africa. On the contrary, precipitation trends in South America and USA have increased net carbon gain over the historical period.

d) Regarding the increased 21st century sink, $CO_2$ fertilization increased NBP by 1.22 PgC/yr between 1990-2016, whilst changes in climate led to a loss of 1.17 PgC/yr. Warming trends increased NPP over the majority of the northern (>30°N) lands, however concurrent rises in soil respiration reversed initial increases in temperate US and Eurasia. Declines in South American NBP are driven by decreases in productivity due to warming and drying trends. Nitrogen deposition increased by only 3% globally since 1990, and as such there was a limited carbon response. Regionally however, changes in nitrogen deposition caused large changes in net carbon uptake. Increased NBP due to deposition in East Asia was on the order of 50% of the total NBP change. Synergistic effects are limited over this period, with only a small response seen in China. This is primarily due to the small spatial footprint of nitrogen increases across the globe, being limited to East Asia and Western Europe, and also because large synergistic effects take years to develop.

e) Therefore, from the results of Chapters 2 and 3, I conclude that the increased global terrestrial sink since the turn of this century is likely not due to increased nitrogen deposition, carbon-nitrogen synergies, or increased atmospheric aerosols related to fossil fuel burning. Accordingly, other drivers and mechanisms must be responsible for the increased sink. Both JULES and CLM4.5-BGC simulate a large $CO_2$ fertilization effect (even with the nitrogen limitation included in CLM). Further, both simulate carbon losses due to changes in climate in the past two decades (studied further in Chapter 4). Other mechanisms not included in these studies such as land-use and land cover change could have driven large changes in vegetation distribution and carbon cycling, impacting the terrestrial carbon balance.

## 5.3 Climate-driven variability and trends in plant productivity over the last three decades based on three global products

Three independent ‘state of the art’ datasets of gross primary production (GPP); upscaled eddy-flux observations (FLUXCOM), a set of process-based terrestrial biosphere models (TRENDY), and a satellite driven light-use efficiency model (LUE) were compared in regard to the interannual variability and trends due to changes in climate over the period 1982-2016. The sensitivity of global, regional, and local GPP to changes in temperature and precipitation was quantified for each product. A summary of the findings from this study is highlighted below:

a) FLUXCOM exhibits much lower IAV than both TRENDY and LUE on global, regional, and local scales. TRENDY and LUE have a mean variation (1σ of detrended annual timeseries) of 1.21 PgC/yr and 1.01 PgC/yr, respectively, whereas FLUXCOM has a smaller IAV of 0.34 PgC/yr. FLUXCOM captures on a portion of the climate-driven GPP signal, and does not contain an vegetation memory effects. Namely, FLUXCOM uses a fixed seasonal cycle of satellite LAI, and therefore IAV and trends in vegetation activity are not captured. However, on inter-annual timescales the products significantly ($p<0.05$) correlate on global and broad regional scales. On grid-cell scale, the products all agree on inter-annual scales in temperate US, grasslands of Eurasia, and savannas and shrublands of the southern hemisphere. LUE grid-cell GPP correlates poorly with both FLUXCOM and TRENDY in tropical regions. Tropical GPP is highly uncertain in all products. FLUXCOM suffers from poor data coverage, and terrestrial biosphere models are unconstrained in this region.

b) Global GPP trends over 1982-2016 differ between the products. FLUXCOM has a small non-significant positive trend of 0.002±0.017 PgC/yr$^2$ compared to the larger significant trends of 0.092±0.057 PgC/yr$^2$ and 0.062±0.027 PgC/yr$^2$ for TRENDY and LUE, respectively. Large-scale northern warming led to increased uptake in TRENDY and LUE models, a finding in line with previous studies which suggest temperature is a primary control on northern photosynthesis. All three products exhibit negative GPP trends in central South America, driven by warming temperatures increasing evaporative demand. Tropical trends are generally less robust, with positive precipitation trends in South East Asia lead to a spatially uniform (albeit small) increase in TRENDYv6 GPP. However, FLUXCOM and LUE simulate no change in the majority of South East Asia (and other tropical forest regions).

c) On grid-cell scale, all products agree in the direction of trend over 58% of the vegetated land surface. Large areas of Eurasia and North America exhibit positive summer trends due to warming. In contrast, warming in central South America has decreased dry season GPP over the study period. Negative precipitation trends in South US and Mongolia/China have reduced GPP, whereas a wetting trend in South Africa has enhanced productivity.

d) The spatial pattern of GPP sensitivity to temperature is similar between all products. Northern lands show a positive sensitivity to temperature (with TRENDY showing highest values), and tropics and southern lands being negatively related to temperature (with LUE have largest negative sensitives). The spatial pattern of GPP precipitation sensitivities varies between the products. FLUXCOM has a significant ($p<0.05$) positive sensitivity ubiquitously across the land surface, whereas TRENDY has significant sensitivities located in northern temperate, tropical, and southern regions. LUE GPP is generally less sensitive to precipitation, with only the grasslands of North America, and grasslands and shrublands of the southern hemisphere showing a positive response.

e) Furthermore, the relative importance of temperature and precipitation in grid scale GPP variability differs across the products. FLUXCOM GPP is controlled by precipitation across the globe, apart from central South America where temperature exerts a dominating influence. Both TRENDY and LUE northern GPP is controlled by temperature. In line with FLUXCOM, TRENDY is controlled by precipitation in grasslands and shrublands across the globe. However, for LUE, large parts of the tropics and southern hemisphere are controlled by temperature variability.

## 5.4 Summary

The terrestrial carbon sink has increased over the past decades due to a myriad of factors including; $CO_2$ fertilization of photosynthesis (Schimel *et al.*, 2015), climate warming leading to longer and more favourable growing seasons (Barichivich *et al.*, 2013), regrowth on abandoned farm land (Kondo *et al.*, 2018), increased diffuse radiation fraction (Mercado *et al.*, 2009), and nitrogen deposition stimulating plant growth (Zaehle, 2013). However, the exact contribution of these drivers and the location of changes in component fluxes and sinks remains uncertain. Identifying the location and driving mechanisms is vital for a holistic understanding of the carbon cycle and the ability to confidently and accurately predict future environmental changes. Of initial interest in this thesis is the apparent increase in terrestrial carbon uptake from the beginning of the 21st century. Enhanced nitrogen deposition and diffuse radiation associated with increased fossil fuel emissions were hypothesised to increase carbon uptake and explain the recent sink (Hansen *et al.*, 2013). Both mechanisms have a positive influence on primary productivity (Mercado *et al.*, 2009, Zaehle, 2013) and have altered regional carbon uptake in the 20th century.

Chapter 2 of this thesis quantified the roles of various drivers on changes in carbon uptake over the first decade of the 21st century. A particular focus was on the impact of changes in fossil fuel emissions on atmospheric aerosol, direct/diffuse light, and subsequently NPP. Previous studies have highlighted the important role of the ratio of diffuse to direct light (Mercado *et al*., 2009, Gu *et al*., 2003). However, this is the first study to quantify the effects of changes in fossil fuel aerosol (along with $CO_2$ fertilization, climate change, and changes in biomass burning aerosol) on carbon uptake since the start of the 21st century. This is of particular importance as the period 2000-2010 saw a large increase in the terrestrial carbon sink (Le Quéré *et al*., 2018), with conflicting reports on the drivers behind the increase (Ballantyne *et* al., 2017, Keenan *et al.,* 2016, Zhu *et al.,* 2018). This study used a 3-model cascade in order to attribute drivers to changes in carbon uptake over 1998-2010. The ability of each model to reproduce observed patterns of AOD, surface solar radiation, and photosynthetic response to direct and diffuse PAR was evaluated. GLOMAP is a comprehensive microphysical aerosol model and successfully reproduced observed AOD trends in fossil fuel dominated regions (North America, Europe, and East Asia) over 1998-2010. Further, modelled incoming surface solar total and diffuse radiation matched observations at forest sites. This study also further evaluated JULES in four northern temperate and boreal forest sites (two broadleaf, two needleleaf), complementing the evaluation performed in previous work (Mercado *et al*., 2009, Rap *et al*., 2015), that JULES is able to capture observed response to varying PAR levels in different biomes and diffuse/direct light regimes. It is important a model is able to reproduce observed patterns in response to changes in incoming PAR when using the same model to simulate future responses to changes in fossil fuel emissions, aerosol concentrations, and subsequent light regime.

The decadal trend in NPP due to changes in fossil fuel aerosol was dominant (compared to other drivers) in localised regions (North America, Europe, East Asia), highlighting the first-order influence of the ratio of direct to diffuse radiation has on canopy photosynthesis. Therefore, all DGVMs should include the influence of diffuse radiation and changes in light regime in historical and future carbon cycle simulations. For example, a comparison of the simulated historical sink (1900-present) using TRENDY DGVMs (Sitch *et al*., 2015) with the residual land sink indicates there is a budget imbalance (difference between two estimates) for any particular year (Le Quéré *et al*., 2018). This imbalance is most pronounced following the eruption of Mt. Pinatubo (1991-1992), whereby the DGVMs are missing processes related to diffuse radiation (Mercado *et al*., 2009).

Importantly, JULES does not include the effects of nitrogen availability on carbon uptake, which is a key determinant of plant growth, due to stoichiometric demands (Cleveland *et al*., 2013). Further, nitrogen is generally a limited resource due to the large energy requirement of converting atmospheric $N_2$ to plant available forms, and losses from the biosphere due to fires, leaching, and denitrification (Vitousek & Howarth, 1991). Chapter 3 expands on the results from Chapter 2 by considering the secondary impact of changes in fossil fuel emissions; effects of nitrogen deposition and carbon-nitrogen interactions on the recent carbon sink. Chapter 3 quantifies the roles of $CO_2$ fertilization, nitrogen deposition, climate and the synergistic effects between them on gross and net carbon fluxes over the historical period. Firstly, the simulated deposition trends (increase in East Asia, decrease in Europe and North America) are in line with observations (Liu *et al*., 2013, De Vries & Posch, 2011, Du *et al*., 2014). The nitrogen deposition induced sink simulated by CLM4.5-BGC matches previous studies well (Thornton *et al*., 2007, Zaehle *et al*., 2010), and the simulated CN-synergistic effect is (to a lesser extent) in further agreement with other models (Churkina *et al*., 2009, Zaehle *et al*., 2010). This study expands on previous work by additionally focusing on changes to the terrestrial carbon cycle relative to a more recent baseline (hereby removing background carbon trends from non-equilibrium conditions; Bonan & Levis, 2010). Over the last two decades, changes in nitrogen deposition and carbon-nitrogen synergistic interactions are important drivers of carbon uptake on regional levels (North America, Europe, and East Asia), however these effects are negligible when integrated to the global scale (due to opposing regional trends). Therefore, carbon-nitrogen interactions do play a pivotal role in terrestrial carbon cycling, but in the context of the strengthening global carbon sink over the last two decades, these processes seem not to be dominant.

Both Chapters 2 and 3 (and numerous other studies; Keenan *et al.*, 2016, Schimel *et al.*, 2015, Sitch *et al.*, 2015) indicate a primary role for $CO_2$ fertilization in the explaining the recent sink. Yet, the $CO_2$ fertilization effect is still largely unconstrained in DGVMs (Arora *et al.,* 2013, Zaehle *et al.*, 2014), as the full interaction with nutrient cycling (e.g. nitrogen, phosphorus) is still largely unknown (Goll *et al.*, 2012, Zaehle *et al.*, 2014). Overall, both the ratio of diffuse to direct light and nitrogen availability are key factors in determining gross and net carbon uptake. The results from Chapters 2 and 3 highlight the regional importance of taking into account spatiotemporal changes in fossil fuel aerosol in determining carbon fluxes, and the need for modelling studies to include all relevant processes. Although these mechanisms appear not responsible for the increased 21st century sink (thus far), future fossil fuel emission trajectories will determine aerosol trends (and hence the light regime and deposition patterns). Therefore, our results stress the need for the inclusion of these necessary processes and mechanisms in DGVMs for future carbon cycle studies, in which emission trajectories are expected to drastically change (Moss *et al.*, 2010).

One of the largest (and most important) uncertainties in future carbon cycle projections is how GPP will evolve (temporally and spatially). Terrestrial GPP is the largest carbon flux into the biosphere and therefore drives other ecosystem functions (e.g. growth and respiration). It is also one of the major fluxes influencing the net carbon sink, which works to offset anthropogenic $CO_2$ emissions. The future evolution of global GPP depends in part on the sensitivity of plant level GPP to local climate (e.g. temperature and precipitation), and how these sensitivities and responses integrate to the global scale. Chapter 4 addresses this question by analysing three global GPP datasets (upscaled FluxNet observations; FLUXCOM, a suite of DGVMs; TRENDYv6, and a LUE model) spanning the period 1982-2016. For TRENDY and LUE, northern warming led to large increases in growing season GPP throughout North America and Eurasia, in agreement with our understanding of temperature constraints on northern productivity (Nemani *et al.*, 2003). However, FLUXCOM shows limited GPP increases in northern latitudes, and FLUXCOM has overall lower GPP variability than the DGVMs and LUE model. Low FLUXCOM GPP variance is highlighted in this study, and is a previously known issue for the product (Jung *et al*., 2011, Tramontana *et al*., 2016). There are noticeable similarities and differences in GPP sensitivities to climate forcings amongst the three products. Overall, the spatial patterns of GPP sensitivity to temperature are consistent between all three products (positive in north, negative in the tropics/south). The consistency between products and also with previous studies (Beer *et al*., 2010, Jung *et al*., 2017) gives confidence in the reported temperature sensitivities. However, IAV in GPP from FLUXCOM is mostly driven by precipitation anomalies across the globe, whereas the corresponding pattern for LUE GPP is only observed in a number of shrubland regions. Thus, the FLUXCOM GPP pattern is inconsistent with "northern regions are temperature limited" paradigm (Nemani *et al*., 2003).

One important feature must be highlighted. The high northern latitudes are generally characterised by cold/dry conditions and relatively low magnitude and variance of GPP, which leads to difficulties in trying to explain the variability using machine learning / empirical methods (i.e. there is nothing to explain). Further, the predictor variables used in the machine learning methods do not capture all drivers of GPP variability (Tramontana *et al*., 2016). For example, there is no information on the IAV of vegetation activity in FLUXCOM. The impact of this on estimated GPP IAV is highlighted by analysing a previous version of upscaled flux tower GPP (FluxNetG), which includes interannual satellite vegetation information. The large northern GPP increase over 1982-2016 estimated by FluxNetG, as well as IAV magnitudes similar to TRENDYv6 and LUE indicate the importance of input data in the machine learning methods. Further, machine learning methods generally perform poorly outside of conditions of the training data, and as there are very few sites in high northern latitudes, the models may not be suitable for these regions.

The dominance of temperature over precipitation regarding IAV in GPP from LUE is most likely due to the structure of the LUE model, which is driven by two climate scalars; a function of temperature, and a function of  VPD. VPD is a measure of moisture in the atmosphere and is heavily influenced by temperature. Therefore, a larger dependence of LUE GPP on temperature in the multiple linear regression is not surprising. Further, the LUE model was parameterised with site observations from northern temperate forests (Robinson *et al.*, 2018, Zhao & Running, 2010), and so using this model in other biomes introduces additional uncertainties. Moreover, the model maybe missing important information on plant water availability by excluding a soil moisture term (Stocker *et al.*, 2018). There are many sources of uncertainty across all products (missing or poorly represented processes), and as such differences in driver attribution to GPP variability is not unexpected. Overall, Chapter 4 highlights robust patterns of GPP change (e.g. northern latitude and Sahel increases, North and South America decreases), however this study also highlights the large uncertainties associated with the underlying drivers and climate sensitivities with all three global GPP products.

## 5.5 Implications for Future Work

The results of this thesis highlight the important role of both the type (direct or diffuse) of incoming radiation and also nitrogen availability on terrestrial carbon fluxes. Chapter 2 indicated that JULES was able to generally capture observed GPP responses to PAR in a range of light conditions, although the model does underestimate GPP in needleleaf forests. This is most likely because I do not tune any model parameters such as the maximum photosynthetic capacity, unlike previous model evaluation (Mercado et al., 2009). Under estimation of JULES carbon uptake has been reported previously (Mercado et al., 2007; Slevin et al., 2015), due to biases in global values for photosynthetic capacity generally underestimating local site conditions. There could therefore be a need to increase the number of PFTs in JULES to account for more of the spatial variability among biomes. Generally for all DGVMs, the separation of diffuse and direct radiation for sunlit and shaded leaves, along with accurate representation of radiative transfer through the canopy is vital for correction simulation of canopy GPP (Mercado *et al.*, 2007). Currently, in modelling intercomparison studies (e.g. TRENDY), the influence of spatiotemporally changing diffuse radiation is neglected. Addressing this should be a high priority for the modelling community.

In Chapter 2, the atmospheric aerosol loading was underestimated, although AOD trends matched well with satellite observations. An underestimation of aerosol will lead to subsequent biases in radiative fluxes in the atmosphere and vegetation canopy. Due to the non-linear relationship between carbon uptake and incoming radiation, the diffuse radiation response simulated here may be overestimated. GLOMAP underestimating aerosol burdens has been reported previously (Mann et al., 2010) and could be due to missing processes such as; underestimation of primary emissions or missing species (eg. nitrate). The first two hypothesis of this thesis are directly related to emissions of fossil fuel gas/aerosol. The emission datasets used in Chapters 2 (MACCity) and 3 (Lamarque et al., 2010) have a low temporal resolution, with annual values calculated by interpolating between decadal means. Therefore, by design our model simulations may not be able to produce the increase in carbon uptake due to increased aerosol or nitrogen deposition around 2000, but instead capture decadal changes. Future work by the community into developing high temporal resolution datasets of emissions would overcome this issue.

Furthermore, future work to improve the modelling studies of Chapters 2 and 3 would be to include additional important processes associated with fossil fuel emissions that are missing from current DGVMs. For example, fossil fuel $SO_2$ contributes to acid deposition, which depletes nutrients in soils and can lead to plant mortality (Driscoll *et al.*, 2001). Further NOx emitted from fossil fuel burning is a precursor to atmospheric ozone, which can cause plant cellular damage (Ashmore, 2005). Although JULES does include the adverse effects of ozone on photosynthesis, they were not considered in this study. Future work should attempt to include all these relevant processes, so a more realistic, combined effect on carbon uptake can be quantified.

In Chapter 3, the importance of carbon-nitrogen interactions in driving the response of the terrestrial biosphere to increases in $CO_2$ and variations in climate is highlighted. Therefore, it is critical DGVMs include a representation of nitrogen availability on carbon uptake, especially in future coupled carbon cycle climate simulations. How terrestrial biosphere models represents inputs and losses of nitrogen, as well as the coupling to the carbon cycle is a key uncertainty that propagates through to other ecosystem processes such as; water and energy fluxes, species composition, stomatal conductance and evapotranspiration (Zaehle & Dalmonech, 2011). Nitrogen limitation in CLM4.5-BGC is implemented via a downscaling of GPP as a function of available plant nitrogen and fixed C:N tissue ratios. Other, more realistic approaches exist whereby the acclimation of photosynthesis to nitrogen stress is simulated by allowing changes in allocation patterns, and foliar nitrogen concentrations (Zaehle et al., 2010). Further, the fixed C:N ratios used in CLM prevent plants acclimating to new conditions. Therefore, CLM may potentially underestimate the carbon impact of additional nitrogen deposited as in-situ studies have shown increasing C:N ratios under increasing $CO_2$ (Finzi et al., 2006; Dybzinkski et al., 2015). Models which include flexible C:N ratios (eg. O-CN (Zahele et al., 2011), Hybrid (Friend et al., 1997), LPJ (Xu-Ri & Prentice, 2008)) have the capacity to capture observed changes in stoichiometry in ecosystem experiments (Norby et al., 2005) and have better agreement with observed foliar nitrogen concentrations at FACE sites (Medlyn et al., 2015). These are all factors modellers should take into account when implementing coupled carbon-nitrogen schemes into DGVMs, in order to accurately capture the carbon response to future global change.

Furthermore, I addressed my first two hypothesis in separate modelling studies. However, including both processes simultaneously would have amplified the carbon response in regions of changing diffuse radiation and aerosol deposition. The global effect however, would most likely have been unchanged as regional compensations would remain. Although both JULES and CLM have been extensively evaluated, the use of a single model in Chapters 2 and 3 may lead to biases due to structural uncertainties in all terrestrial biosphere models (Fisher et al., 2014; Huntzinger et al., 2017). Model inter-comparisons such as TRENDY (Sitch et al., 2015) and MsTMIP (Huntzinger et al., 2013 – Overview and experimental design) provide an opportunity to understand how model structural differences impact estimates of carbon uptake.

Chapter 4 assessed the consistency in IAV and trends for three prominent climate-driven global GPP datasets. Various uncertainties with these products are discussed above. The machine learning methods used in the FLUXCOM product suffer from incomplete predictor variables that do not contain enough information regarding the variability of carbon fluxes (Tramontana *et al.*, 2016).

Inclusion of interannual vegetation information would help to solve this issue. Further, increasing the number of flux tower sites in underrepresented regions (high northern latitudes and tropical forests) will improve the predictive capability of these methods. Additionally, this study used the ensemble mean GPP of 12 DGVMs, all of which have different model structures, and carbon flux sensitivities to climate. A more thorough analysis of each of the individual TRENDY models, indicating regions of agreement and disagreement in GPP variability, trends, and dominant climate drivers would enable a deeper understanding of the simulated patterns. This would then indicate which processes are most important in determining GPP variability, and allow for model development into constraining these processes.

The increased availability of observations via satellites, atmospheric inversions, flux towers, FACE sites, and forest plots provide an opportunity to evaluate terrestrial biosphere models and provide direct estimates of changes to the environment. Satellites offer global coverage at high temporal (daily-weekly) resolution and can observe a range of variables (eg. FPAR, VOD, SIF, LAI) representing various ecosystem functions. FPAR and LAI have been critical in estimating vegetation productivity over the past three decades (Myneni et al., 1997, LAI reference), but are not direct measurements of carbon uptake. Solar-induced fluorescence (SIF) on the other hand is a direct by-product of photosynthesis, and new (~2007) satellite monitoring offers a direct measurement of global GPP (Frankenberg et al., 2011). Further, observations from field data, particularly FACE experiments (Ainsworth & Long, 2004), and forest inventory plots (Brienen et al., 2015) can be used to test model parameterisations and reduce model uncertainty (Medlyn et al., 2015).

This thesis has focused on past changes in the terrestrial carbon cycle and potential driving mechanisms. However, a key topic in carbon/climate research is estimating the evolution of carbon sinks under climate change and evaluating potential carbon-climate feedbacks. All analysis conducted in this thesis used “offline” terrestrial biosphere models. However, all parts of the Earth system interact and are coupled together. Therefore, coupled climate-carbon cycle models that capture relevant processes and feedbacks are required to make accurate projections. A model inter-comparison of coupled carbon-climate models (CMIP5, Friedlingstein et al., 2014) predicts an increased terrestrial sink in the future, however with large differences between models.

## References

Ainsworth E, Long S *et al*. (2004) What have we learned from 15 years of free-air $CO_2$ enrichment (FACE)? A meta-analysis review of the responses of photosynthesis, canopy properties and plant production to rising $CO_2$. New Phytologist, **165**, 351-372.

Arora V, Boer G, Friedlingstein P *et al*. (2013) Carbon-Concentration and Carbon-Climate Feedbacks in CMIP5 Earth System Models. Journal of Climate, **26**, 5289-5314.

Ashmore M (2005) Assessing the future global impacts of ozone on vegetation. Plant, Cell and Environment, **28**, 949-964.

Ballantyne A, Smith W, Anderegg W *et al.* (2017) Accelerating net terrestrial carbon uptake during the warming hiatus due to reduced respiration. Nature Climate Change*,* **7**.

Barichivich J, Briffa KR, Myneni RB *et al.* (2013) Large-scale variations in the vegetation growing season and annual cycle of atmospheric $CO_2$ at high northern latitudes from 1950 to 2011. Global Change Biology*,* **19**, 3167-3183.

Beer C, Reichstein M, Tomelleri E *et al.* (2010) Terrestrial Gross Carbon Dioxide Uptake: Global Distribution and Covariation with Climate. Science*,* **329**, 834-838.

Bonan GB, Levis S (2010) Quantifying carbon-nitrogen feedbacks in the Community Land Model (CLM4). Geophysical Research Letters*,* **37**, L07401-L07401.

Brienen RJW, Phillips OL, Feldpausch TR *et al.* (2015) Long-term decline of the Amazon carbon sink. Nature*,* **519**, 344-348.

Churkina G, Brovkin V, Von Bloh W, Trusilova K, Jung M, Dentener F (2009) Synergy of rising nitrogen depositions and atmospheric $CO_2$ on land carbon uptake moderately offsets global warming. Global Biogeochemical Cycles*,* **23**.

Cleveland C, Houlton B, Smith W, Marklein A *et al*. (2013) Patterns of new versus recycled primary production in the terrestrial biosphere. Proceedings of the National Academy of Sciences of the United States of America, **110**, 12733-7

De Vries W, Posch M (2011) Modelling the impact of nitrogen deposition, climate change and nutrient limitations on tree carbon sequestration in Europe for the period 1900–2050. Environmental Pollution*,* **159**, 2289-2299.

Driscol C, Lawrence G, Bulger A *et al*. (2001) Acidic Deposition in the Northeastern United States: Sources and Inputs, Ecosystem Effects, and Management Strategies: The effects of acidic deposition in the northeastern United States include the acidification of soil and water, which stresses terrestrial and aquatic biota. BioScience, **51**, 180-198.

Du E, Wim De V, James NG, Xueyang H, Jingyun F (2014) Changes in wet nitrogen deposition in the United States between 1985 and 2012. Environmental Research Letters*,* **9**, 095004.

Dybzinski R, Farrior CE, Pacala SW (2015) Increased forest carbon storage with increased atmospheric CO2 despite nitrogen limitation: a game-theoretic allocation model for trees in competition for nitrogen and light. Global Change Biology*,* **21**, 1182-1196.

Finzi AC, Moore DJP, Delucia EH *et al.* (2006) PROGRESSIVE NITROGEN LIMITATION OF ECOSYSTEM PROCESSES UNDER ELEVATED $CO_2$ IN A WARM-TEMPERATE FOREST. Ecology*,* **87**, 15-25.

Fisher JB, Huntzinger DN, Schwalm CR, Sitch S (2014) Modeling the Terrestrial Biosphere. Annual Review of Environment and Resources*,* **39**, 91-123.

Frankenberg C, Fisher J, Worden J *et al*. (2011) New global observations of the terrestrial carbon cycle from GOSAT: Patterns of plant fluorescence with gross primary productivity. Geophysical Research Letters, **38**.

Friedlingstein P, Meinshausen M, Arora VK *et al*. (2014) Uncertainties in CMIP5 Climate Projections due to Carbon Cycle Feddbacks, Journal of Climate, **27**, 511-526

Friend AD, Stevens AK, Knox RG, Cannell MGR (1997) A process-based, terrestrial biosphere model of ecosystem dynamics (Hybrid v3.0). Ecological Modelling*,* **95**, 249-287.

Goll D, Brovkin V, Parida B *et al*. (2012) Nutrient limitation reduces land carbon uptake in simulations with a model of combined carbon, nitrogen and phosphorus cycling. Biogeosciences, **9**, 3547-3569.

Gu L, Baldocchi DD, Wofsy SC, Munger JW, Michalsky JJ, Urbanski SP, Boden T (2003) Response of a Deciduous Forest to the Mount Pinatubo Eruption: Enhanced Photosynthesis. Science*,* **299**, 2035-2038.

Hansen J, Kharecha P, Sato M (2013) Climate forcing growth rates: doubling down on our Faustian bargain. Environmental Research Letters*,* **8**, 011006-011006.

Huntzinger DN, Michalak AM, Schwalm C *et al.* (2017) Uncertainty in the response of terrestrial carbon sink to environmental drivers undermines carbon-climate feedback predictions. Scientific Reports*,* **7**, 4765-4765.

Huntzinger DN, Schwalm C, Michalak A *et al.* (2013) The North American Carbon Program Multi-Scale Synthesis and Terrestrial Model Intercomparison Project - Part 1: Overview and experimental design. Geoscientific Model Development, **6**, 2121-2133.

Jung M, Reichstein M, Margolis H *et al.* (2011) Global patterns of land-atmosphere fluxes of carbon dioxide, latent heat, and sensible heat derived from eddy covariance, satellite, and meteorological observations. Journal of Geophysical Research, **116**, G00J07.

Jung M, Reichstein M, Schwalm CR *et al.* (2017) Compensatory water effects link yearly global land CO2 sink changes to temperature. Nature*,* **541**, 516-520.

Keenan TF, Prentice IC, Canadell JG, Williams CA, Wang H, Raupach M, Collatz GJ (2016) Recent pause in the growth rate of atmospheric $CO_2$ due to enhanced terrestrial carbon uptake. Nature Communications*,* **7**, 13428-13428.

Kondo M, Ichii K, Patra PK *et al.* (2018) Plant Regrowth as a Driver of Recent Enhancement of Terrestrial $CO_2$ Uptake. Geophysical Research Letters*,* **45**, 4820-4830.

Lamarque JF, Bond TC, Eyring V *et al.* (2010) Historical (1850–2000) gridded anthropogenic and biomass burning emissions of reactive gases and aerosols: methodology and application. Atmospheric Chemistry and Physics*,* **10**, 7017-7039.

Liu X, Zhang Y, Han W *et al.* (2013) Enhanced nitrogen deposition over China. Nature*,* **494**, 459-462.

Le Quéré C, Andrew RM, Friedlingstein P *et al.* (2018) Global Carbon Budget 2017. Earth Syst. Sci. Data*,* **1010333739**, 405-448.

Mann GW, Carslaw KS, Spracklen DV *et al.* (2010) Description and evaluation of GLOMAP-mode: a modal global aerosol microphysics model for the UKCA composition-climate model. Geoscientific Model Development Discussions*,* **3**, 651-734.

Medlyn B, Zaehle S, De Kauwe M *et al.* (2015) Using ecosystem experiments to improve vegetation models. Nature Climate Change, **5**, 528-534.

Mercado LM, Huntingford C, Gash JHC, Cox PM, Jogireddy V (2007) Improving the representation of radiation interception and photosynthesis for climate model applications. Tellus, Series B: Chemical and Physical Meteorology*,* **59**, 553-565.

Mercado LM, Bellouin N, Sitch S, Boucher O, Huntingford C, Wild M, Cox PM (2009) Impact of changes in diffuse radiation on the global land carbon sink. Nature*,* **458**, 1014-1017.

Moss R, Edmonds J, Hibbard K *et al*. (2010) The next generation of scenarios from climate change research and assessment. Nature, **463**, 747-756.

Myneni RB, Keeling CD, Tucker CJ, Asrar G, Nemani RR (1997) Increased plant growth in the northern high latitudes from 1981 to 1991. Nature*,* **386**, 698-702.

Nemani RR, Keeling CD, Hashimoto H *et al.* (2003) Climate-driven increases in global terrestrial net primary production from 1982 to 1999. Science (New York, N.Y.)*,* **300**, 1560-1563.

Norby RJ, Delucia EH, Gielen B *et al.* (2005) Forest response to elevated CO2 is conserved across a broad range of productivity. Proceedings of the National Academy of Sciences of the United States of America*,* **102**, 18052-18056.

Rap A, Spracklen DV, Mercado L *et al.* (2015) Fires increase Amazon forest productivity through increases in diffuse radiation. 1-9.

Robinson NP, Alfred BW, Smith WK *et al*., (2018) Terrestrial primary production for the conterminous United States derived from Landsat 30m and MODIS 250m. Remote Sensing in Ecology and Conservation, **4**, 264-280.

Schimel D, Stephens BB, Fisher JB (2015) Effect of increasing $CO_2$ on the terrestrial carbon cycle. Proceedings of the National Academy of Sciences of the United States of America*,* **112**, 436-441.

Sitch S, Friedlingstein P, Gruber N *et al.* (2015) Recent trends and drivers of regional sources and sinks of carbon dioxide. Biogeosciences*,* **12**, 653-679.

Slevin D, Tett S, Williams M (2015) Multi-site evaluation of the JULES land surface model using global and local data. Geoscientific Model Development, **8**, 295-316.

Stocker BD, Zscheischler J, Keenan TF *et al*. (2018) Quantifying soil moisture impacts on light use efficiency acros biomes. New Phytologist, **218**, 1430-1449.

Thornton PE, Lamarque J-F, Rosenbloom NA, Mahowald NM (2007) Influence of carbon-nitrogen cycle coupling on land model response to $CO_2$ fertilization and climate variability. Global Biogeochemical Cycles, **21**, GB4018-GB4018.

Tramontana G, Jung M, Schwalm CR *et al.* (2016) Predicting carbon dioxide and energy fluxes across global FLUXNET sites with regression algorithms. Biogeosciences, **13**, 4291-4313.

Vitousek PM, Howarth RW (1991) Nitrogen Limitation on Land and in the Sea: How Can It Occur? pp Page, Springer.

Xu-Ri, Prentice I (2008) Terrestrial nitrogen cycle simulation with a dynamic global vegetation model. Global Change Biology, **14**, 1745-1764.

Zaehle S, Medlyn BE, De Kauwe MG *et al.* (2014) Evaluation of 11 terrestrial carbon-nitrogen cycle models against observations from two temperate Free-Air $CO_2$ Enrichment studies. New Phytologist, **202**, 803-822.

Zaehle S (2013) Terrestrial nitrogen-carbon cycle interactions at the global scale. Philosophical transactions of the Royal Society of London. Series B, Biological sciences, **368**, 20130125-20130125.

Zaehle S, Dalmonech D (2011) Carbon–nitrogen interactions on land at global scales: current understanding in modelling climate biosphere feedbacks. Current Opinion in Environmental Sustainability, **3**, 311-320.

Zaehle S, Friend AD, Friedlingstein P, Dentener F, Peylin P, Schulz M (2010) Carbon and nitrogen cycle dynamics in the O-CN land surface model: 2. Role of the nitrogen cycle in the historical terrestrial carbon balance. Global Biogeochemical Cycles, **24**, GB1005-GB1005.

Zhao M, Running SW (2010) Drought-Induced Reduction in Global Terrestrial Net Primary Production from 2000 Through 2009. Science, **329**, 940-943.

Zhu Z, Piao S, Yan T, Ciais P, Bastos A, Zhang X, Wang Z (2018) The Accelerating Land Carbon Sink of the 2000s May Not Be Driven Predominantly by the Warming Hiatus. Geophysical Research Letters, **45**, 1402-1409.

# Appendix A

# Supplementary information for Chapter 1

## Text A1

The Joint UK Land Environment Simulator (JULES) is a land-surface model that originated from the Met Office Surface Exchange Scheme (MOSES), initially designed as the land component in weather forecasting and Earth system models (Cox et al., 1999). JULES contains various interacting sub-models representing different parts of the land surface. Surface exchange of energy, water, and momentum as well as snow cover, hydrology (including surface runoff) and soil dynamics (temperature and moisture) are simulated. Soil moisture and temperature couple to the carbon cycle by influencing modelled photosynthesis and respiration (Figure A1 and Best et al., 2011).

JULES describes vegetation in grid cells using a small number of PFTs (broadleaf trees, needleleaf trees, $C_3$ grasses, $C_4$ grasses, and shrubs). Surface carbon fluxes related to photosynthesis and plant respiration are calculated in the plant physiology module on a half hourly timestep. Accumulated carbon fluxes are passed to the vegetation dynamics module, Top-down Representation of Interactive Foliage and Flora Including Dynamics (TRIFFID). Species competition is not simulated in this thesis as all simulations are on short timescales. However, TRIFFID does update vegetation carbon storage and allocation to leaves, wood, and root pools based on each PFTs LAI. After each call to TRIFFID (every 10 days), LAI and canopy height are updated depending on changes in vegetation carbon storage. This influences land-surface parameters (eg. albedo and surface roughness) used in the biophysical sub-model for surface energy fluxes. Leaf phenology is updated (every 10 days) using accumulated temperature-dependent leaf turnover rates. Litterfall calculated from TRIFFID is input to the soil carbon model RothC (Coleman and Jenkinson, 1999) which calculates the rate of microbial decomposition and subsequent $CO_2$ flux back to the atmosphere (depending on carbon content, moisture, and temperature). Plant input is split between four pools: decomposable plant material (DPM), resistant plant material (RPM), biomass (BIO), and humus (HUM).

JULES scales leaf level photosynthesis to canopy scale using a multi-layer scheme. The canopy is split into 10 layers and uses the two-stream approach of Sellers et al. (1985) to calculate surface spectral albedos and absorbed radiation at each layer. This approach considers leaf angle distribution, zenith angle, and describes absorption and scattering of direct and diffuse radiation in visible and near-infared wavebands. At each canopy level, the model also considers sunlit and shaded leaves separately and further accounts for sunfleck penetration (small regions of the vegetation understory exposed to direct sunlight). Therefore, radiative fluxes are split into direct beam radiation, scattered direct radiation, and diffuse radiation. Sunlit leaves absorb all radiation and shaded leaves only absorb diffuse. Leaf photosynthesis is calculated using a vertically varying light limited rate and decreasing photosynthetic capacity ($V_{c\,max}$) down through the canopy. Decreasing $V_{c\,max}$ is implemented by assuming an exponential decline in leaf nitrogen.

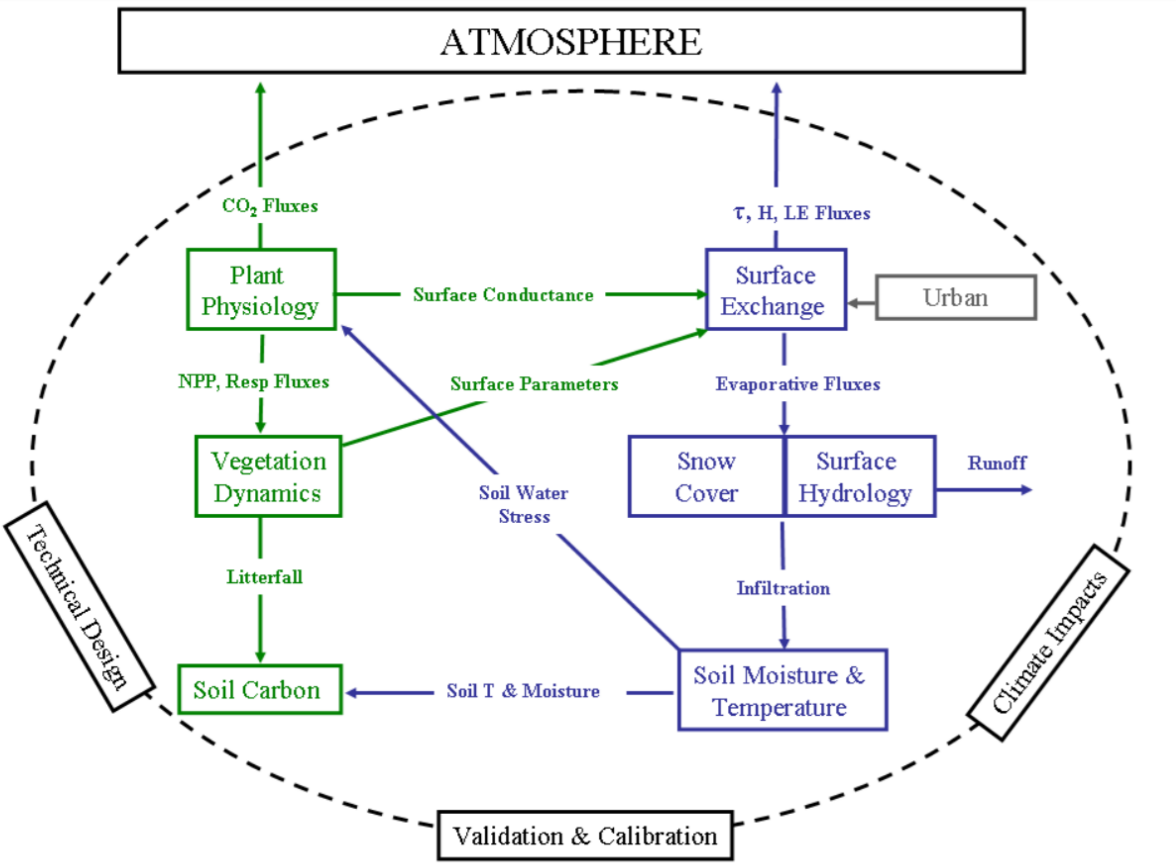

**Figure A.1 - Modular structure of JULES. Boxes show physical processes, and lines show links between modules. Biophysical processes are shown in blue and carbon cycle processes in green. Figure from Best et al., (2011).**

## Text A2

The land component of the Community Earth System Model (CESM), known as the Community Land Model (CLMv4.5; Oleson et al., 2013) represents many aspects of the land surface. CLM has various sub-models relating to biogeophysics, hydrology, biogeochemistry, land-use, and vegetation dynamics (Figure A.2). Like JULES (see Text A1), CLM simulates sub-grid heterogeneity with different land units (here vegetation, lake, urban, wetland, and glacier are included) and various PFTs (8 tree species and 7 herbaceous/understory species). Each PFT has its own LAI and canopy height that varies depending on local conditions. The land-surface component simulates the exchange of energy, water, and momentum with the atmosphere. This thesis focuses on biogeochemical processes and a short description is provided. CLM4.5-BGC is fully prognostic with respect to all carbon and nitrogen pools (vegetation, litter, soil organic matter) as well as phenology (seasonal timing of new growth and litterfall).

Leaf level photosynthesis is based on the Farquhar et al. (1980) model for C3 plants and Collatz et al. (1992) for C4 plants. Simply, leaf photosynthesis is the minimum of three limiting rates: 1) Rubisco limited rate, 2) light limited rate, and 3) rate of transport of photosynthetic products (C3 plants) and PEPCarboxylase limitation (C4 plants). Photosynthesis is calculated separately for sunlit and shaded leaves, and the maximum rate of carboxylation ($V_{c\,max}$) depends on foliar nitrogen content, which exponentially declines throughout the canopy. Stomatal conductance is calculated from the Ball-Berry model as described in Collatz et al. (1991). The model relates stomatal conductance to photosynthesis, scaled by the relative humidity and $CO_2$ concentration at the leaf surface. Soil water stress reduces both the stomatal conductance and $V_{c\,max}$.

After sunlit and shaded photosynthesis is simulated (and scaled through the canopy), potential canopy GPP ($GPP_{pot}$) is calculated. $GPP_{pot}$ is downscaled depending on available nitrogen and required nitrogen by new carbon growth. Actual GPP is defined as:

$$\mathrm{GPP}=\mathrm{GPP}_{\mathrm{pot}} * (1-f),$$

with the nitrogen scaling factor (*f*) defines as:

$$f=\frac{\mathrm{CF}_{\mathrm{avail\_alloc}}\text{-}\mathrm{CF}_{\mathrm{alloc}}}{\mathrm{GPP}_{\mathrm{pot}}}$$

where $CF_{avail\_alloc}$ is the carbon flux from photosynthesis available for new growth, after accounting for maintenance respiration. $CF_{alloc}$ is the actual carbon allocation to new growth, limited by nitrogen availability.

Coupling of the carbon and nitrogen cycles is a major advance on CLM which is briefly outlines here (Figure A.3). As a first step, plant nitrogen demand is calculated depending the amount of carbon available for growth ($CF_{avail\_alloc}$) and fixed C:N ratios for each part of the vegetation (leaves, roots, wood) for each PFT on the soil column. The plant demand for nitrogen is (partially) compensated for by translocating nitrogen from senescing leaves. Total plant nitrogen demand is reduced by the translocating flux to give the plant demand for mineral nitrogen from the soil. The combined demand for all PFTs and heterotrophic demand from the soil (immobilization) compete for available soil nitrogen. The fraction (0-1) of the plant demand that can be met given soil supply is multiplied by plant soil demand to calculate plant nitrogen uptake. The total allocated nitrogen ($NF_{alloc}$) is the sum of translocation and soil uptake. This is then used along with allocation and C:N ratios to calculate carbon allocation, $CF_{alloc}$.

Litter decomposition into soil organic matter is represented as a cascade of transformations between a certain number of decomposing coarse woody debris (CWD), litter, and soil organic matter (SOM) pools, each defined at several vertical levels. The soil decomposition scheme is based on the Century model (Parton et al., 1988) and contains 10 vertical soil layers. The carbon balance of each soil pools is the balance between inputs (directly from litter or "upstream" pools) and outputs (respiration to atmosphere, decay to "downstream" pools) to the pool. Soil respiration is modified by temperature, moisture content, and oxygen levels. A recent addition where respiration decreases exponentially with depth is included (Koven et al., 2013).

Decomposition rates are also influenced by nitrogen availability. For decomposition from each upstream to downstream pool, a nitrogen source/sink term is calculated. In general, if the downstream pool has a much higher C:N ratio than the upstream pool, a new source of nitrogen is created (mineralisation). However, if the upstream pool is nitrogen limited compared to the downstream pool, then the decomposition flux results in a demand for nitrogen (immobilization). Therefore, depending on plant demand for soil nitrogen, decomposition fluxes can be downregulated if nitrogen supply is limited. Nitrogen mineralisation is a critical feedback connecting heterotrophic respiration and plant growth. Not only does decomposition release $CO_2$ to the atmosphere, but also potentially releases nitrogen that can be taken up by plants (see thick orange arrows in Figure A.3).

Finally, in addition to the rapid cycling of nitrogen in the plant-litter-soil system, CLM has a representation of an "external" nitrogen cycle. Inputs to the system come from atmospheric deposition and biological nitrogen fixation

(BNF). Losses are due to denitrification, leaching, and fire. Additions from deposition and NBF are added straight to the mineral $NH_4^+$ pool. Deposition flux represents total reactive nitrogen from lightening NOx formation, NOx and NH3 emissions from wildfire, fossil fuel combustion, deforestation fires, and NH3 from agriculture and animal waste. BNF is assumed to be a function of annual net primary productivity (levelling at high NPP values). Nitrification of NH4+ to NO3- is a function of temperature, moisture, and pH and denitrification depends on NO3- concentrations, carbon consumptions rates, and only occurs in anoxic fractions of the soil.

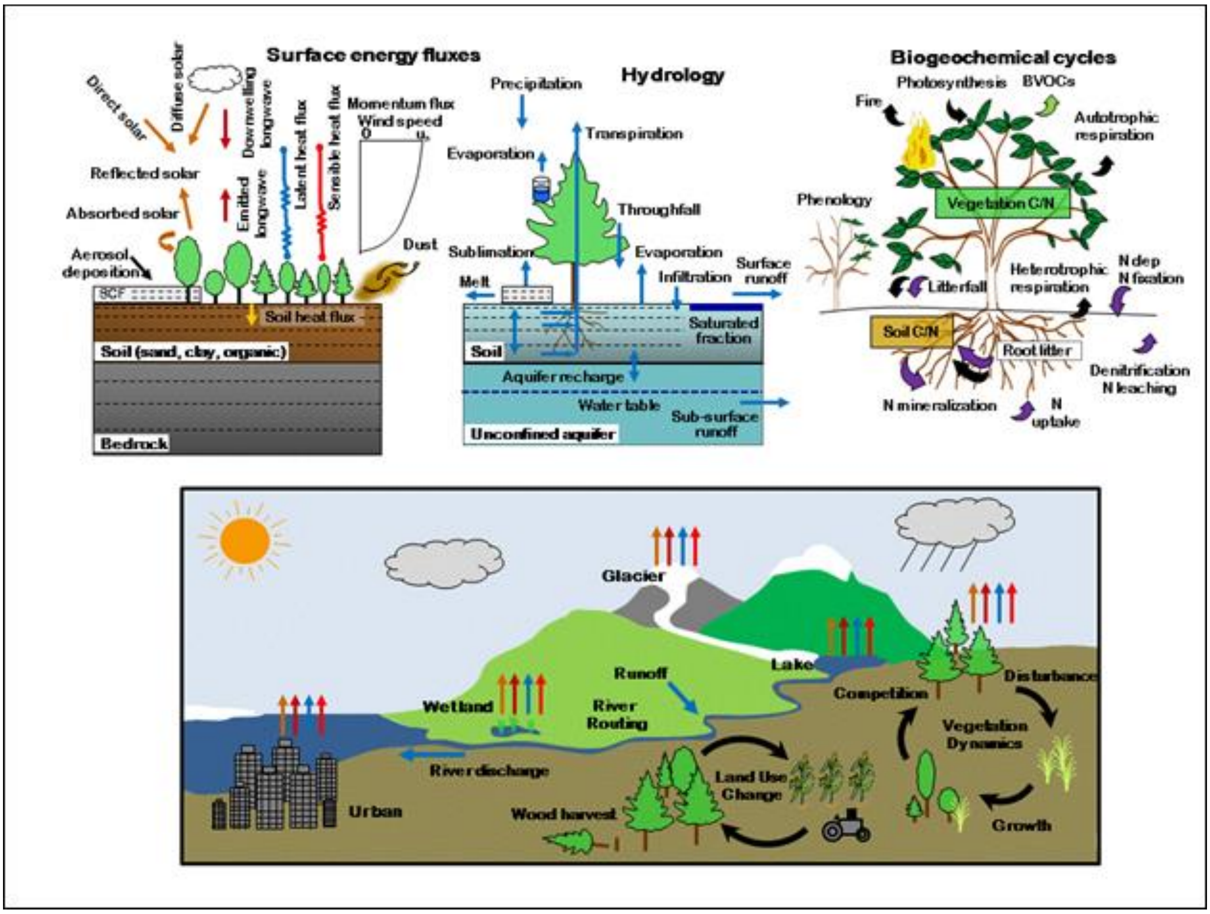

**Figure A.2 - Conceptual design of the Community Land Model version 4.5. Image from www.cesm.ucar.edu/models/clm**

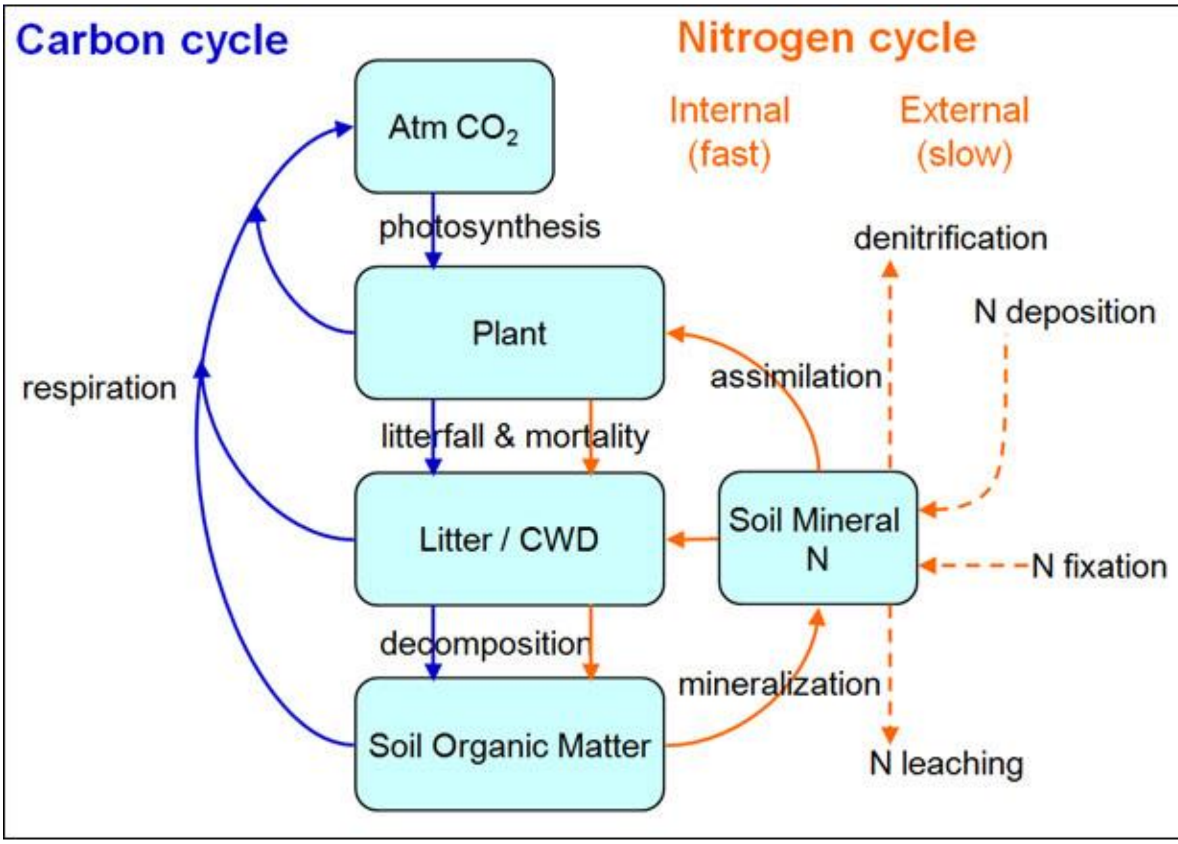

**Figure A.3 - Schematic of the coupled carbon-nitrogen cycles in CLM. Blue arrows represent carbon pathways and orange arrows nitrogen pathways. Figure from Thornton et al. (2009).**

# Appendix B

# Supplementary information for Chapter 2

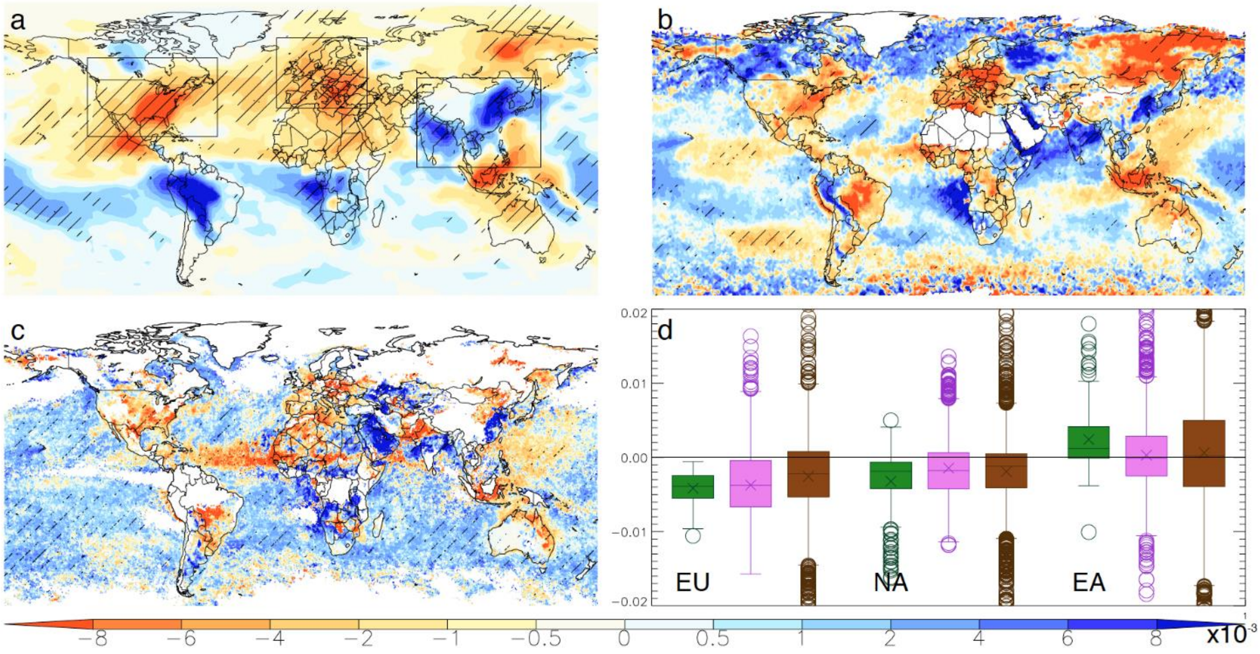

**Figure B.1 - Comparison between modelled and satellite AOD trends ($yr^{-1}$) for the period of overlapping data records 2001-2010. Panels depict linear Jul-Dec half-yearly mean trends for (a) GLOMAP, (b) MODIS, and (c) SeaWiFS. In (d), linear trends in AOD ($yr^{-1}$) between 2001 and 2010 are shown for the three focus regions (land points only): Europe (EU), North America (NA), and East Asia (EA) based on GLOMAP (green), MODIS (violet), and SeaWiFS (brown). The crosses represent the mean trend, the middle bars the median, the boxes the 25th and 75th percentile values and the error bars the minimum and maximum values with circles representing outliers (greater than 1.5 x interquartile range). The three focus regions are depicted in the top left panel. In the maps, white areas in (b) and (c) indicate regions where satellite retrievals were not available and statistically significant ($P<0.05$) trends are highlighted with stippling. In our GLOMAP AOD calculations we did not consider all aerosol size modes and so miss the majority of dust aerosol, which has potential to cause discrepancies between model and observations. To assess whether dust may have a strong influence on the annual AOD trends (Figure 1 in main manuscript), we also computed AOD trends based on Jul-Dec means since at that time dust is generally not dominating the AOD fields specifically in East Asia (Hansen et al., 2013; ref. in main manuscript). Comparing the (GLOMAP) simulated AOD trends with the satellite observed trends generally showed a good agreement specifically in areas where FF aerosol emissions dominate the AOD trends (see also Figure B1). Further, a comparisons of the satellite AOD trends based on annual and half-yearly means also shows good agreement suggesting that dust does not play a dominant role in the observed AOD trends.**

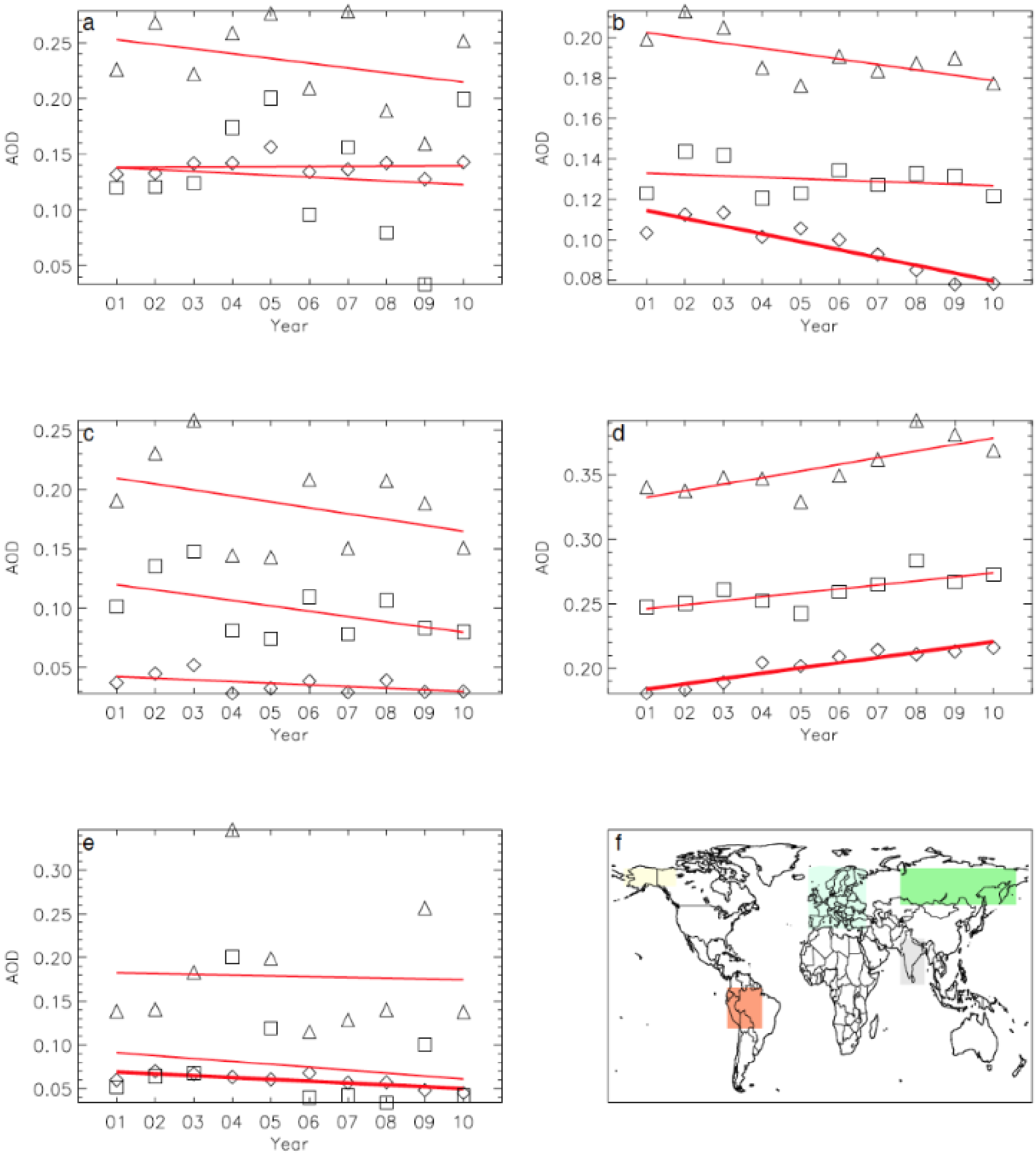

**Figure B.2 - Simulated and observed annual mean AOD time series for five regions where discrepancies between modelled and observed AOD trends at some level were identified (see Figure 1 in main ms): a) Amazon, b) Europe, c) north east Russia, d) India, and e) Alaska. Regions are shown in f). Results are shown for GLOMAP (diamonds), SeaWiFS (squares), and MODIS (triangles). Linear best fit lines are plotted, with statistically significant trends (P<0.05) bolded.**

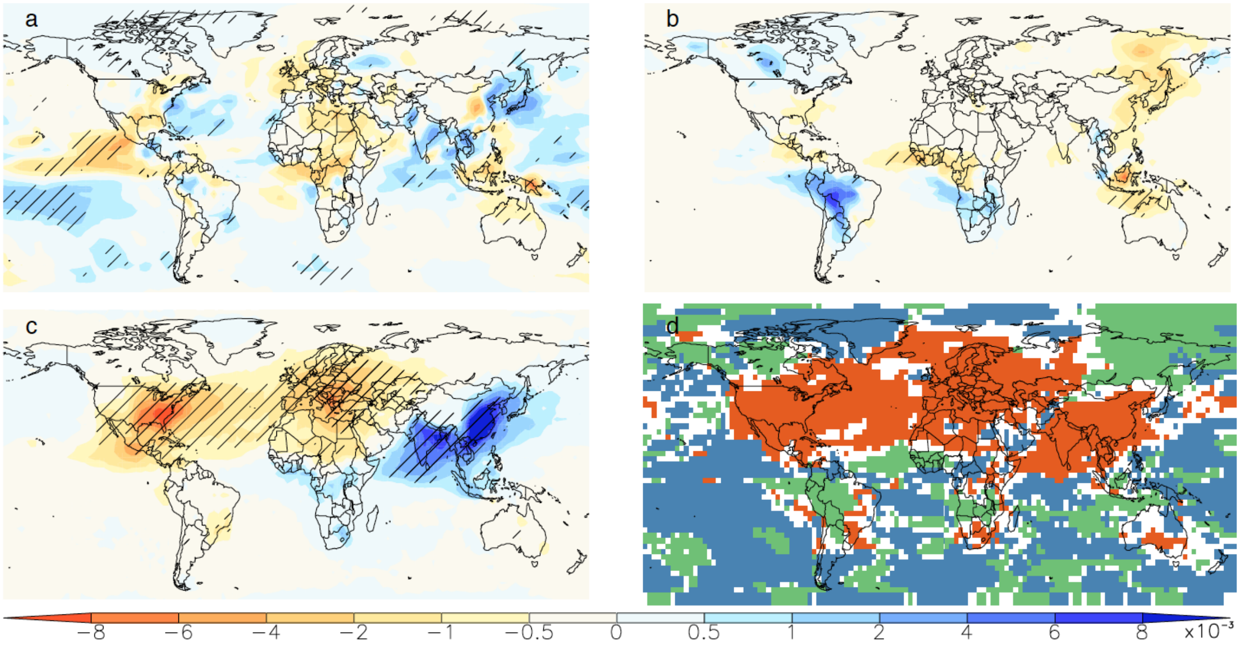

**Figure B.3** - Spatial pattern of linear trends (yr$^{-1}$) in simulated annual AOD due to each factor (a-c) and the dominating driving factor in the trend (d) over 1998-2010. The isolated factors include (a) climate, (b) fire emissions, and (c) fossil fuel emissions. Panel (d) shows the dominating driver with climate (blue), fires (green), and fossil fuels (orange) depicted. White areas depict regions with no factor contributing more than 50% to the total trend (no dominating factor).

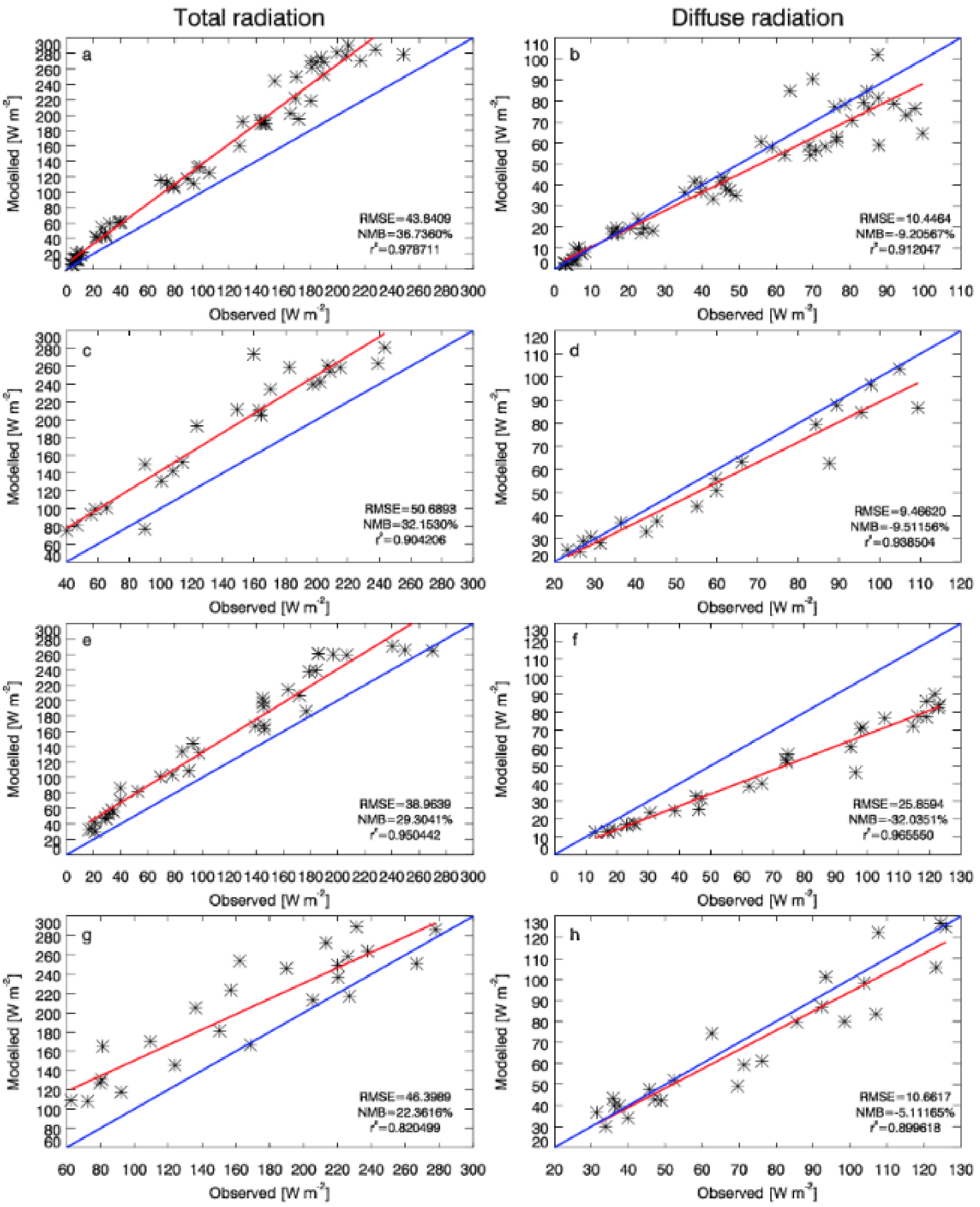

**Figure B.4** - **Scatterplot of monthly mean observed (FluxNet) versus ES modelled (a,c,e,g) total and (b,d,f,h) diffuse radiation at (a,b) Hyytiala, Finland (Hyy) (61.85°N, 24.30°E), (c,d) Bartlett Experimental Forest, New Hampshire, US (Bar) (44.06°N, 71.29°W), (e,f) Loobos, Netherlands (Loo) (52.17° N, 5.74° E), and (g,h) Walker Branch Watershed, Tennessee, US (WBW) (35.96°N, 84.29°W). The normalised mean bias (NMB), $r^2$ and root-mean-square error (RMSE) between model and observations are shown in each panel. Linear best fit lines are also plotted. This data model comparison shows generally a good agreement, albeit with high model bias in total radiation (22%<NMB<37%). Simulated diffuse radiation matched the observations also well (-32%<NMB<-5%), with the $r^2$ value between modelled and observed radiation (total and diffuse) being high at all sites ($r^2$>0.82).**

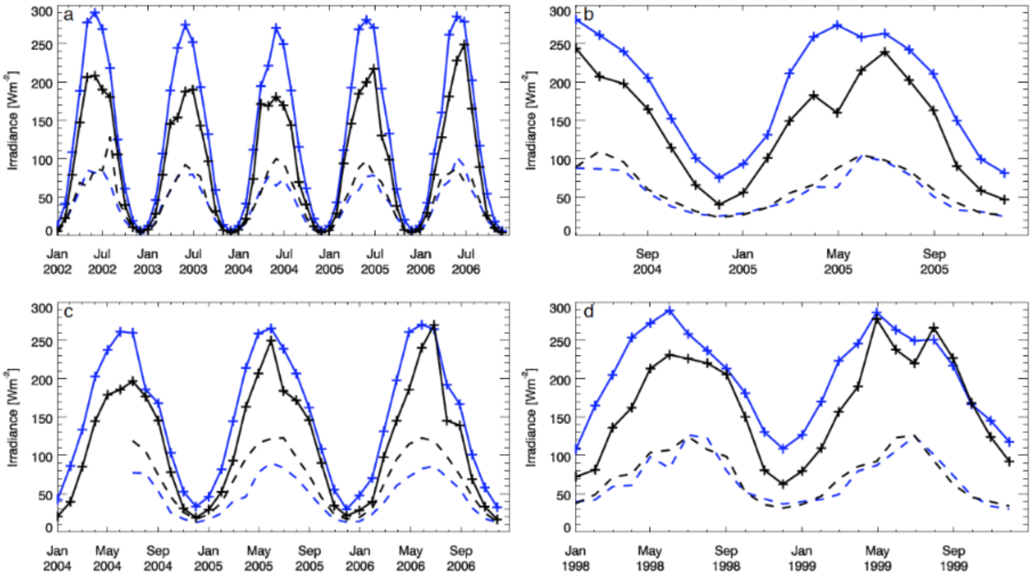

**Figure B.5 - Observed (black) and ES modelled (blue) monthly mean total (solid) and diffuse (dashed) radiation at a) Hyy, b) Bar, c) Loo, and d) WBW. Results show that the model also captures the observed seasonal cycle of surface radiation. The aforementioned high model bias in total radiation (Figure B4) is notable at Hyytiala, however the model performs well at the other three sites, especially in matching observed diffuse radiation trajectories.**

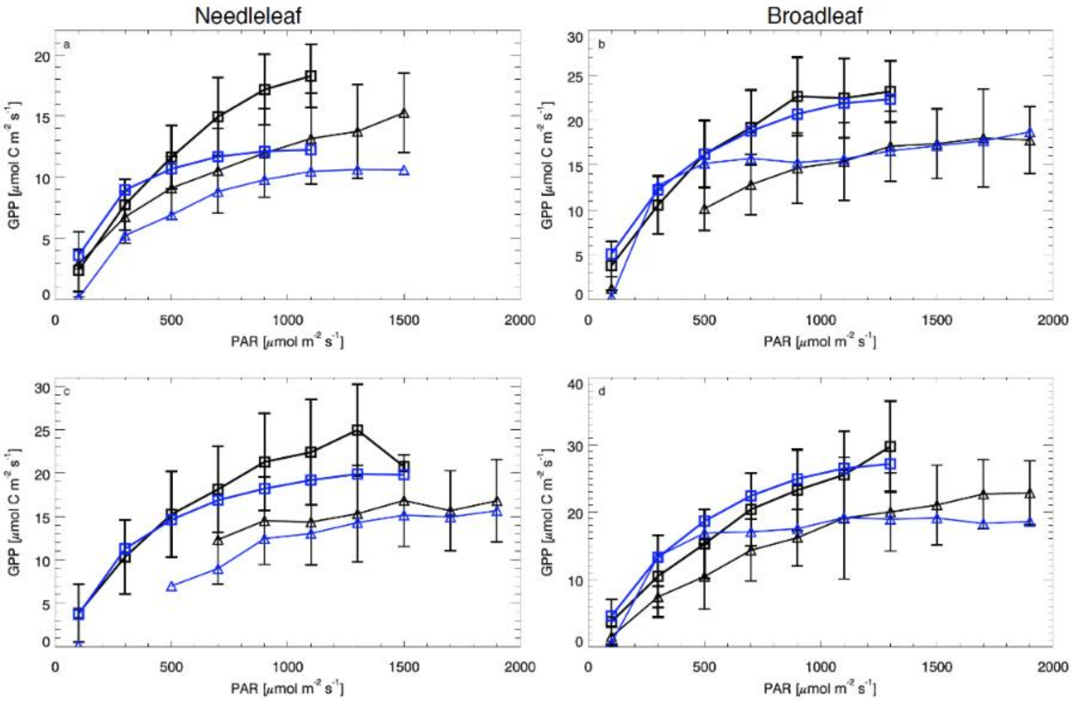

**Figure B.6 - Observed (black) and modelled (blue) GPP response to both direct (triangles) and diffuse (squares) photosynthetic active radiation (PAR) averaged for bins of 200 µmol $m^{-2}s^{-1}$ for the northern summer (Jun-Aug) at (a) Hyy (2002-2006), (b) Bar (2004-2006), (c) Loo (2004-2006), and (d) WBW (1998-1999). Error bars show 1 standard deviation of the range of GPP responses. Data points are split into "diffuse" and "direct" conditions using thresholds of diffuse fractions >80% and <25% to discriminate between the two cases. The two European FluxNet sites, Hyy (panel a) and Loo (c), are needleleaf forests, whereas two North American FluxNet sites, Bar (b) and WBW (d), are broadleaf forests. Results show that observed and simulated GPP increase with PAR, saturating at high light levels. Further, GPP is consistently higher under diffuse light conditions as expected from the theory of radiative transfer in vegetation canopies. It should be noted, that the sensitivity simulations were performed without tuning important model parameters (eg Vcmax, tree height) to site level conditions and, hence, some discrepancies between model and observations are anticipated. Overall, however, this comparison along with the previous validation studies mentioned in the main ms demonstrate that the model can realistically simulate photosynthetic responses in a range of forest types and light regimes.**

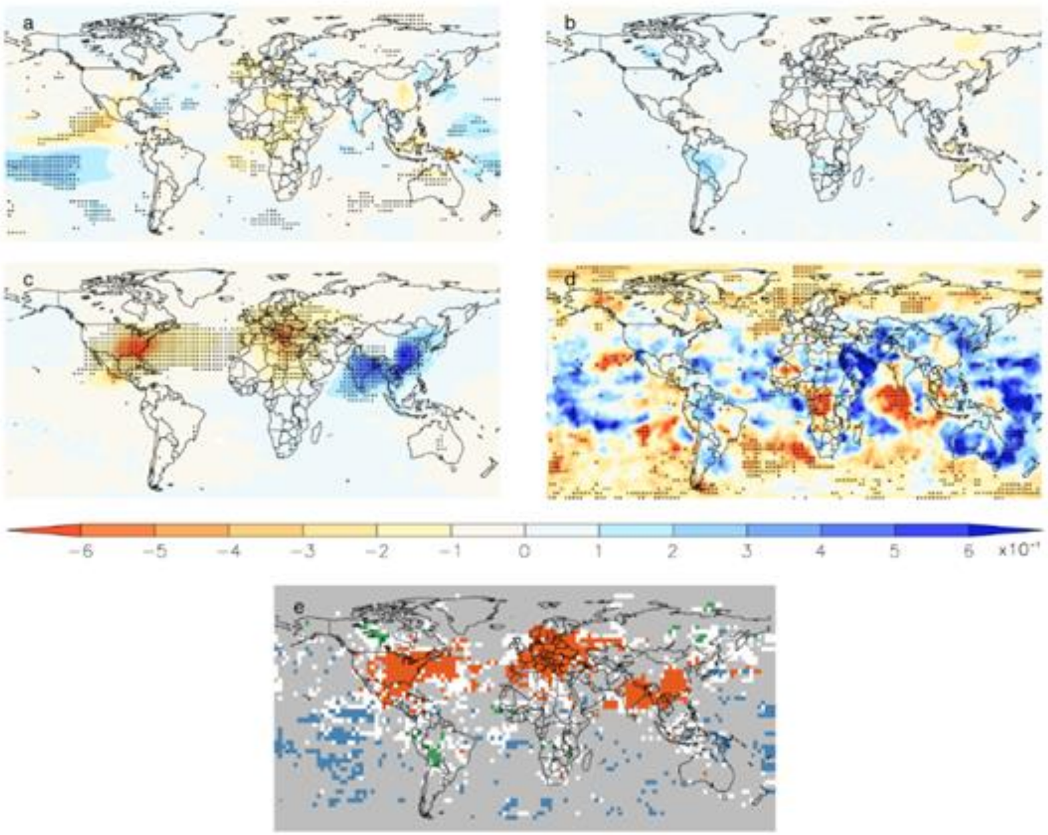

**Figure B.7 - Spatial pattern of linear trends ($Wm^{-2}yr^{-1}$) in simulated annual surface diffuse radiation due to each factor (a-d) and the dominating driving factor in the trend (e) over 1998-2010. The isolated factors include (a) climate, (b) fire emissions, (c) fossil fuel emissions, and (d) clouds. Panel (e) shows the dominating driver with climate (blue), fires (green), fossil fuels (orange), and clouds (grey) depicted. White areas depict regions with no factor contributing more than 50% to the total trend (no dominating factor).**

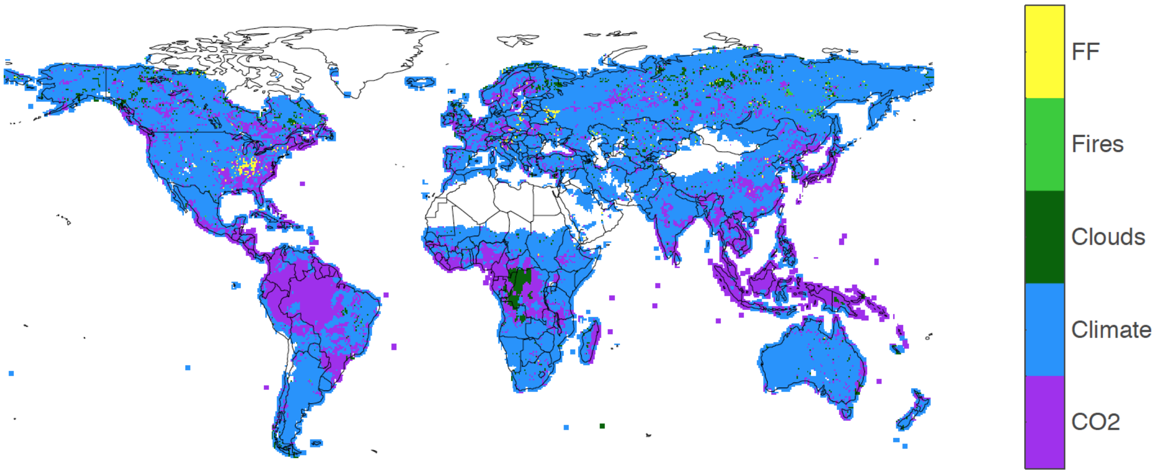

Figure B.8 - Dominant driving factor in simulated (JULES) NPP trend over 1998-2010.

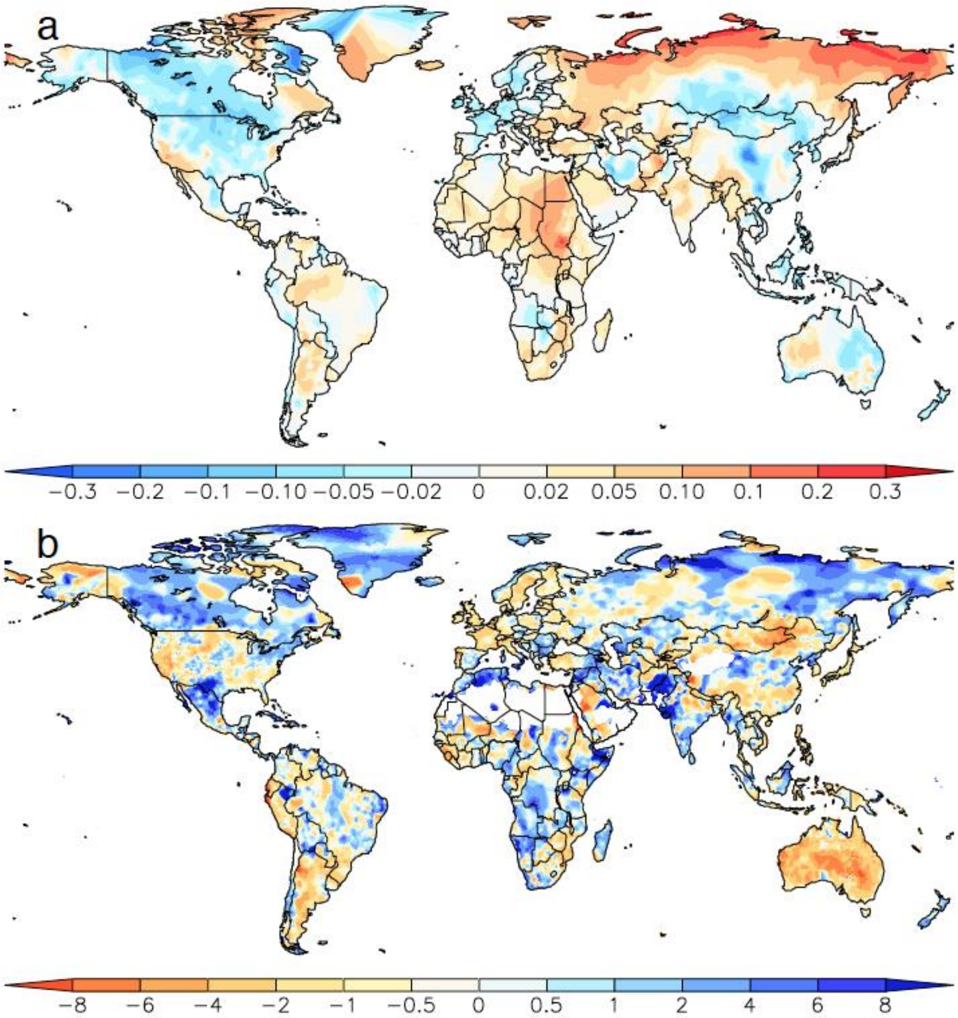

**Figure B.9** - **Spatial distribution of trends in selected land climate drivers for the period 1998-2010, including (a) temperature (°Cyr$^{-1}$) and (b) precipitation (%yr$^{-1}$).**

## Appendix C

# Supplementary information for Chapter 3

**Table C.1 - Regional change in nitrogen deposition (Ndep) (TgN/yr) 1990-1996 to 2010-2016. Percentage change for Ndep shown in parenthesis. Changes in NPP (TgC/yr) and NBP (TgC/yr) due to the direct nitrogen deposition effect (Ndep) and the carbon-nitrogen synergistic effect (CN-syn) are also shown. Regions are defined as follows: East Asia (75°E to 125°E and 10°N to 45°N), East Europe (15°E to 40°E and 45°N to 70°N), North America (120°W to 75°W and 30°N to 45°N), West Europe (10°W to 15°E and 40°N to 60°N), and Central Africa (10°W to 30°E and 5°S to 10°N).**

| Region | ΔNdep (TgN/yr) | ΔNPP (TgC/yr) | | ΔNBP (TgC/yr) | |
|---|---|---|---|---|---|
| | | Ndep | CN-syn | Ndep | CN-syn |
| **Global** | 1.78 (2.6) | 30.9 | 13.3 | 33.0 | 3.0 |
| **East Asia** | 3.74 (26.6) | 96.9 | 8.7 | 49.0 | 1.0 |
| **East Europe** | -0.47 (-11.6) | -16.9 | 0.0 | -6.6 | 0.5 |
| **North America** | -0.89 (-16.2) | -19.7 | -3.0 | -10.9 | -2.7 |
| **West Europe** | 0.22 (7.0) | 9.2 | -0.3 | 3.5 | -0.6 |
| **Central Africa** | -0.52 (-11.2) | -21.8 | -5.6 | -5.9 | -4.4 |

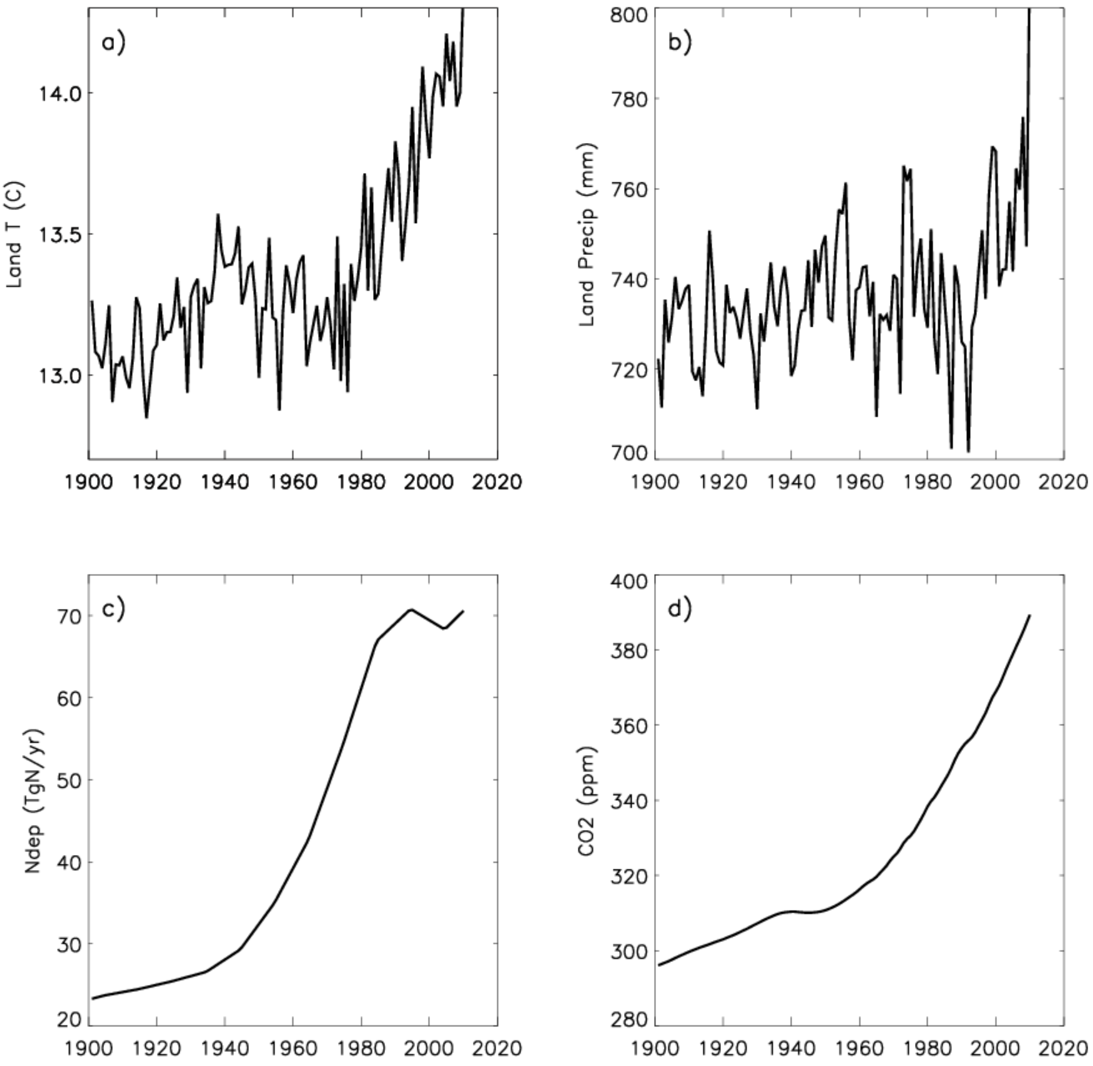

**Figure C.1 - Global mean changes in model drivers from 1901-2016 for a) land surface temperature (C), b) total precipitation over land (mm/yr), c) total atmospheric nitrogen deposition over land (TgN/yr), and d) atmospheric $CO_2$ concentrations (ppm).**

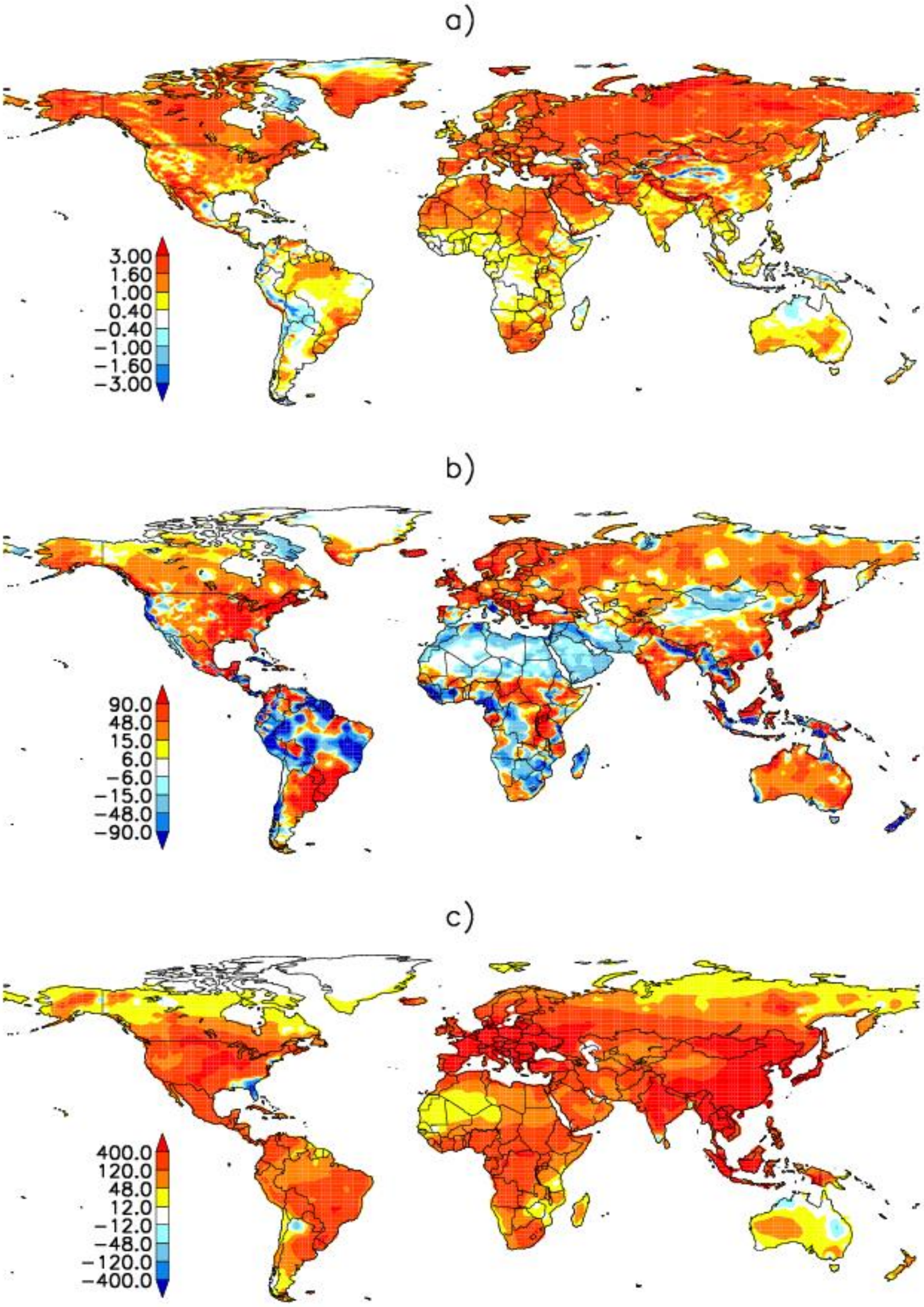

**Figure C.2 - Spatial trends in model drivers over the period (1901-1910) to (2007-2016) for a) land surface temperature (C), b) precipitation (mm/yr), and c) atmospheric nitrogen deposition (mgN/m$^2$/yr).**

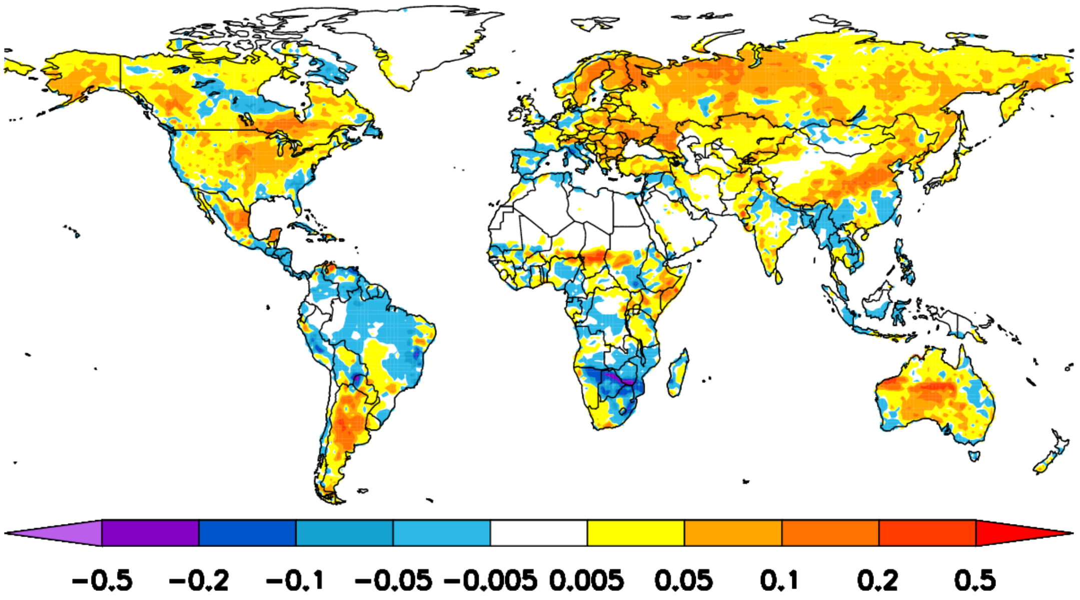

**Figure C.3 - Change in Btran between (1901-1910) and (2007-2016). Btran represents soil water availability in CLM and is a scaling factor (range 0 – 1) on stomatal conductance related to plant-available soil water.**

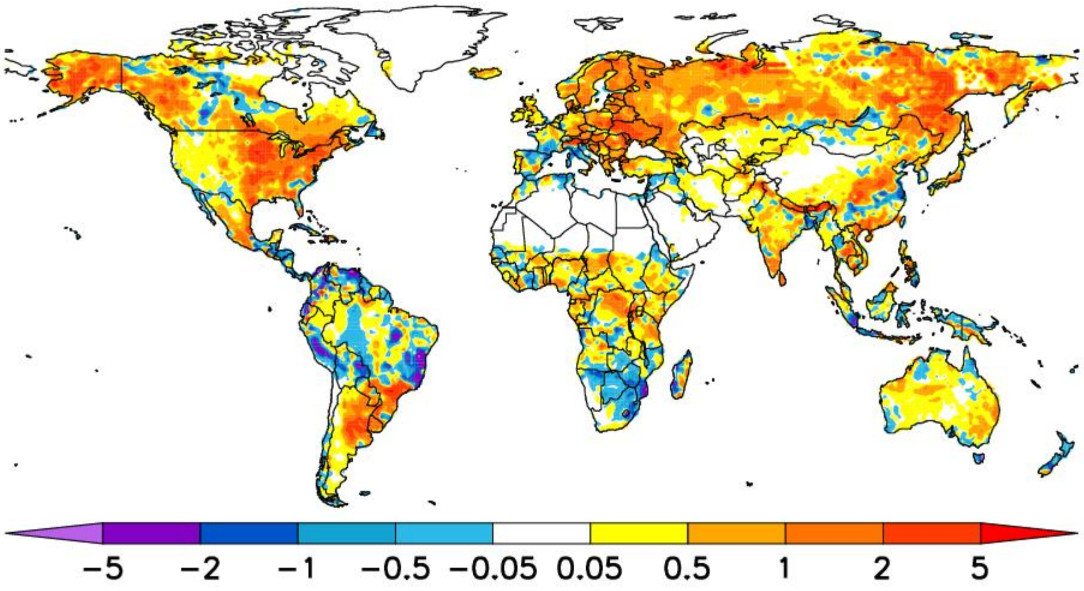

**Figure C.4 - Change in net nitrogen mineralisation (gN/m²/yr) between (1901-1910) and (2007-2016) due to climate forcing alone.**

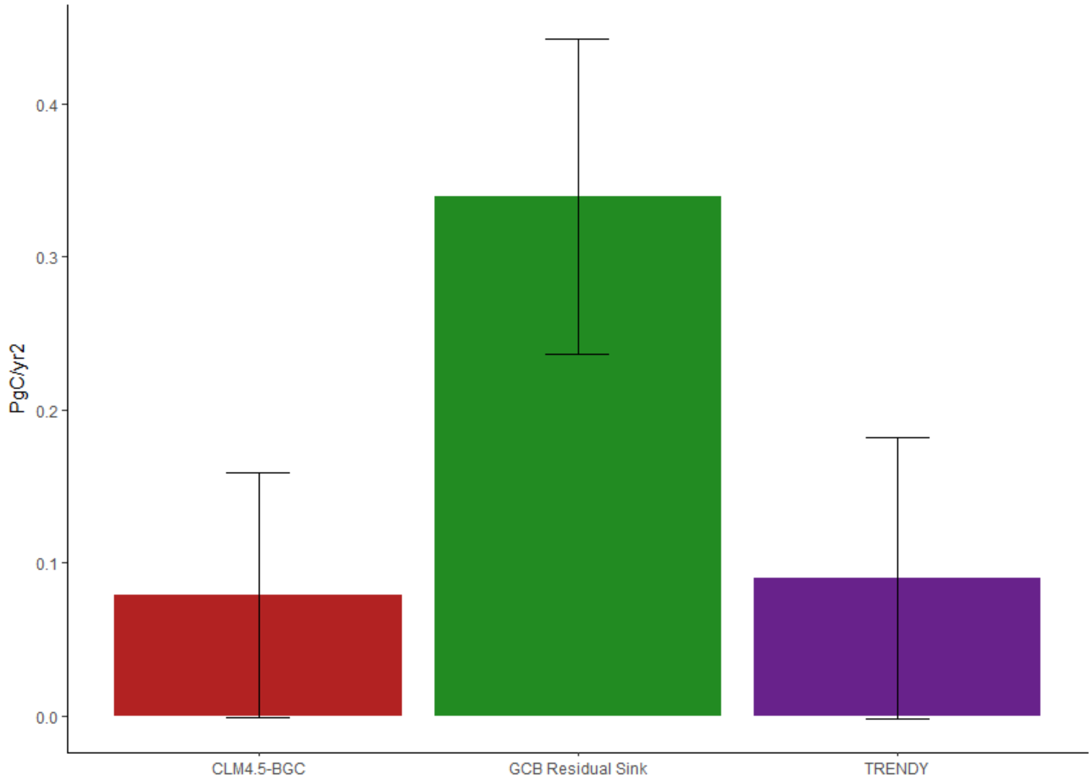

**Figure C.5 - Change in trend in land carbon uptake (PgC/yr2) between 1990-2002 and 2002-2014. Changes in trend are shown for (this study) CLM4.5-BGC, the Global Carbon Budget residual sink (green), and TRENDY multi model mean (purple). The error bars for CLM4.5-BGC and GCB Residual Sink are calculated as the square root of the sums of squares of standard errors of trends for the two periods. The TRENDY error is calculated as the standard deviation of the change in trend across all models.**

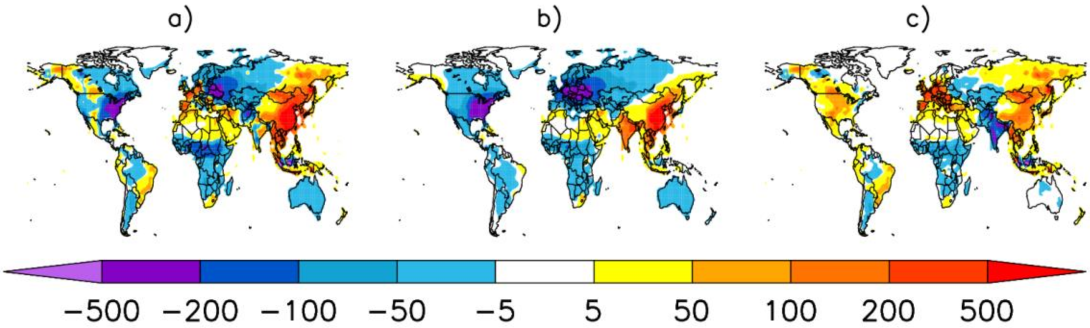

**Figure C.6 - Spatial maps of the change in nitrogen deposition (mgN/m$^2$/yr) between 1990-1996 and 2010-2016 for a) total N deposition, b) NOy deposition, and c) NHx deposition. Since the early 1990s, global nitrogen deposition remained approximately constant (~80 TgN/yr), but there were large regional changes. Comparing the end (2010-2016) to the start (1990-1996) of this period, East Asia [75°E to 125°E and 10°N to 45°N] experienced a 27% increase in annual nitrogen deposition, mostly driven by fossil fuel (NOx) burning, but with a significant contribution from agricultural (NHx) activities (a-c). Reductions in fossil fuel burning in Europe [10°W to 25°E and 40°N to 60°N] and North America [120°W to 75°W and 30°N to 45°N] caused declines in deposition rates (b), however increasing agricultural intensity has countered the fossil fuel trend (c). Overall, the relative changes in nitrogen deposition in Europe and North America are smaller than East Asia, a 3% increase and 16% decrease, respectively.**

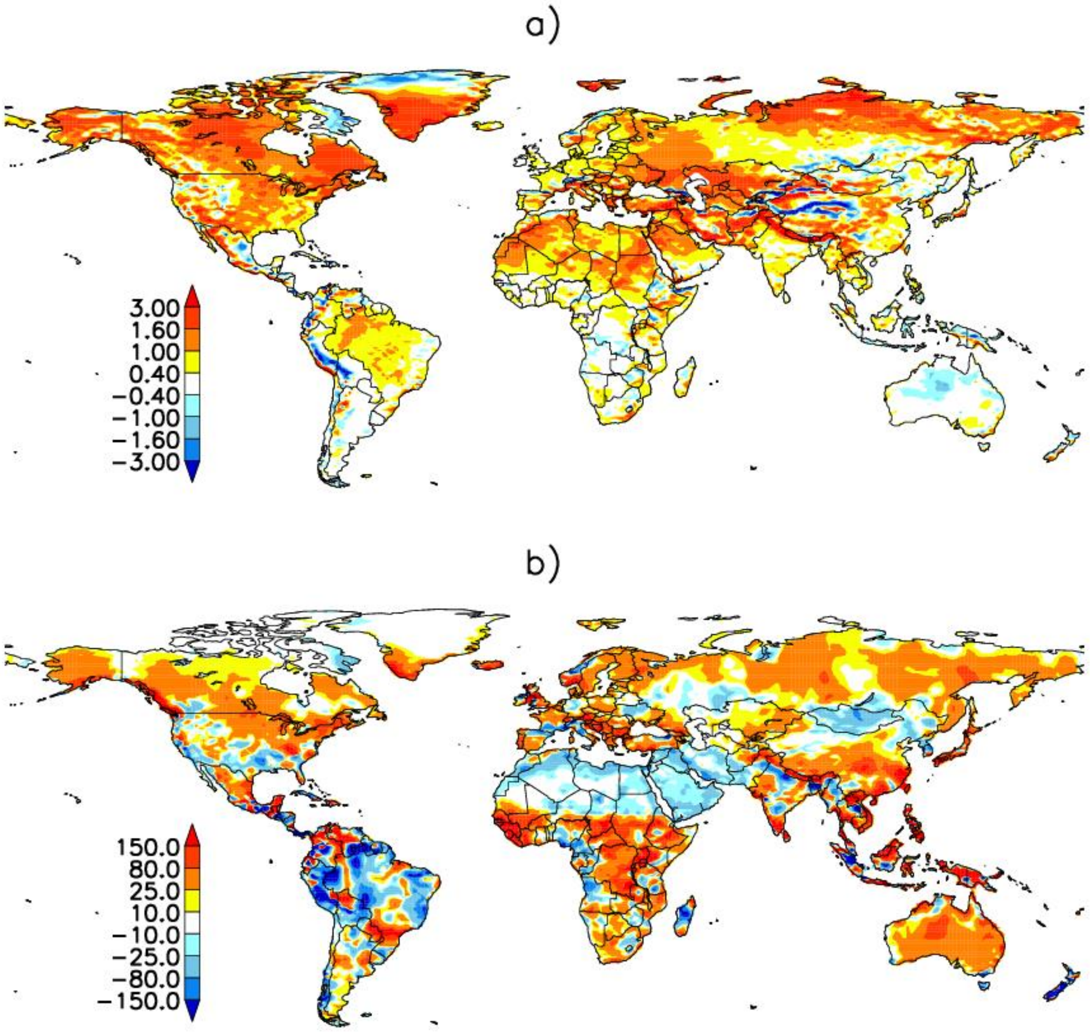

**Figure C.7 - Spatial trends in model drivers over the period (1990-1996) – (2010-2016) for a) land surface temperature (C), b) precipitation (mm/yr).**

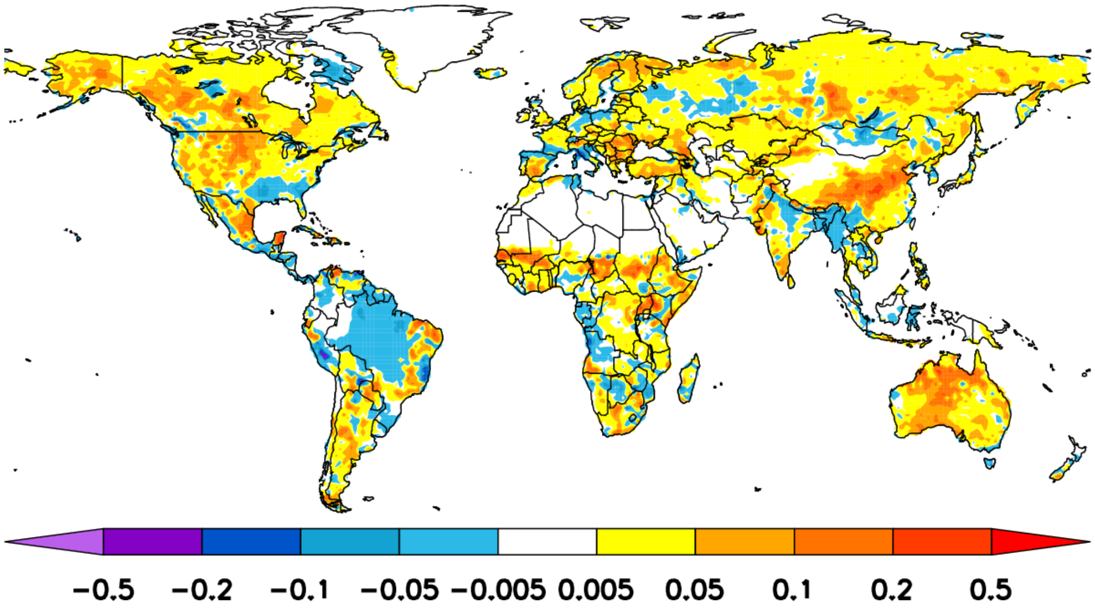

**Figure C.8 - Change in Btran between (1990-1996) and (2010-2016). Btran represents soil water availability in CLM and is a scaling factor (range 0 – 1) on stomatal conductance related to plant-available soil water.**

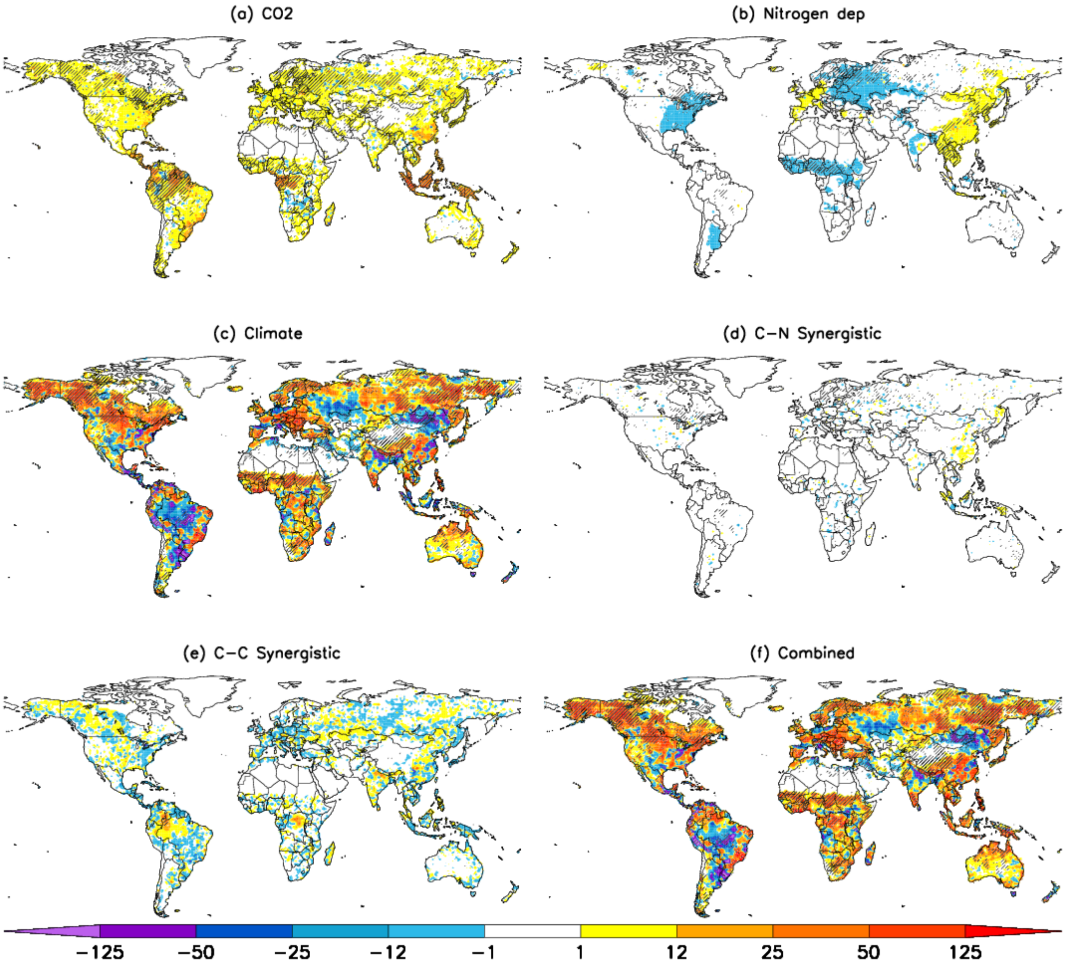

**Figure C.9 - Spatial patterns of heterotrophic respiration change (gC/m$^2$/yr) due to a) CO$_2$ fertilization, b) nitrogen deposition, c) climate, d) CN-synergy, e) CC-synergy, and f) combined effect. The patterns are based on a set of factorial simulations (see Methods). Respiration changes shown here are calculated as the difference between 2010-2016 and 1990-1996 mean values. Significant ($p<0.05$; Mann-Whitney U test) changes highlighted with hatching.**

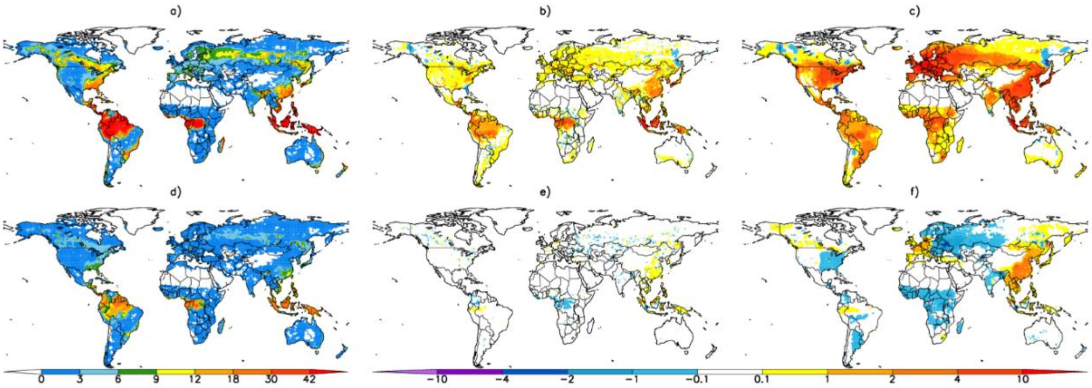

**Figure C.10 - Spatial distribution of Γ (gC/ppm) for the extended (top row) and recent (bottom row) periods calculated from the difference in total ecosystem carbon between the start and end of the study period (see Methods in main ms) for simulations with varying atmospheric $CO_2$, constant climate and constant nitrogen deposition, (a,d). Panels b,e depict the influence of carbon-nitrogen synergy on Γ, and panels c,f depict the combined influence of nitrogen deposition and carbon-nitrogen synergy on Γ.**

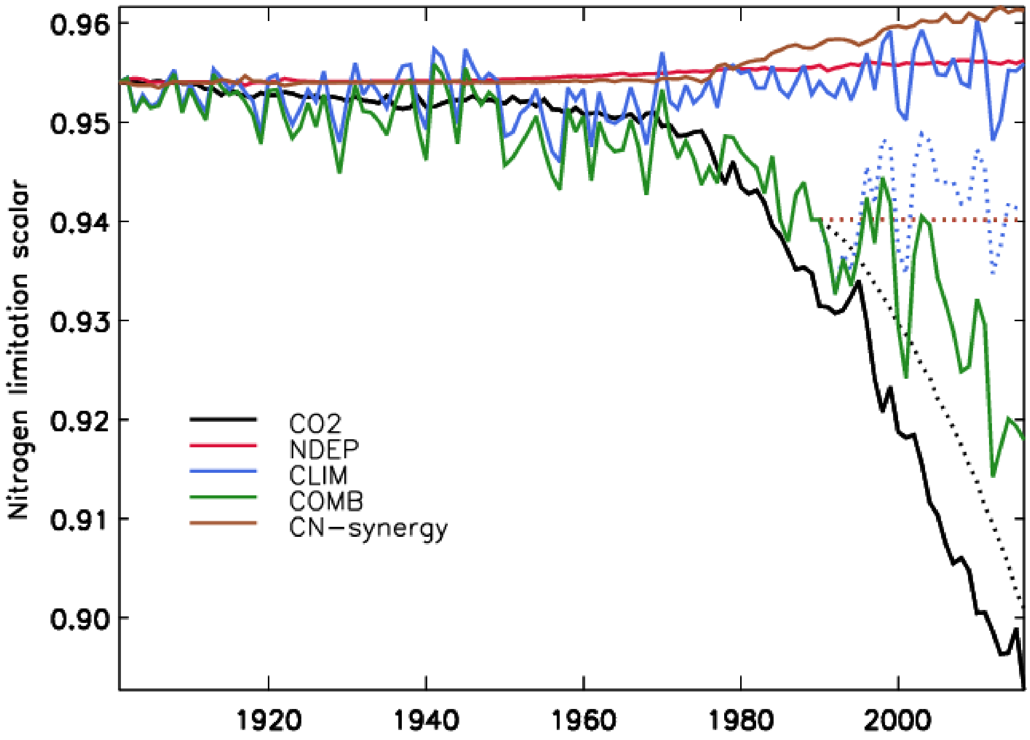

**Figure C.11 - Changes in Amazon N limitation for 1901-2016 (solid) and 1990-2016 (dotted). Changes are relative to a control simulation with no variables changing. Contributions from $CO_2$ (black), nitrogen deposition (red), climate (blue), combined (green), and CN-synergy (yellow) are shown.**

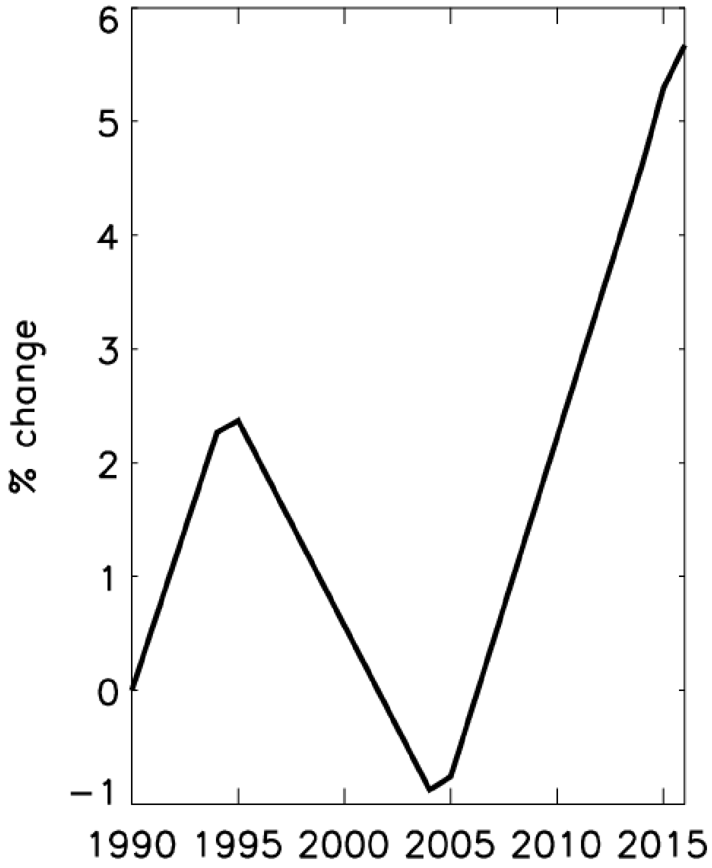

**Figure C.12 - Changes in global nitrogen deposition expressed as a percentage change from the start of the simulation (1990).**

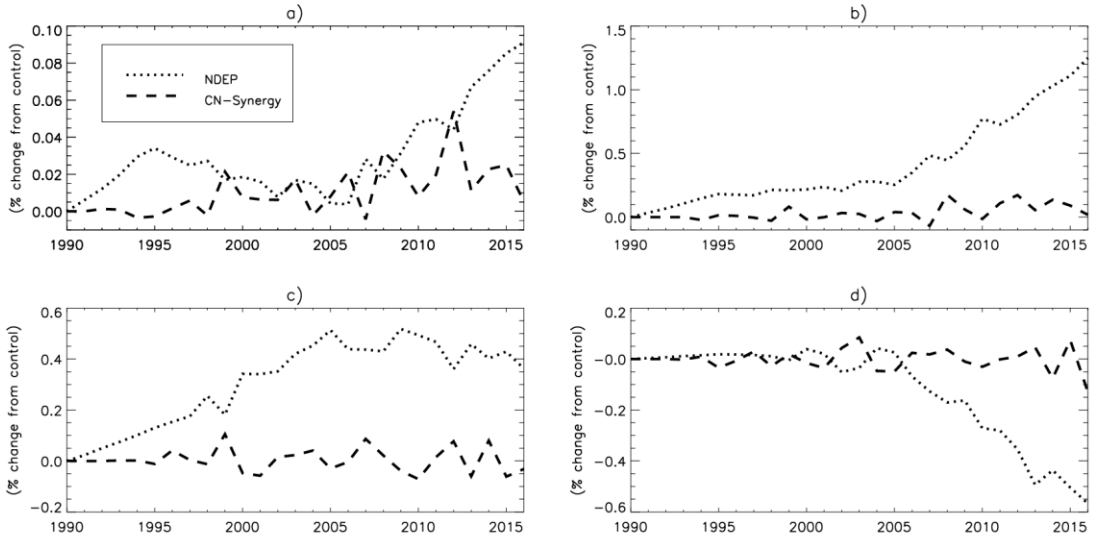

**Figure C.13 - Change (percentage from control run) in nitrogen limitation scalar from 1990 to 2016 using the recent simulations. The direct influence of nitrogen deposition (dotted) and carbon-nitrogen synergy (dashed) are shown. Four regions are shown, namely a) Global, b) East Asia (75°E to 125°E and 10°N to 45°N), c) Western Europe (10°W to 15°E and 40°N to 60°N), and d) North America (120°W to 75°W and 30°N to 45°N).**

# Appendix D

# Supplementary information for Chapter 4

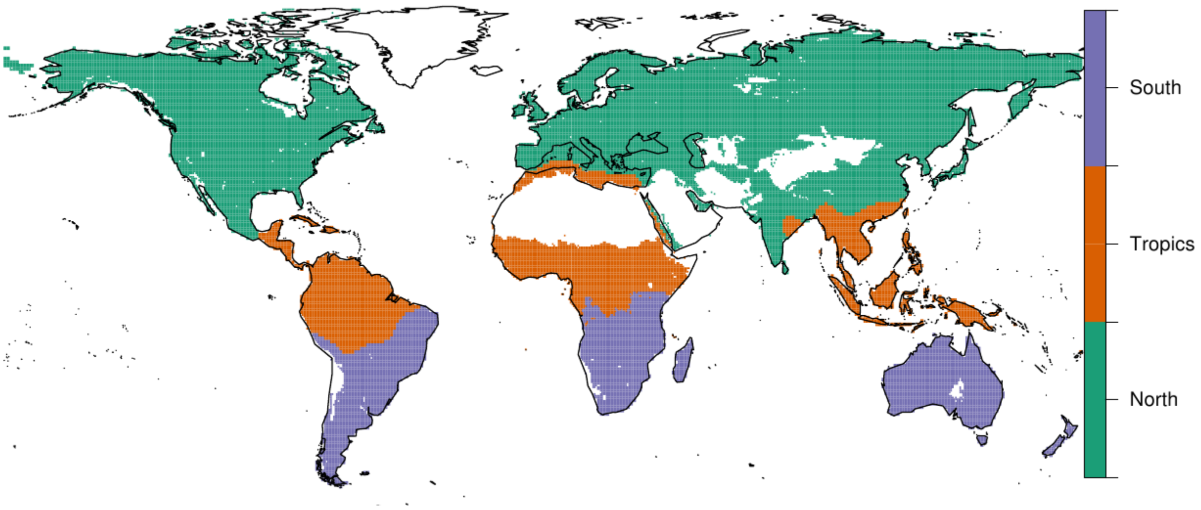

**Figure D.1 - Regions used in the study. Regions are broadly defined from the TRANSCOM-3 experiment. North American boreal, North American temperate, Europe, Eurasian Temperate, and Eurasian boreal are grouped as *North.* South American tropical, North Africa, and tropical Asia are grouped as *Tropics.* We further used the MODIS land over product (MCD12C1) to isolate African tropical forest and included this in the *Tropics* region. Finally, South American temperate, Southern Africa, and Australia are grouped as *South.***

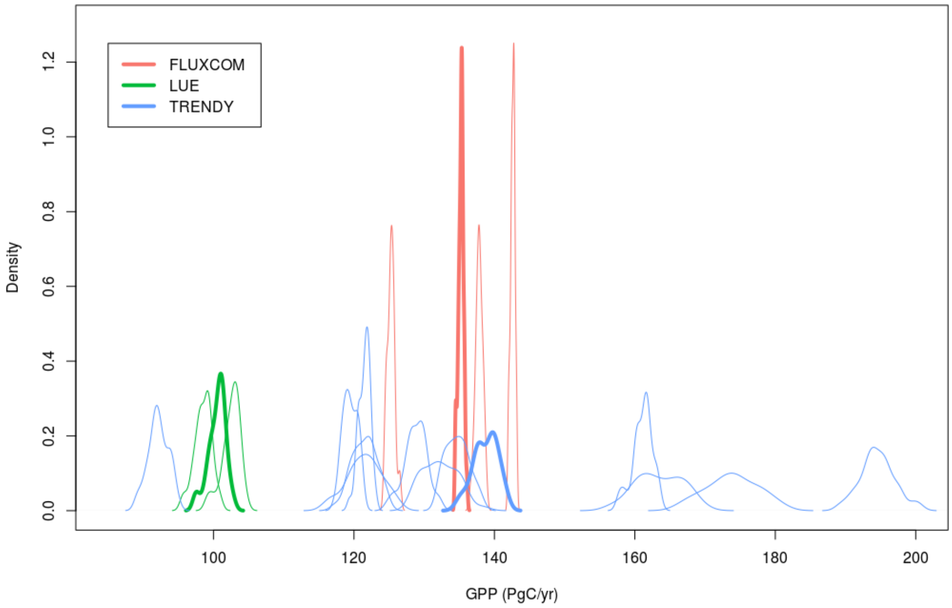

**Figure D.2 - Global annual mean GPP distribution (PgC/yr) over 1982-2016 for each ensemble member of the three products. Ensemble means are shown in bold.**

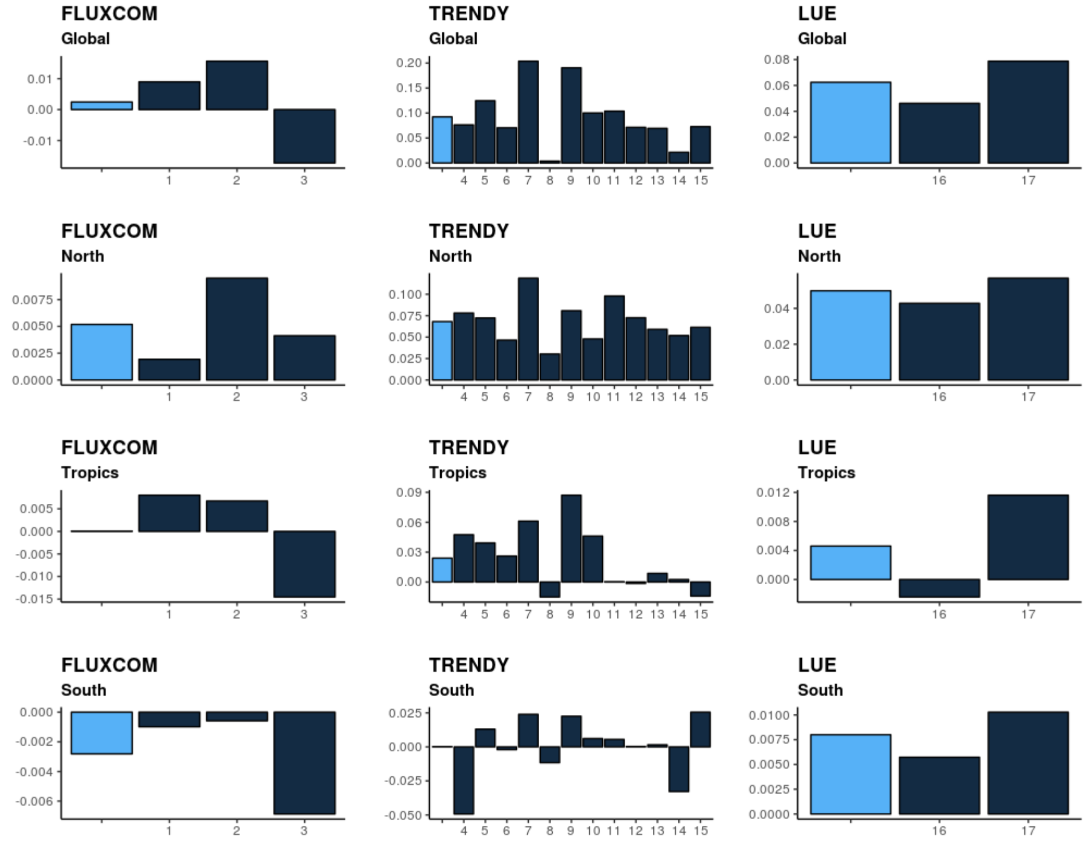

**Figure D.3 - Trends in annual GPP (PgC/yr$^2$) over 1982-2016 in four regions for each ensemble member from FLUXCOM for three upscaling approaches (Artificial Neural Network – ANN, Random Forest – RF, and Multivariate Adaptive Regression – MARS); (1) ANN, (2) RF, (3) MARS, from TRENDY models; (4) CABLE, (5) CLASS-CTEM, (6) CLM4.5-BGC, (7) DLEM, (8) ISAM, (9) JSBACH, (10) JULES, (11) LPJ-GUESS, (12) ORCHIDEE, (13) ORCHIDEE-MICT, (14) VEGAS, and (15) VISIT, and from LUE model for two parameterisations; (16) Zhao & Running, 2010, and (17) Robinson *et al.*, 2018 (references in main manuscript). Ensemble mean trend for each region and product is shown in light blue.**

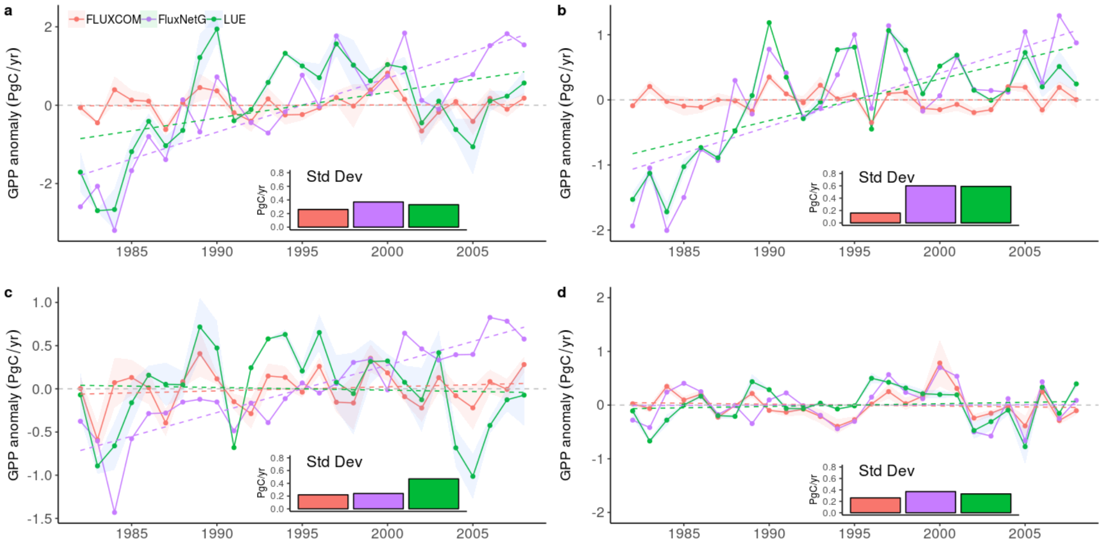

**Figure D.4 – Global and regional variations in annual GPP based on three GPP products. Annual gross primary production (GPP) anomalies (PgC/yr) over the period 1982-2008 estimated by upscaled flux tower observations, FLUXCOM (red), and FluxNetG (purple), and a satellite based light use efficiency model (green). Both FLUXCOM and FluxNetG are based on FLUXNET site-level carbon flux observations. However, FLUXCOM is driven with seasonally varying NDVI whereas FluxNetG incorporates interannually varying NDVI in the upscaling procedure. Further, similarly to FluxNetG, LUE is driven with interannualy varying satellite data (see Methods). GPP anomalies are shown for a) global, b) northern, c) tropical, and d) southern regions, as defined in Figure D1. Shading represents 1σ spread among each products ensemble members (see Methods). Linear trends are depicted with a dashed line. Bar charts show the inter-annual variability of each product as the 1σ (PgC/yr) of the detrended timeseries.**

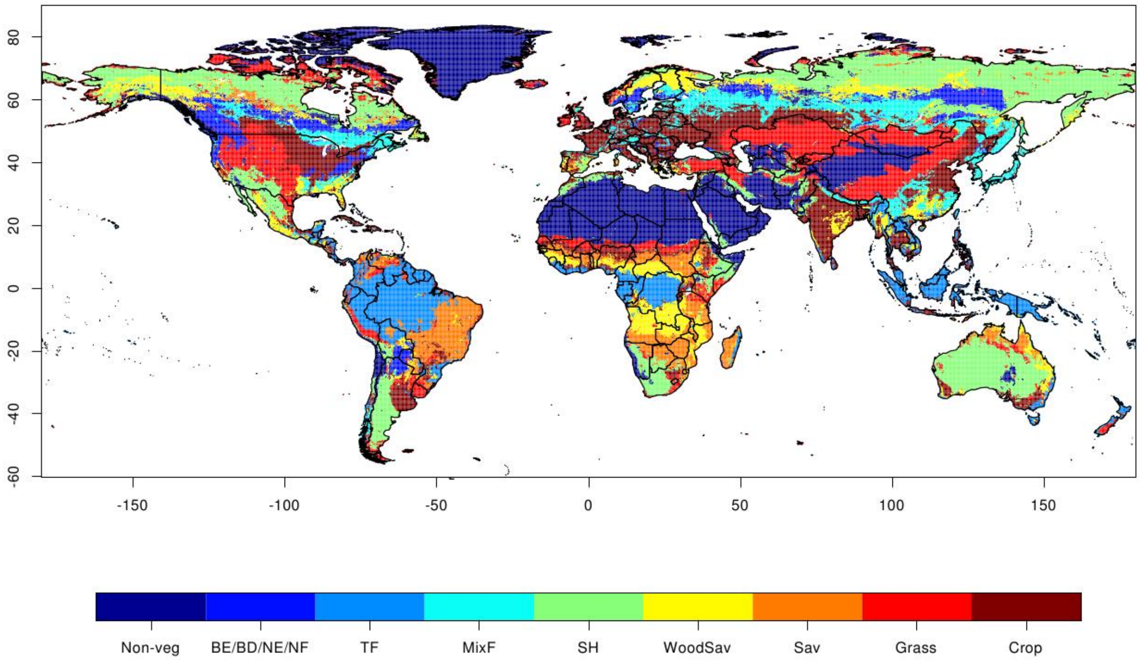

**Figure D.5 – Landcover based on the MODIS product (MCD12C1). Landcover types include Non-vegetated (Non-veg), broadleaf evergreen/broadleaf deciduous/needleleaf evergreen/needleleaf deciduous (BE/BD/NE/ND), tropical forests (TF), mixed forests (MixF), shrubs (SH), woody savanna (WoodSav), savanna (Sav), grassland (Grass), and cropland (Crop).**

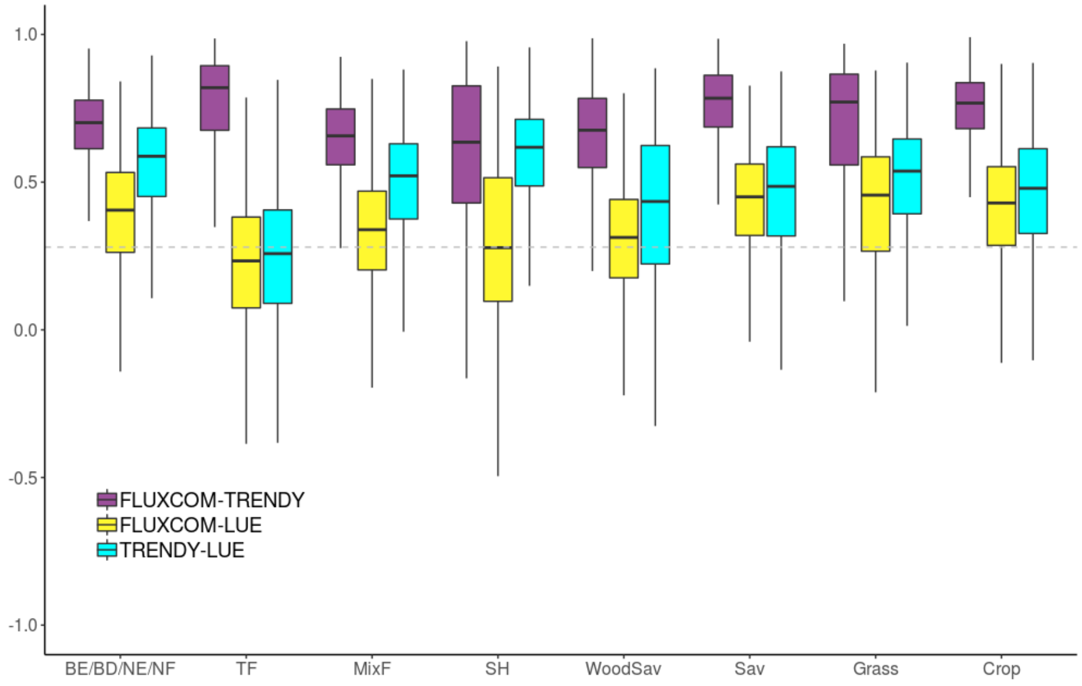

**Figure D.6 - Boxplots of grid scale correlations between FLUXCOM-TRENDY (purple), FLUXCOM-LUE (yellow), and TRENDY-LUE (cyan) for each biome type defined in Figure D5. Grey dashed line (r=0.28) represents significant correlation (P=0.05).**

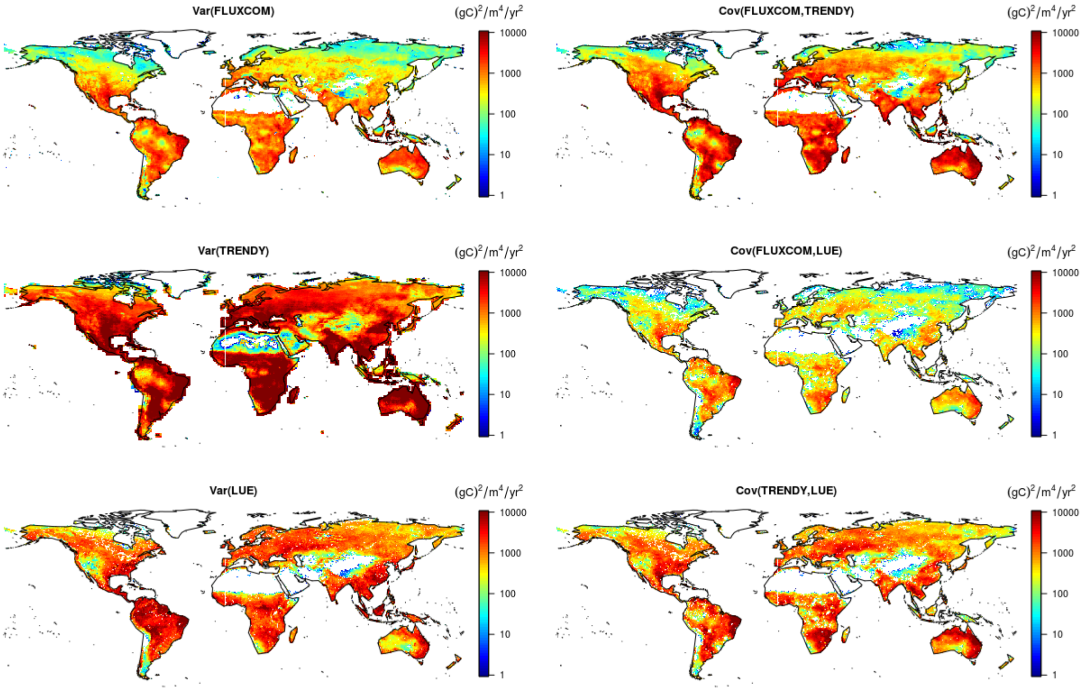

**Figure D.7 - Variance (left column) and covariance (right column) of detrended annual mean GPP for each dataset (FLUXCOM, TRENDY, LUE) and combination of datasets (FLUXCOM-TRENDY, FLUXCOM-LUE, TRENDY-LUE) over the period 1982-2016.**

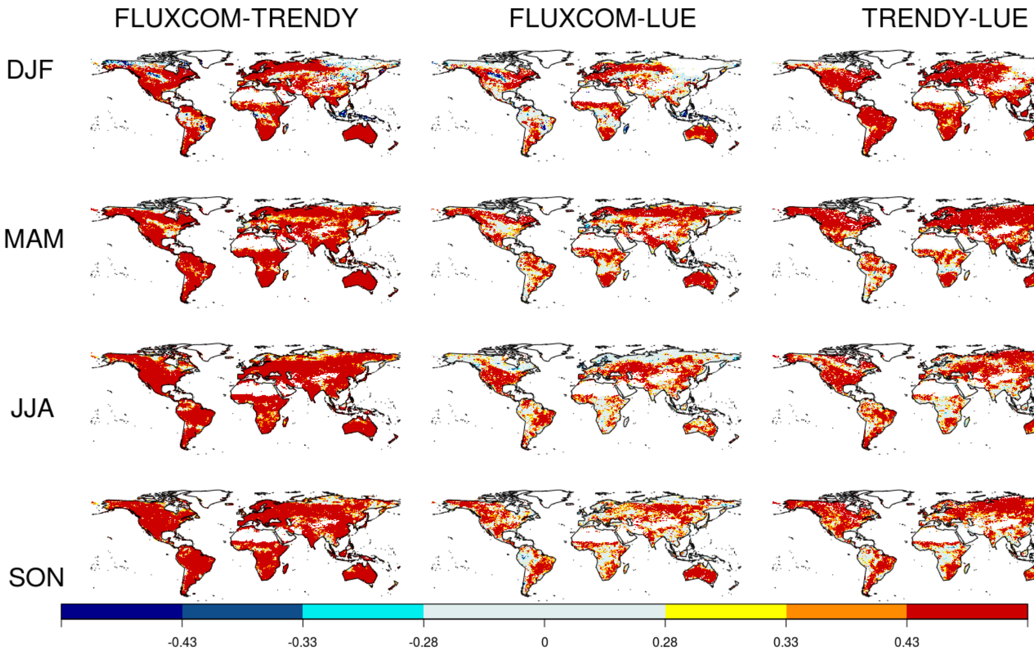

**Figure D.8 - Correlation between detrended seasonal GPP (1982-2016) for each product. Seasons are defined as December-January-February (DJF), March-April-May (MAM), June-July-August (JJA), and September-October-November (SON). Non-significant correlations ($r<0.28$, $P>0.05$) are in grey. Missing data is represented with white. ($r=0.28$, 0.33, 0.43 corresponds to $P=0.1$, $P=0.05$, $P=0.01$).**

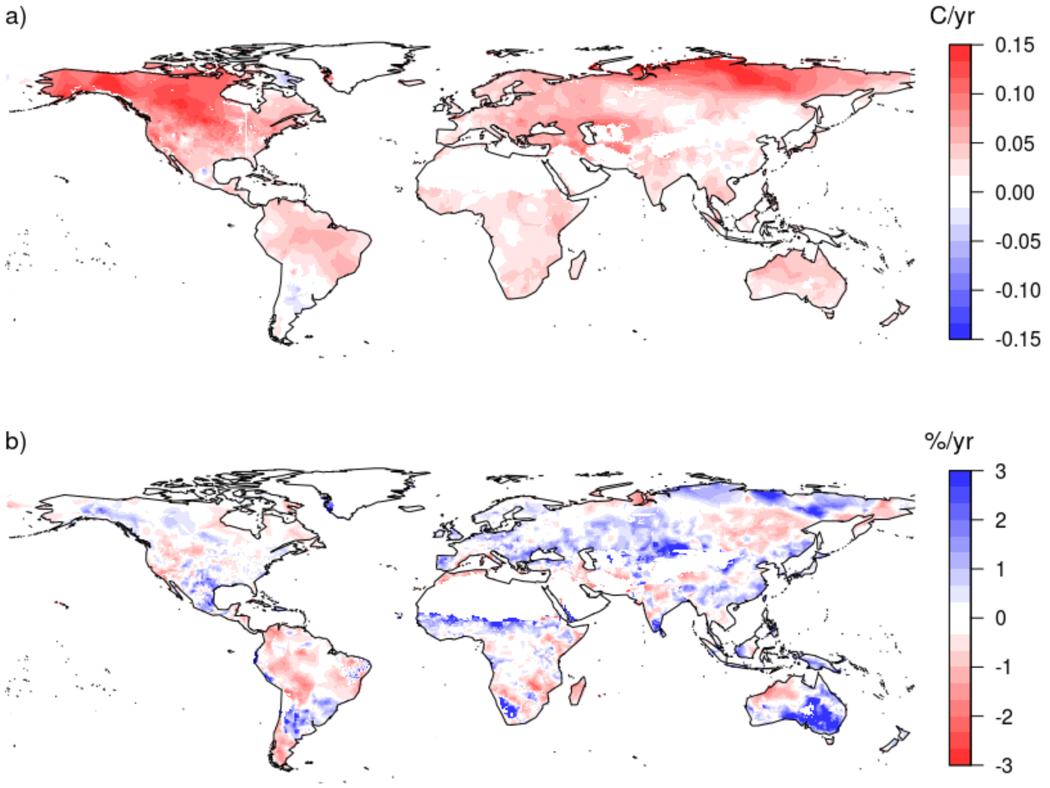

**Figure D.9 - Linear trends in mean annual temperature (°C/yr) and mean annual precipitation (%/yr) from CRUNCEPv8 reanalysis over the period 1982-2016.**

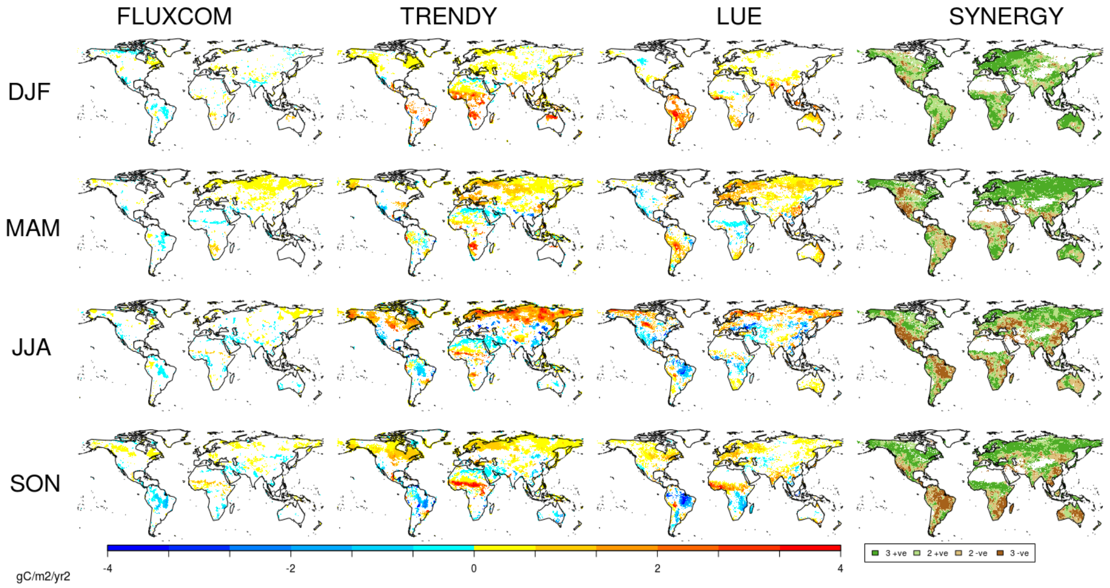

**Figure D.10 - Trends in seasonal GPP (gC/m$^2$/yr$^2$) for each product over the period 1982-2016. The maps depict significant ($P<0.05$) trends and seasons are defined as in Figure D8. Right column shows “synergy” between trends. Dark areas are where all agree on the direction of trend and light areas indicate disagreement (two products agree, and one differs).**

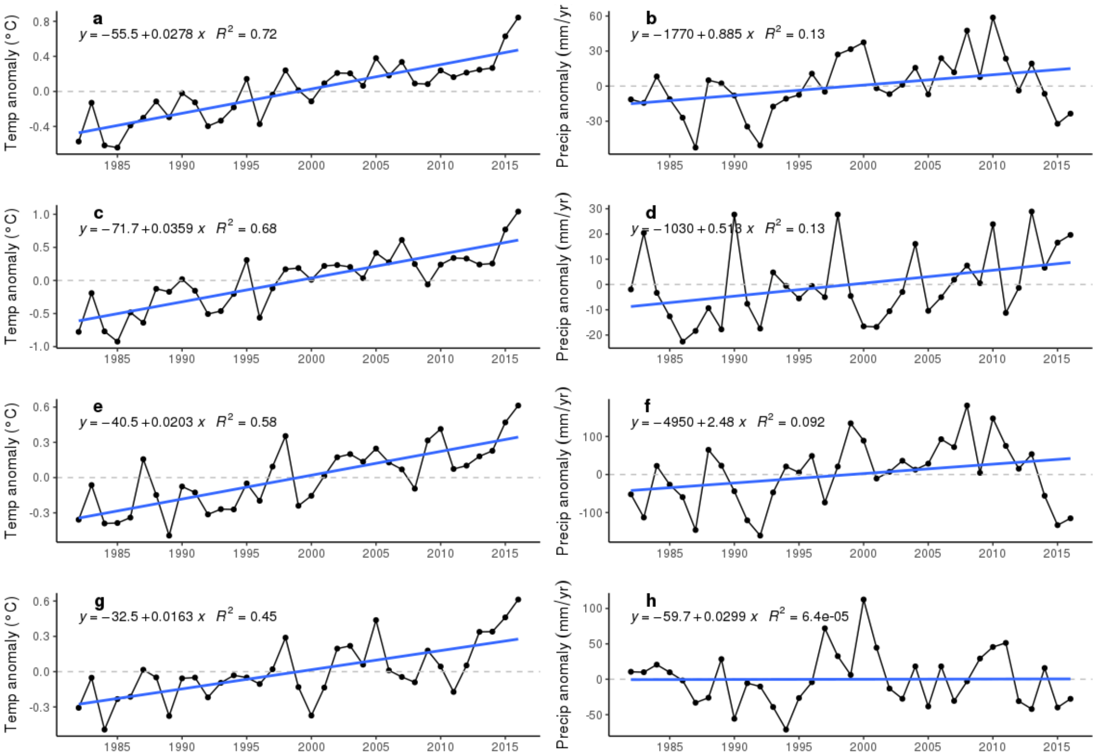

**Figure D.11 - Annual mean (a,c,e,g) temperature (°C) and (b,d,f,h) precipitation (mm/yr) anomalies for (a,b) global, (c,d) northern, (e,f) tropical, and (g,h) southern regions. Best fit lines are shown in blue with slope and intercept depicted on plot.. Data is from CRUNCEPv8.**